

Constructing Exact Correlators In $\mathcal{N} = 4$ SYM Using Integrability

by

Frank Coronado

A thesis
presented to the University of Waterloo
in fulfillment of the
thesis requirement for the degree of
Doctor of Philosophy
in
Physics

Waterloo, Ontario, Canada, 2019

© Frank Coronado 2019

Examining Committee Membership

The following served on the Examining Committee for this thesis. The decision of the Examining Committee is by majority vote.

External Examiner: Leonardo Rastelli
Professor, Dept. of Physics,
Stony Brook University, New York

Supervisor: Pedro Vieira
Faculty, Perimeter Institute for Theoretical Physics
Adjunct Professor, Dept. of Physics and Astronomy,
University of Waterloo

Co-supervisor: Robert Myers
Faculty, Perimeter Institute for Theoretical Physics
Adjunct Professor, Dept. of Physics and Astronomy,
University of Waterloo

Internal Member: Jaume Gomis
Faculty, Perimeter Institute for Theoretical Physics
Adjunct Professor, Dept. of Physics and Astronomy,
University of Waterloo

Internal Member: Niayesh Afshordi
Associate Faculty, Perimeter Institute for Theoretical Physics
Associate Professor, Dept. of Physics and Astronomy,
University of Waterloo

Internal-External Member: Florian Girelli
Associate Professor, Dept. of Applied Mathematics,
University of Waterloo

Author's Declaration

I hereby declare that I am the sole author of this thesis. This is a true copy of the thesis, including any required final revisions, as accepted by my examiners.

I understand that my thesis may be made electronically available to the public.

Abstract

This thesis is devoted to the study of correlation functions in $\mathcal{N} = 4$ superconformal Yang-Mills theory. We focus on a class of four point functions for which we achieve formal results at finite coupling and explicit results at all-loops at weak coupling and strong coupling in the planar 't Hooft limit. We use three approaches to construct them. The first is the conformal OPE expansion for which we work out the necessary conformal data, scaling dimensions and structure constants, using integrability. The second uses a geometric decomposition of the four-punctured worldsheet into hexagonal patches. This renders the four-point function as a form factor series expansion and again thanks to integrability, the components of this series are completely worked out. In the third approach we adopt a bootstrap philosophy, we fix completely a non-trivial four-point function at all loops by assuming it satisfies certain properties which we learned from the weak coupling limit of our previous two approaches. We study the strong coupling limit in our second approach and obtain results that take the expected form for a holographic CFT dual to classical strings in AdS. Finally we compute non-planar corrections in a double scaling limit and manage to perform explicit all-genus resummations in special cases. This thesis is based on the preprints [1, 2, 3, 4].

Acknowledgements

I had the luck of having Pedro Vieira as my PhD advisor. For his enthusiasm, creativity, generosity and hard working it is hard to conceive what a better advisor could be.

I specially thank Shota Komatsu for his collaboration and for being just like another supervisor always available to answer my questions and share his ideas with me.

I am also obliged to my co-advisor Rob Myers, for his patience and guidance in my first project in theoretical physics at Perimeter.

I am very thankful to my collaborators Till Bargheer, Benjamin Basso, Vasco Goncalves, Ho-Tat Lam, Amit Sever, De-liang Zhong, from whom I learned so much.

Finally, I would like to dedicate this thesis to my family. My mother, sister and brothers who have always supported me in all stages of my career.

Table of Contents

Introduction	1
1 Bethe Roots	8
1.1 Summary of the chapter	8
1.2 Introduction	8
1.3 Asymptotic Bethe Ansatz	10
1.3.1 The middle node: $\mathfrak{sl}(2)$ sector	13
1.4 Finding Bethe Roots	14
1.4.1 An algorithm to find all Bethe solutions	15
1.4.2 An example: Bethe solutions in the scalar sector	18
2 Hexagons	21
2.1 Summary of the chapter	21
2.2 Introduction	21
2.3 The BKV Hexagon program	24
2.3.1 The Hexagon Form factor	25
2.3.2 The BKV conjecture for the $\mathfrak{sl}(2)$ structure constant	30
2.4 Structure constants in the full $\mathfrak{psu}(2, 2 4)$ sector	32
2.4.1 Nested Bethe Wave Function	32
2.4.2 Nested Hexagon	34
2.4.3 “Yangian” Symmetry	39
3 Asymptotic Four-Point functions	41
3.1 Summary of the chapter	41
3.2 Introduction	41

3.3	Super OPE and Finite Bethe Roots	42
3.3.1	Reservoir Picture and Asymptotic Four-Point Functions	42
3.3.2	Super Operator Product Expansion	45
3.4	Comparison with Data	46
4	The octagon	51
4.1	Summary of the chapter	51
4.2	Introduction	51
4.3	The octagon	55
4.4	Octagons at weak coupling	58
4.5	Hexagonalization of polarized four-point functions	60
4.5.1	Skeleton graphs and hexagonalization	60
4.5.2	The <i>simplest</i> four-point function	63
4.5.3	The <i>asymptotic</i> four point function	67
4.5.4	An example for finite K and nine loops	69
4.6	The OPE expansion: a test of the hexagonalization prediction	71
5	Bootstrap	76
5.1	Summary of the chapter	76
5.2	Introduction	76
5.3	Analytic properties of octagon	78
5.3.1	Single-Valuedness and Ladders	78
5.3.2	Double-trace OPE channel	78
5.3.3	Null-square limit	79
5.4	Bootstrapping the octagon	80
5.4.1	A Steinmann basis of Ladder integrals	80
5.4.2	Fixing all coefficients with Light-cone asymptotics	82
6	Strong Coupling	84
6.1	Summary of the chapter	84
6.2	Introduction	84
6.3	Derivation	87
6.4	Analysis	90
6.4.1	OPE Limits	92

7	Non-planar	95
7.1	Summary of the chapter	95
7.2	Introduction	95
7.3	A Matrix Model for Large Operators	100
7.4	Matrix Model Simplification and Limits	108
7.4.1	Small Octagon Limit, $\mathbb{O} \rightarrow 0$	111
7.4.2	Large Octagon Limit, $\mathbb{O} \rightarrow \infty$	112
7.4.3	Free Octagon Limit, $\mathbb{O} \rightarrow 1$	114
8	Conclusions	116
	Bibliography	123
A	All-loop Beisert-Staudacher equations	135
B	The $\mathfrak{so}(6)$ Structure Constant at Tree Level	136
B.1	The $\mathfrak{so}(6)$ spin chain	138
B.2	The $\mathfrak{so}(6)$ vertex model	140
B.3	The Algebraic Bethe Ansatz (ABA)	142
B.4	The Yang-Baxter algebra	148
B.5	The coordinate Bethe Ansatz (CBA)	151
B.6	The scalar product: tree level structure constant	153
C	The $\mathfrak{su}(1,1 2)$ spin chain	157
C.1	The coordinate Bethe Ansatz(CBA)	157
C.2	Regularization of singular solutions in the $\mathfrak{su}(1,1 2)$ sector at one loop level	160
D	Superconformal Blocks	162
D.1	Cross ratios	162
D.2	The blocks	163
D.3	The super-block of a long multiplet	165
D.3.1	$\mathfrak{so}(4,2)$ conformal blocks	165
D.3.2	$\mathfrak{so}(6)$ R-symmetry blocks	166
D.4	Perturbative OPE expansion	166

E	Comparison with Data : A Special Case	169
F	Appendices for Octagon	172
F.1	More details on the octagon	172
F.1.1	The mirror states ψ	172
F.1.2	The hexagon form factor $\langle \mathcal{H} \psi \rangle$	173
F.1.3	Summing over flavor indexes	174
F.2	An efficient way to evaluate the mirror integrals	175
F.3	Mirror integrals up to nine loops	178
F.4	Prediction nine loop complete ope data of check	179
G	Non-planar appendices	181
G.1	Constructing Graphs Explicitly	181
G.2	From Minimal to Maximal Graphs	187
G.3	Counting Quadrangulations Including Couplings	190
G.3.1	Introduction	190
G.3.2	Graph Operations	193
G.3.3	Non-BPS Quadrangulations	195
G.3.4	All quadrangulations	198
G.4	Other Results On Quadrangulations	202
G.4.1	$(n + 1)$ -Point Extremal Correlators in DSL	202
G.4.2	n -Point Cyclic Correlators In DSL	204

Introduction

Conformal field theory and four-point functions

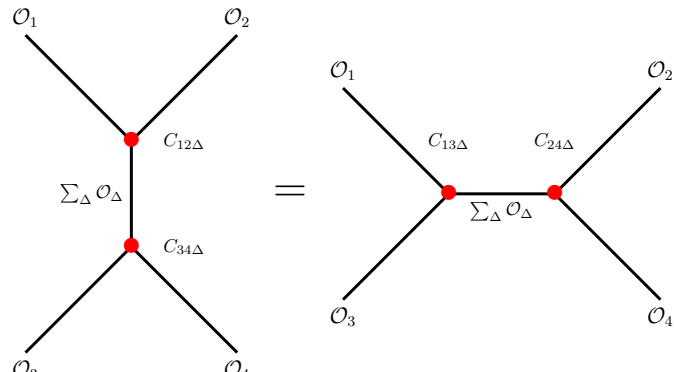
In the landscape of quantum field theories (QFT), conformal field theories (CFT) occupy a special place. It is of fundamental importance to understand their dynamics since they sit at the critical points where the RG flow starts or ends. This could eventually allows us to explore the RG flows around them and get access to more generic QFTs.

A CFT is defined by the conformal data $\{\Delta, C_{ijk}\}$ which is manifest in the local operator product expansion (OPE):

$$\mathcal{O}_1(x)\mathcal{O}_2(0) = \sum_k C_{12k} \frac{1}{x^{\Delta_1+\Delta_2-\Delta_k}} \mathcal{O}_k(0) \quad (1)$$

with scaling dimensions Δ and structure constants C_{123} .

This OPE is also associative and implies the crossing symmetry equation in a four-point correlator:



$$(2)$$

This also implies strong constraints in the conformal data Δ s and C_{ijk} s. It is non-perturbative as it holds for any value of the parameters of the theory, including the coupling of interaction. However this crossing equation(s) is hard to solve in higher dimensions as it typically has an infinite number of exchanged operators in both sides. The best we can do is to study it in some special kinematics [12, 13, 14] or numerically with the aim of finding bounds on the lowest data [15, 16, 17, 18]. In fact, this latter option has proven very successful in carving out the space of CFTs by finding boundaries or islands in the space of consistent conformal data.

In principle, thanks to the OPE, the conformal data suffices to obtain higher-point correlation functions. For the four-point function this goes as a decomposition into conformal blocks :

$$\langle \mathcal{O}_1 \mathcal{O}_2 \mathcal{O}_3 \mathcal{O}_4 \rangle = \sum_{\{\Delta\}} C_{12\Delta} C_{\Delta 34} G_{\Delta} \quad (3)$$

where the blocks G_{Δ} are completely fixed by conformal symmetry, although the full sum is not and is very theory-dependent.

It is, however, impractical to re-sum the series and obtain a manageable expression for the four-point function. It is typically more feasible to compute directly the four-point function by other means and from there have access to the conformal data through the OPE expansion. For instance, we could compute it by a diagrammatic expansion using perturbation theory if a Lagrangian is available. The drawback with this method is the typical high degeneracy of operators at weak coupling which prevents us from extracting individual conformal data¹. In this regard non-perturbative methods for the direct computation would be of better use.

The importance of four-point functions goes beyond being a source of conformal data. They also have interesting kinematical limits that give us access to different physical information in Euclidean or Lorentzian configurations of the four points. Among these we have the double-light-cone limit, Regge limit, Bulk point limit [21, 22, 23]. The former, for instance, was shown to relate the correlator with the expectation value of a Wilson loop in conformal gauge theories [24]. Also in holographic conformal theories, the other two limits, have a relevant interpretation in terms of scattering in Anti-de-Sitter space.

In this thesis we will present non-perturbative or all-loop results on conformal data and four-point functions including some of their kinematical limits. This we achieve in a special theory, the four-dimensional supersymmetric conformal gauge theory known as $\mathcal{N} = 4$ SYM. Thanks to its maximal supersymmetry this theory has exact conformal symmetry for any value of the gauge coupling g_{YM} . Furthermore when the rank of the gauge group $SU(N_c)$ is taken to infinity $N_c \rightarrow \infty$ there is an enhancement of symmetries [25] (integrability) which provides a bigger toolbox for the computation of the aforementioned observables. As we will show, in this so-called planar limit we are able to compute scaling dimensions and structure constants by direct non-perturbative methods. We will also have access to (a class of) four-point functions, not only by the reconstructive method (3), but also by more direct methods obtaining explicit expressions suitable to study more physics of the correlators.

$\mathcal{N} = 4$ SYM

This theory is not only a good toy model to explore the physics of conformal theories. It is also the most attractive example of the AdS/CFT correspondence, which establishes the duality of $\mathcal{N} = 4$ SYM with type IIB string theory in $AdS_5 \times S^5$ [26, 27].

¹Though sometimes we can still resolve the degeneracy with the knowledge of various correlators. For an instance of such resolution of mixing see [19, 20]

This duality is better spelled in the ‘t hooft limit [28] of the gauge theory established by $N_c \rightarrow \infty$ with $\lambda = g_{YM}^2 N_c$ held fixed. In this limit the observables, such as a four point function, organize into topologies in a series of $1/N_c$ as:

$$\mathcal{F}(\lambda, N_c) = \sum_{g=0}^{\infty} N_c^{2-2g} \mathcal{F}^{(g)}(\lambda) \quad (4)$$

where the term $\mathcal{F}^{(g)}$ stands for the re-summation of all (fat) Feynman diagrams with topology of genus g and its contribution comes suppressed by a power of $1/N_c$ controlled by the corresponding genus. The ‘t Hooft coupling λ is kept fixed at first but can later be taken to be small, weak coupling, or large, strong coupling.

In this limit, the duality establishes the expansion in $1/N_c$ in the gauge theory side corresponds to the expansion in the string coupling g_s that controls the splitting and joining of strings in AdS. In this way $\mathcal{F}^{(0)}$ corresponds to the tree level interaction of strings and $\mathcal{F}^{(1)}$ gives the one-loop string interaction.

Furthermore, it also establishes a weak-strong duality between the ‘t Hooft coupling λ and the inverse of the string tension α' which controls the quantum fluctuations of strings. More precisely we have the identification $\alpha' \sim \frac{1}{\sqrt{\lambda}}$. So when at strong coupling $\lambda \rightarrow \infty$ in the gauge theory side we have dual classical strings described by a classical sigma model with AdS target space or point like excitations described by supergravity in AdS. While at weak coupling $\lambda \rightarrow 0$ we have very quantum string in AdS side. This renders this duality hard to test or to prove as when one side admits a perturbative expansion the other side does not. On the bright side this allows us to access the strong coupling limit of the gauge theory side by performing computations in the classical sigma model or supergravity (depending on the type of operators involved).

The AdS/CFT dictionary establishes that for each operator of the CFT there is a dual field or string state in the AdS side. A simple set of operators is the $\frac{1}{2}$ -BPS operators, these are gauge invariant operators of the form $\text{tr}(Z^L)$ (and other $\mathfrak{so}(6)$ rotations), where Z is one of the six scalars in $\mathcal{N} = 4$ SYM. The two and three point functions of these operators are protected as shown by non-renormalization theorems. However, their four-point function is not protected as can be inferred from their OPE which includes protected short-multiplets as well as non-protected long-multiplets.

For $L = 2$ this corresponds to the short-multiplet of the stress tensor in the CFT which is dual to the supergravity multiplet in AdS. Other higher values of L correspond to Kaluza-Klein modes. However when L is of order \sqrt{N} it gives a macroscopic classical string.

We will focus on the four-point functions of these protected operators whose OPE contains a wealth of non-protected conformal data of long-multiplets. At weak coupling we will present results which can be compared with the low loop orders in the literature, up to three loops in the gauge theory side.

In order to achieve these all-loop and strong coupling results we will be exploiting the integrability of the worldsheet in the planar limit $\mathcal{F}^{(0)}$ in (4).

Integrability was discovered on both sides of the duality at weak coupling in the dilatation generator and at strong coupling in the classical sigma model. Conjectured to hold at all loops, it allows to interpolate between the two regimes in a single unifying description. This is better appreciated starting with the spectrum problem.

Integrability and the spectrum problem

In planar $\mathcal{N} = 4$ SYM the problem of finding the (anomalous) scaling dimensions of single-trace operators at any value of the coupling can be mapped to finding the spectrum of an integrable two-dimensional QFT in finite volume. This is the effective worldsheet that appears in the 't Hooft limit, spanning a cylinder. The hamiltonian of this latter system is isomorphic to the planar (anomalous) dilatation generator and the size of the periodic direction in the cylinder, is set by a $U(1)$ R-charge of the single-trace operator.

One way to address this problem is to first consider the system in infinite volume and then incorporate finite size corrections. Once in infinite volume the spectrum of this periodic system consists of multi-particle asymptotic states whose energies are given by the sum of the individual energies. Furthermore, their interaction can be described by the S-matrix which factorises into pairwise scattering, thanks to the higher conserved charges of integrability. This S-matrix also plays a key role in finding the finite size corrections.

The first finite-size corrections are of order $1/L$, with L given by the $U(1)$ R-charge, and come from the quantisation condition on the momenta imposed by periodicity over the length L of the circle. This condition is established by the Bethe equations, which for diagonal scattering are given by:

$$e^{ip_1 L} \prod_{j \neq 1} S(p_1, p_j) = 1 \quad (5)$$

which sets to 1 the total phase of translation and scattering obtained by making a particle travel around the finite size circle of length L .

The second source of finite-size corrections come from virtual or mirror particles living in the mirror space. These are related to the physical particles in the circle by a double-Wick rotation which exchanges the energy and momentum. Nevertheless, unlike the physical particles, their momenta is not quantised since the mirror space has effectively infinite length.

These mirror particles wrap around the circle and interact with physical particles along the way. More importantly their contributions to the finite-volume spectrum are exponentially suppressed according to their mirror energy and the length they travel around $e^{-E_{\text{mirror}} L}$. In the so-called asymptotic limit $L \gg 1$ these corrections are negligible and the finite-volume spectrum just comes from the sum of energies of the individual particles with the quantisation condition (5). However for small length L these wrapping corrections are important and have to be re-summed. In integrable systems this re-summation can be achieved by the so-called Thermodynamic Bethe Ansatz (TBA).

In $\mathcal{N} = 4$ SYM this TBA has been superseded by the ultimate description for the scaling dimensions known as the Quantum spectral curve. This reformulates the spectrum problem as a Riemann-Hilbert problem and it is highly efficient in obtaining numerical and analytic results for any value of the coupling λ and for any value of the $U(1)$ R-charge L , specially for small values—all of this without the necessity to perform the cutting and gluing just described.

Nevertheless, this de-compactification procedure is still of high relevance to start addressing other observables apart from the spectrum problem. For instance correlators of operators O_i^w living in the 2D world-sheet can be found through a decompactification limit or form factor expansion as:

$$\langle O_1^w O_2^w \rangle_{2D} = \sum_{mirror} \langle O^w | \psi_{mirror} \rangle \langle \psi_{mirror} | O^w \rangle e^{-E_{mirror} r_{12}}. \quad (6)$$

where r_{12} is the distance between the operators in the compact direction.

The form factors $\langle O^w | \psi_{mirror} \rangle$ are the central objects in this expansion. In integrable theories they must satisfy a set of consistency conditions or axioms that go under the name of integrable form factor bootstrap program. Our ability to find solutions to this program depends on the theory at hand and whether or not the specific operators O^w respect some extra symmetries which give further constraints for the form factors or even fix them uniquely.

An important question is which are the operators O^w in the 2D world-sheet relevant for the computation of observables, such as structures or higher-point functions, in the four-dimensional theory. Some of these relevant operators are hexagons, octagons, etc and their corresponding form factors which play a central role in this thesis.

Hexagons and higher-point functions

The authors of [5] established that the three-point function of single-trace operators is given by the finite volume correlator of two hexagon operators in the 2D world-sheet:

$$\langle \mathcal{O}_1 \mathcal{O}_2 \mathcal{O}_3 \rangle_{4D} \sim \langle \hat{\mathcal{H}}_1 \hat{\mathcal{H}}_2 \rangle_{2D} \quad (7)$$

The form factor decomposition is, however, more complicated than the one described in (6). In order to fully accomplish the decompactification we need to perform three cuts that decompose the “pair of pants” (worldsheet with three punctures) into two hexagon form factors:

$$\langle \mathcal{H} | \Psi_1 \rangle_{phys} | \psi_{12} \rangle_{mirror} | \Psi_2 \rangle_{phys} | \psi_{23} \rangle_{mirror} | \Psi_3 \rangle_{phys} | \psi_{13} \rangle_{mirror} \quad (8)$$

These are hexagonal patches of worldsheet space-time which have three physical edges, two in the past and one in the future (or viceversa). These host the physical states Ψ_i that described the external operators \mathcal{O}_i . There are also three mirror edges which host mirror states ψ_{ij} that we need to sum over in this form factor expansion.

It was subsequently shown in [6] that the hexagon program can be extended to compute higher-point functions:

$$\langle \mathcal{O}_1 \cdots \mathcal{O}_n \rangle_{4D} \sim \langle \hat{\mathcal{H}}_1 \cdots \hat{\mathcal{H}}_{2n-2} \rangle_{2D} \quad (9)$$

In this case the worldsheet has n punctures and to decompactify we perform $3(n-1)$ cuts. In this way we obtain a triangulation that gives the maximal decomposition of the worldsheet. For each triangle we insert a hexagon² and we need to sum over all mirror states propagating on the edges of the triangles.

The form factors (8) are known at finite coupling λ thanks to the work in [5] where the relevant form factor bootstrap program was solved. Still, in order to recover (7) or (9) we need to perform a re-summation over the mirror states ψ_{ij} . Fortunately their contribution comes exponentially suppressed due to the propagation along the distances that separate the hexagons $e^{-E_{\psi_{ij}} l_{ij}}$ where l_{ij} counts the number of Wick contractions between a pair of operators. Hence in the limit where all or some $l_{ij} \gg 1$ we have a controllable expansion which can be truncated. This is the regime where we will focus in this thesis.

In this thesis we will step on the shoulders of this hexagon program and will use it to obtain results for a class of four-point functions of large operators. We will show formal expressions at finite coupling and very explicit results at all-loops (weak coupling) and at strong coupling.

Outline

- In [Chapter 1](#) we review the asymptotic Bethe Ansatz of $\mathcal{N} = 4$ SYM which identifies large non-protected operators with so-called Bethe roots. We also provide a novel algorithm, combining traditional methods, to obtain these Bethe roots.
- In [Chapter 2](#) we review the hexagon program to compute structure constants of large single-trace operators. We complete this program for the structure constant of a generic non-protected operator and two protected operators, finding explicit compact formulas that depend on the Bethe roots.
- In [Chapter 3](#) we combine the knowledge of scaling dimensions and structures constants from [Chapter 1](#) and [Chapter 2](#) to reconstruct a class of four-point functions of large operators in the OPE expansion
- In [Chapter 4](#) we use hexagonalization to compute the same class of four-point functions of large operators. We simplify the construction and obtained our result as an infinite series at finite coupling. We also expand this at weak coupling, learning about the basis of functions that appear up to nine loops. Furthermore we test this nine-loop prediction against an OPE reconstruction in the spirit of [Chapter 3](#).
- In [Chapter 5](#) we perform a bootstrap exercise where we use three defining properties of the *simplest* four-point function to completely fix it at all loops.

²Our hexagons reduce to triangles if we only count the mirror edges

- In [Chapter 6](#) we take the strong coupling limit of our results in [Chapter 4](#) and analyse various OPE limits.
- In [Chapter 7](#) we consider a double scaling limit which requires the resummation of non-planar contributions. We introduce a matrix model to find all these non-planar corrections and obtained explicit resummed expressions in certain limits.
- In [Chapter 8](#) we conclude.

Chapter 1

Bethe Roots

1.1 Summary of the chapter

In this chapter we present the integrability description of the planar spectrum of $\mathcal{N} = 4$ SYM. We focus in the asymptotic regime of operators with large scaling dimensions, where we can identify each (super-primary) operator with a (finite) solution of the Beisert-Staudacher equations. Each solution is given by a list of so-called Bethe roots. We introduce a method to find these roots by combining the Beisert-Staudacher equations and the direct diagonalization of the higher conserved charges of the $\mathcal{N} = 4$ spin chain. Using this method we identify hundreds of super-conformal multiplets that we later use in [Chapter 3](#) and [Chapter 4](#) to reconstruct four-point correlators in the OPE limit.

1.2 Introduction

In the planar free theory the basis of conformal operators is spanned by the single-traces:

$$O(x) = \text{tr} \left(Z \bar{Z} \Psi_1 X \bar{X} D_\mu D^\mu Z \right) (x) \quad (1.1)$$

where each letter $Z, X, \Psi \dots$ stands for bosonic or fermionic fields and D for covariant derivatives. These are $N_c \times N_c$ matrix valued fields and the trace on their product guarantees gauge invariance.

In the free theory any state of the form [1.1](#) has a definite scaling dimension given by the sum of the classical dimensions of the composite fields. However this is not the case in the interacting theory. When turning on the coupling we need to perform a wave-function renormalization to render finite the two-point functions of operators of the form [\(1.1\)](#). This is reflected in the quantum corrections to the dilatation generator:

$$\mathcal{D} = \mathcal{D}^{(0)} + g^2 \mathcal{D}^{(1)} + g^4 \mathcal{D}^{(2)} + \dots \quad \text{with} \quad g^2 = \frac{\lambda}{16\pi^2} \quad (1.2)$$

Furthermore there is mixing, which means that at loop order only adequate linear combinations of operators (1.1) have definite scaling dimensions. In order to find these new operators we need to diagonalize the anomalous dilatation generator $\delta\mathcal{D} \equiv \mathcal{D} - \mathcal{D}^{(0)}$. Fortunately, by explicitly finding the one-loop generator $\mathcal{D}^{(1)}$ [30, 31], a remarkable feature was observed at the planar level: its integrability.

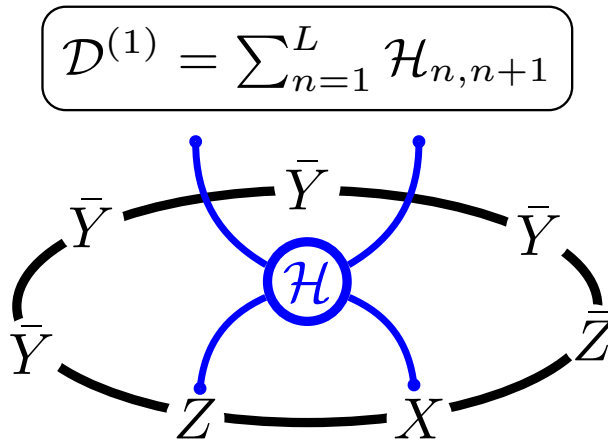


Figure 1.1: The planar one-loop dilatation generator as a nearest-neighbour spin chain Hamiltonian.

By thinking of the trace as a closed spin chain and the elementary fields as the spin degrees of freedom, the planar dilatation generator $\mathcal{D}^{(1)}$ stands as the nearest-neighbour Hamiltonian of an integrable quantum spin chain with $\mathfrak{psu}(2, 2|4)$ symmetry [32] i.e. the superconformal symmetry of $\mathcal{N} = 4$. Under this map the anomalous dimensions of conformal single-trace operators are found as the spectrum of the spin chain Hamiltonian.

The zero-energy states represent operators in short $\frac{1}{2}$ -BPS multiplets whose scaling dimensions are protected from loop corrections. One of such operators made out of only one type of scalar is $\text{tr}(Z^L)$. It serves as a reference state for the spin chain of length L and it is known as the BMN vacuum.

The higher energy levels correspond to non-protected operators in long multiplets. Their eigenvalues or anomalous dimensions can be found using the Bethe Ansatz [33, 34]. This machinery provides a set of equations whose solutions, a set of complex numbers known as Bethe roots, identify uniquely the states of the spectrum. In the $\mathcal{N} = 4$ spin chain these equations are known as Beisert-Staudacher(BS) equations¹, worked out for $\mathcal{D}^{(1)}$ in [31].

The minimal form of these equations appears in the so-called $\mathfrak{sl}(2)$ subsector spanned by operators containing only one type of scalars Z and arbitrary number of light-cone covariant derivatives D . For a state with Lorentzian spin K and L scalars $\text{tr}(D^K Z^L)$ the

¹Throughout this thesis we will be referring to them as BS equations or Bethe equations indistinctively.

Bethe equations are:

$$\text{periodicity: } e^{ip(u_k)L} \prod_{k \neq j}^M S(u_k, u_j) = 1 \quad \text{and} \quad \text{cyclicity: } \prod_{k=1}^M e^{ip(u_k)} = 1 \quad (1.3)$$

with:

$$e^{ip(u_j)} = \frac{u + \frac{i}{2}}{u - \frac{i}{2}} \quad \text{and} \quad S(u, v) = \frac{u - v + i}{u - v - i} \quad (1.4)$$

Physically the Bethe roots parametrize the momenta of K magnons interacting on top of the BMN vacuum of length L . This interaction is controlled by their two-particle S-matrix and the Bethe equations are the quantization conditions on the momenta imposed by periodicity and cyclicity of the wave-function.

At higher loop orders integrability was observed to persist by explicitly working out the corrections to the dilatation generator in some closed subsectors, reaching up to four loops in the $\mathfrak{su}(2)$ subsector. These corrections now lead to a long-range spin chain Hamiltonian with a range of interaction that grows with the loop order. Its spectrum was found to be encoded in suitable loop deformations of the phases (1.4) in the Bethe Ansatz quantization conditions (1.3). Furthermore assuming integrability holds at all loops, the all-loop BS equations were conjectured in [35], including the all-loop generalization of the phases in (1.4), although the Hamiltonian for high loop orders remains unknown.

However, these all-loop BS equations are only exact in the asymptotic regime i.e. at loop orders smaller than the length L of the chain. At higher loop orders the spin chain description breaks down as the range of the Hamiltonian becomes larger and starts wrapping around the chain.

Beyond this asymptotic regime the description of the integrability of the system is more akin to that of a 2D integrable QFT in finite volume, see Figure 1.2. In this description the wrapping effects are represented by virtual particles that live on the mirror space, edges of the cylinder, and wrap around the circle of length L interacting with the magnons of the physical space. At this point one must switch to more sophisticated integrability machinery such as the Y-system [41], the Thermodynamic Bethe ansatz [42], finite integral equations [43] or, the current *spectrum problem Ferrari*, the quantum spectral curve [44].

In this thesis we focus only in the so-called asymptotic regime. This is spanned by the spectrum of large operators for which wrapping corrections can be safely disregarded. We will later refer to the virtual particles in subsequent chapters where they will play a major role.

1.3 Asymptotic Bethe Ansatz

A conformal single-trace operator is identified by a list of Bethe roots that furnishes a solution of the BS equations (see Appendix A for explicit form). These roots are grouped

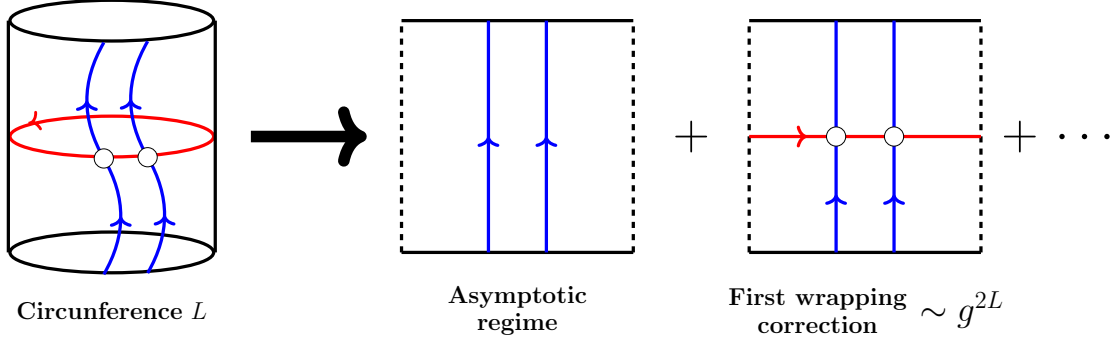


Figure 1.2: 2D QFT in finite volume

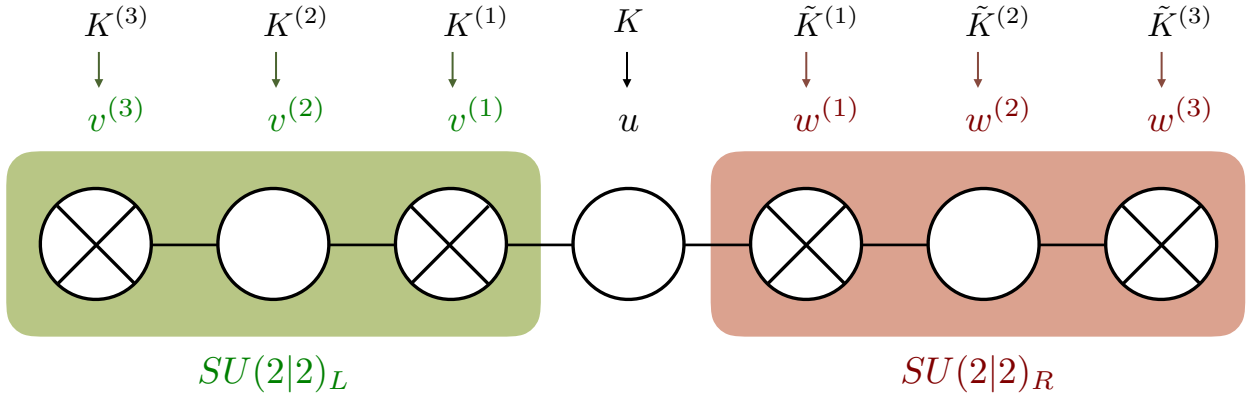


Figure 1.3: $PSU(2, 2|4)$ Dynkin diagram and Bethe roots.

into seven sets, each associated to a node in the $\mathfrak{psu}(2, 2|4)$ Dynkin diagram, see [Figure 1.3](#). We use u_j to denote the *middle node* Bethe roots which obey the middle node equations with a spin-chain length L . Then we have a set of three type of Bethe roots $v_j^{(1)}, v_j^{(2)}, v_j^{(3)}$ describing one of the $\mathfrak{su}(2|2)$ wings and another set of roots $w_j^{(1)}, w_j^{(2)}, w_j^{(3)}$ describing the other $\mathfrak{su}(2|2)$ wing. We use K to denote the number of middle node roots and $K^{(a)}$ and $\tilde{K}^{(a)}$ with $a = 1, 2, 3$ to indicate the number of Bethe roots in each of the wings.

The number of Bethe roots necessary to describe an operator is determined by its charges at zero coupling. These are the global charges under the classical super-conformal group of the free theory. In this thesis we focus only in the super-primaries that appear in the OPE of two identical protected operators. Their corresponding global numbers and representations under the Lorentz and R-symmetry groups are:

Scaling dimension	Lorentz $\mathfrak{su}(2) \times \mathfrak{su}(2)$	$\mathfrak{so}(6)$ R-charge
$\Delta = \Delta_0 + \delta\Delta$	$[s, s]$	$[n - m, 2m, n - m]$

where Δ_0 and $\delta\Delta$ denote the classical and anomalous dimensions respectively.

Due to the symmetry in their Lorentz and R-charge representations these class of

operators have the wings occupation numbers identified:

$$\tilde{K}^{(a)} = K^{(a)} \quad \text{with} \quad a = 1, 2, 3 \quad (1.5)$$

and the exact relation between classical charges and occupation numbers is

$$\Delta_0 = L - K^{(1)} + K^{(3)} + K - 2 \quad (1.6)$$

$$s = K - K^{(1)} - K^{(3)} - 2 \quad (1.7)$$

$$n = L/2 + K^{(3)} - K^{(2)} - 1 \quad (1.8)$$

$$m = L/2 + K^{(2)} - K^{(1)} - 1 \quad (1.9)$$

From the knowledge of the middle node Bethe roots we can compute the anomalous dimension in the asymptotic regime²:

$$\delta\Delta = \sum_{j=1}^K \frac{2g^2}{x^+(u_j)} - \frac{2g^2}{x^-(u_j)} \quad (1.10)$$

where we use the short-hand notation for the Zhukovsky variable $x_j^\pm \equiv x(u_j \pm \frac{i}{2})$ which incorporates the coupling as:

$$x(u) = \frac{u + \sqrt{u^2 - 4g}}{2g} \quad \text{or} \quad x(u) + \frac{1}{x(u)} = \frac{u}{g} \quad (1.11)$$

The wing roots do not enter explicitly formula (1.10) but they are coupled with the middle node roots through the BS equations. Their role is to account for the flavour degrees of freedom in the $\mathfrak{psu}(2, 2|4)$ chain, see [Section 2.4.1](#) in [Chapter 2](#).

Bethe equations admit solutions with finite roots and other solutions that include roots at infinity. In fact any solution with only finite Bethe roots can be deformed by adding roots at infinity while still satisfying Bethe equations with shifted occupations numbers but with the same value of anomalous dimension (add $x_{\text{extra}}^\pm = \infty$ in (1.10)). This means finite solutions and its deformations with roots at infinity are related in the same way as a super-primary and its descendants in a super-conformal multiplet³. So instead of associating a finite Bethe solution with a single operator we should consider it actually represents a full super-conformal multiplet, although we typically pick a representative in this multiplet as the super-primary.

For the Bethe equations to admit finite solutions the occupation numbers usually need to decrease as we go from the middle node occupation K into the wing extremities $K^{(3)}$, see e.g. [\[35, 46, 47\]](#). Besides being the quantum numbers in [\(3.7–3.10\)](#) all non-negative integers also puts restrictions over the length L and the occupation numbers K and $K^{(a)}$. In [Table 1.3](#) we provide instances of global and occupation numbers indicating the subsector they belong to.

²Up to higher loop wrapping corrections which, as mentioned above, we are discarding throughout this work.

³Adding different arrangements of roots at infinity in some or all seven nodes would correspond to descendants obtained by the action of different lowering generators of the super-conformal algebra on the super-primary.

$\{\Delta_0, s, n, m\}$	K^3	K^2	K^1	K	\tilde{K}^1	\tilde{K}^2	\tilde{K}^3
$\{24, 2, 10, 10\}$	4						
$\{6, 2, 2, 0\}$	2		4	2			
$\{24, 0, 10, 10\}$	1		2	4	2	1	

Table 1.1: Examples of global numbers and occupation numbers of Bethe roots. The green and blue nodes correspond to the closed subsectors $\mathfrak{sl}(2)$ and $\mathfrak{su}(1, 1|2)$ respectively.

1.3.1 The middle node: $\mathfrak{sl}(2)$ sector

Super-conformal multiplets in the $\mathfrak{sl}(2)$ subsector are described by middle node roots and empty wings. Some operators forming part of a super-conformal multiplet in this sector have composite fields of the form⁴:

$$\text{Tr}(D^{K-2}Z^{L-1}\bar{Z}) \quad \text{and} \quad \text{Tr}(D^K Z^L) \quad \text{and} \quad \text{Tr}(D^{K-2}Z^L X X) \quad (1.12)$$

The corresponding BS equations have the same form as in (1.3) but with deformations of the momentum and S-matrix in (1.4) that now depend on the coupling g through the Zhukovsky variable:

$$\begin{aligned}
 & \text{All-loops} & \text{Leading order, } g = 0 \\
 1 = \left(\frac{x_j^+}{x_j^-} \right)^L \prod_{\substack{k=1 \\ k \neq j}}^K \underbrace{\frac{x_j^+ - x_k^-}{x_j^- - x_k^+} \frac{1 - \frac{1}{x_k^- x_j^+}}{1 - \frac{1}{x_k^+ x_j^-}}}_{= S(u_j, u_k)} \frac{1}{\sigma^2(u_j, u_k)} & \xrightarrow{g \rightarrow 0} & 1 = \left(\frac{u_j + \frac{i}{2}}{u_j - \frac{i}{2}} \right)^L \prod_{\substack{k=1 \\ k \neq j}}^K \frac{u_j - u_k + i}{u_j - u_k - i}
 \end{aligned} \quad (1.13)$$

The function $\sigma(u_j, u_k) = 1 + \mathcal{O}(g^8)$ is the so-called dressing phase, see [36].

These equations are only valid in the asymptotic regime, for loop order below or equal to L . In order to solve them we typically first search for the solutions at leading order $g = 0$ and then we simply solve for each loop correction one by one from a linearized system of equations. For instance, for $K = 2$ and even L in (1.13) we have $L/2$ different solutions,

⁴For $K = 2$ and $L = 2$ these are operators in the Konishi multiplet. Each of them can be the super-primary depending on the grading we use, $\text{tr}(Z\bar{Z})$ in the beauty grading, $\text{tr}(D^2 Z^2)$ in the $\mathfrak{sl}(2)$ grading and $\text{tr}(ZZXX)$ in the $\mathfrak{su}(2)$ grading.

each given by a pair of Bethe roots with opposite signs.

$$u_{n,\pm} = \pm \left(\frac{1}{2} \cot \left(\frac{n\pi}{L+1} \right) + g^2 \frac{2(L+2) \sin \left(\frac{2n\pi}{L+1} \right)}{L+1} + \mathcal{O}(g^4) \right) \quad \text{with } n = 1, \dots, \frac{L}{2} \quad (1.14)$$

and the corresponding anomalous dimension up to four loops is :

$$\delta\Delta_n = g^2 16 \sin^2 \left(\frac{n\pi}{L+1} \right) + g^4 \frac{64 (L+3 + 2 \cos \left(\frac{2n\pi}{L+1} \right) \sin^4 \left(\frac{n\pi}{L+1} \right))}{L+1} + \mathcal{O}(g^6) \quad (1.15)$$

for $L = 2$ and $K = 2$ the latter expression provides the two-loop anomalous dimension of Konishi, the non-protected super-multiplet with the lowest scaling dimension. At four loops we already need to incorporate contributions from virtual particles.

Finding analytical solutions for higher K and L is almost impossible, but we can access them numerically. The solutions in this sector only have real roots, so by bringing the equations in manifestly real form we can use MATHEMATICA to find all solutions, see for instance [104]. This method is also applicable to higher rank sectors, with finite roots on the wings, but it misses the complex solutions. In the following section we present an alternative to find all solutions.

1.4 Finding Bethe Roots

Finding all (complex) solutions of the leading order Bethe equations is a hard task. It also comes with extra complications such as the presence of singular solutions, which make some components on the Bethe equations diverge. Besides this type of solutions can be unphysical and it is necessary to develop a regularization and criteria to discriminate between physical and unphysical solutions. This problem has been addressed for instance in [53] for states in the $\mathfrak{su}(2)$ subsector, but the extension of this analysis to the full $\mathfrak{psu}(2, 2|4)$ has not been performed yet.

More recently an algorithm based on the reformulation of the one-loop Bethe equations, in terms of so-called Q-functions, has proven efficient in finding all physical solutions for small to moderately large global numbers $\{\Delta_0, s, m, n\}$. These Q-functions satisfy a set of difference equations which combined with their polynomiality condition can be found using the algorithm of [56, 57]. The Bethe roots are read from the zeros of these polynomials.

In [57] all super-conformal multiplets with classical dimension below $\Delta_0 < \frac{13}{2}$ are identified by their Bethe solutions. This data was very useful for the one-loop tests presented in Chapter 3. However, to perform the nine-loop tests in Chapter 4 we needed to find Bethe solutions corresponding to scalar operators with classical dimension $\Delta_0 = 24$. In order to deal with these larger operators we engineered an algorithm that combines the approaches of direct diagonalization and Bethe equations to find the Bethe roots. We provide the details in the following section.

1.4.1 An algorithm to find all Bethe solutions

Before constructing our algorithm we start by summarizing the advantages and disadvantages of the direct diagonalization of the dilatation generator and solving Bethe equations.

- **Direct diagonalization of the Dilatation generator:**

The first obstacle is to know explicitly the anomalous dilatation generator $\delta\mathcal{D}$. This generator receives corrections at each loop order and its full explicit form is only known at one-loop $\delta\mathcal{D} = g^2\mathcal{D}^{(1)} + \dots$.

For a given space of nearly degenerate states with classical global numbers $\{\Delta_0, s, m, n\}$ the matrix representation of $\mathcal{D}^{(1)}$ is not dense and hence is more suitable for a direct diagonalization. This is thanks to planarity which implies $\mathcal{D}^{(1)}$ can only have nearest-neighbour interactions.

As the global numbers grow $\{\Delta_0, s, m, n\}$ also the number of nearly-degenerate states grow and at some point the diagonalization becomes unfeasible, even for just $\mathcal{D}^{(1)}$. However a numerical diagonalization is still doable for a moderately large space.

By performing the diagonalization of $\mathcal{D}^{(1)}$ we only get access to the anomalous dimensions and that is not enough information to obtain the Bethe roots. These latter are needed to identify the super-conformal multiplets uniquely.

- **Bethe equations:**

The BS equations can be solved in an expansion in the coupling: $u = u^{(1)} + g^2 u^{(2)} + \dots$. We can first solve them at $g = 0$ and then find the loops corrections one at the time by solving the linearized BS equations which takes the lower loop orders as a seed.

The first step is the hardest and in general the space of solutions contains (singular) unphysical solutions which do not correspond to any super-conformal multiplet in $\mathcal{N} = 4$.

Considering the advantages of the two approaches we propose a procedure that combines the direct diagonalization of $\mathcal{D}^{(1)}$ and the use of linearized BS equations to find the Bethe roots and all its loop corrections. An important ingredient we need to incorporate is the complete set of local conserved charges of the one-loop integrable spin chain. As we will explain their eigenvalues provides us with enough information to find the Bethe roots at leading order.

Our algorithm follows the red dashed path in [Figure 1.4](#). In what follows we describe its steps in more detail and provide some explicit results.

1. Cyclicity and highest weight space:

In order to evaluate the dilatation generator as a matrix we first construct a basis of states for the space with global numbers $\{\Delta_0, s, m, n\}$. This is spanned by all single-traces $\text{tr}(\dots)$ with field content constrained by the aforementioned charges.

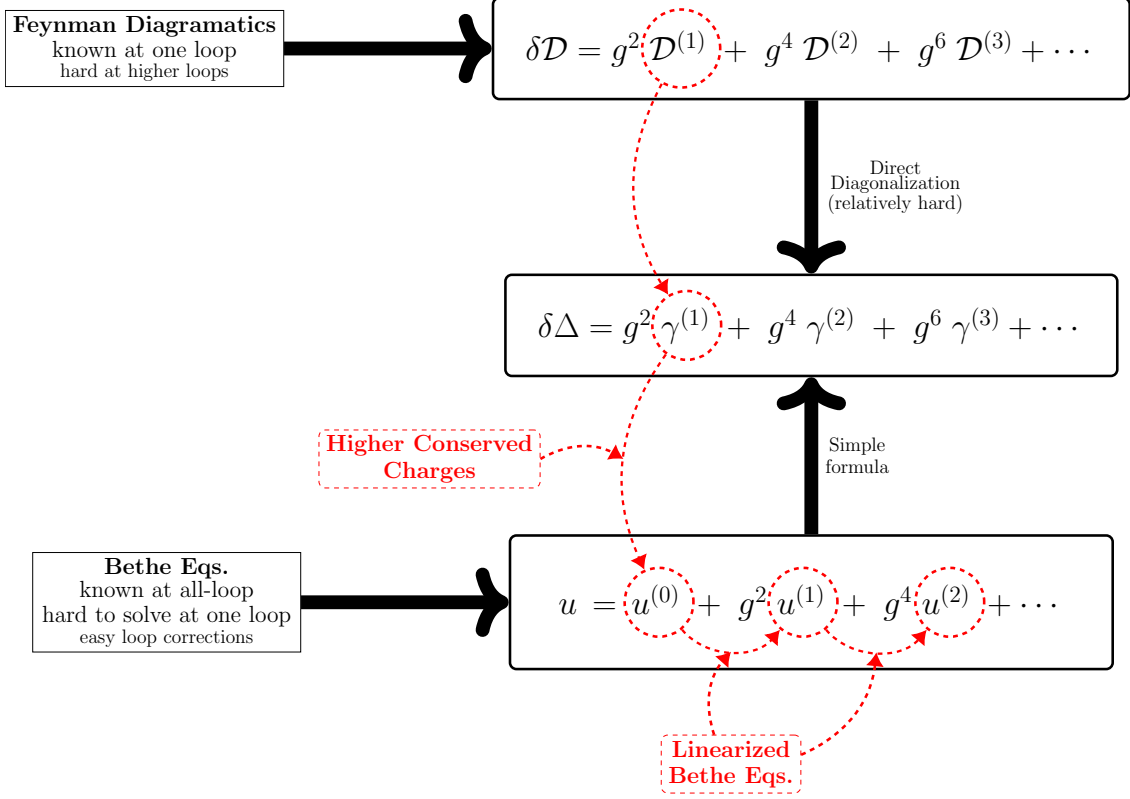


Figure 1.4: An alternative method to find all Bethe roots.

For instance for the scalar sector $\{\Delta_0 = L, s = 0, n, m\}$ some of the basis elements have the form

$$\text{tr}(Z^{\frac{L}{2}+m} X^{n-m} \bar{Z}^{\frac{L}{2}-n}) \equiv |Z^{\frac{L}{2}+m} X^{n-m} \bar{Z}^{\frac{L}{2}-n}\rangle + \text{cyclic permutations} \quad (1.16)$$

On the right hand side we present the spin chain interpretation of the trace as a sum of all cyclic permutations. The other elements of the basis are obtained by considering other (cyclically inequivalent) orderings of the fields within the trace and also by replacing singlet pairs $Z\bar{Z}$ by $X\bar{X}$ or $Y\bar{Y}$.

To further reduce the dimension of the basis we should project over the space of highest weights. These corresponds to finding linear combinations of states of the form (1.16) that are annihilated by the raising generators of the super-conformal group. The dimension of the resulting basis already provides the number of super-conformal multiplets we should find.

2. Diagonalization of local charges and middle node Bethe roots

The next step is to evaluate the anomalous dilatation generator $\mathcal{D}^{(1)}$ on the basis previously constructed and diagonalize it. In this way we obtain all anomalous dimensions but in general we still get some degenerate subspaces. In order to completely lift the degeneracy we use the higher conserved charges of the spin chain.

These local conserved charges are a family of L commuting operators that are responsible for the integrability of the spin chain of length L . According to the Bethe Ansatz they are obtained from the expansion of the so-called transfer matrix T as:

$$\log T(w) = \sum_{k=1}^L w^k \mathcal{Q}_k \quad (1.17)$$

The commutativity of transfer matrices $[T(w), T(v)] = 0$ for any parameter w, v guarantees the commutation of the conserved charges. For details on this Bethe Ansatz construction see [Fadeev] or check appendix where we present a novel construction for the $\mathfrak{so}(6)$ spin chain.

The local conserved charge \mathcal{Q}_k can be written in terms of a density operator that acts over k sites of the spin chain. The first two are notable, the first charge is the momentum or shift-operator of the spin chain and the second charge is its nearest-neighbour Hamiltonian. This latter is proportional to the one-loop dilatation operator:

$$\mathcal{Q}_1 = e^{iP} = 1 \quad \text{and} \quad \mathcal{Q}_2 = \frac{1}{2} \mathcal{D}^{(1)} = \sum_{j=1}^L \mathcal{H}_{j,j+1} \quad (1.18)$$

the next charge has the form $\mathcal{Q}_3 = \sum_{j=1}^L [\mathcal{H}_{j,j+1}, \mathcal{H}_{j+1,j+2}]$ and higher charges are increasingly more complicated.

The eigenvalues $\{\lambda_1, \lambda_2, \dots, \lambda_L\}$ of a state under the L conserved charges are related to the corresponding middle node Bethe roots as:

$$\prod_{k=1}^K \frac{u_k + \frac{i}{2}}{u_k - \frac{i}{2}} = \lambda_1 = 1 \quad \text{and} \quad \sum_{k=1}^K \left(\frac{1}{(u + \frac{i}{2})^{k-1}} - \frac{1}{(u - \frac{i}{2})^{k-1}} \right) = \lambda_{k \geq 2} \quad (1.19)$$

The first eigenvalue is one for all cyclic states (traces) and the second eigenvalue is proportional to the anomalous dimension $\gamma^{(1)} = 2\lambda_2$.

Formulas (1.19) are typically used to go from the knowledge of the Bethe roots to the conserved charges but they can be equally used in the reverse direction. In fact it is enough to know the first K eigenvalues to determine uniquely the complete set of K middle node roots.

Continuing with our diagonalization procedure, after finding the spectrum of $\mathcal{Q}_2 = \mathcal{D}^{(1)}$ we diagonalize \mathcal{Q}_3 within each degenerate subspace and store the corresponding eigenvalues. Then we do the same with the next higher charges one by one. At each step some degeneracy is further lifted. After reaching the K -th charge the degeneracy is not lifted anymore. If there is some remaining degeneracy at all, it will be due to the roots at the wings as we explain in the next step.

Concerning the middle node Bethe roots they can be found as:

$$\{\lambda_1, \dots, \lambda_K\} \xrightarrow{(1.19)} \{u_1, \dots, u_K\} \quad (1.20)$$

3. Wing roots from wing Bethe equations:

In order to find the roots at the wings we can use the eigenvalues of the nested local charges. Then relations analog to (1.19) will give us access to the wings $\{v\}_N$ and $\{w\}_N$, where N denotes the total number of them.

Alternatively we can use directly the Bethe equations to solve for the wings. This is now much more tractable as we input the middle node roots found in (1.20).

The solutions we found can be classified into two groups:

(a) Symmetric wings

The wings are identical $\{v\}_N = \{w\}_N$, so there is only one Bethe solution $\{\{w\}_N, \{u\}_K, \{w\}_N\}$ in the space labeled by eigenvalues $\{\lambda_1 \cdots \lambda_K\}$.

(b) Non-symmetric wings

The wings are different $\{v\}_N \neq \{w\}_N$ and this leads to two different solutions related by swapping the wings: $\{\{w\}_N, \{u\}_K, \{v\}_N\}$ and $\{\{v\}_N, \{u\}_K, \{w\}_N\}$. This explains the residual two-fold degeneracy found in some spaces $\{\lambda_1 \cdots \lambda_K\}$

4. Finding loop corrections

This step is straightforward, we plug in the leading order Bethe roots as a seed and solve for the corrections loop by loop from a linearized system of Bethe equations.

1.4.2 An example: Bethe solutions in the scalar sector

Using the method of the previous section we find Bethe solutions in the scalar sector with classical global numbers $\{\Delta_0 = L, s = 0, n = \frac{L}{2} - 2, m = \frac{L}{2} - 2\}$. These correspond to states with $\mathfrak{so}(6)$ R-charge $[0, L - 4, 0]$ and have four middle node Bethe roots. We find all solutions for even $L = 6, 8, \dots, 24$. The number of solutions classified according to their symmetry on the wings is reported in Table 1.2. For the lowest values of $L = 2, \dots, 12$

L	6	8	10	12	14	16	24
{sym,no-sym}	{8,1}	{24,5}	{52,14}	{100,28}	{166,53}	{260,87}	{966,371}

Table 1.2: Number of solutions of the $\mathfrak{so}(6)$ spin chain of length L and roots $\{2, 4, 2\}$. We classify them according to {symmetric wings, non-symmetric wings}. The total number of solutions is given by $(\text{sym} + 2 \times \text{no-sym})$.

our results are in perfect agreement with the algorithm of [90].

All these Bethe solutions, specially the ones with $\Delta_0 = L = 24$, are used in Chapter 4 to perform a nine-loop test of the computation of four-point functions there exposed. Among these solutions we encountered some with Bethe roots in approximately singular positions, see Table 1.3. These have a pair of complex conjugate Bethe roots such that $u_3 - u_4 - i \approx 0$. This factor renders singular the Bethe equations and also the main formulas of Chapter 2 for structure constants. We needed to carry our method with high numerical precision to

find the deviation of these roots from the singular point $u_3 - u_4 - i \approx 10^{-45}$ and be able to check they satisfy the Bethe equations and used them in the computation of structure constants.

u_1	u_2	$u_3 \ \& \ u_4$
-3.775756759	-0.07391374823	0.0151079602 \pm 0.5000000000 i
-1.829135907	-0.1511209049	0.0266840879 \pm 0.5000000000 i
-1.162800880	-0.2355067318	0.0341089969 \pm 0.5000000000 i
-0.8184936558	-0.3323810079	0.0383217165 \pm 0.5000000000 i
-0.6026135491	-0.4499760493	0.0402087653 \pm 0.5000000000 i

Table 1.3: Five almost singular solutions with $\{\Delta_0 = 24, s = 0, n = 10, m = 10\}$. We provide the four middle node Bethe roots $\{u_1, u_2, u_3, u_4\}$ at leading order in g and with 10 digits of precision only. To see their deviation from the singular positions $\pm \frac{i}{2}$ we need to go up to precision 10^{-35} and in particular 10^{-45} for the solution highlighted in [blue](#).

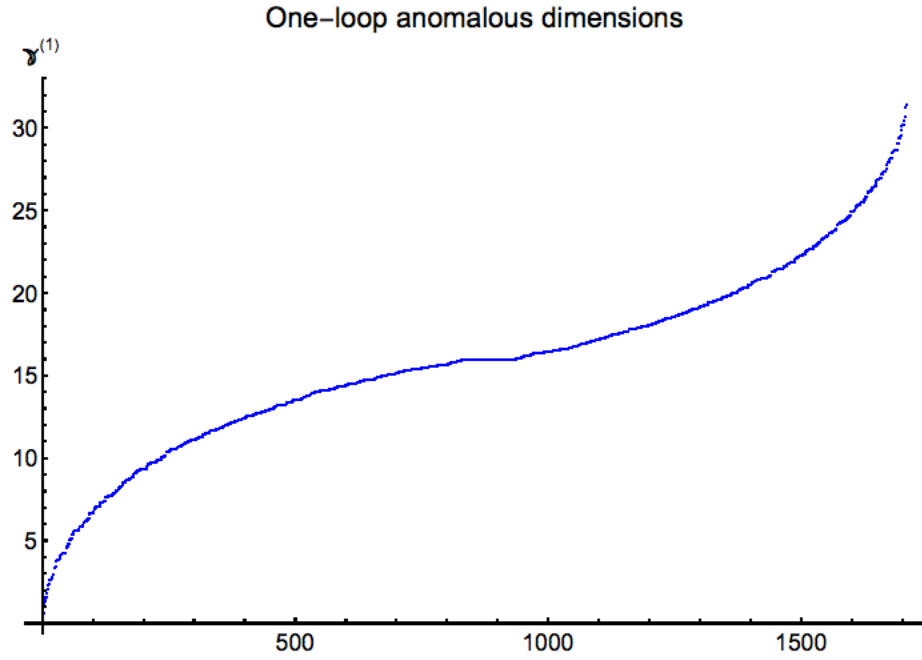


Figure 1.5: A ListPlot of the anomalous dimensions $\gamma^{(1)}$ of the 1708 super-conformal multiplets with global numbers $\{\Delta_0 = 24, s = 0, n = 10, m = 10\}$. The flat region in the middle corresponds to 90 degenerate multiplets with anomalous dimension $\gamma^{(1)} = 16$. This degeneracy is (partially) lifted when considering the higher-conserved charges.

Chapter 2

Hexagons

2.1 Summary of the chapter

In this chapter we introduce the hexagon program for the computation of structure constants. We study the case of one non-protected operator and two protected operators and focus only in the asymptotic limit. We review the all-loop hexagon conjecture for the rank one subsector $\mathfrak{sl}(2)$. We further extend this conjecture to the full $\mathfrak{psu}(2, 2|4)$ sector by incorporating the nested wing wave-functions in the hexagon program. The resulting formula makes manifest a selection rule for three-point functions of non-protected and two protected operators. We comment on the symmetry responsible for this.

2.2 Introduction

Another important piece of the CFT data are the OPE structure constants which can be found on the three-point functions of conformal operators:

$$\mathcal{C}_{123} \sim \langle \mathcal{O}_1(0) \mathcal{O}_2(1) \mathcal{O}_3(\infty) \rangle \quad (2.1)$$

In the planar limit, thanks to integrability, we also have access to them using non-perturbative or all-loop methods.

In order to address the problem of structure constants in the language of the underlying 2D integrable system we now need to consider this in a finite volume space with topology of a pair of pants where the states at the three entries represent the conformal operators or Bethe states. As in the case of the spectrum we can tackle this problem by performing a tailoring procedure: cut and glue. This consists on cutting open the pair of pants considering the asymptotic limit first and then glue back incorporating finite size corrections as the contributions of the mirror states living on the cuts. While for the cylinder one cut was enough to go from finite to large volume, now for the pair of pants we need to perform three cuts resulting into two hexagons as shown in [Figure 2.2](#). Each cut removes one of

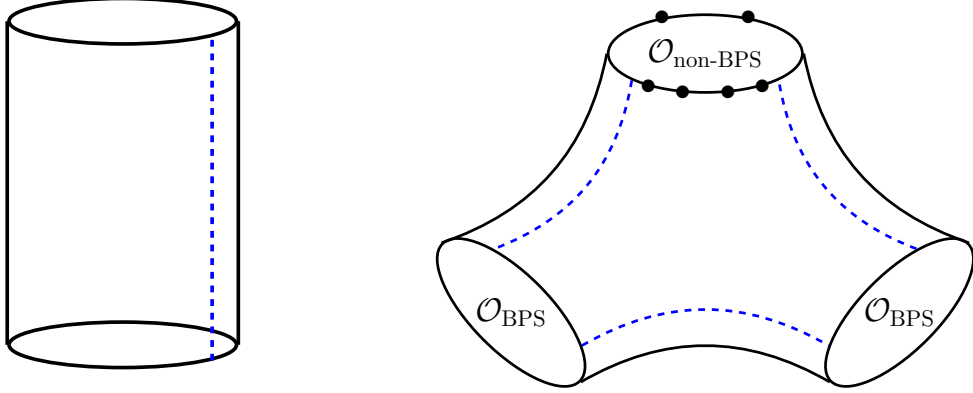


Figure 2.1: Cutting-open worldsheets with topologies of cylinder and pairs of pants. Algebraically a cut corresponds to an insertion of a resolution of the identity given by the mirror spectrum.

the three bridge lengths $l_{ij} = \frac{L_i + L_j - L_k}{2}$ (number of Wick contractions at tree level). These come back when gluing back the hexagons and control the contributions of the mirror states as $e^{-E_{\text{mirror}} l_{ij}} \sim (g^2)^{l_{ij}}$, where E_{mirror} stands for the energy.

In this thesis we will only consider the asymptotic limit corresponding to very large bridge lengths $l_{ij} \gg 1$ (needs $L_i \gg 1$) such that we can ignore the contributions of mirror states and the gluing becomes trivial. Still to compute the structure constants in this asymptotic regime we need to address two important questions:

1. How do we cut the Bethe states representing the non-protected operators?
2. How do we evaluate the two hexagons obtained after cutting the pair of pants?

The answers to these equations at all-loops are the subject of the following sections. Let us briefly comment on the early steps taken at weak coupling.

The standard perturbative computation consists on first finding explicitly the eigenstates of the anomalous dilatation generator that represent the non-protected conformal operators. Then proceed with the Feynman diagrammatic expansion performing Wick contractions at tree level and decorating with loops at loop level. In particular, for the tree level computation we need the one-loop eigenstates of $\mathcal{D}^{(1)}$ ¹. These can be found from a direct diagonalization of $\mathcal{D}^{(1)}$ or through the Bethe Ansatz construction of the eigenstates, which works perfectly at this order. However at higher loops the necessary explicit knowledge of the eigenstates is one of the main drawbacks of this perturbative program, as no

¹This is necessary to lift the degeneracy of the naive tree-level conformal operators. In general, to access the structure constant at loop order n we will need the eigenstates of the dilatation generator at loop order $n + 1$.

systematic construction of them is available².

Fortunately, hints to answer the two questions above appeared already at tree level and one-loop computations of structure constants involving operators in the rank-one sectors $\mathfrak{sl}(2)$, $\mathfrak{su}(2)$ and $\mathfrak{su}(1|1)$ [9, 10, 11]. At tree-level the structure constant of one non-protected operator \mathcal{O}_1 described by a $\mathfrak{sl}(2)$ Bethe state with roots $\mathbf{u} \equiv \{u_1, \dots, u_k\}$ and two protected operators $\mathcal{O}_2, \mathcal{O}_3$ can be computed by Wick contractions and was found to be given by a sum over bi-partitions $\alpha \cup \bar{\alpha}$ of the magnons \mathbf{u} :

$$\mathcal{C}_{123}(\mathbf{u}) \sim \sum_{\alpha \cup \bar{\alpha} = \mathbf{u}} w_{\alpha, \bar{\alpha}; l_{12}} \mathcal{H}_{\alpha} \times \mathcal{H}_{\bar{\alpha}} \quad (2.2)$$

A suggestive interpretation of the components in this latter formula associates it with the tailoring. The phase factor $w_{\alpha, \bar{\alpha}; l_{12}}$ appears as a result of the scattering between magnons in different partitions and the propagation of magnons in $\bar{\alpha}$ along the bridge l_{12} to reach the second hexagon, see equation (2.31). The form factors \mathcal{H}_{α} and $\mathcal{H}_{\bar{\alpha}}$ can be understood as the hexagons evaluated on each partition of the Bethe roots. At leading order they were found to factorized into two-magnon interactions:

$$\mathcal{H}_{\mathbf{u}} = \prod_{i < j}^K h(u_i, u_j) \quad \text{with} \quad h(u, v) = \frac{u - v}{u - v - i} \quad (2.3)$$

with these satisfying a simple relation with the two-magnon S-matrix:

$$\text{Watson equation:} \quad \frac{h(u, v)}{h(v, u)} = S(u, v) \quad (2.4)$$

Furthermore, the same structure in (2.2) with a one-loop deformation of its components was found to reproduce the one-loop structure constants obtained from the OPE of one-loop correlators of four protected operators. One of the important lessons we learned was that the details of the complicated Bethe states are finally encoded into the much simpler components of (2.2).

Finally, the authors of [5] provided an all-loop generalization of (2.2). They found the all-loop hexagon form factors $\mathcal{H}_{\mathbf{u}}$ using its residual supersymmetry $\mathfrak{psu}(2|2)$ and the axioms of the integrable form factor bootstrap program³ without resorting to the explicit form of the Bethe states. In the next section we review the relevant components of this hexagon program for the asymptotic regime of large operators⁴.

In Section 2.4.1 we address the case when the non-protected operator is in a higher rank sector of $\mathfrak{psu}(2, 2|4)$ whose description requires auxiliary wing roots \mathbf{v} and \mathbf{w} . For

²At higher loop orders the standard Bethe Ansatz receives local corrections whose exact pattern has not been worked out beyond two loops. This simply says that we do not have access to the Bethe states at higher loop orders, which is an important drawback for the perturbative computation.

³These are a set of consistency relations that any form factor in an integrable theory must satisfy. Among these relations we have the Watson equation.

⁴For the computation of structure constants of small operators we refer the reader to where details are provided on how to incorporate the finite size corrections with the mirror basis at the three cuts.

this we incorporate the nested Bethe wave-functions of the left $|\psi_{\mathbf{v}}\rangle$ and right $|\psi_{\mathbf{w}}\rangle$ wings. We will show that after simplifying the contraction of these nested wave-functions with the hexagons the formula for the corresponding structure constant receives a minimal modification with respect to the $\mathfrak{sl}(2)$ case:

$$\mathcal{C}_{123}(\mathbf{u}, \mathbf{v}, \mathbf{w}) \sim \langle \psi_{\mathbf{v}} | \psi_{\mathbf{w}} \rangle \times \sum_{\alpha \cup \bar{\alpha} = \mathbf{u}} w_{\alpha, \bar{\alpha}; \mathbf{v}; l_{12}} \mathcal{H}_{\alpha} \times \mathcal{H}_{\bar{\alpha}} \quad (2.5)$$

We obtain an extra phase in the weight factor due to the scattering of middle node roots \mathbf{u} and wing \mathbf{v} . And more importantly, we obtain a pre-factor given by the scalar product of the nested left and right wave-functions which vanishes for $\mathbf{v} \neq \mathbf{w}$. This constitutes a novel selection rule much stronger than the ones set by global symmetry. In [Section 2.4.3](#) we comment on the symmetry responsible for it.

In [Appendix B](#) we provide a tree level derivation of (2.5) for the $\mathfrak{so}(6)$ sector. This derivation is independent of the hexagon formalism and required developing a novel construction through Algebraic Bethe Ansatz for the one-loop conformal operators in this sector. In [Appendix C](#) we provide a construction through coordinate Bethe Ansatz of the one-loop conformal operators in the $\mathfrak{psu}(1,1|2)$ sector which we also used to test the validity of (2.5) at tree level.

2.3 The BKV Hexagon program

The hexagon program regards the structure constant, pair of pants, as a finite volume correlator of two hexagon operators $\langle \mathcal{H} \mathcal{H} \rangle_{2D}$ that live in a two-dimensional integrable theory worldsheet. As such it admits a decomposition into form factors achieved by the insertion of complete sets of states ψ , forming a resolution of the identity $1 = \sum_{\psi} |\psi\rangle\langle\psi|$, in between the two hexagons. In the tailoring language these are the states living in the mirror edges that result from the cutting. Since we perform three cuts to isolate the hexagons we obtain three of theses complicated sums over complete sets of mirror states $\psi_{12}, \psi_{23}, \psi_{31}$. Fortunately their contribution is damped by the factor $e^{-E_{\psi_{ij}} l_{ij}}$ that depends on their energy and the “distances” between the hexagons given by the bridge lengths l_{ij} . Therefore in the asymptotic limit $l_{ij} \gg 1$ we can safely consider only the contribution of the mirror vacuum state with zero energy. In the weak coupling approximation $e^{-E_{\psi_{ij}} l_{ij}} \sim (g^2)^{l_{ij}}$ this asymptotic regime includes all loop orders below the minimum of the three bridge lengths l_{ij} .

In this asymptotic limit the non-trivial contribution comes entirely from the states that live at the closed boundaries of the pair of pants. These 2D-states are trivial when corresponding to protected operators, just the BMN vacuum of the 2D-space, or very non-trivial when representing non-protected operators of the 4D-space. These are the Bethe states which contain magnons with momenta quantized by the Bethe equations (1.13) that impose the periodicity of their wave-function.

Upon cutting these magnons can end in any of the two hexagons and we must sum over all the ways of distributing them with an appropriate weight factor, see [Figure 2.3](#). After

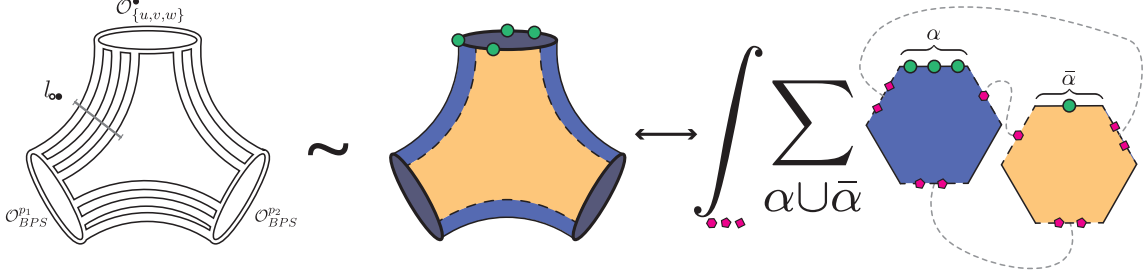


Figure 2.2: Pictorial representation of the BKV hexagon conjecture. We cut the “pair of pants” into two hexagons and sum over all the partitions of physical excitations while integrating over virtual particles to glue back the mirror edges. In the asymptotic limit, this latter contribution can be neglected.

this decompactification the important dynamical piece is encoded in the infinite volume hexagon form factors introduced in the following section.

2.3.1 The Hexagon Form factor

The hexagon operator can be described by its form factors. The most generic form factor has arbitrary states of physical or mirror magnons at the six boundaries:

$$\langle \mathcal{H} | 1 \rangle_{phys} \otimes | 2 \rangle_{mirror} \otimes | 3 \rangle_{phys} \otimes | 4 \rangle_{mirror} \otimes | 5 \rangle_{phys} \otimes | 6 \rangle_{mirror} \quad (2.6)$$

In the asymptotic limit we just need to consider the vacuum at the mirror edges. Besides since we only consider one non-protected operator, we only need to study the form factor with magnons at a single physical edge. Nevertheless starting from this form factor we can obtain all the other form factors by using the mirror transformations (double-Wick rotations) that map a magnon from one (physical or mirror) edge to the next (mirror or physical) edge.

The form factor we are interested in quantifies the absorption or annihilation of a state at a single physical edge of the hexagon:

$$\mathcal{H}_{A_1 \dot{A}_1, \dots, A_n, \dot{A}_n}(\mathbf{u}) \equiv \langle \mathcal{H} | \mathcal{X}_{A_1 \dot{A}_1}(u_1) \cdots \mathcal{X}_{A_n \dot{A}_n}(u_n) \rangle \quad (2.7)$$

where the Ket is an infinite-length Bethe state of magnons given by a (complicated) linear combination of plane-waves with polarizations or flavours $\mathcal{X}_{A\dot{A}}$ and momenta $p(u_i)$ representing magnons that move on top of a sea of scalars Z i.e. a BMN vacuum of infinite length. As an asymptotic state the rapidities need not to satisfy any quantization conditions. However, later we will assume these magnons come from a closed chain of large length L and impose the periodicity condition given by Bethe equations. For now we can consider the rapidities to be off-shell.

The flavour indexes undotted A and dotted \dot{A} lie in the fundamental representations of the left and right copies of the symmetry group $\mathfrak{psu}_L(2|2) \otimes \mathfrak{psu}_R(2|2)$, the residual supersymmetry preserved by the BMN vacuum. More explicitly we have the factorization:

$$\mathcal{X}_{A\dot{A}} \equiv \mathcal{X}_A \otimes \mathcal{X}_{\dot{A}} \quad (2.8)$$

This undotted (dotted) index can take on four values, two bosonic and two fermionic, $\mathcal{X}_A \in \{\phi_1, \phi_2, \psi_1, \psi_2\}$. This gives a total of 16 different flavours for the one-magnon state in this bi-fundamental representation. For a specific choice of indexes we obtain, for instance, the $\mathfrak{sl}(2)$ states with magnons charged as light-cone derivatives:

$$D_+ \equiv D_{1\dot{2}} \equiv \psi_1 \otimes \psi_{\dot{2}} \quad (2.9)$$

Under residual symmetry $\mathfrak{psu}(2|2)^2$:

$$|D_{1\dot{2}}(u_1) \cdots D_{1\dot{2}}(u_n)\rangle$$

In the $\mathfrak{psu}(2, 2|4)$ chain:

$$\sim \text{Tr}(D_+^n Z \cdots Z) \quad (2.10)$$

On the right-hand side we only show the field content of the corresponding state in the $\mathcal{N} = 4$ chain with the covariant derivative D_+ in a light-cone direction. The actual state is a linear combination of traces with the derivatives on different sites of the chain, for a explicit form see for instance [Non-compact] for the two-loop state or for the one-loop state see appendix B (specialized to the $\mathfrak{sl}(2)$ sector by removing the wings). However the explicit state will not be needed since we can have access to the form factor (2.7) at all-loops by other means, as we explain below.

The hexagon form factor (2.7) is in general a complicated tensor whose number of terms grows exponentially with the number of magnons. Nevertheless this object can be bootstrapped at all-loops thanks to the symmetry of the hexagon and the conditions imposed by integrability on form factors. Here we briefly describe three of the important conditions that constrain the hexagon form factor and conclude presenting a solution for them. For more details on this bootstrap and its solution we refer the reader to [BKV] and the pedagogical set of lectures in [3pointLectures].

1. Watson equation

The action of the S -matrix in an integrable theory simply reshuffles the momenta of the particles:

$$\begin{aligned} \hat{S}_{12} |\mathcal{X}_{A_1 \dot{A}_1}(u_1) \mathcal{X}_{A_2 \dot{A}_2}(u_2) \mathcal{X}_{A_3, \dot{A}_3}(u_3) \cdots \rangle = \\ \mathbb{S}(u_1, u_2)_{A_1 \dot{A}_1, A_2 \dot{A}_2}^{B_1 \dot{B}_1, B_2 \dot{B}_2} |\mathcal{X}_{B_2 \dot{B}_2}(u_2) \mathcal{X}_{B_1 \dot{B}_1}(u_1) \mathcal{X}_{A_3, \dot{A}_3}(u_3) \cdots \rangle \end{aligned} \quad (2.11)$$

where we assume summation over repeated flavour indexes. This is a manifestation of the lack of particle production and the conservation of the individual momentum of the magnons due to the higher conserved charges that furnish the integrability symmetry.

The Watson equation states that the action of the S-matrix on the state before computing the form factor does not change the value of this latter. In other words, we can swap the ordering of the rapidities in the form factor at the cost of multiplying by the S-matrix. For the hexagon form factor this simply says:

$$\mathcal{H}_{A_1\dot{A}_1,A_2\dot{A}_2,\dots}(u_1, u_2, \dots) = \mathbb{S}(u_1, u_2)_{A_1\dot{A}_1,A_2\dot{A}_2}^{B_1\dot{B}_1,B_2\dot{B}_2} \mathcal{H}_{B_2\dot{B}_2,B_1\dot{B}_1,\dots}(u_2, u_1, \dots) \quad (2.12)$$

The two-body S-matrix $\hat{\mathbb{S}}$ is composed of an overall abelian phase and a factorized tensor structure with one copy for undotted and another identical copy for dotted indexes:

$$\hat{\mathbb{S}}(u_1, u_2) = S(u_1, u_2) \hat{\mathcal{S}}(u_1, u_2) \otimes \hat{\mathcal{S}}(u_1, u_2) \quad (2.13)$$

where $S(u_1, u_2)$ is the all-loop abelian phase that appears in the $\mathfrak{sl}(2)$ Bethe equations in (1.13) and $\hat{\mathcal{S}}$ is proportional to the $\mathfrak{su}(2|2)$ Beisert S-matrix⁵. Both satisfy the unitary relation:

$$S(u, v)S(v, u) = 1 \quad \text{and} \quad \hat{\mathcal{S}}(u_1, u_2)\hat{\mathcal{S}}(u_2, u_1) = \hat{1} \quad (2.14)$$

The latter also satisfies the Yang-Baxter relation:

$$\hat{\mathcal{S}}(u_2, u_3)\hat{\mathcal{S}}(u_1, u_3)\hat{\mathcal{S}}(u_1, u_2) = \hat{\mathcal{S}}(u_1, u_2)\hat{\mathcal{S}}(u_1, u_3)\hat{\mathcal{S}}(u_2, u_3) \quad (2.15)$$

which directly implies $\hat{\mathbb{S}}$ satisfies it as well. This equation establishes that all orderings of scattering are equivalent in an integrable theory with pairwise factorized scattering.

Our normalization for $\hat{\mathcal{S}}$ is such that for a $\mathfrak{sl}(2)$ state only the abelian phase enters. So for a two-particle state we have:

$$\mathcal{H}_{D_{1\dot{2}}D_{1\dot{2}}}(u_1, u_2) = S(u_1, u_2) \mathcal{H}_{D_{1\dot{2}}D_{1\dot{2}}}(u_1, u_2) \quad (2.16)$$

As mentioned in the introduction of this chapter this relation was observed at leading order and now we demand it holds at all loops in its most generic form (2.12).

2. Kinematical pole

This axiom associates the presence of a simple pole to the decoupling of a pair of identical particles at opposite (physical or mirror) edges which are taken away from the core of the hexagon. By using a crossing transformation we can rephrase this as the decoupling of a pair of particle and anti-particle at the same edge.

This axiom also establishes the residue at the pole is given simply by the hexagon form factor of the remaining particles, providing us with a recursion relation:

$$\frac{1}{i} \text{Res}_{u=v} \langle \mathcal{H} | \underbrace{\mathcal{X}(u^{2\gamma})\mathcal{X}(v)}_{\text{singlet}} \mathcal{X}(w) \dots \rangle = \langle \mathcal{H} | \mathcal{X}(w) \dots \rangle \quad (2.17)$$

The right hand side is set to one in case there are not extra particles.

⁵We follow the conventions of appendix A in [8]

For a generic operator the right hand side of (2.17) has an extra term. This is better understood in the picture of the identical pair decoupling which in a typical space-time patch with four edges, two physical and two mirror, it can happen along the left side or it can happen on the right side, including a product of S-matrices in this latter case due to the scattering with the other particles. For the hexagon however when moving the bottom particle to the right the identical pair does not face each other and can not decouple. The hexagon is an instance of a twist-like operator that creates an excess angle in the space-time patch. The decoupling axiom for this class of operators has been postulated in [37], where they appear in computations of entanglement entropy (replica trick) in a quantum integrable model.

3. Residual diagonal symmetry

The hexagon respects a diagonal symmetry $\mathfrak{psu}_D(2|2)$ of the two copies $\mathfrak{psu}(2|2)_L \times \mathfrak{psu}_R(2|2)$. This corresponds to the residual symmetry preserved by 3 (rotated) BMN vacua at three different spacetime positions (e.g. at 0, 1 and ∞). It imposes the annihilation of the hexagon by the generators of the group in the presence of an arbitrary state:

$$\langle \mathcal{H} | \hat{\mathcal{J}} | \dots \rangle = 0 \quad (2.18)$$

where $\hat{\mathcal{J}}$ represents a generator of $\mathfrak{psu}(2|2)_D$. For their explicit form as linear combinations of the left and right generators see [5].

This implies the hexagon form factors must be $\mathfrak{psu}(2|2)_D$ invariant tensors. For the one-magnon state this condition is enough to set:

$$\mathcal{H}_{A\dot{A}} \equiv \langle \mathcal{H} | \mathcal{X}_{A\dot{A}} \rangle = \begin{cases} \langle \mathcal{H} | \psi_\alpha \psi_{\dot{\beta}} \rangle = \sqrt{\mu(u)} \epsilon_{\alpha\dot{\beta}} \\ \langle \mathcal{H} | \phi_a \psi_{\dot{\beta}} \rangle = \langle \mathcal{H} | \psi_\alpha \phi_{\dot{b}} \rangle = 0 \\ \langle \mathcal{H} | \phi_a \phi_{\dot{b}} \rangle = i\sqrt{\mu(u)} \epsilon_{a\dot{b}} \end{cases} \quad (2.19)$$

where $\phi_{a=1,2}$ and $\psi_{\alpha=1,2}$ form the quartet of A indexes. Being the antisymmetric tensors $\epsilon_{\alpha\dot{\beta}}$ and $\epsilon_{a\dot{b}}$ the only $\mathfrak{psu}_D(2|2)$ invariants that can be constructed with a pair of $A\dot{A}$ indexes. The prefactor $\sqrt{\mu(u)}$ is not fixed by the symmetry and should be interpreted as the cost of creating or absorbing a particle by the hexagon. We will be later referring about it as the measure.

Likewise, this diagonal symmetry and Watson equation fix the two-magnon form factor up to an overall factor “ h ”:

$$\mathcal{H}_{A_1\dot{A}_1, A_2\dot{A}_2}(u_1, u_2) = h(u_1, u_2) (-1)^f \mathcal{S}(u_1, u_2)_{A_1\dot{A}_2}^{B_1B_2} \mathcal{H}_{B_1\dot{A}_1} \mathcal{H}_{B_2\dot{A}_2} \quad (2.20)$$

where $\mathcal{H}_{A\dot{A}}$ are the one-magnon form factors defined with anti-symmetric tensors in (2.19). The grading $(-1)^f$ gets a (-1) when an undotted and dotted fermion index get swap in the reordering: $A_1\dot{A}_1 A_2\dot{A}_2 \rightarrow A_1 A_2 \dot{A}_1 \dot{A}_2$.

This symmetry does not fix the multi-magnon form factor but still constitutes a strong constraint.

The solution

A solution to all these constraints was provided in [5]. They conjecture the multi-magnon hexagon form factor is composed of a dynamical part and a matrix part as:

$$\langle \mathcal{H} | \mathcal{X}_{A_1 \dot{A}_1}(u_1) \dots \mathcal{X}_{A_n \dot{A}_n}(u_n) \rangle = \prod_{i < j} h(u_i, u_j) \times \mathcal{M}_{A_1 \dot{A}_1, \dots, A_n \dot{A}_n}, \quad (2.21)$$

The dynamical part is given by a pairwise product of the two-magnon abelian function:

$$h(u, v) = \frac{x^-(u) - x^-(v)}{x^-(u) - x^+(v)} \frac{1 - \frac{1}{x^-(u)x^+(v)}}{1 - \frac{1}{x^+(u)x^+(v)}} \frac{1}{\sigma(u, v)} \xrightarrow{g \rightarrow 0} \frac{u - v}{u - v - i} + O(g^2) \quad (2.22)$$

given in terms of the Zhukovsky variable in (1.11) and the dressing phase [36]. This can be checked to satisfy the Watson equation $\frac{h(u, v)}{h(v, u)} = S(u, v)$.

The matrix part is given in terms of a scattering matrix with $\mathfrak{psu}(2|2)_D$ symmetry:

$$\mathcal{M}(u_1, u_2, \dots)_{A_1 \dot{A}_1, A_2 \dot{A}_2, \dots} = (-1)^f \mathcal{S}(u_1, u_2, u_3, \dots)_{A_1 \dot{A}_2, \dots}^{B_1 B_2, \dots} \mathcal{H}_{B_1 \dot{A}_1} \mathcal{H}_{B_2 \dot{A}_2} \dots \quad (2.23)$$

where $\mathcal{H}_{A \dot{A}}$ is the one-particle form factor defined as in (2.19) with measure:

$$\mu(u) = \frac{\left(1 - \frac{1}{x^+ x^-}\right)^2}{\left(1 - \frac{1}{(x^+)^2}\right) \left(1 - \frac{1}{(x^-)^2}\right)} \quad (2.24)$$

and the overall sign $(-1)^f$ is determined by the product all the (-1) we pick each time we swap two fermionic indexes when reordering: $(A_1 \dot{A}_1) \dots (A_n \dot{A}_n) \rightarrow (A_1 \dots A_n)(\dot{A}_1 \dots \dot{A}_n)$.

The multi-magnon scattering matrix reverses the ordering of the magnons as:

$$\hat{\mathcal{S}}(u_1, u_2, \dots, u_n) : \{u_1, u_2, \dots, u_n\} \rightarrow \{u_n, \dots, u_2, u_1\} \quad (2.25)$$

and it is explicitly given by a factorized product of the Beisert two-magnon S-matrix as depicted.

$$\hat{\mathcal{S}}(u_1, u_2, \dots) = \prod_{i < j} \hat{\mathcal{S}}(u_i, u_j) \quad (2.26)$$

When all magnons have the same flavour, as in the rank one sectors $\mathfrak{sl}(2)$ and $\mathfrak{su}(2)$, the scattering matrix (2.26) is just a scalar phase and the hexagon form factor only has a dynamical part. For instance, in the $\mathfrak{sl}(2)$ sector we have⁶:

$$\mathcal{H}_{\mathbf{u}} \equiv \langle \mathcal{H} | D_{1\dot{2}}(u_1) \dots D_{1\dot{2}}(u_n) \rangle = \prod_{i < j} h(u_i, u_j) \times \prod_{i=1}^n \sqrt{\mu(u_i)} \quad (2.27)$$

Similarly in the $\mathfrak{su}(2)$ sector spanned by the scalars $Y_{1\dot{2}}$ the corresponding form factor is obtained by replacing:

$$h(u, v) \rightarrow h_{\mathfrak{su}(2)}(u, v) = h(u, v) \text{ complete} \quad (2.28)$$

In the following section we use the form factor (2.27) to build the structure constant in the $\mathfrak{sl}(2)$ sector. In Section 2.4.1 we address the case when the magnons have different polarizations.

⁶The sign $(-1)^f$ cancels with a sign we obtain from the scattering matrix in (2.26).

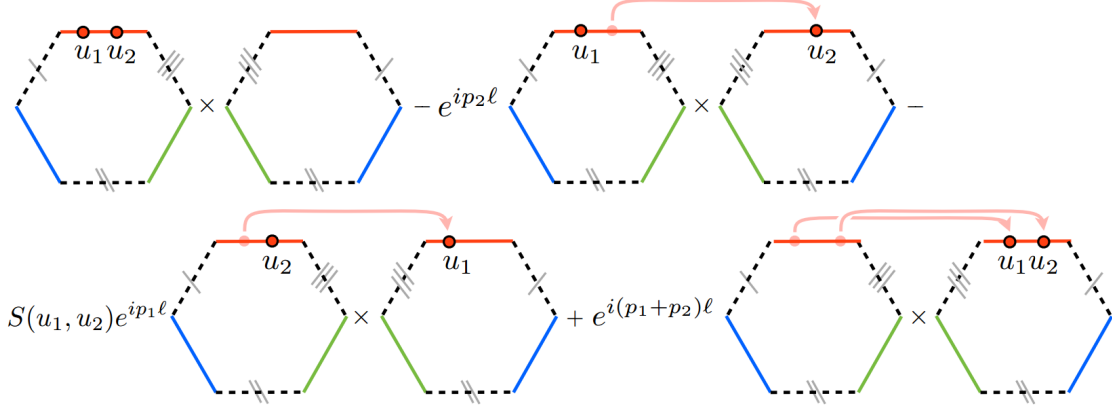


Figure 2.3: Figure slightly adapted from [5]. Visualization of the factor $\omega(\alpha, \bar{\alpha})$ for two excitations (u_i, u_j) .

2.3.2 The BKV conjecture for the $\mathfrak{sl}(2)$ structure constant

Now we consider the tailoring of a pair of pants with one of its boundaries containing a Bethe state $|\mathbf{u}\rangle$ representing a non-protected operator in the $\mathfrak{sl}(2)$ sector:

$$|\mathbf{u}\rangle \equiv |D_{1\dot{2}}(u_1) \cdots D_{1\dot{2}}(u_n)\rangle_L \quad (2.29)$$

Where the subscript indicates that before cutting this state lives on a closed chain of size L and must have a periodic wave-function. This condition imposes that the set of rapidities \mathbf{u} must furnish a solution of the $\mathfrak{sl}(2)$ Bethe equations described in 1.3.1.

When performing the cutting of the pair of pants, the BKV prescription instructs us to distribute the set of magnons \mathbf{u} between the two hexagons in all possible ways and add up the contribution of each bi-partition to obtain the structure constant⁷:

$$C_{\mathbf{u}}^{\bullet\circ\circ} \sim \sum_{\alpha \cup \bar{\alpha} = \mathbf{u}} w_{\alpha, \bar{\alpha}, l} \mathcal{H}_{\alpha} \times \mathcal{H}_{\bar{\alpha}} \quad (2.30)$$

where \mathcal{H}_{α} and $\mathcal{H}_{\bar{\alpha}}$ are the $\mathfrak{sl}(2)$ hexagon form factors defined in (2.27).

The partition dependent weight factor contains three components:

$$w_{\alpha, \bar{\alpha}} = (-1)^{|\bar{\alpha}|} \prod_{u_j \in \bar{\alpha}} e^{ip(u_j)l} \prod_{\substack{i < j \\ u_i \in \bar{\alpha}, u_j \in \alpha}} S(u_i, u_j) \quad (2.31)$$

described as:

⁷This will turn into an equal sign once we properly normalize the right-hand side, see equation (2.34).

- The product of S-matrices due to the reordering of the magnons within the $\mathfrak{sl}(2)$ Bethe state before cutting:

$$\hat{\mathbb{S}}_{\mathbf{u} \rightarrow \alpha \bar{\alpha}} |\mathbf{u}\rangle = \left(\prod_{\substack{i < j \\ u_i \in \bar{\alpha}, u_j \in \alpha}} S(u_i, u_j) \right) |\alpha\rangle \otimes |\bar{\alpha}\rangle \quad (2.32)$$

The action of $\hat{\mathbb{S}}$ is diagonal since all magnons have the same polarization. The resulting partitions $|\alpha\rangle$ and $|\bar{\alpha}\rangle$ are also Bethe states that when evaluated on the hexagons give the form factors \mathcal{H}_α and $\mathcal{H}_{\bar{\alpha}}$.

- A phase $e^{ip(u)l}$ due to the propagation of the magnons in the $\bar{\alpha}$ -partition over the distance l to cross from the first to second hexagon. The momentum is given by

$$e^{ip(u)} = \frac{x^+(u)}{x^-(u)} \quad (2.33)$$

and the bridge length l is set by the number of tree-level Wick contractions between the non-protected operator and the protected operator to its right⁸.

- The sign $(-1)^{|\bar{\alpha}|}$ should have a geometrical origin related to the change of frame from the first to second hexagon. However a clear explanation for it is still unknown. Although an ad-hoc sign thus far its correctness has passed several tests⁹.

Finally the conjecture for the normalized $\mathfrak{sl}(2)$ structure constant can be compactly written as:

$$\left(\frac{C_{123}^{\bullet\circ\circ}}{C_{123}^{\circ\circ\circ}} \right)^2 = \frac{\prod_{k=1}^K \mu(u_k)}{\langle \mathbf{u} | \mathbf{u} \rangle \prod_{i < j} S(u_i, u_j)} \mathcal{A}^2. \quad (2.34)$$

On the left-hand side we divide the structure constant by a structure constant of three BPS operators with the same length to get rid of combinatorial factors. On the right-hand side we have the measure (2.24), the sum over partitions rewritten as:

$$\mathcal{A} = \prod_{i < j} h(u_i, u_j) \sum_{\alpha \cup \bar{\alpha} = \mathbf{u}} (-1)^{|\bar{\alpha}|} \prod_{j \in \bar{\alpha}} e^{ip(u_j)l} \prod_{i \in \alpha, j \in \bar{\alpha}} \frac{1}{h(u_i, u_j)}. \quad (2.35)$$

and in the denominator the norm of the Bethe state in finite volume. This is given by a product of the abelian phase of the S -matrix and the Gaudin-norm defined as the following determinant:

$$\langle \mathbf{u} | \mathbf{u} \rangle = \det \partial_{u_i} \phi_j \quad (2.36)$$

⁸On the support of the Bethe equations it can be shown that the two possible choices of bridges to cross l and $L - l$ are equivalent.

⁹At tree level its origin can be traced to the exchange algebra of the creation and annihilation operators of the Algebraic Bethe Ansatz. These are used in the computation of the spin chain scalar product that accounts for the Wick contractions in the tree level computation.

where ϕ_j represents that logarithm of product of phases that appear in the Bethe equations (1.13):

$$e^{i\phi_j} = e^{ip(u_j)L} \prod_{\substack{k=1 \\ k \neq j}}^K S(u_j, u_k) \quad (2.37)$$

2.4 Structure constants in the full $\mathfrak{psu}(2, 2|4)$ sector

In this section we find a compact formula for the structure constant of two protected operators with any non-protected operator in the full $\mathfrak{psu}(2, 2|4)$ sector. As discussed in Chapter 1 the Bethe Ansatz description of these latter operators includes Bethe roots at the wings \mathbf{v} and \mathbf{w} . We encounter that the corresponding structure constant vanishes unless the wings are identical $\mathbf{v} = \mathbf{w}$. In the last section we comment on the underlying Yangian symmetry responsible for this selection rule.

In what follows we start by introducing the so-called nested Bethe wave-function necessary to guarantee the periodicity of the Bethe state when confined to a chain of length L . This completes the description of the single-trace conformal operators, eigenstates of the dilatation generator, in higher-rank sectors (non-trivial wings). Then we cut the Bethe state and contract the nested wave-function with the hexagon form factors (2.21) to obtain our main formula (2.56).

2.4.1 Nested Bethe Wave Function

To describe single-trace operators in higher rank sectors we should consider Bethe states with magnons with generic $\mathfrak{psu}(2|2)^2$ polarization in a closed chain of (large) length L :

$$|\mathcal{X}_{A_1 \dot{A}_1}(u_1) \cdots \mathcal{X}_{A_n \dot{A}_n}(u_n)\rangle_L \quad (2.38)$$

However, unlike the $\mathfrak{sl}(2)$ states in (2.29), the states (2.38) with generic flavour indexes do not diagonalize the action of the scattering matrix (see equation (2.11)). This raises two issues in the application of the hexagon program.

The first is a technical issue and concerns the proliferation of flavour indexes we need to sum over when cutting the Bethe state and distributing the magnons between the two hexagons, see Figure 2.4.2. This involves the use of the S-matrix and becomes increasingly complicated as the number of magnons grows. To this we should also add the complicated structure of the matrix part of the hexagon form factors for multi-magnon states which also depends on the S-matrix.

The second issue is more physical and concerns the periodicity of the Bethe state before cutting. To impose this condition we typically carry a magnon around the chain and demand that the acquiring phase equates to unity. However if the scattering is non-diagonal, instead of a simple phase we obtain a complicated tensor given by the product

of $\mathfrak{su}(2|2)^2$ S-matrices:

$$\prod_{j=2}^n \hat{S}_{1j} = \left(\prod_{j=2}^n S(u_1, u_j) \right) \hat{T} \otimes \hat{T} \quad (2.39)$$

Up to an overall phase, this product naturally factorizes into a left (undotted) and right (dotted) copies of the $\mathfrak{su}(2|2)$ transfer matrix:

$$\hat{T} = \prod_{j=1}^n \hat{S}_{1j} \quad (2.40)$$

So it is clear that to address these issues we must find the linear combination of states (2.38) that diagonalize the action of the S-matrix and more specifically diagonalizes both copies of the transfer matrix (2.40). The solution is given by the nested Bethe Ansatz (NBA) worked out in [84, 85] for $\mathfrak{su}(2|2)$.

To construct the NBA we first pick as a reference state a chain of derivatives $D_{1\dot{2}} = \psi_1 \otimes \psi_2$. On top of this state we create nested left and right magnons with momentum v and w introducing waves with new flavours ϕ_2 and $\phi_{\dot{1}}$ respectively. For instance a nested one-magnon state with left flavour ϕ_2 corresponds to the linear combination:

$$|\Psi_{\mathbf{u}}^{v,\emptyset}\rangle = \sum_{n=1}^K \left(\prod_{i=1}^n f(w, u_i) \right) |D_{1\dot{2}} \cdots \underbrace{\Psi_{2\dot{2}}^{\downarrow}}_{\phi_2 \otimes \psi_2} \cdots D_{1\dot{2}}\rangle \quad (2.41)$$

where the phase $f(v, u)$ stands for the scattering of v with the “inhomogeneties” $\mathbf{u} = \{u_1, \dots, u_K\}$ of the nested spin chain and the symbol \emptyset simply denotes the right wing is turned off. When this latter is turned on it can be simply superposed with the left wave-function thanks to the factorization of left and right indexes. For the construction of nested multi-magnon states see [85].

These states of the first nested level serve to simplify the diagonalization of the transfer matrix $T_{\mathfrak{su}(2|2)}$ to a simpler transfer matrix with smaller residual symmetry $T_{\mathfrak{su}(2|1)}$. To further this simplify new object we need to add more nested levels until there is not residual transfer matrix to diagonalize. We denote the complete set of auxiliary roots as $\mathbf{w} = \{\mathbf{w}^{(1)}, \mathbf{w}^{(2)}, \mathbf{w}^{(3)}\}$ for the left wing and $\mathbf{v} = \{\mathbf{v}^{(1)}, \mathbf{v}^{(2)}, \mathbf{v}^{(3)}\}$ for the right wing. Furthermore at each level of the nesting the rapidities must satisfy the nested Bethe equations, see Appendix A, to guarantee the diagonalization of the transfer matrix of the corresponding level.

The generic form of the left and right wave-functions is:

$$\begin{aligned} |\Psi_{\mathbf{u}}^{\mathbf{v}}\rangle &= \sum_{\chi_n = \phi_{1,2}, \psi_{1,2}} \psi_{\chi_1 \cdots \chi_K}(\mathbf{v}|\mathbf{u}) |\chi_1(u_1) \chi_2(u_2) \cdots \chi_K(u_K)\rangle, \\ |\Psi_{\mathbf{u}}^{\mathbf{w}}\rangle &= \sum_{\dot{\chi}_n = \phi_{1,\dot{2}}, \psi_{1,\dot{2}}} \psi_{\dot{\chi}_1 \cdots \dot{\chi}_K}(\mathbf{w}|\mathbf{u}) |\dot{\chi}_1(u_1) \dot{\chi}_2(u_2) \cdots \dot{\chi}_K(u_K)\rangle, \end{aligned} \quad (2.42)$$

with the complete wave-function given by the tensor product:

$$|\Psi_{\mathbf{u}}^{\mathbf{v}, \mathbf{w}}\rangle = |\Psi_{\mathbf{u}}^{\mathbf{v}}\rangle \otimes |\Psi_{\mathbf{u}}^{\mathbf{w}}\rangle \quad (2.43)$$

This wave-function has two important properties that abelianized the periodicity condition. It diagonalizes the action of the S-matrix as

$$\mathbb{S}_{i, i+1} |\Psi_{u_1, \dots, u_K}^{\mathbf{v}, \mathbf{w}}\rangle = S(u_i, u_{i+1}) |\Psi_{u_1, \dots, \textcolor{red}{u}_{i+1}, u_i, \dots, u_K}^{\mathbf{v}, \mathbf{w}}\rangle, \quad (2.44)$$

with $S(u, v)$ being an abelian phase. Furthermore when \mathbf{w} (\mathbf{v}) satisfy the Bethe equation for higher levels, the right(left) wave function has an additional “nested periodicity” property,

$$|\Psi_{u_{k+1}, \dots, u_K, \textcolor{red}{u}_1, \dots, u_k}^{\mathbf{w}}\rangle = \left(\prod_{i=1}^k f(u_i, \mathbf{w}) \right) |\Psi_{u_1, \dots, u_K}^{\mathbf{w}}\rangle, \quad (2.45)$$

where f is phase later defined.

With these two properties, one can rewrite the right hand side of the periodicity condition of the full wave function,

$$|\Psi_{u_1, \dots, u_K}^{\mathbf{v}, \mathbf{w}}\rangle = e^{ip_1 L} \left(\prod_{i=2}^K \mathbb{S}_{1, i} \right) |\Psi_{u_1, \dots, u_K}^{\mathbf{v}, \mathbf{w}}\rangle, \quad (2.46)$$

in the following way:

$$\begin{aligned} e^{ip_1 L} \left(\prod_{i=2}^K \mathbb{S}_{1, i} \right) |\Psi_{u_1, \dots, u_K}^{\mathbf{v}, \mathbf{w}}\rangle &= e^{ip_1 L} \left(\prod_{i=2}^K S(u_1, u_i) \right) |\Psi_{u_2, \dots, u_K, \textcolor{red}{u}_1}^{\mathbf{v}, \mathbf{w}}\rangle \\ &= e^{ip_1 L} f(u_1, \mathbf{v}) f(u_1, \mathbf{w}) \left(\prod_{i=2}^K S(u_1, u_i) \right) |\Psi_{u_1, \dots, u_K}^{\mathbf{w}}\rangle. \end{aligned} \quad (2.47)$$

This leads to the Bethe equation for the middle node roots:

$$e^{ip_1 L} \left(\prod_{i=2}^K S(u_1, u_i) \right) f(u_1, \mathbf{v}) f(u_1, \mathbf{w}) = 1. \quad (2.48)$$

given explicitly in (A.4) from which the phase f can be read off.

2.4.2 Nested Hexagon

After identifying the nested structured of the finite-length Bethe states in higher rank sectors of $\mathfrak{psu}(2, 2|4)$ we now use the hexagon program to compute the corresponding structure constant $C^{\bullet\bullet\bullet}(\mathbf{u}, \mathbf{v}, \mathbf{w})$. Seemingly the computation is now much more complicated since

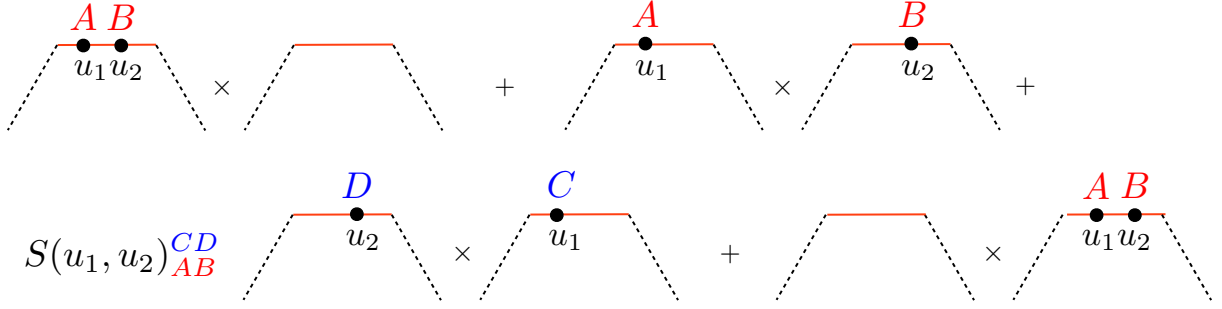


Figure 2.4: Splitting a two-particle state with indices. When the first particle passes through the second particle, it gets multiplied by a S-matrix $S(u_1, u_2)$. The resulting state is a complicated object which includes a summation over indices (C and D in the figure).

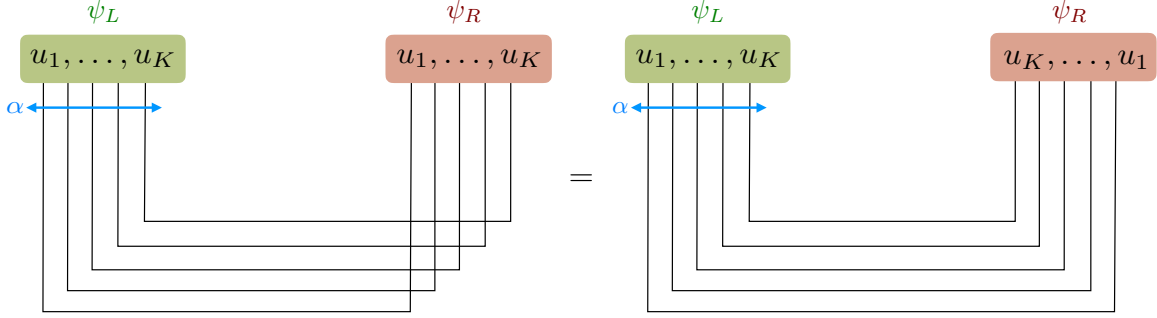


Figure 2.5: Matrix part for $\bar{\alpha} = \emptyset$: One can simply act the S-matrix to the right wave function ψ_R and simplify the structure. Note we are using the normalization of the matrix part, in which the abelian part ($\mathfrak{sl}(2)$ S-matrix) is unity.

the contraction with the nested wave function¹⁰ “couples” the contribution from the two hexagons. However thanks to the aforementioned properties of the wave-function the complicated structure of indexes can be simplified to arrive to a compact expression.

To apply the hexagon formalism, we first reorder the magnons (or equivalently the momentum-carrying roots) and split them into two subsets α and $\bar{\alpha}$. Thanks to the property of the nested Bethe wave function, the state we get after reordering is as simple as

¹⁰Note that the “wave functions” that we discuss in this section are all about the wave functions for the indices; in the nested Bethe ansatz language they are the wave functions at the nested level. This is in contrast to the perturbative computation at weak coupling in which one also needs to talk about the wave function of magnons themselves (in other words, the wave function for the middle node). The structure of the wave function of magnons themselves is already taken into account by the hexagon form factors, and we simply need to figure out how to efficiently deal with the index structure. This is the main theme of this section.

the original one:

$$|\Psi_{\mathbf{u}}\rangle = \left(\prod_{\substack{i < j \\ u_i \in \bar{\alpha}, u_j \in \alpha}} S(u_i, u_j) \right) |\Psi_{\alpha\bar{\alpha}}\rangle. \quad (2.49)$$

Here $S(u, v)$ is the S-matrix in the $\mathfrak{sl}(2)$ sector.

The next step is to contract the nested wave function with the hexagon form factor. When $\bar{\alpha}$ is empty, this can be done easily since the hexagon is essentially given by a product of S-matrices which are already diagonalized by the wave function. As a result, we obtain

$$\mathcal{H}_{\alpha=\mathbf{u}, \bar{\alpha}=\emptyset} = \left(\prod_{i < j} h(u_i, u_j) \right) \langle \overset{\leftarrow}{\Psi}_{\bar{\mathbf{u}}} | \Psi_{\mathbf{u}} \rangle \quad (2.50)$$

where $\langle \overset{\leftarrow}{\Psi}_{\bar{\mathbf{u}}} | \Psi_{\mathbf{u}} \rangle$ represents a contraction of right $\dot{\Psi}$ and left Ψ wings defined pictorially in figure 2.5. More precisely, for the following two states in the $\mathfrak{psu}(2|2)$ spin chain with the opposite orderings of the inhomogeneities,

$$\begin{aligned} |\Psi_{\mathbf{u}}\rangle &= \sum_{\chi_n = \phi_{1,2}, \psi_{1,2}} \psi_{\chi_1 \dots \chi_K} |\chi_1(u_1) \chi_2(u_2) \dots \chi_K(u_K)\rangle, \\ |\dot{\Psi}_{\bar{\mathbf{u}}}\rangle &= \sum_{\dot{\chi}_n = \dot{\phi}_{1,2}, \dot{\psi}_{1,2}} \psi_{\dot{\chi}_1 \dots \dot{\chi}_K} |\dot{\chi}_1(u_K) \dot{\chi}_2(u_{K-1}) \dots \dot{\chi}_K(u_1)\rangle, \end{aligned} \quad (2.51)$$

the overlap is defined by

$$\langle \overset{\leftarrow}{\Psi}_{\bar{\mathbf{u}}} | \Psi_{\mathbf{u}} \rangle \equiv \sum_{\substack{\chi_n = \phi_{1,2}, \psi_{1,2} \\ \dot{\chi}_n = \dot{\phi}_{1,2}, \dot{\psi}_{1,2}}} \psi_{\chi_1 \dots \chi_K} \psi_{\dot{\chi}_1 \dots \dot{\chi}_K} \prod_{n=1}^K \mathcal{H}_{\chi_n \dot{\chi}_{K+1-n}}, \quad (2.52)$$

with $\mathcal{H}_{\chi\dot{\chi}}$ being the one-particle hexagon form factor defined in (2.19).

By contrast, when $\bar{\alpha}$ is not an empty set, things are a little bit more involved. In the diagram that computes the matrix part, the magnons for the right wing are in the order $\bar{\alpha}\alpha$ (see how the lines enter into the leftmost blue dotted box in figure 2.6) while the wave function $\dot{\Psi}$ (in the same figure) is originally defined in the order $\alpha\bar{\alpha}$. To simplify the computation, we rewrite the wave function $\dot{\Psi}$ in the order $\bar{\alpha}\alpha$ (rightmost dotted box in figure 2.6). This can be done by using the nested periodicity (2.45), and it produces a product of phase factors f , which can be read off from the asymptotic Bethe equation for the momentum-carrying root:

$$f(u) = \prod_{v_i^{(1)} \in \mathbf{v}^{(1)}, v_k^{(3)} \in \mathbf{v}^{(3)}} \frac{x^-(u) - x(v_i^{(1)})}{x^+(u) - x(v_i^{(1)})} \frac{1 - 1/x^-(u)x(v_k^{(3)})}{1 - 1/x^+(u)x(v_k^{(3)})}. \quad (2.53)$$

Note that we should only take factors which depend on v 's since f is the phase factor coming just from the right wing. After doing so, we can straightforwardly contract the

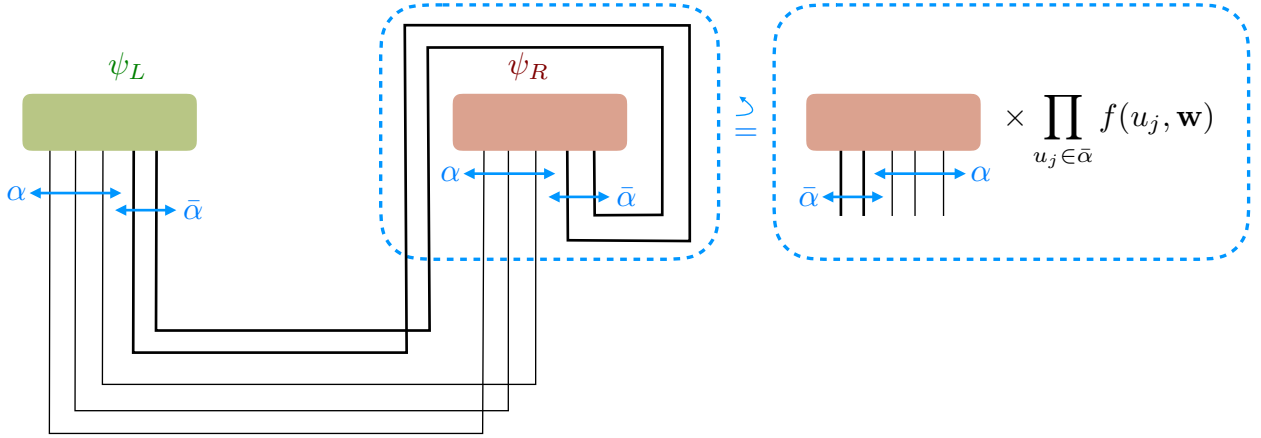


Figure 2.6: Matrix part for $\bar{\alpha} \neq \emptyset$: The magnons for the right wing are in a different order from those in the wave function. To contract the wave function with the hexagon, we have to rewrite it using the “nested periodicity” (2.45).

wave functions with the hexagons and act the S-matrices on the wave functions. This leads to an expression

$$\mathcal{H}_{\alpha, \bar{\alpha}} = \left(\prod_{u_i \in \bar{\alpha}} f(u_i) \right) \left(\prod_{\substack{i < j \\ u_i, u_j \in \alpha}} h(u_i, u_j) \right) \left(\prod_{\substack{i < j \\ u_i, u_j \in \bar{\alpha}}} h(u_i, u_j) \right) \langle \bar{\Psi}_{\bar{\alpha}\bar{\alpha}}^{\leftarrow} | \Psi_{\alpha\bar{\alpha}} \rangle \quad (2.54)$$

In order to compute the contraction $\langle \bar{\Psi}_{\bar{\alpha}\bar{\alpha}}^{\leftarrow} | \Psi_{\alpha\bar{\alpha}} \rangle$ we need the explicit form of the nested $\mathfrak{su}(2|2)$ wave-functions which can be found in [84, 85]. By performing this computation in the $\mathfrak{psu}(1, 1|2)$ subsector with corresponding $\mathfrak{su}(1|1)$ wings we learn that on the support of the Bethe equations (on-shell condition):

$$\langle \bar{\Psi}_{\bar{\alpha}\bar{\alpha}}^{\leftarrow} | \Psi_{\alpha\bar{\alpha}} \rangle = \langle \bar{\Psi}_{\mathbf{u}} | \Psi_{\mathbf{u}} \rangle \quad (2.55)$$

where the right hand side is the usual scalar product of the spin chain and is independent of the ordering of the momentum-carrying roots. Hence it can be taken out of the sum over partitions as a partition-independent prefactor.

We did not perform the same computation in the full sector but conjecture that equality (2.55) still holds when the full $\mathfrak{su}(2|2)$ wings are excited¹¹.

Furthermore, because of the orthogonality of two different on-shell states, the scalar product (2.55) vanishes unless all the roots of left and right wings are identical, namely

¹¹This assumption leads to the main formula (2.56) which we have extensively tested as shown in section 3.4. See also appendix E where we analyze a state with all seven types of Bethe roots. Furthermore, for the $\mathfrak{so}(6)$ sector at tree level, we derived (2.56) from scratch, namely without ever resorting to the hexagon formalism, by developing the algebraic Bethe ansatz for that sector. This provides another independent support for the formula (2.56). See Appendix B for details.

$$\left(\begin{array}{cccccc} \frac{\partial}{\partial v_k^3} \phi_{v_j^3} & \frac{\partial}{\partial v_k^2} \phi_{v_j^3} & & \frac{\partial}{\partial u_k} \phi_{v_j^3} & & \\ \frac{\partial}{\partial v_k^3} \phi_{v_j^2} & \frac{\partial}{\partial v_k^2} \phi_{v_j^2} & \frac{\partial}{\partial v_k^1} \phi_{v_j^2} & & & \\ & \frac{\partial}{\partial v_k^2} \phi_{v_j^1} & \frac{\partial}{\partial v_k^1} \phi_{v_j^1} & \frac{\partial}{\partial u_k} \phi_{v_j^1} & & \\ \frac{\partial}{\partial v_k^3} \phi_{u_j} & & \frac{\partial}{\partial v_k^1} \phi_{u_j} & \frac{\partial}{\partial u_k} \phi_{u_j} & \frac{\partial}{\partial w_k^1} \phi_{u_j} & \frac{\partial}{\partial w_k^3} \phi_{u_j} \\ & & \frac{\partial}{\partial u_k} \phi_{w_j^1} & \frac{\partial}{\partial w_k^1} \phi_{w_j^1} & \frac{\partial}{\partial w_k^2} \phi_{w_j^1} & \\ & & & \frac{\partial}{\partial w_k^1} \phi_{w_j^2} & \frac{\partial}{\partial w_k^2} \phi_{w_j^2} & \frac{\partial}{\partial w_k^3} \phi_{w_j^2} \\ & & & & \frac{\partial}{\partial w_k^2} \phi_{w_j^3} & \frac{\partial}{\partial w_k^3} \phi_{w_j^3} \end{array} \right)$$

$$\langle \mathbf{v} | \mathbf{v} \rangle = \det \left(\begin{array}{c} \text{green} \end{array} \right) = \det \left(\begin{array}{c} \text{red} \end{array} \right), \langle \mathbf{u} | \mathbf{u} \rangle = \det \left(\begin{array}{cc} \text{red} & \text{yellow} \\ \text{yellow} & \text{blue} \end{array} \right)$$

Figure 2.7: Definitions of the Gaudin norms $\langle \mathbf{u} | \mathbf{u} \rangle$ and $\langle \mathbf{v} | \mathbf{v} \rangle$: $\phi_{u,v,w}$ is a logarithm of the nested Bethe equation, $e^{i\phi_{u,v,w}} = 1$. $\langle \mathbf{u} | \mathbf{u} \rangle$ is a determinant of the full matrix shown above whereas $\langle \mathbf{v} | \mathbf{v} \rangle$ is a determinant of the upper (or equivalently lower) diagonal matrix shown in red (green). The missing matrix elements are vanishing, as a result of the structure of the $\mathfrak{psu}(2,2|4)$ BAEs (e.g., there is no interaction between auxiliary roots w and v lying on different wings).

$\mathbf{v}^{(i)} = \mathbf{w}^{(i)}$. This suggests the existence of a hidden symmetry, which forces infinitely many structure constants to vanish. In the next subsection, we explicitly construct such a symmetry using the transfer matrix of $\mathfrak{psu}(2|2)$.

Putting together all the elements, we obtain our main formula for the structure constant in higher rank sectors,

$$\left(\frac{C_{123}^{\bullet\circ\circ}}{C_{123}} \right)^2 = \frac{\langle \mathbf{v} | \mathbf{v} \rangle^2 \prod_{k=1}^K \mu(u_k)}{\langle \mathbf{u} | \mathbf{u} \rangle \prod_{i < j} S(u_i, u_j)} \mathcal{A}^2. \quad (2.56)$$

Here $\mu(u)$ is the measure [5] and \mathcal{A} is a higher-rank generalization of the sum over partitions, which reads

$$\mathcal{A} = \prod_{i < j} h(u_i, u_j) \sum_{\alpha \cup \bar{\alpha} = \mathbf{u}} (-1)^{|\bar{\alpha}|} \prod_{j \in \bar{\alpha}} f(u_j) e^{ip(u_j)\ell_{31}} \prod_{i \in \alpha, j \in \bar{\alpha}} \frac{1}{h(u_i, u_j)}. \quad (2.57)$$

The factor $\langle \mathbf{u} | \mathbf{u} \rangle$ denotes the Gaudin norm of the full $\mathfrak{psu}(2,2|4)$ spin chain whereas $\langle \mathbf{v} | \mathbf{v} \rangle$, equivalent to (2.55), is the norm for the (left) wing. Their precise definitions are given in

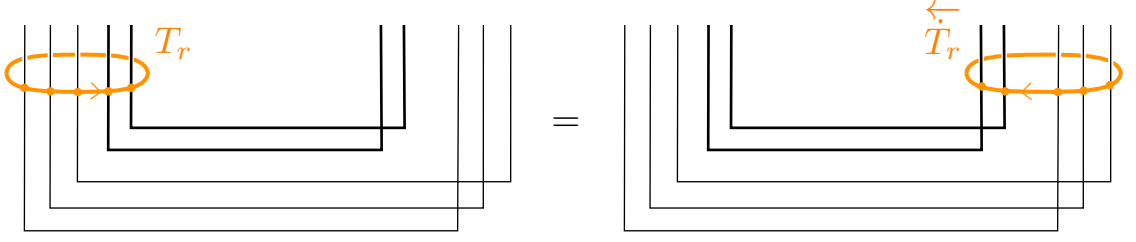


Figure 2.8: “Yangian” symmetry for three-point functions. The thin black lines denote the magnons in the first hexagon (α) whereas the thick bold lines denote the magnons in the second hexagon $\bar{\alpha}$. Using the Yang-Baxter equation, one can move the transfer matrix from the left to the right.

figure 2.7. In the $\mathfrak{sl}(2)$ sector there are not wings so we have $\langle \mathbf{v} | \mathbf{v} \rangle = 1$ and $f(u) = 1$ such that (2.56) reduces to equation (2.34)

In section 3.4, we will use this formula to reproduce the data obtained by the OPE decomposition of the four-point functions.

2.4.3 “Yangian” Symmetry

As we saw above, the structure constant vanishes unless the roots in the two wings are identical. Below we uncover the underlying symmetry responsible for such a super-selection rule.

Let us take a look again at the matrix part of $C_{123}^{\circ\circ\bullet}$. Using the Yang-Baxter relation, we can show that the difference of transfer matrices acting on two wings must always vanish if the state is contracted with the hexagons (see figure 2.8):

$$(\langle \mathcal{H} | \otimes \langle \mathcal{H} |) (T_r(u) - \overleftarrow{T}_r(u)) = 0. \quad (2.58)$$

Here r can be any representation of $\mathfrak{psu}(2|2)$ and T and \overleftarrow{T} denote the forward and the backward transfer matrices acting on the left and the right $\mathfrak{psu}(2|2)$ respectively.

As is well-known, the expansion of transfer matrices yields mutually commuting charges. Thus, the relation (2.58) is manifestation of infinitely many conservation laws hidden in the three-point function. With a slight abuse of the word, we call it “Yangian symmetry”.

When the state we contract is the on-shell nested Bethe state, we can replace the symmetry generator $T_r(u) - \overleftarrow{T}_r(u)$ by its eigenvalue. Then it follows from (2.58) that, unless

$$T_r(u) - \overleftarrow{T}_r(u) = 0 \quad (2.59)$$

is satisfied as an eigenvalue equation, the structure constant must vanish. The eigenvalues of these transfer matrices are expressed in terms of nested roots [49] and the only possible

way to satisfy (2.59) is to set the rapidities of two wings to be identical. This is the symmetry origin¹² of our super-selection rule.

In integrable systems, an infinite number of commuting charges are often accompanied by a real Yangian symmetry, namely a set of non-commutative non-local charges. An explicit construction of such a symmetry for our case is an interesting open problem for the future.

¹²The symmetry we constructed here is reminiscent of the “monodromy relations” studied at weak coupling in [50]. It would be interesting to understand the relation between the two.

Chapter 3

Asymptotic Four-Point functions

3.1 Summary of the chapter

We reconstruct a family of asymptotic four-point functions using the OPE conformal data worked out in the previous two chapters. We test our proposal at one loop against available data.

3.2 Introduction

Four-point correlation functions are probably the most interesting entities in a conformal field theory. While two- and three-point functions are kinematically constrained by conformal symmetry, four point functions can depend on conformal cross-ratios and will be strikingly different for different conformal theories with different physics.

In principle, the spectrum and operator product expansion (OPE) coefficients of a conformal field theory entail a full non-perturbative solution of a conformal field theory since they can be put together to construct any higher point function. *In practice*, it is usually unpractical to compute *all* needed spectra and three point functions and then perform the sum over *all* possible exchanged operators appearing in the OPE to finally obtain the four point correlator.

In planar $\mathcal{N} = 4$ Super Yang-Mills theory integrability comes to the rescue and renders this task feasible. In this chapter, we will construct planar four point functions of *large* BPS operators at any value of the 't Hooft coupling from the knowledge of two- and three-point functions which in turn can be computed by means of integrability. We shall be dealing with large enough external operators so that so-called wrapping corrections can be discarded; we denote such four point functions as *Asymptotic Four Point Functions*.

To compute these four point functions we need to compute the three point functions between two BPS operators and *any* non-BPS operator appearing in its OPE. These non-BPS operators are described using integrability by a set of (at most) seven different type of

Nested Bethe roots [35]. As we showed in Chapter 2 the intimidating Nested Bethe ansatz can actually be described very simply within the hexagon formalism [5] leading to very compact expressions for the relevant three-point functions and hence for the asymptotic four point functions alluded to above.

In section 3.3 we discuss four point functions, their operator product decomposition and the precise limits which allow one to discard finite size corrections. In section 3.4 we check the integrability predictions against perturbative data.

3.3 Super OPE and Finite Bethe Roots

Defined as

$$G^{(p)}(z, \bar{z}, \alpha, \bar{\alpha}) \equiv \frac{\langle \mathcal{O}_1 \mathcal{O}_2 \mathcal{O}_3 \mathcal{O}_4 \rangle}{\langle \mathcal{O}_1 \mathcal{O}_2 \rangle \langle \mathcal{O}_3 \mathcal{O}_4 \rangle} \quad \text{where} \quad \mathcal{O}_i \equiv \text{tr}((y_i \cdot \phi(x_i))^p), \quad (3.1)$$

the reduced correlator is a nice conformal invariant quantify. It is a function of the $SO(2, 4)$ and $SO(6)$ cross-ratios

$$z\bar{z} \equiv \frac{x_{12}^2 x_{34}^2}{x_{13}^2 x_{24}^2}, \quad (1-z)(1-\bar{z}) \equiv \frac{x_{14}^2 x_{23}^2}{x_{13}^2 x_{24}^2}, \quad \alpha\bar{\alpha} \equiv \frac{y_{12} y_{34}}{y_{13} y_{24}}, \quad (1-\alpha)(1-\bar{\alpha}) \equiv \frac{y_{14} y_{23}}{y_{13} y_{24}}, \quad (3.2)$$

where $x_{ij}^2 = (x_i - x_j)^2$ and $y_{ij} = y_i \cdot y_j$ with y_j being the standard six-dimensional null vectors parametrizing the orientation of the external BPS operators which are inserted at four-dimensional positions x_j .

3.3.1 Reservoir Picture and Asymptotic Four-Point Functions

Let us recall some well-understood facts about the correlator (3.1). We will describe it through its infinite OPE series governing what flows from operators 1, 2 to operators 3, 4. In principle, all the multi-trace operators can show up in this OPE representation. However, at large N there is an important simplification: only single- and double-trace operators contribute. Then the four-point function can be expanded as

$$\begin{aligned} G^{(p)} = & 1 + \overbrace{N^{-2} \sum_{\substack{\text{single-trace} \\ \text{BPS super-conformal} \\ \text{primaries of twist } L = 2, 4, \dots, 2p-2}} L \times \mathcal{F}_L^{\text{BPS}}(z, \bar{z}, \alpha, \bar{\alpha})}^{\text{SUSY protected, coupling independent part}} + \overbrace{N^{-2} \sum_{\substack{\text{single-trace} \\ \text{non-BPS super-conformal} \\ \text{primaries}}} (C_p^{\circ\circ\bullet})^2 \mathcal{F}_{\Delta, s, n, m}(z, \bar{z}, \alpha, \bar{\alpha})}^{\text{more interesting coupling dependent part}} \\ & + \text{extremal and double trace contribution.} \end{aligned} \quad (3.3)$$

where the conformal blocks \mathcal{F} in the first line are fixed by super-conformal symmetry and are summarized in appendix D. Our main focus here is on the last term in the first line

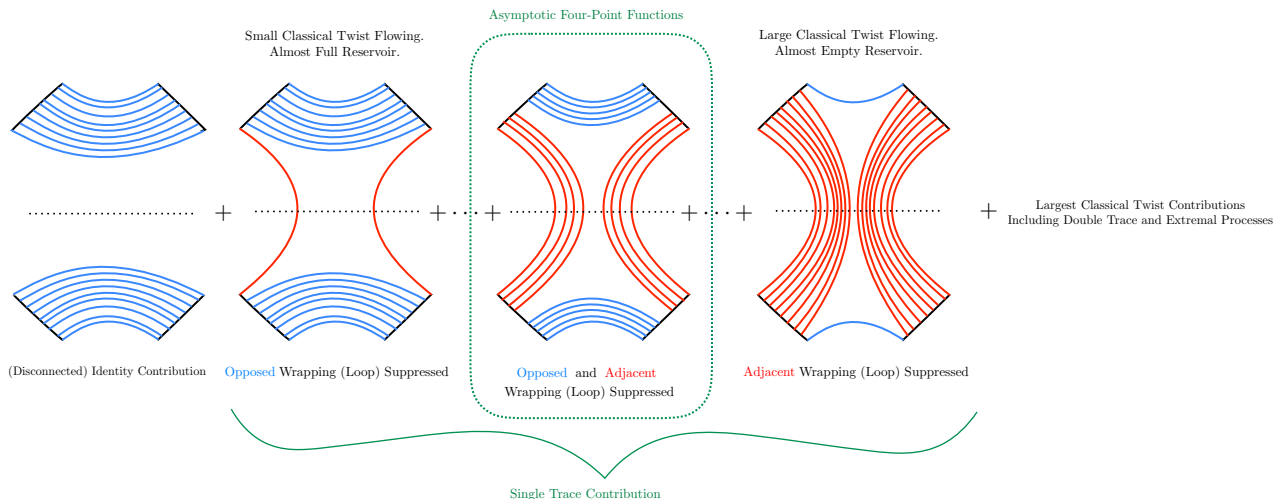


Figure 3.1: Various contributions to the 4pt function.

corresponding to the contribution of single-trace non-protected operators, whose three-point functions can be computed by the hexagon approach [5]. A priori, it is non-trivial to disentangle the double-trace contribution from the single-trace contributions since, at finite coupling, they can have the same twist and mix with each other.¹ However, in perturbation theory the twist of each exchanged operator is close to its classical value and this allows us to neatly separate the single- and double-trace contributions – especially if we consider large external operators with $p \gg 1$ – since the exchanged double traces will have classical twist $\tau \geq 2p$. Hence, in the OPE limit where z, \bar{z} are small and the ratio z/\bar{z} is fixed, for all twists $\tau \leq 2p - 2$ we can safely restrict our attention to single-trace operators as schematically depicted in figure 3.1.

As illustrated in that figure, we can think of operators in the OPE, organized by twist, as originating from a big “reservoir” of propagators at the bottom (and top). Operators with a small twist τ flowing in the OPE arise from opening up a few links at the bottom. As such, they will have small side bridges but very large bottom and top bridges. For these operators wrapping in the so-called opposed channel is greatly suppressed in perturbation theory [5, 131]. (The adjacent wrapping does matter eventually, at $\tau/2 + 2$ loops to be precise.) In the other extreme case we have the contribution of operators with twist close to the double trace threshold, $\tau = 2p - O(1)$. Those have huge side bridges which soak up the reservoirs almost completely. For these large twist operators it is thus the adjacent wrapping which is greatly suppressed. (On the other hand, the bottom and top bridges can now be small so that opposed wrapping eventually kicks in at $p - \tau/2 + 1$ loops.)

Finally we have the intermediate regime which is the most relevant one for the present chapter. For operators whose twist is very large and yet far from emptying the reservoir, $1 \ll \tau \ll 2p$ – as depicted in the middle of figure 3.1 – wrapping is suppressed in both the

¹At large N the corresponding anomalous dimensions can cross, in this integrable theory. At finite N this crossing is resolved as discussed in [39].

adjacent and the opposed channels. For such contributions we can thus ignore wrapping contributions altogether and use only the so-called asymptotic prediction for the three point coefficients in the OPE expansion.

By playing with the polarization vectors we can easily make sure the adjacent bridges are very large, see e.g. [10]. The basic idea is that if operators \mathcal{O}_1 and \mathcal{O}_2 have a large non-zero combined R-charge then by R-charge conservation the operators in their OPE must have a large twist, at least as large as the R-charge. For example, we could choose \mathcal{O}_1 to be

$$\mathcal{O}_1^{ZX} = \text{tr}(Z^{p-q} X^q) + \text{permutations} = \left(\frac{\partial}{\partial \beta_1} \right)^q \text{tr}(y_1 \cdot \phi)^p \Big|_{\beta_1=0} \quad \text{where } y_1 = (1, i, \beta_1, i\beta_1, 0, 0), \quad (3.4)$$

and \mathcal{O}_2 to be made out of the same Z 's and the complex conjugate \bar{X} 's. For the top we proceed similarly using the remaining complex scalars Y 's and \bar{Y} .² Combined, the total X $U(1)$ charge of operators 1 and 2 cancels out but the Z $U(1)$ charge does not. Instead there are $2p - 2q$ units of such R -charge. As such, in the OPE of such operators we have operators whose twist is at least $\tau = 2(p - q)$. Those leading twist operators would have side bridges of length $l = p - q$. Operators with subleading twists will have even larger side bridges. In sum, for the correlator

$$\langle O_1^{ZX} O_2^{Z\bar{X}} O_3^{\bar{Z}Y} O_4^{\bar{Z}\bar{Y}} \rangle = \left(\frac{\partial}{\partial \beta_1} \frac{\partial}{\partial \beta_2} \frac{\partial}{\partial \beta_3} \frac{\partial}{\partial \beta_4} \right)^q \langle O_1 O_2 O_3 O_4 \rangle \Big|_{\beta_i=0} \quad (3.6)$$

with p and $p - q$ both very large, the side wrapping effects in the OPE channel 12 can be delayed tremendously as they will only kick in at $p - q + 2$ loops. Furthermore, if q is also very large then the bottom wrapping is also very suppressed since there will be a huge bottom bridge connecting the X 's and \bar{X} 's which requires a lot of twist to eat up. More precisely, for a flowing twist $\tau = 2p - 2q + 2n < 2p - 2$ bottom wrapping corrections will only show up at $q + 1 - n$ loops. Only for very subleading twist with n very large will these effect become relevant. To summarize: At weak coupling, for most practical purposes we can ignore *all* wrapping corrections when computing (3.6). Such four point functions are thus dubbed *asymptotic four-point functions*.

²All in all,

$$\begin{aligned} O_2^{Z\bar{X}} &= \left(\frac{\partial}{\partial \beta_2} \right)^q \text{tr}(y_2 \cdot \phi)^p \Big|_{\beta_2=0} \quad \text{where } y_2 = (1, i, \beta_2, -i\beta_2, 0, 0), \\ O_3^{\bar{Z}Y} &= \left(\frac{\partial}{\partial \beta_3} \right)^q \text{tr}(y_3 \cdot \phi)^p \Big|_{\beta_3=0} \quad \text{where } y_3 = (1, -i, 0, 0, \beta_3, i\beta_3), \\ O_4^{\bar{Z}\bar{Y}} &= \left(\frac{\partial}{\partial \beta_4} \right)^q \text{tr}(y_4 \cdot \phi)^p \Big|_{\beta_4=0} \quad \text{where } y_4 = (1, -i, 0, 0, \beta_4, -i\beta_4). \end{aligned} \quad (3.5)$$

3.3.2 Super Operator Product Expansion

In the OPE (3.3) we sum over super-conformal primaries only. The descendants are automatically taken into account by the super-conformal blocks \mathcal{F} which we summarized out in appendix D.

In the integrability context each single trace operator is described by a set of seven kind of Bethe roots satisfying so called Beisert-Staudacher Bethe equations [35, 36]. In this chapter we can disregard finite size corrections as explained in the previous section so that the Beisert-Staudacher equations will suffice in what follows.

Now, not all solutions to Bethe equations suit our purpose. Super-conformal primaries are solutions to Bethe equations where all Bethe roots are finite. Furthermore, we should exclude solutions where $x(v^{(1)}) = x(w^{(1)}) = 0$ which also correspond to super descendants³[35] *unless* these solutions are part of exact strings in which case the corresponding solutions are denoted as *singular solutions* and should a priori be considered.⁴ The sum in (3.3) stand therefore for a sum over such finite Bethe roots configurations.

The number of Bethe roots of each kind can be read of from the quantum numbers of the exchanged operator. Since our external operators are all BPS, the three-point functions preserve a diagonal $\mathfrak{su}(2|2)$ subgroup [5, 45] which immediately implies that the occupation numbers of the wings must be identified to yield a non-zero result, $\tilde{K}_a = K_a$. The relation between the Bethe ansatz occupation numbers and length and the labels

Scaling dimension	Lorentz $\mathfrak{su}(2) \times \mathfrak{su}(2)$	$\mathfrak{so}(6)$ R -charge
Δ	$[s, s]$	$[n - m, 2m, n - m]$

which show up in (3.3) is then

$$\Delta - \delta\Delta = L - K^{(1)} + K^{(3)} + K - 2 \quad (3.7)$$

$$s = K - K^{(1)} - K^{(3)} - 2 \quad (3.8)$$

$$n = L/2 + K^{(3)} - K^{(2)} - 1 \quad (3.9)$$

$$m = L/2 + K^{(2)} - K^{(1)} - 1 \quad (3.10)$$

where the anomalous dimension $\delta\Delta = \sum_j \frac{2ig}{x^+(u_j)} - \frac{2ig}{x^-(u_j)}$ up to higher loop finite size corrections which, as mentioned above, we are discarding throughout this work. The quantum numbers in (3.7–3.10) are all non-negative integers. This puts restrictions over the length L and the occupation numbers K and $K^{(a)}$. Also, for the Bethe equations to admit finite solutions the occupation numbers usually need to decrease as we go from the middle node occupation K into the wing extremities $K^{(3)}$, see e.g., [35, 46, 47].

To summarize, we should a priori find *all* finite solutions to Bethe equations with $K^{(a)} = \tilde{K}^{(a)}$, read of their quantum numbers from (3.7–3.10), compute their three-point functions

³By means of a dynamic transformation introduced in [35] we can map a root $x(v^{(1)}) = 0$ to a root $x(v^{(3)}) = \infty$ which corresponds to a descendant of the state without the root at ∞ .

⁴Coincidentally or not we found out that – on all examples we checked – these singular solutions yield a vanishing three-point function.

using the hexagon approach [5] and add them up as in (3.3) using the super-conformal blocks summarized in appendix D.

It turns out that a version of Yangian symmetry, Chapter 2, actually implies much more than the global symmetry constraint $K^{(a)} = \tilde{K}^{(a)}$. To get a non-vanishing OPE contribution we must in fact have absolutely symmetrical wings *root by root*, that is $v_j^{(a)} = w_j^{(a)}$. This is a very sharp and novel space-time implication of the world-sheet integrability.

3.4 Comparison with Data

In this section we combine the previous two sections. Namely, we put the integrability predictions of Chapter 1 and Chapter 2 to test by comparing them with the OPE expansion described in section 3.3 of perturbative four point functions.

Integrability yields predictions for individual structure constants given a set of Bethe roots corresponding to the non-BPS operator at hand. These operators have different quantum dimensions Δ as read off from their Bethe roots but classically there is a large number of operators with the same classical dimension $\Delta_{\text{classical}} = \Delta - \delta\Delta$ – the right hand side of (3.7). In perturbation theory, what shows up in the OPE of a four-point function are sum rules over these degenerate operator spaces. The summand is the square of the structure constants weighted by powers of the quantum anomalous dimension $\delta\Delta$.

This was illustrated in detail for the simplest $\mathfrak{sl}(2)$ sector in [10], see for example formulae (56–65) therein summarizing some of those sum rules. Here we are dealing with the full nested space so the sum rules are a bit more involved; they are sums over all finite solutions to Bethe equations whose occupation numbers K, K_j and length L yield the same $\mathfrak{psu}(2, 2|4)$ classical charges appearing in the right hand side of (3.7–3.10).

Up to one loop, for instance, we can easily use the perturbative results of [51] to extract predictions for the sum rules $\mathcal{P}^{(0,0)}$, $\mathcal{P}^{(0,1)}$ and $\mathcal{P}^{(1,1)}$ defined as⁵

$$\sum_{\text{Bethe solutions with fixed r.h.s. of (3.7–3.10)}} (C^{\circ\circ\bullet})^2 e^{y\delta\Delta} \equiv \mathcal{P}^{(0,0)} + g^2 \mathcal{P}^{(1,0)} + g^2 y \mathcal{P}^{(1,1)} + \mathcal{O}(g^4) \quad (3.11)$$

These predictions are summarized in table 3.1 for one loop OPE data extracted from the four point function of 1/2 BPS operators of length $p = 4$. We provide the sum rules corresponding to non-BPS operators with $\mathfrak{so}(6)$ charges $0 \leq m \leq n \leq 2$ and twist $\tau \leq 2p - 2$. At twist $\tau = 2p$ the OPE would be contaminated by double trace contributions and we could no longer cleanly test the single trace integrability predictions against it.⁶ To

⁵In other words, $\mathcal{P}^{(0,0)} \equiv \sum_{\{u\}} (C_{\mathbf{u}}^{(0)})^2$, $\mathcal{P}^{(1,0)} \equiv \sum_{\{u\}} 2 C_{\mathbf{u}}^{(0)} C_{\mathbf{u}}^{(1)}$ and $\mathcal{P}^{(1,1)} \equiv \sum_{\{u\}} \gamma_{\mathbf{u}}^{(1)} (C_{\mathbf{u}}^{(0)})^2$ where $\delta\Delta = g^2 \gamma_{\mathbf{u}}^{(1)} + g^4 \gamma_{\mathbf{u}}^{(2)} + \dots$ and $C_{\mathbf{u}}^{\circ\circ\bullet} = C_{\mathbf{u}}^{(0)} + g^2 C_{\mathbf{u}}^{(1)} + g^4 C_{\mathbf{u}}^{(2)} + \dots$.

⁶Of course, we could simply consider larger external operators to delay the double trace contribution as much as we want. It would also be interesting to play with the OPE analysis varying the external dimensions in order to isolate the double trace contribution from the extremal one. This would provide valuable data for guiding an integrability based approach towards studying extremal or double trace correlation functions.

generate this table we used a four point function with external operators of length $p = 4$ so that at one loop we can test integrability predictions in the OPE involving operators of twist 2, 4 and 6. Had we used a larger p and we could have tested those twists (the result would be the same at this loop order) and more.

Having predictions for the right hand side of (3.11) we turn to the left hand which we will now generate using integrability.

To reproduce this OPE data from integrability we first find all (wing-symmetric) solutions⁷ of Beisert-Staudacher Bethe equations with finite Bethe roots. First we set $g = 0$ and solve these equations to leading order at weak coupling. This part is hard. Then to get the quantum corrections to the Bethe roots we simply correct the Bethe roots perturbatively by linearizing the $\mathcal{O}(g^2)$ Bethe equations around each tree level seed solution. This part is straightforward. Once we get the Bethe roots we plug them into the Hexagon prediction (2.56) with $l = L/2$, sum over all solutions as indicated in the left hand side of (3.11). The result is then compared with the OPE predictions for the right hand side of (3.11) which we extracted from perturbative data and summarized in table 3.1.

To find all the Bethe ansatz solutions at tree level we resorted to various pieces of technology. The simplest Bethe equations correspond to the $\mathfrak{sl}(2)$ sector where we only excite the middle node and Bethe solutions for operators of spin s are given by sets of real roots $\{u_1, \dots, u_s\}$. Solving Bethe equations in the $\mathfrak{sl}(2)$ sector in Mathematica is absolutely straightforward, see for example [104]. Checks of OPE data against integrability conjectures were already performed in [5] and earlier in [10]. The sums $\mathcal{P}^{(a,b)}$ for this sector are highlight in red in table 3.1.

For other sectors such as higher rank sectors with excited wing nodes, Bethe equations become more complicated and also admit complex solutions including at times so called exceptional solutions [53, 54]. It is the existence of complex solutions which renders the problem of finding all solutions to the Bethe equations much more challenging in this case. One way to proceed which we found quite useful is to use a Baxter formulation of Bethe equations and solve directly for the Baxter polynomials and the transfer matrix eigenvalues rather than individual Bethe roots. Another useful numerical method is the so-called Homotopy continuation method [55] where one starts from some simpler equations and adiabatically deform them until they become the Beisert-Staudacher equations. For $\mathfrak{su}(2)$ solutions this was proposed in [55] and its generalization to the nested case also works very well. The third method – and the one we found to be the most convenient – is however to use the very powerful recently proposed analytic solver of [56, 57] based on the Q -system⁸. This provided us with the complete set of Bethe solutions needed to reproduce all the number in blue in tables 3.1 using the hexagon conjecture (2.56).

To illustrate what goes into these computations consider the following example. For global charges $\Delta - \delta\Delta = 8$, $s = 2$, $n = 2$ and $m = 0$ there are 20 wing-symmetric Bethe

⁷Bethe solutions with asymmetric wings give a vanishing structure constant $C^{\circ\circ\bullet}$. We exclude as well symmetric solutions with $w^1 = v^{(1)} = 0$, as they do not render highest weights.

⁸We are very grateful to C. Marboe and D. Volin for sharing a working code of the fast analytic solver for $\mathfrak{psu}(2, 2|4)$.

solutions, each of them with 6 middle node roots $\{u\}$ and 2 roots in the first left and right fermionic nodes $\{w^{(1)}\}$ and $\{v^{(1)}\}$. Performing the sum over Bethe solutions with a high numerical precision we obtain:

$$\sum_{20 \text{ solutions}} (C^{\circ\circ\bullet})^2 = 0.194805\mathbf{194805194805194805194805} - g^2 \mathbf{1.81175390266299357208448117539026629935720844} \quad (3.12)$$

we then recognize this renders the rational numbers:

$$\sum_{20 \text{ solutions}} (C^{\circ\circ\bullet})^2 = \frac{15}{77} - g^2 \frac{1973}{1089} \quad (3.13)$$

In an attached `Mathematica` notebook the reader can find our conjecture (2.56) coded up to one loop order and how the twenty solutions beautifully add to this nice rational number which perfectly reproduces the perturbative OPE data. All other blue numbers in table 3.1 were checked in the same way.

Note in particular that there is no data in table 3.1 when $s + n - m$ is odd although there exist Bethe solutions with these global charges. Their absence is imposed by the symmetry of the OPE under the exchange of the pair of identical external operators. It is nice to see how this selection rule comes about from our integrability construction. The sum over partitions (2.57) is written in terms of the bridge length ℓ_{31} . However, nothing in the original problem singles out this particular adjacent channel. We can find an equivalent formula expressed in terms of the complementary bridge length ℓ_{23} when the Bethe state is on shell and cyclic. Namely, using the ABA equations, $e^{ip_{\bar{\alpha}}L_3} f(u_{\bar{\alpha}})^2 S_{\bar{\alpha}\alpha} = 1$ and $f(u_{\alpha})f(u_{\bar{\alpha}}) = 1$, the permutation property of the hexagon form factor $h_{\alpha\bar{\alpha}} S_{\bar{\alpha}\alpha} = h_{\bar{\alpha}\alpha}$, and the zero momentum condition $e^{-ip_{\bar{\alpha}}} = e^{ip_{\alpha}}$, one easily derives that

$$\sum_{\alpha} (-1)^{|\bar{\alpha}|} f(u_{\bar{\alpha}}) e^{ip_{\bar{\alpha}}\ell_{31}} \frac{1}{h_{\alpha\bar{\alpha}}} = (-1)^K \sum_{\alpha} (-1)^{|\bar{\alpha}|} f(u_{\bar{\alpha}}) e^{ip_{\bar{\alpha}}\ell_{23}} \frac{1}{h_{\alpha\bar{\alpha}}}, \quad (3.14)$$

where $K = |\alpha| + |\bar{\alpha}|$ is the total number of magnons. For two identical operators, the spin chain is split into two equal parts of length $\ell_{13} = \ell_{23} = L_3/2$ and the previous relation turns into a selection rule : $\mathcal{A} = 0$ for K odd. In terms of the quantum numbers of the superconformal primary, see equation (3.7), it happens whenever $(-1)^K = (-1)^{s+n-m} = -1$, in agreement with the symmetry property of the 4-point function.

Finally, it is worth stressing that while all the checks we performed worked like a charm, they do not exhaust the available perturbative data by any stretch. Even at tree level and one loop we only confirmed the predictions in blue in table 3.1. From a Bethe ansatz point of view, most of these solutions are not general enough as they do not excite roots associated with all $\mathfrak{psu}(2, 2|4)$ Dynkin nodes. The only solutions which contain roots of type $v^{(3)}$ and $w^{(3)}$ are the ones which contribute to $\mathbb{P}_{\tau=6, s=0}^{n=0, m=0}$ in table 3.1. These solutions have some peculiarities, such as the appearance of odd powers of g in the rapidities, which

are explained in Appendix E. It would be very interesting – even at this low loop order – to perform a few higher twist checks and probe various Bethe solutions in full generality. It would also be very interesting to expand Bethe ansatz further and compare the integrability predictions with the available data at two [58], three [59] or even four loops [60]. When going to higher loops we should either start including finite size corrections to the three-point functions [61, 131, 48] (hard) or increase the length p of the external operators as explained in section 3.3 (easy).

Table 3.1: The sum of $\mathcal{P}^{(a,b)}$ from superconformal block expansion $\mathbb{P}_{\tau,s}^{[n,m]} = \mathcal{P}^{(0,0)} + g^2 \mathcal{P}^{(1,0)} + g^2 y \mathcal{P}^{(1,1)}$ of operators with twist $\tau = \Delta_{\text{classical}} - s$ and spin s . The data in color has been checked against integrability and the data in red is for the $\mathfrak{sl}(2)$ sector.

s	0	2	4	6
$\mathbb{P}_{2,s}^{[0,0]}$	$\frac{1}{3} - 4g^2 + 4g^2y$	$\frac{1}{35} - \frac{205}{441}g^2 + \frac{10}{21}g^2y$	$\frac{1}{462} - \frac{1106}{27225}g^2 + \frac{7}{165}g^2y$	$\frac{1}{6435} - \frac{14380057}{4509004500}g^2 + \frac{761}{225225}g^2y$
$\mathbb{P}_{4,s}^{[0,0]}$	$\frac{2}{15} - \frac{79}{75}g^2 + \frac{14}{15}g^2y$	$\frac{13}{378} - \frac{9223}{23814}g^2 + \frac{71}{189}g^2y$	$\frac{1}{198} - \frac{137053}{2044900}g^2 + \frac{431}{6435}g^2y$	$\frac{43}{72930} - \frac{1514205197}{173746973400}g^2 + \frac{905}{102102}g^2y$
$\mathbb{P}_{4,s}^{[1,1]}$	$\frac{7}{5} - 8g^2 + 8g^2y$	$\frac{16}{63} - \frac{196}{81}g^2 + \frac{22}{9}g^2y$	$\frac{29}{858} - \frac{1873528}{4601025}g^2 + \frac{892}{2145}g^2y$	$\frac{46}{12155} - \frac{12573551}{239320900}g^2 + \frac{419}{7735}g^2y$
$\mathbb{P}_{6,s}^{[0,0]}$	$\frac{13}{210} - \frac{31}{63}g^2 + \frac{7}{15}g^2y$	$\frac{23}{660} - \frac{566107}{1633500}g^2 + \frac{557}{1650}g^2y$	$\frac{7}{825} - \frac{1448972527}{15030015000}g^2 + \frac{35891}{375375}g^2y$	$\frac{37}{25194} - \frac{19377905081}{1052328186000}g^2 + \frac{184}{9945}g^2y$
$\mathbb{P}_{6,s}^{[1,1]}$	$\frac{4}{5} - \frac{1264}{245}g^2 + \frac{172}{35}g^2y$	$\frac{47}{110} - \frac{20891}{5445}g^2 + \frac{208}{55}g^2y$	$\frac{368}{3575} - \frac{5619351}{5112250}g^2 + \frac{3932}{3575}g^2y$	$\frac{149}{8398} - \frac{9215599347}{43197422450}g^2 + \frac{31709}{146965}g^2y$
$\mathbb{P}_{6,s}^{[2,0]}$	$\frac{4}{15} - 2g^2 + 2g^2y$	$\frac{15}{77} - \frac{1973}{1089}g^2 + \frac{20}{11}g^2y$	$\frac{2}{39} - \frac{84593}{152100}g^2 + \frac{329}{585}g^2y$	$\frac{98}{10659} - \frac{57003741}{511212100}g^2 + \frac{1284}{11305}g^2y$
$\mathbb{P}_{6,s}^{[2,2]}$	$\frac{26}{7} - 12g^2 + 12g^2y$	$\frac{12}{11} - \frac{2494}{363}g^2 + \frac{76}{11}g^2y$	$\frac{12}{55} - \frac{15917}{8450}g^2 + \frac{124}{65}g^2y$	$\frac{145}{4199} - \frac{9212823}{25560605}g^2 + \frac{831}{2261}g^2y$
s	1	3	5	7
$\mathbb{P}_{4,s}^{[1,0]}$	$\frac{1}{5} - 2g^2 + 2g^2y$	$\frac{3}{77} - \frac{521}{1089}g^2 + \frac{16}{33}g^2y$	$\frac{1}{195} - \frac{10909}{152100}g^2 + \frac{43}{585}g^2y$	$\frac{2}{3553} - \frac{4415079}{511212100}g^2 + \frac{101}{11305}g^2y$
$\mathbb{P}_{6,s}^{[1,0]}$	$\frac{1}{4} - \frac{20}{9}g^2 + \frac{13}{6}g^2y$	$\frac{9}{104} - \frac{1179}{1300}g^2 + \frac{9}{10}g^2y$	$\frac{3}{170} - \frac{1179497}{5664400}g^2 + \frac{249}{1190}g^2y$	$\frac{25}{9044} - \frac{2070147901}{57971452140}g^2 + \frac{41291}{1139544}g^2y$
$\mathbb{P}_{6,s}^{[2,1]}$	$\frac{8}{7} - 8g^2 + 8g^2y$	$\frac{29}{78} - \frac{5186}{1521}g^2 + \frac{134}{39}g^2y$	$\frac{69}{935} - \frac{11553}{14450}g^2 + \frac{69}{85}g^2y$	$\frac{335}{29393} - \frac{30397561}{219090900}g^2 + \frac{3207}{22610}g^2y$

Chapter 4

The octagon

4.1 Summary of the chapter

We use hexagonalization to compute four-point correlation functions of long BPS operators with special R-charge polarizations. We perform the computation at weak coupling and show that at any loop order our correlators can be expressed in terms of single-valued polylogarithms with uniform maximal transcendentality. As a check of our results we extract nine-loop OPE data and compare it against sum rules of (squared) structures constants of non-protected exchanged operators described by hundreds of Bethe solutions.

4.2 Introduction

Hexagonalization [6]¹ provides a non-perturbative method, any value of the ‘t Hooft coupling, which relies on the integrability of the two-dimensional effective world-sheet of $\mathcal{N} = 4$ SYM. In this chapter we will use this approach to compute some four-point functions explicitly. However, in order to achieve this we will have to restrict to the asymptotic limit $K_i \gg 1$ at weak ‘t Hooft coupling $g^2 \rightarrow 0$. As it will become clear this is the regime where this method is most efficient.

In this integrability approach we use a map of the 4D planar four-point function into a finite volume 2D correlator of four hexagon operators², with the volume determined by the external scaling dimensions K_i :

$$\langle \mathcal{O}_{K_1} \mathcal{O}_{K_2} \mathcal{O}_{K_3} \mathcal{O}_{K_4} \rangle_{4D} \implies \langle \mathcal{H}_1 \mathcal{H}_2 \mathcal{H}_3 \mathcal{H}_4 \rangle_{2D} \quad (4.1)$$

This 2D correlator is then computed by a spectral decomposition whose ingredients, the 2D mirror spectrum and the hexagon form factors, are known at finite coupling thanks to supersymmetry and integrability. This provides a series expansion where each element gives a

¹See also [112] for similar ideas on tessellations introduced at tree level.

²A n -point correlator in the 4D space is mapped to a finite volume correlator of $2(n - 2)$ hexagon operators in the 2D effective world-sheet

finite coupling contribution but there are an infinite number of them and a resummation has to be performed to get back the four-point function with finite K_i . See figure 4.1 for a representation of hexagonalization and the parameters entering this form factor expansion.

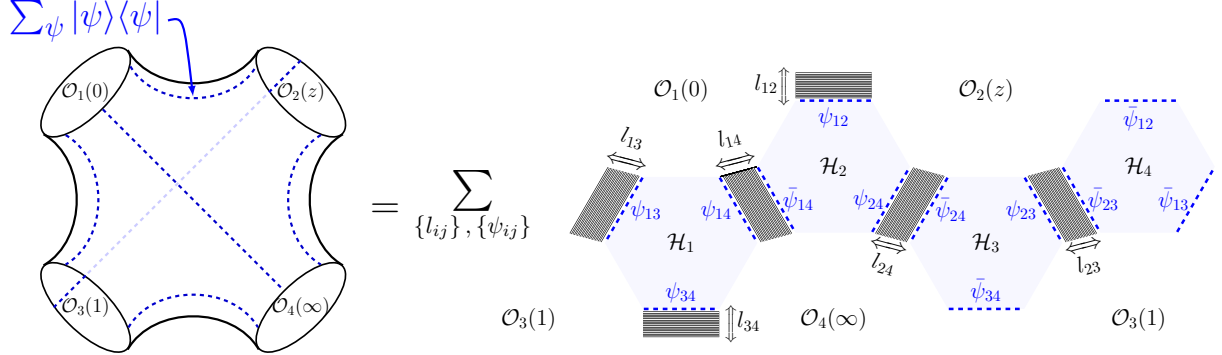


Figure 4.1: On the left, the effective world-sheet that resums all planar Feynman graphs. On the right, hexagonalization: we start with the tree level planar graphs characterized by the Wick contractions or bridge lengths $\{l_{ij}\}$ constrained by $K_1 = l_{12} + l_{13} + l_{14}$ (and likewise for the other three operators). Each of these graphs is tessellated into four hexagons by inserting a complete basis of 2D intermediate states $1 = \sum |\psi\rangle\langle\psi|$ on six mirror cuts performed along each bridge l_{ij} . The coupling (g^2) dependence is incorporated by the hexagon form factors $\langle\mathcal{H}|\psi_{ij}\rangle$ and chemical potentials such as the Boltzmann factor $e^{-E_{\psi_{ij}} l_{ij}}$. To get back the planar four-point function we need to sum over all mirror states $\{\psi_{ij}\}$ for each graph $\{l_{ij}\}$.

The resummation of this form factor series is very challenging at finite coupling. However this changes as we go to weak coupling where hexagonalization becomes suitable for the perturbative study of correlators of long operators. This is evident when analyzing the Boltzmann factors that weight the contributions of the intermediate 2D states ψ_{ij} . These depend on the energy $E_{\psi_{ij}}$ and the bridge length l_{ij} or number of Wick contractions between operators \mathcal{O}_i and \mathcal{O}_j : $e^{-E_{\psi_{ij}} l_{ij}}$. At weak coupling these weights scale as $(g^2)^{l_{ij}}$ for the non-trivial lowest states and even more suppressed for heavier states. As a consequence at a given loop order and for large enough l_{ij} all intermediate states are projected out and only the vacuum propagates on this bridge. In the strict limit $l_{ij} \rightarrow \infty$ this remains valid at any loop order. Thus the only contributions come from intermediate states propagating through small bridges.

In this chapter we accompany the limit $K_i \gg 1$ with specific choices of R -charge polarization for the external operators. This allows us to achieve the greatest simplification in the perturbative regime, see figure 4.2. This consists on fixing a large R -charge flowing between pairs of operators in order to enforce a large bridge stretching between them. Such that we are left only with two non-adjacent small bridges, the only two that can host non-trivial intermediate states.

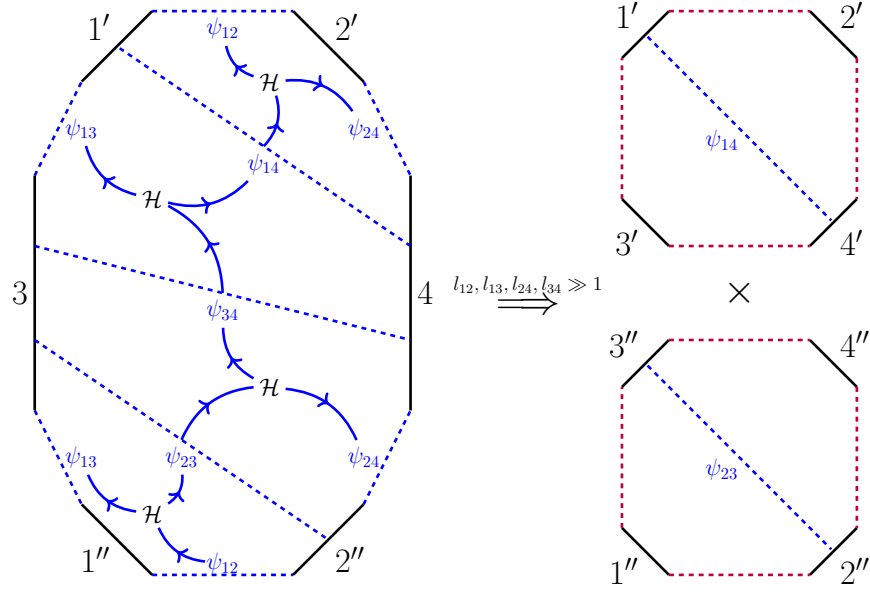


Figure 4.2: Sequence of transitions caused by acting with hexagon operators \mathcal{H} . Each state ψ_{ij} picks a Boltzmann factor $e^{-E_{\psi_{ij}} l_{ij}}$ when propagating through the bridge connecting operators i and j . A sequence of transitions such as $\psi_{12} \xrightarrow{\mathcal{H}} \psi_{23} \xrightarrow{\mathcal{H}} \psi_{34} \xrightarrow{\mathcal{H}} \psi_{14} \xrightarrow{\mathcal{H}} \psi_{12}$ wraps around operators \mathcal{O}_1 and \mathcal{O}_3 as well as \mathcal{O}_2 and \mathcal{O}_4 . It is in general given by a complicated contraction of the four tensors $\langle \psi_{ij} | \mathcal{H} \rangle$. This simplifies when we have large bridges $l_{12}, l_{13}, l_{24}, l_{34} \gg 1$ which only let the vacuum propagate through them. This leads to a factorization of the present polygon into two octagons $\mathbb{O}_{l_{14}}$ and $\mathbb{O}_{l_{23}}$, composed by the two top and the two bottom hexagons respectively.

We consider two instances of four-point functions of polarised operators with equal dimension K . At tree level these correlators are given schematically by the Wick contractions:

$$\mathbb{S}^{(0)} \sim \begin{array}{c} \text{Diagram with four vertices } O_1, O_2, O_3, O_4 \text{ in a square. } O_1 \text{ and } O_2 \text{ are connected by multiple red lines. } O_3 \text{ and } O_4 \text{ are connected by multiple red lines. } O_1 \text{ and } O_3 \text{ are connected by multiple black lines. } O_2 \text{ and } O_4 \text{ are connected by multiple black lines.} \end{array} \quad \text{and} \quad \mathbb{A}^{(0)} \sim \sum_{l=0}^{K/2} \begin{array}{c} \text{Diagram with four vertices } \hat{O}_1, \hat{O}_2, \hat{O}_3, \hat{O}_4 \text{ in a square. } \hat{O}_1 \text{ and } \hat{O}_2 \text{ are connected by multiple red lines. } \hat{O}_3 \text{ and } \hat{O}_4 \text{ are connected by multiple blue lines. } \hat{O}_1 \text{ and } \hat{O}_3 \text{ are connected by multiple black lines. } \hat{O}_2 \text{ and } \hat{O}_4 \text{ are connected by multiple black lines. A double-headed arrow labeled } l \text{ is between } \hat{O}_1 \text{ and } \hat{O}_2. \end{array} \quad (4.2)$$

where the colors represent the complex scalar R -charges X , Y and Z .

As hexagonalization prescribes, when turning on the coupling we dress the tree level graph(s) with mirror particles. In the limit $K \gg 1$, our polarized correlators only receive contributions from graphs where the simplification described in figure 4.2 applies.

Schematically this gives the results:

$$\mathbb{S} \sim \mathbb{O}_{l=0}^2 \quad \text{and} \quad \mathbb{A} \sim \sum_{l=0}^{K/2} \mathbb{O}_l^2 \quad (4.3)$$

where \mathbb{O}_l denotes the octagon form factors depicted on the right panel of figure 4.2. These are composed of two hexagons glued by summing over all intermediate states along a common edge.

The main goal of this chapter is to first provide a finite coupling representation for the octagon form factor \mathbb{O}_l and second, at weak coupling, a useful representation for the octagon and the polarized correlators in (4.2), in terms of analytic functions at arbitrary loop order. To achieve this we take the following steps:

Outline

In section 4.3 we construct the finite coupling octagon form factor by gluing two hexagons. We show how the matrix parts of the hexagon form factors simplified when contracted. This allow us to express the final result in terms of n -particle contributions, each of them containing n sums and n integrals to perform on an abelianized integrand.

In section 4.4 we take the weak coupling limit ($g^2 \rightarrow 0$) of the octagon and show the structure it takes when expressed in terms of well known Ladder integrals at each loop order. In appendix F.2 we provide technical details on how to efficiently perform the n -particle integrals by residues. We also provide explicit expressions for the non-vanishing integrals up to nine loops in appendix F.3.

In section 4.5 we use hexagonalization to construct the polarized four-point functions. We start by reviewing the hexagonalization prescription focusing on the skeleton graphs. Then we work out in detailed how to express the *simplest* and *asymptotic* four point functions in terms of the octagons of sections 4.3 and 4.4. In this way we obtain expressions for these correlators up to arbitrary loop order provided the external scaling dimensions are large enough. In appendix D.1 we provide a comprehensive list of cross ratios we use throughout this section and the next.

In section 4.6 we test our results up to nine loops. For this we extract nine-loop OPE data from our octagon prediction for the *asymptotic* correlator. Then we reproduce these OPE coefficients by solving Beisert-Staudacher equations and using the BKV hexagon formula for three-point functions. The agreement is perfect.

This section is supplemented by appendix D.3 containing the 4D long super-conformal blocks and their OPE expansion in radial coordinates, appendix D.4 that shows the organization of the OPE data into sum rules at weak coupling, appendix F.4 containing some explicit nine-loop sum rules

4.3 The octagon

In this section we construct the octagon form factor which will serve as a building block of our polarized four-point functions. We consider an octagon with four physical and four mirror edges with the corresponding BMN vacuum at each edge. This octagon depends on

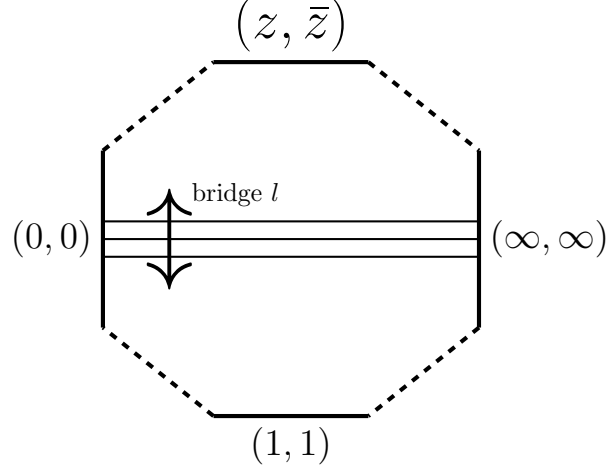


Figure 4.3: octagon

the bridge length l given by the number of Wick contractions between physical edges at $(0, 0)$ and (∞, ∞) . It also depends on the spacetime cross ratios (z, \bar{z}) and the R -charge cross ratios $(\alpha, \bar{\alpha})$, which in figure 4.3 come as the coordinates of the top physical edge.

The octagon can be decomposed into two hexagons by means of the insertion of a complete set of states along a mirror cut. We consider this cut to stretch between the operators connected by the bridge length l . Gluing back the two hexagons by resumming all intermediate states ψ we recover the octagon as:

$$\mathbb{O}_l = \sum_{\psi} \begin{array}{c} (z, \bar{z}) \\ \text{Hexagon } \mathcal{H}_2 \\ \psi \\ \text{Bridge } l \\ \bar{\psi} \\ \text{Hexagon } \mathcal{H}_1 \\ (1, 1) \end{array} \begin{array}{c} (0, 0) \\ \text{---} \\ (\infty, \infty) \end{array} = \sum_{\psi} \langle \mathcal{H}_2 | \psi \rangle \mu_{\psi} e^{-E_{\psi} l} \langle \psi | \mathcal{H}_1 \rangle \quad (4.4)$$

The measure μ_ψ gives the cost to create the state ψ at the mirror cut. The Boltzmann factor $e^{-E_\psi l}$ which controls this expansion weighting each state according to its energy E_ψ and the bridge length l it propagates through. We also use the short-hand notation $\langle \mathcal{H}_i | \psi \rangle$ (or the conjugate $\langle \psi | \mathcal{H}_i \rangle$) for the hexagon form factors which have a single non-trivial state ψ .

Both hexagon operators \mathcal{H}_1 and \mathcal{H}_2 can be brought to the standard hexagon \mathcal{H} defined in appendix F.1.2, which is independent of the cross ratios and only depends on the coupling. This is achieved by means of a similarity transformation which when acted upon the mirror states brings new chemical potentials:

$$\mathbb{O}_l(z, \bar{z}, \alpha, \bar{\alpha}) = \sum_{\psi} \langle \mathcal{H} | \psi \rangle \mu_\psi e^{-E_\psi l} e^{i p_\psi \log(z\bar{z})} e^{i L_\psi \phi} e^{i R_\psi \theta} e^{i J_\psi \varphi} \langle \psi | \mathcal{H} \rangle \quad (4.5)$$

The cross ratios now enter through the angle variables:

$$\phi = -\frac{i}{2} \log\left(\frac{z}{\bar{z}}\right) \quad \theta = -\frac{i}{2} \log\left(\frac{\alpha}{\bar{\alpha}}\right) \quad \varphi = \frac{1}{2} \log\left(\frac{\alpha\bar{\alpha}}{z\bar{z}}\right) \quad (4.6)$$

and the corresponding conjugate charges are: the angular momentum L_ψ , the R-charges R_ψ and J_ψ . Including also the momentum p_ψ conjugate to translation.

Using the details about the multi-particle mirror basis ψ and the hexagon form factors $\langle \mathcal{H} | \psi \rangle$ provided in appendix F.1, we can express the octagon as a sum over the number of particles n . Including an integral over the rapidity u_i and a sum over the bound state number a_i for each particle. More precisely this is:

$$\mathbb{O}_l(z, \bar{z}, \alpha, \bar{\alpha}) = 1 + \sum_{n=1}^{\infty} \mathcal{X}_n(z, \bar{z}, \alpha, \bar{\alpha}) \times \mathcal{I}_{n,l}(z, \bar{z}) \quad (4.7)$$

where the unity stands for the vacuum contribution and the factor \mathcal{X}_n that we name the character is given by:

$$\mathcal{X}_n(z, \bar{z}, \alpha, \bar{\alpha}) = \frac{(\mathcal{X}^+)^n + (\mathcal{X}^-)^n}{2} \quad (4.8)$$

with:

$$\mathcal{X}^+ = -\frac{(z - \alpha)(\bar{z} - \alpha)}{\alpha} \quad \text{and} \quad \mathcal{X}^- = -\frac{(z - \bar{\alpha})(\bar{z} - \bar{\alpha})}{\bar{\alpha}} \quad (4.9)$$

The n -particle sum and integral $\mathcal{I}_{n,l}$ is given by:

$$\mathcal{I}_{n,l}(z, \bar{z}) = \frac{1}{n!} \sum_{a_1=1}^{\infty} \cdots \sum_{a_n=1}^{\infty} \int du_1 \cdots \int du_n \prod_{j=1}^n \bar{\mu}_{a_j}(u_j, l, z, \bar{z}) \times \prod_{j < k}^n P_{a_j a_k}(u_j, u_k) \quad (4.10)$$

The integrand contains the coupling dependence and is composed as follows:

- The one-particle effective measure $\bar{\mu}$ where we package the chemical potentials for each particle:

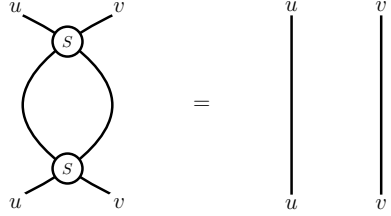
$$\bar{\mu}_a(u, l, z, \bar{z}) = \frac{1}{\sqrt{z\bar{z}}} \frac{\sin a\phi}{\sin \phi} \times \mu_a(u) \times e^{-E_a(u)l} \times (z\bar{z})^{-i p_a(u)} \quad (4.11)$$

where the one-particle measure $\mu_a(u)$, energy $E_a(u)$ and momentum $p_a(u)$ are defined in (F.2).

- The (abelian) symmetric product of two-particle hexagon form factors $P_{ab}(u, v)$ defined in (F.8).

Two comments are in order regarding the simplicity of the integrand (4.10) and the structure of the character (4.8):

- **The matrix part simplifies:** The hexagon form factors are in general complicated tensors with as many $\mathfrak{su}(2|2)^2$ flavour indexes as the number of particles. For a n -particle state this matrix part is constructed multiplying n copies of the $\mathfrak{su}(2|2)$ Beisert's S -matrix (see appendix F.1.2). Fortunately when contracting $\langle\psi|\mathcal{H}\rangle$ and $\langle\mathcal{H}|\psi\rangle$ these tensors simplified as shown in figure 4.4, thanks to the unitarity of the S -matrix:


(4.12)

This simplification does not happen when the hexagons have other non-trivial states on different edges. These non-trivial cases will not show up in our polarized four-point functions of section 4.5.

- **Prescription for character \mathcal{X}_n :** A complete knowledge of the mirror basis is an essential ingredient to carry on with hexagonalization. However its construction as representations of $\mathfrak{psu}(2|2)^2$ comes with ambiguities associated to the action of super-charges which, in principle, can introduce an arbitrary number of so-called Z -markers (see section 5.1 in [6]). These markers represent the insertion or deletion of the vacuum field Z and change the R -charge J_ψ in (4.5).

We still lack a physical interpretation of how to correctly take them into account in the mirror basis. Nevertheless an empirical prescription was proposed in [6] for the one-particle states and generalized to multi-particle states in [7]. We are instructed to include these markers in two different ways and then take the average. This results in the average that takes place in the definition of the character \mathcal{X}_n , see equation (4.8).

This prescription has so far only been tested at one loop and it is important to remark that at this order other prescriptions could work. In order to get rid of this ambiguity, in this chapter, we will perform a test as far as nine loops using our polarized four-point functions. At this order we receive for the first time a contribution from $\mathcal{X}_{n=3}$ and this will give us strong evidence for this prescription.

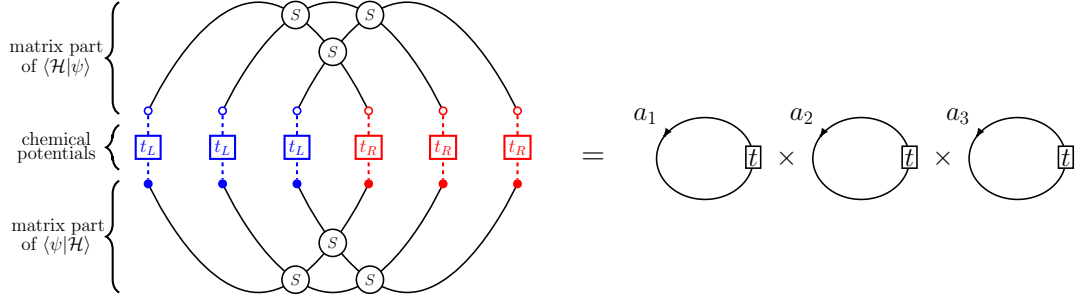


Figure 4.4: On the left the tensorial contraction of two hexagon form factors of three mirror particles with bound state numbers a_i . The dashed lines denote the sum over $\mathfrak{psu}(2|2)_L \times \mathfrak{psu}(2|2)_R$ flavour indexes on each representation a_i . The twists $t_{L,R}$ account for the chemical potentials which act on each copy $\mathfrak{psu}(2|2)_L$ and $\mathfrak{psu}(2|2)_R$. Using the invariance of $\mathfrak{psu}(2|2)$ Beisert's S -matrix under the twists and unitarity (4.12) we simplify this contraction. The result is a product of three twisted transfer matrices (with twist $t = t_L t_R$) on representations a_i .

4.4 Octagons at weak coupling

In this section we take the weak coupling limit of the mirror integrals (4.10). The coupling enters in the components of the integrand exclusively through the Zhukovsky variable:

$$x^{[\pm a]}(u) = x(u \pm \frac{i}{2}a) \quad \text{and} \quad x(u) = \frac{u + \sqrt{u^2 - 4g^2}}{2g} \quad (4.13)$$

This square-root branch cut whose size is controlled by the magnitude of the coupling develops in to a series of poles in the limit $g \rightarrow 0$:

$$x^{[\pm a]} = \frac{u \pm \frac{i}{2}a}{g} - \frac{g}{u \pm \frac{i}{2}a} - \frac{g^3}{(u \pm \frac{i}{2}a)^3} - \frac{2g^5}{(u \pm \frac{i}{2}a)^5} - \frac{5g^7}{(u \pm \frac{i}{2}a)^7} + \mathcal{O}(g)^9 \quad (4.14)$$

These poles lie on the imaginary axis $\pm \frac{i}{2}a$ and their degree match the exponent of g .

This simple structure of poles is inherited by the mirror integrand. In more detail, the integrand only contains poles on single variables with generic form $(u_j \pm \frac{i}{2}a_j)^\#$. This can be appreciated on the leading order expansion of the one-particle component:

$$\begin{aligned} \mu_a(u) &= a \frac{g^2}{(u^2 + \frac{a^2}{4})^2} + \mathcal{O}(g)^4 \\ e^{-E_a(u)} &= \frac{g^2}{(u^2 + \frac{a^2}{4})} + \mathcal{O}(g)^4 \quad \text{and} \quad p_a(u) = u + \mathcal{O}(g)^2 \end{aligned} \quad (4.15)$$

and the two-particle interaction:

$$P_{ab}(u, v) = g^4 \frac{\left((u-v)^2 + \frac{(a-b)^2}{4} \right) \left((u-v)^2 + \frac{(a+b)^2}{4} \right)}{(u^2 + \frac{a^2}{4})^2 (v^2 + \frac{b^2}{4})^2} + \mathcal{O}(g)^6 \quad (4.16)$$

This latter component contains differences between rapidities $(u-v)$, but these only appear in the numerator and can be easily expanded out. By doing so we are able to disentangle the integration variables and with that the integrals that we need to evaluate.

The upshot of this analysis is that the multivariable mirror integrals can be expanded at weak coupling into sums of products of one-variable integrals. In appendix F.2 we identify a basis of these one-variable integrals and use it to algorithmically find the mirror integrals, in principle, at arbitrary loop order. The result is explicitly obtained in terms of polylogarithms.

Another observation that adds to the simplicity of this expansion is the delay of the n -particle state to start contributing only at $n(n+l)$ -loop order:

$$\prod_{j=1}^n \bar{\mu}_{a_j}(u_j) \times \prod_{j < k} P_{a_j a_k}(u_j, u_k) = \mathcal{O}(g^2)^{n(n+l)} \quad (4.17)$$

For instance we would have to reach nine loops to have a first contribution from the three-particle mirror state (when $l = 0$). This is the reason we go to this high loop order in section 4.6 to test our results.

Using a **Mathematica** implementation of the algorithm described in appendix F.2 we made an explicit computation of the mirror integrals up to $n = 4$ and up to 17 loops for bridges $l = 0, 1, 2$. In all these cases we were able to express our results as:

$$\mathcal{I}_{n,l} = \sum_{j=n(n+l)}^{\infty} (g^2)^j \sum_{k_1+\dots+k_n=j} d_{l;k_1,\dots,k_n} F_{k_1} \cdots F_{k_n} \quad (4.18)$$

where we only consider positive integer partitions $\{k_1, \dots, k_n\} \in \mathbb{Z}^+$ and the basis of singled-valued conformal ladder integrals is given by [108]:

$$F_L(z, \bar{z}) = \frac{1}{z - \bar{z}} \sum_{m=0}^L \frac{(-1)^m (2L-m)!}{L!(L-m)!m!} (\log(z\bar{z}))^m (\text{Li}_{2L-m}(z) - \text{Li}_{2L-m}(\bar{z})) \quad (4.19)$$

The coefficients $d_{l;k_1,\dots,k_n}$ depend on the bridge length l and could be zero for some integer partitions. We know them explicitly up to high loop orders for the cases aforementioned, but we were unable to find them in closed form.

This way of expressing our results makes manifest single-valuedness in the Euclidean regime and also the uniform and maximal transcendentality at each loop order.

In (4.20) we present the octagon form factor with bridge length $l = 0$ up to nine loops. We highlight the $n = 1, 2, 3$ mirror integrals $\mathcal{I}_{n,l=0}$ in red, blue and magenta respectively, they go dressed with the corresponding character \mathcal{X}_n as:

$$\begin{aligned}
\mathbb{O}_{l=0} = & 1 + g^2 (\mathcal{X}_1 F_1) + g^4 (-2 \mathcal{X}_1 F_2) + g^6 (6 \mathcal{X}_1 F_3) + g^8 \left(-20 \mathcal{X}_1 F_4 + \mathcal{X}_2 \left(-\frac{F_2^2}{3} + F_1 F_3 \right) \right) \\
& + g^{10} (70 \mathcal{X}_1 F_5 + \mathcal{X}_2 (F_2 F_3 - 6 F_1 F_4)) \\
& + g^{12} \left(-252 \mathcal{X}_1 F_6 + \mathcal{X}_2 \left(-\frac{9 F_3^2}{5} + \frac{4 F_2 F_4}{5} + 28 F_1 F_5 \right) \right) \\
& + g^{14} \left(92 \mathcal{X}_1 F_7 + \mathcal{X}_2 \left(\frac{36 F_3 F_4}{5} - 16 F_2 F_5 - 120 F_1 F_6 \right) \right) \\
& + g^{16} \left(-3432 \mathcal{X}_1 F_8 + \mathcal{X}_2 \left(-\frac{486 F_4^2}{35} - \frac{9 F_3 F_5}{7} + \frac{690 F_2 F_6}{7} + 495 F_1 F_7 \right) \right) \\
& + g^{18} \left(12870 \mathcal{X}_1 F_9 + \mathcal{X}_2 \left(\frac{465 F_4 F_5}{7} - \frac{1203 F_3 F_6}{14} - \frac{979 F_2 F_7}{2} - 2002 F_1 F_8 \right) \right. \\
& \quad \left. + \mathcal{X}_3 \left(-\frac{F_3^3}{20} + \frac{F_2 F_3 F_4}{5} - \frac{3 F_1 F_4^2}{5} - \frac{F_2^2 F_5}{3} + F_1 F_3 F_5 \right) \right) \\
& + \mathcal{O}(g)^{20}
\end{aligned} \tag{4.20}$$

This octagon is the building block of the *simplest* four-point function introduced in section 4.5.2. We have similar expression for other octagons with different bridge lengths which are relevant for the *asymptotic* four point function introduced in 4.5.3. In appendix F.3 we provide all non-vanishing mirror integrals up to nine loops.

4.5 Hexagonalization of polarized four-point functions

In this section we use hexagonalization to compute some polarised four-point functions of protected operators with equal scaling dimension. We consider a limit of large R-charges which leads to a factorization of the correlator into octagon form factors. We first review the starting point of the hexagonalization prescription: the skeleton graphs. Then in sections 4.5.2 and 4.5.3 we construct the projected correlators named as *simplest* and *asymptotic* using octagons.

4.5.1 Skeleton graphs and hexagonalization

As prescribed in [6] to compute a planar four-point function we first need to identify the skeleton graphs. We start by considering a four-point function of scalar $\frac{1}{2}$ -BPS operators with generic $\mathfrak{so}(6)$ polarizations and scaling dimension K :

$$\mathcal{O}(x_i, y_i) = \text{Tr} (y_i \cdot \Phi(x_i))^K \tag{4.21}$$

where x_i gives the space-time position and y_i is a six dimensional null vector $y_i \cdot y_i = 0$ that specifies the $\mathfrak{so}(6)$ R-charge when contracted with the vector of six real scalars $\Phi = (\phi_1 \phi_2 \phi_3 \phi_4 \phi_5 \phi_6)$.

For the planar connected four-point function of operators (4.21) the skeleton graphs are given by the Wick contractions in the tree level correlator³

$$\begin{aligned}
\langle \mathcal{O}(x_1, y_1) \mathcal{O}(x_2, y_2) \mathcal{O}(x_3, y_3) \mathcal{O}(x_4, y_4) \rangle^{(0)} = & \\
& \sum_{l_{12}=1}^{K-1} \left(\text{Diagram 1} \right) + \sum_{l_{14}=1}^{K-1} \left(\text{Diagram 2} + \text{Diagram 3} \right) \\
& + \sum_{l_{14}=1}^{K-2} \sum_{l_{12}=1}^{K-l_{14}-1} \left(\text{Diagram 4} + \text{Diagram 5} \right) \quad (4.22)
\end{aligned}$$

The diagrams represent skeleton graphs with four vertices $\mathcal{O}_1, \mathcal{O}_2, \mathcal{O}_3, \mathcal{O}_4$. Diagram 1 shows a square with multiple lines between adjacent vertices, labeled l_{12} for the top edge. Diagram 2 shows a square with multiple lines between adjacent vertices, labeled l_{14} for the top edge. Diagram 3 shows a square with multiple lines between adjacent vertices, labeled l_{14} for the top edge. Diagram 4 shows a square with multiple lines between adjacent vertices, labeled l_{12} for the top edge and l_{14} for the top edge. Diagram 5 shows a square with multiple lines between adjacent vertices, labeled l_{12} for the top edge and l_{14} for the top edge.

where each line connecting two operators \mathcal{O}_i and \mathcal{O}_j represents a tree level propagator $\frac{y_i \cdot y_j}{x_{ij}^2}$ and their number is given by the bridge length l_{ij} . The bridges left implicit are fixed by the condition $K = K_i = \sum_{j \neq i}^4 l_{ij}$. In particular this sets the identifications: $l_{12} = l_{34}$, $l_{13} = l_{24}$, $l_{14} = l_{23}$ for all skeleton graphs.

It is useful to make manifest conformal invariance by defining a reduced correlator after stripping out a simple factor:

$$\mathcal{G}_K(u, v, \sigma, \tau) = \left(\frac{x_{12}^2 x_{34}^2}{(y_1 \cdot y_2)(y_3 \cdot y_4)} \right)^{\frac{K}{2}} \langle \mathcal{O}(x_1, y_1) \mathcal{O}(x_2, y_2) \mathcal{O}(x_3, y_3) \mathcal{O}(x_4, y_4) \rangle \quad (4.23)$$

This reduced four-point function only depends on the spacetime cross ratios:

$$u = z\bar{z} = \frac{x_{12}^2 x_{34}^2}{x_{13}^2 x_{24}^2} \quad \text{and} \quad v = (1-z)(1-\bar{z}) = \frac{x_{14}^2 x_{23}^2}{x_{13}^2 x_{24}^2} \quad (4.24)$$

and R -charge cross ratios:

$$\sigma = \alpha\bar{\alpha} = \frac{(y_1 \cdot y_2)(y_3 \cdot y_4)}{(y_1 \cdot y_3)(y_2 \cdot y_4)} \quad \text{and} \quad \sigma = (1-\alpha)(1-\bar{\alpha}) = \frac{(y_1 \cdot y_4)(y_2 \cdot y_3)}{(y_1 \cdot y_3)(y_2 \cdot y_4)} \quad (4.25)$$

At tree level the reduced four-point function can be expressed as:

$$\mathcal{G}_K^{(0)}(u, v, \sigma, \tau) = \sum_{r=1}^{K-1} (G_{0,r,K-r} + G_{r,0,p-r} + G_{r,K-r,0}) + \sum_{r=2}^{K-1} \sum_{s=1}^{r-1} G_{s,r-s,K-r} \quad (4.26)$$

³ In the general unpolarized case disconnected graphs may need to be included as skeleton graphs, see appendix F in [99]. However for our polarized correlators they will not play a role.

where our notation $G_{l_{14}, l_{13}, l_{12}}$ serves to identify a skeleton graph through the non-identical bridges and also provides the tree level Wick contractions in terms of cross ratios as:

$$G_{l_{14}, l_{13}, l_{12}} \equiv \begin{cases} 2 \left(\frac{u}{\sigma}\right)^{l_{14}+l_{13}} \left(\frac{\tau}{v}\right)^{l_{14}}, & \text{if } l_{12} \neq 0 \& l_{13} \neq 0 \& l_{14} \neq 0, \\ \left(\frac{u}{\sigma}\right)^{l_{14}+l_{13}} \left(\frac{\tau}{v}\right)^{l_{14}}, & \text{otherwise} \end{cases} \quad (4.27)$$

The first three terms in (4.26) correspond to the three type of skeleton graphs at the top of (4.22). The fourth term represents the two types at the bottom of (4.22), which have the same spacetime dependence and can be simply combined explaining the factor of two in (4.27).

To incorporate the coupling dependence [6] prescribes to dress the skeleton graphs (4.22) with four hexagons which meet along six mirror cuts where we pose multi-particle mirror states. To recover the full-four-point function we must sum over all intermediate states on each cut on each skeleton graph:

$$\langle \mathcal{O}(x_1, y_1) \mathcal{O}(x_2, y_2) \mathcal{O}(x_3, y_3) \mathcal{O}(x_4, y_4) \rangle =$$

$\sum_{\{\psi_{ij}\}}$

$+ \dots + \sum_{\{\psi_{ij}\}}$

(4.28)

where the ellipsis accounts for the other skeleton graphs in (4.22).

When dealing with generic polarizations we need to consider every possible configuration of mirror states $\{\psi_{ij}\}$ on a tessellation. Technically speaking the taming of each of these contributions comes with different degrees of difficulty.

The simplest cases are given by configurations where only one mirror cut hosts non-trivial states and the other five only host the vacuum or when two non-adjacent cuts, such as 1-4 and 2-3, host non-trivial states and the other four only the vacuum. The former case is accounted by an octagon and the latter by the product of two octagons. As we pointed out in section 4.3, the octagon has a simple structure thanks to the outstanding simplicity of the tensor contraction of the two hexagons form factors in figure 4.4.

On the other hand the configurations that include non-trivial states on different edges of the same hexagon are significantly harder to deal with. These show up in the non-trivial gluing of three or four hexagon form factors. The simplest of this type of contributions corresponds to the two-particle string in figure 4.5. The tensor contraction in this case does not simplify and its complexity grows with the bound state number of the particles [7]⁴. Having non-trivial states turn on in all six mirror cuts is the most challenging case and would demand a huge effort even just to find its leading order contribution.

⁴In this reference the two-particle string was tamed at leading order in the context of five-point functions.

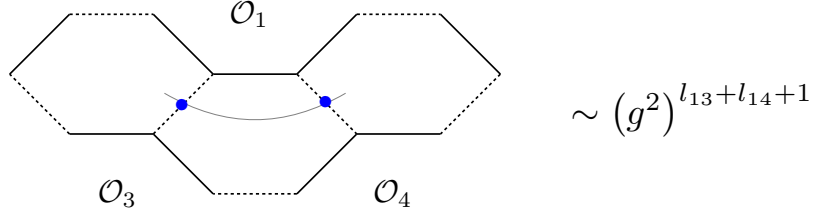


Figure 4.5: Two-particle string

We would like to consider a regime where the contributions of these “strings” of mirror particles can be neglected. This can be partially achieved in the limit of large external dimension $K \gg 1$. As this limit enforces large bridges in many skeleton graphs delaying their contributions to high loop orders. However it is not simple enough yet, as there are still some graphs which allow strings to kick in at low loop orders, such as $G_{l_{14}=0, l_{13}=K-1, l_{12}=1}$. In order to completely get rid of these strings we further consider special choices of R -charge external polarizations which project out these troublesome graphs. This will be such that by R -charge conservation only graphs containing four large bridges and two non-adjacent small bridges will contribute to the correlator.

In the next sections we present two instances of such polarized four-point functions which can be computed by composition of the octagons described in the previous section. We name these correlators as the *simplest* and *asymptotic* four-point functions.

Let us conclude this section by stressing we will be working in the weak coupling regime $g \rightarrow 0$ so we are considering an expansion of the four-point function as:

$$\mathcal{G}_K(u, v, \sigma, \tau) = \mathcal{G}_K^{(0)}(u, v, \sigma, \tau) + \sum_{m=1}^{\infty} (g^2)^m \mathcal{G}_K^{(m)}(u, v, \sigma, \tau) \quad (4.29)$$

4.5.2 The *simplest* four-point function

Our simplest choice of polarised external operators consists of:

$$\begin{aligned} O_1 &= Tr(Z^{\frac{K}{2}} \bar{X}^{\frac{K}{2}}) + \text{cyclic permutations} & O_2 &= Tr(X^K) \\ O_3 &= Tr(\bar{Z}^K) & O_4 &= Tr(Z^{\frac{K}{2}} X^{\frac{K}{2}}) + \text{cyclic permutations} \end{aligned} \quad (4.30)$$

where cyclic permutation means that we only keep one instance of all permutations that are cyclically identified. At tree level this correlator is given by a single graph as shown in figure 4.6.

This *simplest* four-point can be extracted from the general correlator by choosing the

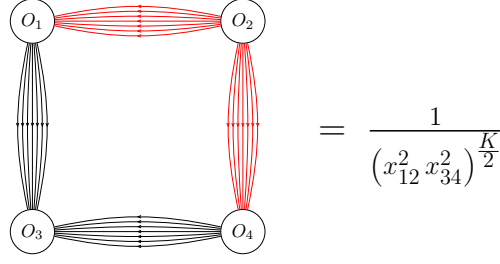


Figure 4.6: The *simplest* four-point function with projected external operators $O_1(0) = \text{Tr} \left(Z^{\frac{K}{2}} \bar{X}^{\frac{K}{2}} \right)$, $O_2(z) = \text{Tr} \left(X^K \right)$, $O_3(1) = \text{Tr} \left(\bar{Z}^K \right)$ and $O_4(\infty) = \text{Tr} \left(Z^{\frac{K}{2}} \bar{X}^{\frac{K}{2}} \right)$. The Wick contractions form a perimeter with four bridges of width $\frac{K}{2}$.

polarization vectors as:

$$\begin{aligned} y_1 &= \frac{1}{\sqrt{2}}(1, i, 0, 0, \beta_1, i\beta_1) & y_2 &= \frac{1}{\sqrt{2}}(0, 0, 0, 0, 1, -i) \\ y_3 &= \frac{1}{\sqrt{2}}(1, -i, 0, 0, 0, 0) & y_4 &= \frac{1}{\sqrt{2}}(1, i, 0, 0, \beta_4, i\beta_4) \end{aligned} \quad (4.31)$$

performing $\frac{K}{2}$ derivatives with respect to each auxiliary parameter β_1 and β_4 , to then set them to zero:

$$\begin{aligned} \langle O_1(x_1)O_2(x_2)O_3(x_3)O_4(x_4) \rangle &= \\ &= \left(\frac{\partial}{\partial \beta_1} \frac{\partial}{\partial \beta_4} \right)^{\frac{K}{2}} \langle \mathcal{O}(x_1, y_1) \mathcal{O}(x_2, y_2) \mathcal{O}(x_3, y_3) \mathcal{O}(x_4, y_4) \rangle \Big|_{\beta_1, \beta_4=0} \end{aligned} \quad (4.32)$$

We can as well define this projection as an operation on the R -charge cross ratios σ, τ of the super-correlator. For this we first define the reduce *simplest* four-point function as:

$$\mathbb{S}_K(z, \bar{z}) = (x_{12}^2 x_{34}^2)^{\frac{K}{2}} \langle O_1(x_1)O_2(x_2)O_3(x_3)O_4(x_4) \rangle \quad (4.33)$$

From this definition it follows we can effectively perform the projection on the reduced super-correlator by extracting the coefficient of $\sigma^{-\frac{K}{2}}$ and setting $\tau = 0$:

$$\mathbb{S}_K(z, \bar{z}) = \mathcal{G}_K(u, v, \sigma, \tau) \Big|_{\text{Coefficient of } \sigma^{-\frac{K}{2}}, \tau \rightarrow 0} \quad (4.34)$$

At tree level this gives:

$$\mathbb{S}_K^{(0)} = u^{\frac{K}{2}} = (z\bar{z})^{\frac{K}{2}} \quad (4.35)$$

We are interested in finding the loop corrections for this four-point function in the limit $K \gg 1$. Following hexagonalization, in this regime, we expect to have only the vacuum state on the large bridges $l_{12}, l_{13}, l_{24}, l_{34} \gg 1$. With this simplification we now only need

to consider the effect of the polarization on the skeleton graph(s) when dressed by two octagons, with mirror particles along cuts 1-4 and 2-3:

$$\begin{array}{c} \text{?} \\ \neq 0 \end{array} \quad (4.36)$$

Coefficient of $\sigma^{-\frac{K}{2}}, \tau \rightarrow 0$

For this we need to focus on the character \mathcal{X}_n , which is responsible for changing the original R -charge dependence of a skeleton graph and allow it to survive our *simplest* projection. In order to find out which are these surviving graphs we rewrite the character in terms of cross ratios σ and τ :

$$\mathcal{X}_n = \frac{\left(\frac{-(z-\alpha)(\bar{z}-\alpha)}{\alpha}\right)^n + \left(\frac{-(z-\bar{\alpha})(\bar{z}-\bar{\alpha})}{\bar{\alpha}}\right)^n}{2} = \sum_{k=-n}^n \sigma^k f_{n,k}(z, \bar{z}, \tau) \quad (4.37)$$

In these variables the n -particle character can be written as a finite series on σ with integer exponents ranging from $-n$ to n and coefficients given by the polynomials $f_{n,k}(z, \bar{z}, \tau)$. From this we learn the character \mathcal{X}_n can change the exponent of σ in a skeleton graph by a shift of at most $\pm n$. Later these shifts are further enhanced when considering the product of the two octagons. On the other hand, due to the polynomiality of $f_{n,k}$ in τ , the effect of the character over graphs with τ dependence such as those with $l_{14}, l_{23} \neq 0$ is to maintain it or increase its positive exponent. Thus we do not need to include this type of graphs as they will vanish when taking $\tau \rightarrow 0$ in our projection.

In conclusion, the graphs that survive the *simplest* projection have $l_{14} = l_{23} = 0$ and can have some shifts on the other bridge lengths compare to the length $\frac{K}{2}$ in the original tree level graph of figure 4.6. These shifts depend on the loop order as this truncates the number of mirror particles n . For instance at one-loop only one-particle states show up, exclusively on cut 1-4 or cut 2-3, and only the three skeleton graphs in figure 4.7 contribute. These are the original tree level graph and two neighbors which survive thanks to the character \mathcal{X}_1 . At two-loops we can have a one-particle state in each mirror cut 1-4 and 2-3, which gives \mathcal{X}_1^2 and with that a maximal of shift of ± 2 on the bridges at the perimeter. As we go to higher loops the admissible number of particles increases and with that also the number of neighboring skeleton graphs.

loop order Λ	1	2	3	4	5	6	7	8	9	10	11	12	13
m_Λ	1	2	2	2	3	3	3	4	4	4	4	4	5

Table 4.1: Maximal shifts m_Λ at each loop order Λ

In table 4.1 we present the maximal shift $\pm m_\Lambda$ at loop order Λ . At this order we

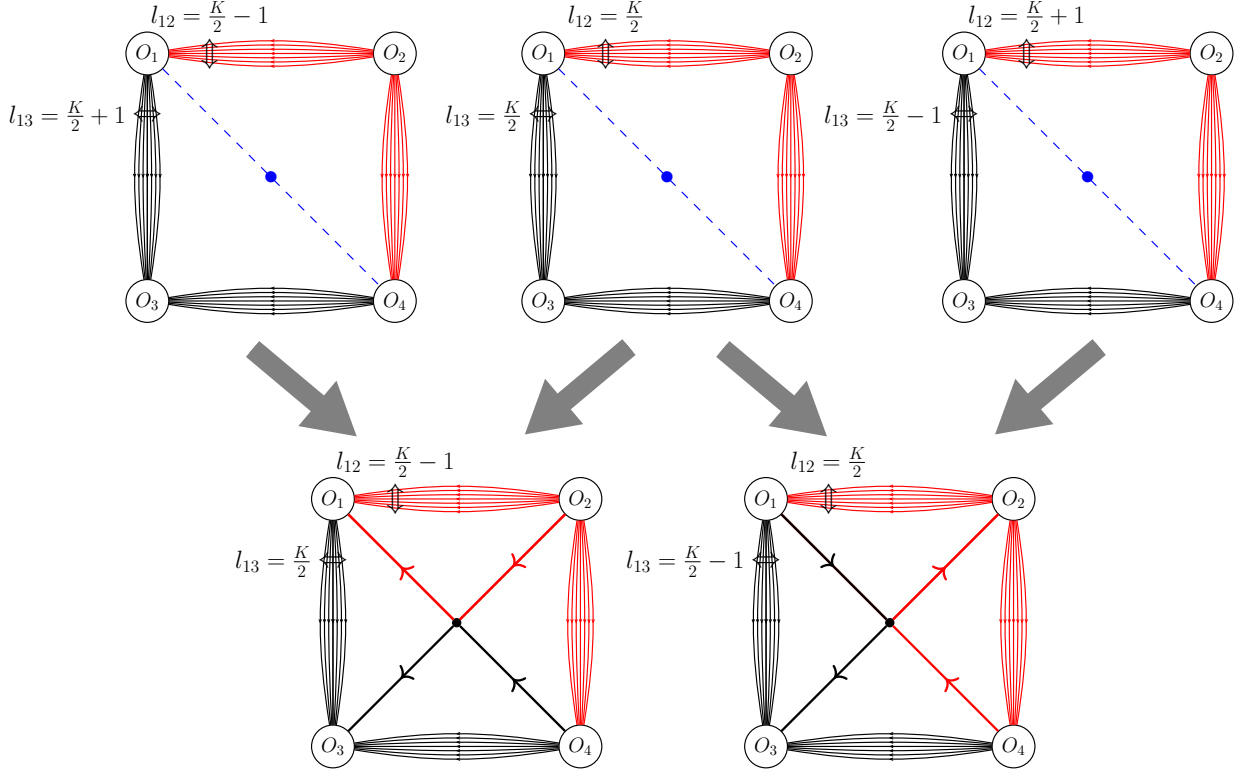


Figure 4.7: At the top the skeleton graphs that we need to hexagonalize and add up to obtain the one-loop *simplest* four-point function. At the bottom an interpretation of the neighboring graphs in terms of Feynman diagrams.

need to include skeleton graphs with σ powers going from σ^{-K-m_Λ} to σ^{-K+m_Λ} . Thus the hexagonalization of the *simplest* correlator at the first loop orders goes schematically as:

$$\begin{aligned}
\mathbb{S}_K^{(0)} &= u^{\frac{K}{2}} \\
\mathbb{S}_K^{(1)} &= \left(\frac{u}{\sigma}\right)^{\frac{K}{2}} \left(\frac{1}{\sigma} + 1 + \sigma\right) (1 + \mathcal{X}_1 \mathcal{I}_{1,0})^2 \Big|_{\text{coefficient of } (g^2 \sigma^{-K/2}), \tau \rightarrow 0} \\
\mathbb{S}_K^{(2)} &= \left(\frac{u}{\sigma}\right)^{\frac{K}{2}} \left(\frac{1}{\sigma^2} + \frac{1}{\sigma} + 1 + \sigma + \sigma^2\right) (1 + \mathcal{X}_1 \mathcal{I}_{1,0})^2 \Big|_{\text{coefficient of } (g^4 \sigma^{-K/2}), \tau \rightarrow 0} \\
&\vdots \\
\mathbb{S}_K^{(5)} &= \left(\frac{u}{\sigma}\right)^{\frac{K}{2}} \left(\frac{1}{\sigma^3} + \frac{1}{\sigma^2} + \frac{1}{\sigma} + 1 + \sigma + \sigma^2 + \sigma^3\right) (1 + \mathcal{X}_1 \mathcal{I}_{1,0} + \mathcal{X}_2 \mathcal{I}_{2,0})^2 \Big|_{\text{coefficient of } (g^{10} \sigma^{-K/2}), \tau \rightarrow 0}
\end{aligned} \tag{4.38}$$

The contributions of these new skeleton graphs can be resummed at each loop order and then repackaged to obtain a compact expression for the *simplest* correlator, valid at

any loop order for sufficiently large K :

$$\mathbb{S}_K = u^{\frac{K}{2}} \times \mathbb{O}_{l=0}^2 \big|_{\mathcal{X}_n \rightarrow \mathcal{X}_n^{(s)}} \quad (4.39)$$

This is simply the original tree level correlator times the squared of the octagon in (4.20) with the character replaced by the polarized effective character:

$$\mathcal{X}_n^{(s)} = (-v)^n = (-(1-z)(1-\bar{z}))^n \quad (4.40)$$

Given the simplicity of (4.39), with the dependence on K totally factorized in the prefactor, we are tempted to claim this expression should be valid at finite coupling provided $K \rightarrow \infty$.

The regime of validity for finite K

We can have an estimate for the smallest value of K for which (4.39) holds up to a given loop order Λ . In our criteria we demand that all neighboring skeleton graphs have bridge lengths l_{12} or l_{13} larger than Λ . This guarantees we can neglect including mirror particles along those bridges.

Considering the smallest bridge is given by $\frac{K}{2} - m_\Lambda$, see table 4.1, our criteria sets the lower bound:

$$K \geq 2\Lambda + 2m_\Lambda \quad (4.41)$$

Below this bound, for instance $K = 2\Lambda + 2m_\Lambda - 2$ (we only consider even K), at loop order Λ we need to start including mirror particles over the non-zero bridges l_{12} and l_{13} and also the two-particle strings of figure 4.5 over bridges l_{14} - l_{13} or l_{14} - l_{12} .

This criteria might not be optimal and our estimated lower bound maybe too large. To be more rigorous we would need to take into account the R-charge dependence of the two-particle strings and see at which loop order they survive the *simplest* projection. We leave this for future work and for now we just stick to the possibly exaggerated bound (4.41).

4.5.3 The *asymptotic* four point function

In this section we consider the four-point function already studied in [1] from the OPE point of view, but now using hexagonalization. This consists of external operators:

$$\begin{aligned} \tilde{O}_1 &= Tr(Z^{\frac{K}{2}} \bar{X}^{\frac{K}{2}}) + \text{cyclic permutations} & \tilde{O}_2 &= Tr(\bar{X}^{\frac{K}{2}} Z^{\frac{K}{2}}) + \text{cyclic permutations} \\ \tilde{O}_3 &= Tr(\bar{Z}^{\frac{K}{2}} \bar{Y}^{\frac{K}{2}}) + \text{cyclic permutations} & \tilde{O}_4 &= Tr(Y^{\frac{K}{2}} \bar{Z}^{\frac{K}{2}}) + \text{cyclic permutations} \end{aligned} \quad (4.42)$$

The corresponding R -charge polarization are:

$$\begin{aligned} y_1 &= \frac{1}{\sqrt{2}}(1, i, 0, 0, \beta_1, -i\beta_1) & y_2 &= \frac{1}{\sqrt{2}}(1, i, 0, 0, \beta_2, i\beta_1) \\ y_3 &= \frac{1}{\sqrt{2}}(1, -i, \beta_3, -i\beta_3, 0, 0) & y_4 &= \frac{1}{\sqrt{2}}(1, -i, \beta_4, i\beta_4, 0, 0) \end{aligned} \quad (4.43)$$

and the *asymptotic* four-point is obtained by differentiating the super-correlator respect to the parameters β_i :

$$\langle \tilde{O}_1(x_1) \tilde{O}_2(x_2) \tilde{O}_3(x_3) \tilde{O}_4(x_4) \rangle = \left(\frac{\partial}{\partial \beta_1} \frac{\partial}{\partial \beta_2} \frac{\partial}{\partial \beta_3} \frac{\partial}{\partial \beta_4} \right)^{\frac{K}{2}} \langle \mathcal{O}(x_1, y_1) \mathcal{O}(x_2, y_2) \mathcal{O}(x_3, y_3) \mathcal{O}(x_4, y_4) \rangle \Big|_{\beta_i=0} \quad (4.44)$$

It is convenient to define the reduced correlator which only depends on the conformal cross ratios:

$$\mathbb{A}_K(z, \bar{z}) = (x_{12}^2 x_{34}^2)^{\frac{K}{2}} \langle \tilde{O}_1(x_1) \tilde{O}_2(x_2) \tilde{O}_3(x_3) \tilde{O}_4(x_4) \rangle \quad (4.45)$$

Then the R-charge projection can be effectively performed over (4.29) as:

$$\mathbb{A}_K(z, \bar{z}) = \mathcal{G}_K(u, v, \sigma, \tau) \Big|_{\text{Coefficient of } \sigma^{-K/2}, \tau \rightarrow 1} \quad (4.46)$$

At tree level the graphs surviving this projection satisfy $l_{12} = \frac{K}{2}$ and $l_{13} + l_{14} = \frac{K}{2}$, see figure 4.8. In the notation of (4.27) this is:

$$\mathbb{A}_K^{(0)} = \sum_{l=0}^{K/2} G_{l, \frac{K}{2}-l, \frac{K}{2}} = u^{\frac{K}{2}} + 2 \sum_{l=1}^{\frac{K}{2}-1} \frac{u^{\frac{K}{2}}}{v^l} + \frac{u^{\frac{K}{2}}}{v^{\frac{K}{2}}} \quad (4.47)$$

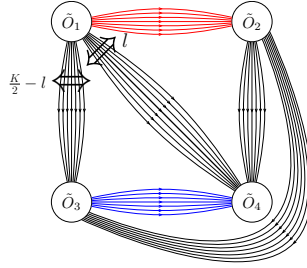


Figure 4.8: A tree level graph of the *asymptotic* four-point function with projected external operators $\tilde{O}_1(0) = \text{Tr}(Z^{K/2} \textcolor{red}{X}^{K/2})$, $\tilde{O}_2(z) = \text{Tr}(\textcolor{red}{X}^{K/2} Z^{K/2})$, $\tilde{O}_3(1) = \text{Tr}(\bar{Z}^{K/2} \textcolor{blue}{Y}^{K/2})$ and $\tilde{O}_4(\infty) = \text{Tr}(\bar{Z}^{K/2} \bar{\textcolor{blue}{Y}}^{K/2})$.

In the limit $K \gg 1$, to find the loop corrections, we need to identify the small bridge lengths which can host mirror particles. In this regime, we can have skeleton graphs with $l_{14}(l_{23})$ small and $l_{13}(l_{24}) \sim \frac{K}{2}$ large or the other way around but not both small at the same time, see figure 4.9. Thus the *asymptotic* correlator receives two types of contributions. The first(second) type comes from mirror particles on small bridges l_{14} and l_{23} (l_{13} and l_{24}). The first type is accounted by the product of two octagons with bridge parameters $l = l_{14} = l_{23}$ and cross ratios z, α (and conjugates). While the second type is also given by two octagons but now with bridge parameter $l = l_{13} = l_{24}$ and cross ratios $\frac{z}{z-1}, \frac{\alpha}{\alpha-1}$ ⁵ (and

⁵This change of cross ratios follow from the different relative positions of the physical edges, see figure 5 in [6]

conjugates). Then the loop corrections are obtained by simply adding up these two types of independent contributions.

As explained in the previous section, at loop level we can have new skeleton graphs with $l_{13} + l_{14} \neq \frac{K}{2}$ which survive the *asymptotic* projection (4.46) when dressed with mirror particles. We repeat the same exercise as in equation (4.38) identifying all skeleton graphs that survive at each loop order. Resumming those contributions we find the *asymptotic* correlator can be expressed as a sum over the original tree level graphs in (4.47), each dressed by a new effective octagon squared. We define this octagon as the *asymptotic* octagon:

$$\tilde{\mathbb{O}}_l(z, \bar{z}) = \mathbb{O}_l|_{\mathcal{X}_n \rightarrow \tilde{\mathcal{X}}_n} = 1 + \sum_{n=1}^{\infty} \tilde{\mathcal{X}}_n(z, \bar{z}) \mathcal{I}_{n,l}(z, \bar{z}) \quad (4.48)$$

with the corresponding effective character:

$$\tilde{\mathcal{X}}_n(z, \bar{z}) = (1 - v)^n = (z + \bar{z} - z\bar{z})^n \quad (4.49)$$

Using this definition the *asymptotic* four-point function is expressed in terms of the z -channel with mirror particles on $l_{14} = l_{13} = l$, and the $\frac{z}{z-1}$ -channel with mirror particles on $l_{13} = l_{24} = \frac{K}{2} - l$:

$$\mathbb{A}_K(z, \bar{z}) = \sum_{l=0}^{\frac{K}{2}} G_{l, \frac{K}{2}-l, \frac{K}{2}} \Big|_{\substack{\sigma \rightarrow 1 \\ \tau \rightarrow 1}} \left(\tilde{\mathbb{O}}_l^2(z, \bar{z}) + \tilde{\mathbb{O}}_{\frac{K}{2}-l}^2\left(\frac{z}{z-1}, \frac{\bar{z}}{\bar{z}-1}\right) - 1 \right) \quad (4.50)$$

or under a simple change of summation index:

$$\mathbb{A}_K(z, \bar{z}) = \sum_{l=0}^{\frac{K}{2}} \left(G_{l, \frac{K}{2}-l, \frac{K}{2}} \Big|_{\substack{\sigma \rightarrow 1 \\ \tau \rightarrow 1}} \times \tilde{\mathbb{O}}_l^2(z, \bar{z}) + G_{\frac{K}{2}-l, l, \frac{K}{2}} \Big|_{\substack{\sigma \rightarrow 1 \\ \tau \rightarrow 1}} \times \tilde{\mathbb{O}}_l^2\left(\frac{z}{z-1}, \frac{\bar{z}}{\bar{z}-1}\right) \right) - \mathbb{A}_K^{(0)}(z, \bar{z}) \quad (4.51)$$

where the (-1) in (4.50) and $(-\mathbb{A}_K^{(0)})$ in (4.51) remove the overcounting of tree level graphs.

Prediction (4.51) is only valid for loop orders below $\frac{K}{2}$. So in practice various octagons there can just be set to one, such as: $\tilde{\mathbb{O}}_{l=\frac{K}{2}} = 1 + O(g^{K+2})$.

4.5.4 An example for finite K and nine loops

Here we choose the minimum value of K for which prediction (4.50) is valid up to nine loops. For this we need to make sure the skeleton graphs surviving the *asymptotic* projection only admit particles on bridges l_{14} and l_{23} or exclusively on l_{13} and l_{24} . Under this criteria we set the minimum value as $K = 22$. In this case, at nine loops, the skeleton graphs to take into account are in the range:

$$9 \leq l_{13} + l_{14} \leq 15 \quad (4.52)$$

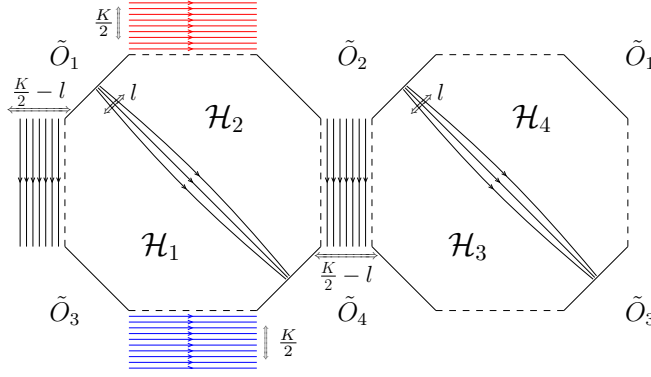


Figure 4.9: At a given loop order for sufficiently large K and small bridge l we have two decouple octagons: $\mathcal{H}_1 \cup \mathcal{H}_2$ and $\mathcal{H}_3 \cup \mathcal{H}_4$. When $l \sim \frac{K}{2}$, then the small bridge is $\frac{K}{2} - l$ and the decouple octagons are $\mathcal{H}_2 \cup \mathcal{H}_3$ and $\mathcal{H}_1 \cup \mathcal{H}_4$.

This lower bound on $l_{13} + l_{14}$ guarantees that we can ignore two-particle strings on l_{13} - l_{14} , as these would kick in at order $(g^2)^{l_{13}+l_{14}+1}$. There is yet a subtlety as this range also includes graphs with $l_{12} = 7$ and $l_{12} = 8$, which can host one-particle states at nine loops. However we have checked that these contributions do not survive the projection, so we ignore them.

Resumming the contributions from the skeleton graphs in (4.52) and using the *asymptotic* octagon we express the four point function in terms of graphs satisfying $l_{13} + l_{14} = 11$ only:

$$\mathbb{A}_{22}(z, \bar{z}) = \sum_{l=0}^{11} G_{l, 11-l, 11} \Big|_{\substack{\sigma \rightarrow 1 \\ \tau \rightarrow 1}} \left(\tilde{\mathcal{O}}_l^2(z, \bar{z}) + \tilde{\mathcal{O}}_{11-l}^2\left(\frac{z}{z-1}, \frac{\bar{z}}{\bar{z}-1}\right) - 1 \right) \quad (4.53)$$

This prediction can only be trusted up to nine loops. In this respect the corrections to $\mathbb{A}_{22}^{(0)}$ come more explicitly from:

$$\begin{aligned} \mathbb{A}_{22}(z, \bar{z}) - \mathbb{A}_{22}^{(0)}(z, \bar{z}) &= u^{11} \left(\tilde{\mathcal{O}}_{l=0}^2(z, \bar{z}) - 1 \right) + 2 \sum_{l=1}^8 \frac{u^{11}}{v^l} \left(\tilde{\mathcal{O}}_l^2(z, \bar{z}) - 1 \right) \\ &\quad + \left(z \rightarrow \frac{z}{z-1}, \bar{z} \rightarrow \frac{\bar{z}}{\bar{z}-1} \right) \end{aligned} \quad (4.54)$$

where we have only kept octagons which contribute non-trivially up to nine loops and $(z \rightarrow \frac{z}{z-1}, \bar{z} \rightarrow \frac{\bar{z}}{\bar{z}-1})$ denotes a contribution analog to the first line on the right hand side with the cross ratios changed as indicated.

In the following section we use this prediction to perform a OPE test up to nine loops. In appendix F.3 we provide the relevant mirror integrals that contribute to (4.54).

4.6 The OPE expansion: a test of the hexagonalization prediction

An alternative and more standard way of decomposing a four-point correlator is through the conformal operator product expansion. This is also realized through the insertion of a complete set of states but now along a physical cut as depicted in (4.55). In the effective world-sheet these are realized as closed string states and they correspond to the local operators in the spectrum of our 4D CFT, the eigenstates of the dilatation operator. This decomposition effectively expands the four-point function into products of three point functions, depicted as pair of pants⁶ in (4.55), of the exchanged operators and the external protected operators.

The diagram illustrates the operator product expansion (OPE) of a four-point correlator. On the left, a four-point correlator is represented as a genus-2 surface (a torus with two handles). The four boundary components are labeled \mathcal{O}_{BPS} . An arrow points to the center of the surface, labeled $\sum_{\Psi} |\Psi\rangle\langle\Psi|$ and "physical states BPS & non-BPS". This is set equal to a sum over "Bethe solutions". The summand is a squared term in large parentheses: $\left(\sum_{\text{Bethe roots } \alpha \cup \bar{\alpha}} \sum_{\text{Bethe roots}} \right)^2$. Inside the parentheses is a "pair of pants" diagram, which is a three-point function. It has two boundary components at the bottom labeled \mathcal{O}_{BPS} and one at the top labeled $\mathcal{O}_{\text{non-BPS}}$. The top boundary is further labeled with $\bar{\alpha}$ and α . The entire expression is multiplied by a "(super) conformal block". The equation is labeled (4.55) on the right.

In Chapter 2 we prescribed how to build all three-point functions necessary to, in principle, reconstruct the *asymptotic* four-point function \mathbb{A}_K in the limit of $K \gg 1$, see Chapter 3. There we performed a one-loop check of this prescription by constructing the three-point functions of the lowest lying operators dominating the OPE expansion in the channel $z, \bar{z} \rightarrow 0$ and comparing them against the coefficients in the OPE series of the one-loop correlator known from the literature.

We now endeavour to perform the same exercise but now up to nine-loops, comparing the OPE reconstruction against our octagon-based nine-loop prediction (4.53) for the *asymptotic* four-point function. We perform a minimal check in the sense that we will only match the leading OPE coefficients, but due to mixing, this already requires summing over hundreds of exchanged super-primaries. So we consider that this still constitutes a very non-trivial consistency check of the integrability methods we used to realized both mirror (hexagonalization) and physical (OPE) decompositions.

In short, our test consists in comparing the OPE data in tables 4.3, 4.4 extracted from the octagon prediction against the results of tables 4.5, 4.6 and 4.2 obtained from Bethe roots and the BKV hexagon formula for structure constants. In what follows we provide some of the details of this successful test.

⁶Here we only depict single-trace operators in this planar OPE, but in general double-trace operators should be present as well. However, as explained in Chapter 3, our asymptotic correlators only favoured single-traces in this OPE channel.

Extracting OPE data from octagon prediction and comparing with BKV hexagon prediction

At weak coupling the OPE data appears in sum rules containing the contributions of nearly-degenerate operators that share the same classical scaling dimension and global charges, see [Appendix D.4](#). Depending on whether we use ordinary conformal blocks or super-conformal blocks⁷ these sum rules will contain conformal primaries or only super-conformal primaries respectively. In the former case we identify the primary by its scaling dimension and spin $\{\Delta, s\}$ and in the latter case we need to include the $\mathfrak{so}(6)$ R-charge to identify the super-primary $\{\Delta, s, m, n\}$. Hence the super-expansion is a more refined decomposition that makes manifest the full symmetry.

Unfortunately this super-decomposition is only possible when we know the correlator with generic external R-charge polarizations, so can we can use the exponents of the cross ratios σ and τ (or α and $\bar{\alpha}$) to read off the R-charges of the states in the super-OPE. This is not the case for our asymptotic four-point function with specific polarizations. The best we can do in this case is use ordinary blocks and extract sum rules of nearly-degenerate conformal primaries. We report in [Table 4.3](#) and [Table 4.4](#) the lowest and next-to-lowest twist OPE data extracted from the nine-loop octagon-based prediction (4.53). The ordinary primary sum rules $P_{\{\Delta_0, s\}}^{(a,b)}$ are defined with the generating function:

$$\sum_{(\Delta, s) \in \text{Class}\{\Delta_0, s\}} C_{12(\Delta, s)} C_{(\Delta, s)34} r^\Delta = r^{\Delta_0} \sum_{a=0}^{\infty} (g^2)^a \sum_{b=0}^a \log(r)^b P_{\{\Delta_0, s\}}^{(a,b)} \quad (4.56)$$

where r is just a book keeping variable (or the radial coordinate of appendices [D.3, D.4](#)) and $\text{Class}\{\Delta_0, s\}$ stands for the family of conformal primaries (Δ, s) which become degenerate at zero-coupling ($g = 0$) with tree-level charges $\{\Delta_0, s\}$.

In order to perform our test we first need to find out how to write primary OPE sums in terms of super-primary OPE sums and then compute these latter by using finite Bethe roots and the BKV hexagon formula. The first task is easily achieved by performing the R-charge projection (4.46) over an Ansatz of the super-expansion and then expand it into ordinary conformal blocks. In this way we obtained the relations in [Table 4.5](#) and [Table 4.6](#), where the super-OPE sum rules $\mathcal{P}_{\{\Delta_0, s, n, m\}}^{(a,b)}$ are defined as:

$$\sum_{(\Delta, s, m, n) \in \text{Super-Class}\{\Delta_0, s, n, m\}} C_{KK(\Delta, s, m, n)}^2 r^\Delta = r^{\Delta_0} \sum_{a=0}^{\infty} (g^2)^a \sum_{b=0}^a \log(r)^b \mathcal{P}_{\{\Delta_0, s, n, m\}}^{(a,b)} \quad (4.57)$$

where *Super-Class* $\{\Delta_0, s, n, m\}$ stands for the family of super-conformal primaries (Δ, s, n, m) which become degenerate with tree-level charges $\{\Delta_0, s, n, m\}$ when turning off the coupling.

⁷A ordinary conformal block accounts for the contribution of a conformal multiplet: conformal primary and all its $\mathfrak{so}(4, 2)$ conformal descendants. While a super-block packages the contribution of a super-conformal multiplet which includes super-descendants, $\mathfrak{so}(4, 2)$ conformal and $\mathfrak{so}(6)$ R-symmetry descendants.

Finally we computed each individual structure constant on the left-hand side of (4.57) using our novel formula (2.56) for structure constants in higher-rank sectors. For this we first needed to identify each super-conformal multiplet in a given *Super-Class* $\{\Delta_0, s, n, m\}$ by finding the corresponding Bethe roots using the method introduced in Chapter 1. We report them in table 4.2 including the number of super-multiplets we identified on each *Super-Class*.

$\{\Delta_0, s, n, m\}$	# of Bethe solutions or super-multiplets	$\mathcal{P}^{(9,9)}$	$\mathcal{P}^{(9,0)}$
$\{20, 0, 9, 9\}$	10	$\frac{4978688}{945}$	-2755264512
$\{22, 0, 10, 10\}$	11	$\frac{4978688}{945}$	-2755264512
$\{24, 0, 11, 11\}$	12	$\frac{4978688}{945}$	-2755264512
$\{22, 2, 9, 9\}$	369	$\frac{632354992917077}{7440174000}$	$-\frac{3880272703256846017844314261170552101}{1008907523437500000000000000}$
$\{24, 2, 10, 10\}$	486	$\frac{2990537878301}{29760696}$	$-\frac{25906812477093695541612336367}{562220051373121536}$
$\{26, 2, 11, 11\}$	626	$\frac{1012348238189803}{8630601840}$	$-\frac{24206493839806735477486708172518503089}{445073004000599941716074496}$
$\{24, 0, 11, 9\}$	478	$\frac{1344109856}{19845}$	-41148586528
$\{24, 0, 10, 10\}$	$966 + 2 \times \textcolor{red}{371}$	$\frac{181961001311}{1086750}$	$-\frac{1561516641881791110594032737679}{1796875000000000000000}$

Table 4.2: The number of Bethe solutions or number of long super-multiplets on each of the 8 super-classes involved in our consistency check. The highlighted $\textcolor{red}{371}$ is number of $\mathfrak{so}(6)$ Bethe solutions with non-identical wings, which have vanishing structure constants according to the integrability-based selection rule found in Chapter 2.

With this super-data we were able to reconstruct the primary sum rules $\mathbf{P}_{\{\Delta_0, s\}}^{(9,0)}$ in tables 4.5 and 4.6, finding a perfect match with the octagon-based predictions in tables 4.3 and 4.4 (see also appendix F.4). We have also reconstructed all sum rules $\mathbf{P}_{\{\Delta_0, s\}}^{(a,b)}$ with $9 \geq a \geq b \geq 1$, finding perfect agreement as well.

Some final (technical) comments regarding this nine-loop test:

- We needed to work with a high numerical precision for the Bethe roots. This allowed us to obtain the sum rules with many decimal digits and be able to recognize the (complicated) rational numbers they represent.

In particular the existence of the nearly-exact strings of table 1.3 demands us to work with very high numerical precision when finding the loop corrections of the Bethe roots:

$$u_j^{(0)} \rightarrow u_j^{(1)} \rightarrow \dots \rightarrow u_j^{(9)} \quad (4.58)$$

The reason being that when we go from $u_j^{(0)}$ to $u_j^{(9)}$ the numerical precision severely drops and it is important that the decreased precision of $u_j^{(9)}$ is higher than 10^{-45} so it can still recognize the deviation from $\frac{i}{2}$ of the nearly-singular positions of $u_j^{(0)}$. This is important to not lose this information when using the BKV formula where combinations of the form $u_j^{(0)} \times u_j^{(9)}$ can appear.

- When constructing the super sum rules $\mathcal{P}_{\{24,0,10,10\}}^{(9,a)}$ we excluded the 371 $\mathfrak{so}(6)$ Bethe solutions with non-identical wings. This can be considered as a test of the vanishing of those structure constants according to the integrability selection rule found in [Chapter 2](#).
- Regarding the octagon, in detailed, this perfect matching at nine loops constitutes a successful test of the three-particle mirror integral $\mathcal{I}_{n=3,l=0}$ in [\(F.36\)](#) and with that also a test of the prescription of [\[6\]](#) for the \mathcal{Z} -markers on the mirror basis, which is manifest in [\(F.13\)](#) and the character [\(4.8\)](#).

Twist-22	Twist-24
$P_{\{24,2\}}^{(9,0)} = -2755264512$	$P_{\{24,0\}}^{(9,0)} = -2755264512$
$P_{\{26,4\}}^{(9,0)} = -\frac{25906812477093695541612336367}{562220051373121536}$	$P_{\{26,2\}}^{(9,0)} = -\frac{13565855042891885605834502859803364601}{1008907523437500000000000000}$

Table 4.3: Nine-loop sum rule $P_{\{\Delta_0,s\}}^{(9,0)}$. Appears in the non-logarithmic part of the OPE

Twist-22	Twist-24
$P_{\{24,2\}}^{(9,9)} = \frac{4978688}{945}$	$P_{\{24,0\}}^{(9,9)} = \frac{4978688}{945}$
$P_{\{26,4\}}^{(9,9)} = \frac{2990537878301}{29760696}$	$P_{\{26,2\}}^{(9,9)} = \frac{546998336876863}{1860043500}$

Table 4.4: Nine-loop sum rule $P_{\{\Delta_0,s\}}^{(9,9)}$. Goes dressed by $\log(z\bar{z})^9$ in the OPE.

Twist-22	Twist-24
$P_{\{24,2\}}^{(9,0)} = \mathcal{P}_{\{22,0,10,10\}}^{(9,0)}$	$P_{\{24,0\}}^{(9,0)} = \mathcal{P}_{\{20,0,9,9\}}^{(9,0)} - \mathcal{P}_{\{22,0,10,10\}}^{(9,0)} + \mathcal{P}_{\{24,0,11,11\}}^{(9,0)}$
$P_{\{26,4\}}^{(9,0)} = \mathcal{P}_{\{24,2,10,10\}}^{(9,0)}$	$P_{\{26,2\}}^{(9,0)} = (\text{see appendix } \a href="#">F.4)$

Table 4.5: Decomposition of sum rules $P^{(9,0)}$ into super-sum rules $\mathcal{P}^{(9,0)}$.

Twist-22	Twist-24
$\mathbf{P}_{\{24,2\}}^{(9,9)} = \mathcal{P}_{\{22,0,10,10\}}^{(9,9)}$	$\mathbf{P}_{\{24,0\}}^{(9,9)} = \mathcal{P}_{\{20,0,9,9\}}^{(9,9)} - \mathcal{P}_{\{22,0,10,10\}}^{(9,9)} + \mathcal{P}_{\{24,0,11,11\}}^{(9,9)}$
$\mathbf{P}_{\{26,4\}}^{(9,9)} = \mathcal{P}_{\{24,2,10,10\}}^{(9,9)}$	$\mathbf{P}_{26,2}^{(9,9)} = \mathcal{P}_{\{22,2,9,9\}}^{(9,9)} - \mathcal{P}_{\{24,0,10,10\}}^{(9,9)} + \mathcal{P}_{\{24,0,11,9\}}^{(9,9)} - \frac{526199}{350175} \mathcal{P}_{\{24,0,11,11\}}^{(9,9)} + \mathcal{P}_{\{26,2,11,11\}}^{(9,9)}$

Table 4.6: Decomposition of sum rules $\mathbf{P}^{(9,9)}$ into super-sum rules $\mathcal{P}^{(9,9)}$.

Chapter 5

Bootstrap

5.1 Summary of the chapter

We present the full form of a four-point correlation function of large BPS operators in planar $\mathcal{N} = 4$ Super Yang-Mills to any loop order. We do this by following a bootstrap philosophy based on three simple axioms pertaining to (i) the space of functions arising at each loop order, (ii) the behaviour in the OPE in a double-trace dominated channel and (iii) the behaviour under a double null limit. We discuss how these bootstrap axioms are in turn strongly motivated by empirical observations up to nine loops unveiled through integrability methods in our previous work [116] on this *simplest* correlation function.

5.2 Introduction

Integrability methods have shaped a new path for the explicit evaluation of correlators of local operators in planar $\mathcal{N} = 4$ SYM [5, 6, 7, 112, 1] and also non-planar [114, 115, 113], specially for four-point functions of large protected single-trace operators. In [116] we used integrability-based methods to find the loop corrections to the polarized four-point function we named as the *simplest*. This correlator consists of four external protected operators with R -charge polarizations chosen as shown in figure 5.1. In the limit of long operators¹ ($K \gg 1$), we argued this four-point function admits a factorization into the tree level part which carries all the dependence on the external scaling dimension K and the loop corrections which are given by the squared of the function \mathbb{O} (the octagon)

$$\langle O_1 O_2 O_3 O_4 \rangle = \left[\frac{1}{x_{12}^2 x_{13}^2 x_{24}^2 x_{34}^2} \right]^{\frac{K}{2}} \times \mathbb{O}^2(z, \bar{z}) \quad (5.1)$$

¹ The rank of the gauge group $N_c \rightarrow \infty$ is the largest parameter followed by K . Then the planar correlator is expanded in powers of the 't Hooft coupling g^2 .

where the cross ratios are defined in terms of the spacetime positions as:

$$z\bar{z} = u = \frac{x_{12}^2 x_{34}^2}{x_{13}^2 x_{24}^2} \quad \text{and} \quad (1-z)(1-\bar{z}) = v = \frac{x_{14}^2 x_{23}^2}{x_{13}^2 x_{24}^2}$$

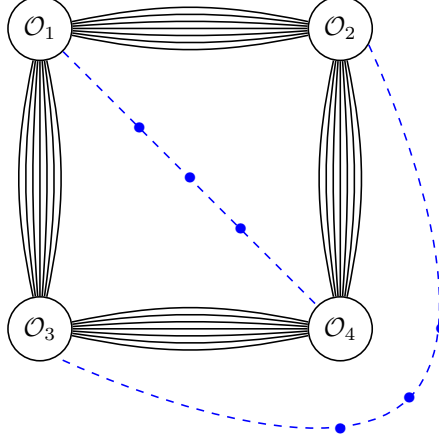


Figure 5.1: The *simplest* four-point function with external operators $O_1(0,0) = \text{Tr}(Z^{\frac{K}{2}} \bar{X}^{\frac{K}{2}}) + \text{cyclic permutations}$, $O_2(z,\bar{z}) = \text{Tr}(X^K)$, $O_3(1,1) = \text{Tr}(\bar{Z}^K)$ and $O_4(\infty,\infty) = \text{Tr}(Z^{\frac{K}{2}} \bar{X}^{\frac{K}{2}}) + \text{cyclic permutations}$. The Wick contractions form a perimeter with four bridges of width $\frac{K}{2}$. According to Hexagonalization [6] in the limit $K \gg 1$ the loop corrections are obtained by summing over $2D$ intermediate multiparticle states ψ_{in} and ψ_{out} on mirror cuts 1-4 and 2-3 respectively, with both sums evaluating to \mathbb{O} . Alternatively the octagon \mathbb{O} represents the resummation of planar Feynman diagrams drawn inside(outside) the perimeter.

In this chapter we present some of the analytic properties of the octagon \mathbb{O} which follow from the explicit nine-loop results in Chapter 4. These properties include a restriction on the space of functions that appear at any loop order and the remarkable simplicity of the octagon in two different kinematical limits: the OPE limit ($z \rightarrow 1, \bar{z} \rightarrow 1$) and the double light-cone limit ($z \rightarrow 0, \bar{z} \rightarrow \infty$).

We also state that these three analytic properties can be used to uniquely define the octagon and with that also the *simplest* correlator (5.1). We show how to solve this bootstrap problem by first introducing a Steinmann basis of Ladders which resolve two of the aforementioned analytic properties. Then using the third property to completely fix the coefficients in an Ansatz constructed with the Steinmann basis.

This bootstrap approach reproduces the explicit results obtained from perturbation theory and integrability and allows us to easily extend them to arbitrary loop order. We accompany this letter with an ancillary file with our explicit results up to 24 loops.

5.3 Analytic properties of octagon

The following analytic properties were observed up to nine loops from the explicit results in [116]. These empirically found properties will then be converted into bootstrap axioms used to fully determine our correlator. Some of these empirical observations can be a posteriori derived and better understood as discussed in more detail in [119].

5.3.1 Single-Valuedness and Ladders

Our explicit results in [116] provided the octagon² as a multilinear combination of Ladder integrals:

$$\mathbb{O} = 1 + \sum_{n=1}^{\infty} \sum_{J=n^2}^{\infty} \sum_{\vec{j} \in Z_n^+(J)} g^{2J} \times d_{\vec{j}} \times f_{j_1} \cdots f_{j_n} \quad (5.2)$$

where $Z_n^+(J)$ represents the group of sets of positive integers $\vec{j} \equiv \{j_1, \dots, j_n\}$ which add up to $j_1 + \dots + j_n = J$. The rational coefficients $d_{\vec{j}}$ are not known in closed form and could be zero for some integer partitions. The basis of conformal Ladder integrals is given by [117]

$$f_p = -v \sum_{j=p}^{2p} \frac{j!(p-1)! [-\log(z\bar{z})]^{2p-j}}{(j-p)!(2p-j)!} \left[\frac{\text{Li}_j(z) - \text{Li}_j(\bar{z})}{z - \bar{z}} \right]$$

where $v = (1-z)(1-\bar{z})$.

This expansion of \mathbb{O} makes manifest its single-valuedness and its uniform maximal transcendentality at each loop order.

5.3.2 Double-trace OPE channel

Here we consider the OPE expansion in channel 2-3, see figure 5.1. Unlike the other two-channels³ (1-2 and 2-4), this one receives double-trace contributions already at leading twist $2K$.

This OPE limit corresponds to $z \rightarrow 1, \bar{z} \rightarrow 1$ (or $v \rightarrow 0, u \rightarrow 1$). At weak coupling we find the behaviour of the octagon in this kinematics to be given by⁴

$$\lim_{z, \bar{z} \rightarrow 1} \mathbb{O}(z, \bar{z}) = \mathbf{a}(z, \bar{z}, g^2) + \mathbf{b}(z, \bar{z}, g^2) \log v \quad (5.3)$$

where both functions \mathbf{a} and \mathbf{b} have a series expansion in the coupling g^2 and the cross ratios $(1-z)$ and $(1-\bar{z})$.

²here we are referring to the polarized octagon form factor which only depends on spacetime cross ratios z, \bar{z} and has bridge parameter $l = 0$. For the more general octagon see [116]

³The 1-2 channel was considered in [116]. In this channel, at weak coupling, we only get single-traces between the leading twist K and the double-trace threshold $2K$.

⁴Similar truncations have been observed in the study of extremal three-point functions in [118]

In the limit of large operators where the expression 5.1 holds up to arbitrary loop order this octagon limit (5.3) implies that the *simplest* four-point function has at most a $\log^2 v$ singularity. This type of truncations is expected in the planar limit for OPE channels dominated by double-trace operators hence we dub this channel as the double trace channel [119].

5.3.3 Null-square limit

This limit corresponds to the kinematics where the external operators become light-like separated: $x_{12}^2, x_{24}^2, x_{34}^2, x_{13}^2 \rightarrow 0$ forming a null square. This limit of the four-point function was considered in [120] for smaller operators where a relationship between null correlators and null polygonal Wilson loops was established.

For our *simplest* four-point function, see (5.1), the non-trivial part of this null limit is given by the limit of the octagon⁵

$$\lim_{z \rightarrow 0, \bar{z} \rightarrow \infty} \log \mathbb{O}(z, \bar{z}) = -\tilde{\Gamma}(g) \log^2(z/\bar{z}) + \frac{1}{2} g^2 (\log^2(-z) + \log^2(-1/\bar{z})) \quad (5.4)$$

where the coefficient $\tilde{\Gamma}$ admits an expansion in the coupling

$$\tilde{\Gamma}(g) = \frac{1}{2} g^2 - \frac{1}{6} \pi^2 g^4 + \frac{8}{45} \pi^4 g^6 - \frac{68}{315} \pi^6 g^8 + \mathcal{O}(g)^{10}$$

To appreciate better the simplicity of (5.4) we contrast it against the result for short operators, $K = 2$

- For the case $K = 2$ the coefficient $\tilde{\Gamma}$ is replaced by the cusp anomalous dimension Γ_{cusp} which is associated to the energy density of the flux tube between the Wilson lines. It also appears in the anomalous dimension of the large spin leading twist-operator $tr(ZD^S Z)$ dominating the light-cone OPE

$$\Delta = S + 2 + \Gamma_{cusp}(g) \log S + \mathcal{O}(1/S)$$

For our *simplest* correlator the operator(s) dominating the light-cone OPE is of the form $tr(Z^{\frac{K}{2}} D^S X^{\frac{K}{2}})$. Furthermore the limit $K \gg 1$ implies a huge number of nearly-degenerate operators at leading twist K . It would be interesting to analyze how these two latter considerations account for the difference between $\tilde{\Gamma}$ and Γ_{cusp} . In particular the latter contains odd zeta-numbers while the former only even zeta-numbers.

- In (5.4) the exponents of $\log(-z)$ and $\log(-1/\bar{z})$ truncate at degree two while for the case $K = 2$ there is an extra complicated function of the cross ratios determined in [122] which accounts for the backreaction of the flux-tube on the heavy particle that propagates along the null square, see [120].

⁵We also know this limit at strong coupling [119] at which the isolated g^2 term is absent. This makes us believe that its presence in (5.4) is only a curious artifact of the weak coupling limit.

We expect these differences can be explained following an analysis similar to [122, 123] including the non-trivial R -charge and large $K \gg 1$ limit of our *simplest* correlator [119]. It would also be interesting to see if $\tilde{\Gamma}$ satisfies a linear integral equation as is the case for⁶ Γ_{cusp} [36].

5.4 Bootstrapping the octagon

We now postulate that the analytic properties described in the previous section are valid at all loops and can be used to define a bootstrap problem. More specifically we establish that the perturbative expansion of the *simplest* four-point function is defined by

- (i) **Ladder integrals:** These span the family of functions that appear in the loop corrections of the correlator. They appear in multilinear combinations with uniform maximal transcendentality at any loop order.
- (ii) **Steinmann relations:** The octagon satisfy these relations which establish the vanishing of its double discontinuity

$$\text{Disc}_1 \text{Disc}_1 \mathbb{O}(z, \bar{z}) = 0 \quad (5.5)$$

where Disc_1 denotes the discontinuity after performing the analytic continuation $(1 - z) \rightarrow (1 - z)e^{i\pi}$ and $(1 - \bar{z}) \rightarrow (1 - \bar{z})e^{i\pi}$. This condition guarantees the truncation to $\log v$ in the OPE expansion $z \rightarrow 1, \bar{z} \rightarrow 1$ at weak coupling.

- (iii) **Light-cone asymptotics:** in the null-square limit $z \rightarrow 0$ and $z \rightarrow \infty$ we demand a simple asymptotics of the logarithm of the octagon:

$$\begin{aligned} \lim_{z \rightarrow 0, \bar{z} \rightarrow \infty} \log \mathbb{O}(z, \bar{z}) &= a_{0,0} + a_{1,0} \log(-z) + a_{0,1} \log(-1/\bar{z}) \\ &\quad + a_{1,1} \log(-z) \log(-1/\bar{z}) \\ &\quad + a_{2,0} \log^2(-z) + a_{0,2} \log^2(-1/\bar{z}) \end{aligned} \quad (5.6)$$

where the relevant condition is the absence of higher logs and we do not impose any conditions on the coefficients $a_{i,j}$.

In the following sections we show how to resolve these three conditions to determine the octagon and the *simplest* four-point function at any loop order.

5.4.1 A Steinmann basis of Ladder integrals

The vanishing of the double discontinuity (ii) motivates the search for a basis of functions that satisfy this property. Here we combine (i) and (ii) to look for this basis of functions

⁶Thanks to B. Basso for comments on this point

in the space of Ladder integrals. We start with an Ansatz of the form

$$\mathcal{S}_i^{(m,n)} = \sum_{k_1+\dots+k_n=m} d_{k_1,\dots,k_n}^{(i)} f_{k_1} \cdots f_{k_n} \quad (5.7)$$

With this Ansatz we are assuming an organization of our Steinmann basis into families $\mathcal{S}^{(m,n)}$ whose elements have uniform transcendentality of order m and are constructed with n Ladders. We are provisionally using the sub-index i to label the different elements $\mathcal{S}_i^{(m,n)}$ on each family.

In order to find our basis we simply need to take into account the discontinuities of the Ladders:

$$\begin{aligned} \text{Disc}_1 f^{(n)}(z, \bar{z}) &\sim 2\pi i [\log(z\bar{z})]^{n-1} \log\left(\frac{z}{\bar{z}}\right) \\ \text{Disc}_1 \text{Disc}_1 f^{(n)}(z, \bar{z}) &= 0 \end{aligned}$$

then imposing the Steinmann relations

$$\text{Disc}_1 \text{Disc}_1 \mathcal{S}_i^{(m,n)} = 0 \quad (5.8)$$

we solve for the coefficients d in the ansatz (5.7).

This exercise was performed in [121] where some solutions to (5.8) were presented and identified with fishnet Feynman integrals. Here we will provide all solutions but without a Feynman integral interpretation.

We solved equation (5.8) for various m, n . From these we gather the following data:

- For $m < n^2$ there are no solutions.
- For $m = n^2$ and $m = n^2 + 1$ there is only one solution.
- All solutions we found admit determinant representations.

This experience allows us to propose a Steinmann basis of Ladders in the form of determinants. In short, the elements of our Steinmann basis can be identified with the minors of the infinite dimensional matrix

$$\begin{pmatrix} f_1 & f_2 & f_3 & \cdots \\ f_2 & f_3 & \cdots & \cdots \\ f_3 & \cdots & \cdots & \cdots \\ \vdots & \cdots & \cdots & \cdots \end{pmatrix}$$

more specifically we label these minors as

$$M_{i_1, i_2, \dots, i_n} = \begin{vmatrix} f_{i_1} & f_{i_2-1} & \cdots & f_{i_n-n+1} \\ f_{i_1+1} & f_{i_2} & \cdots & f_{i_n-n+2} \\ \vdots & \vdots & \ddots & \vdots \\ f_{i_1+n-1} & f_{i_2+n-2} & \cdots & f_{i_n} \end{vmatrix} \quad (5.9)$$

where the subindexes on M_{i_1, i_2, \dots, i_n} correspond to the elements on the diagonal and the subindexes on the first row of the matrix must satisfy

$$0 < i_1 < i_2 - 1 < \dots < i_n - n + 1$$

Using these minors we define our Steinmann basis of Ladders as:

$$S_{k_1, \dots, k_n} = \left[\prod_{o=1}^n p_{k_o} \right] M_{k_1, \dots, k_n} \quad (5.10)$$

where the rescaling $p_k = \frac{1}{k!(k-1)!}$ is just performed for later convenience. The families $\mathcal{S}^{(m,n)}$ are spanned as follows

$$S_{k_1, \dots, k_n} \in \mathcal{S}^{(m,n)} \text{ if } k_1 + \dots + k_n = m$$

Lastly considering the property of maximal transcendentality we use our Steinmann basis $\mathcal{S}^{(m,n)}$ to build an Ansatz for each loop order of a function \mathbb{O} satisfying (i) and (ii).

$$\mathbb{O} = 1 + \sum_{n=1}^{\infty} \sum_{m=n^2}^{\infty} (g^2)^m \sum_{S \in \mathcal{S}^{(m,n)}} c_{k_1, \dots, k_n} S_{k_1, \dots, k_n} \quad (5.11)$$

5.4.2 Fixing all coefficients with Light-cone asymptotics

In order to fix the coefficients c_{k_1, \dots, k_n} in the Ansatz we impose the third analytic property (iii). This condition of exponentiation in the null-square limit allows us to relate coefficients of high loop orders to the ones at lower loops. To take this limit in our Ansatz we simply need to consider the light-cone limit of the Ladders.

$$\lim_{z \rightarrow 0, \bar{z} \rightarrow \infty} f_j(z, \bar{z}) = \sum_{m=0}^j \sum_{n=0}^j b_{m,n}^{(j)} \log^m(-z) \log^n(-1/\bar{z}) \quad (5.12)$$

where $b_{m,n} = 0$ if $m + n$ is odd or otherwise:

$$b_{m,n}^{(j)} = \frac{j!(j-1)!(2 - 2^{m+n-2j+2}) (2j - m - n)!}{(-1)^m m! n! (j-m)! (j-n)!} \zeta_{2j-m-n}$$

Notice light-cone Ladder (5.12) is manifestly symmetric under the exchange of cross-ratios $z \leftrightarrow -1/\bar{z}$ and our Ansatz of Ladders directly inherits this feature.

We then enforce the condition of truncation of the exponents of $\log(z)$ and $\log(-1/\bar{z})$ up to degree two. These provides a set of equations which we can be easily solved at each loop order. Up to four-loops the solution looks like:

$$c_2 = -2c_1^2 \quad c_3 = 6c_1^3 \quad c_4 = -20c_1^4 \quad c_{1,3} = c_1^4$$

Likewise we find that we can fix all coefficients c in (5.11) and $a_{i,j}$ in (5.6) at arbitrary loop order in terms of the single one-loop coefficient c_1 . This latter coefficient can be associated to the definition of the coupling g^2 and in order to match with the conventions in the literature we set it to $c_1 = 1$. This finally shows that properties (i), (ii) and (ii) uniquely define the octagon \mathbb{O} and with that our *simplest* correlator (5.1) at arbitrary loop order.

Furthermore, we have been able to identify the analytic form of an infinite family of coefficients:

$$c_{\underbrace{1,3,\dots,2n-1}_n, 2n+1+m} = \binom{2m+4n}{m} \quad \text{with } m \geq 0$$

In particular the coefficients $c_{1,3,5,\dots,2n-1} = 1$ of the noteworthy elements of our basis $\mathcal{S}_{1,3,5,\dots,2n-1}$ which have been identified in [121] as the fishnet Feynman integrals

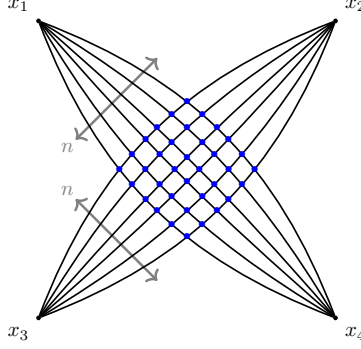


Figure 5.2: Fishnet identified with $\mathcal{S}_{1,3,\dots,2n-1}$

It is interesting to ask whether other elements of the Steinmann basis of Ladders or perhaps linear combinations of them can be identified with other families of Feynman integrals. Finding such identification could be the guiding principle to find the closed form of all coefficients of our (possibly rotated) Steinmann basis. Then all would be set to attempt a resummation and get access to the finite or strong coupling limit. This is a question we hope to address in the future.

Chapter 6

Strong Coupling

6.1 Summary of the chapter

The octagon function is the fundamental building block yielding the correlation function of four large BPS operators at any value of the 't Hooft coupling and at any genus order (see [Chapter 7](#)). Here we compute the octagon at strong coupling and discuss its various interesting limits and implication both at the planar and non-planar level.

6.2 Introduction

The octagon function $\mathbb{O}(z, \bar{z}|\lambda)$ was introduced in [\[2\]](#) and provides a finite 't Hooft coupling representation for four point correlation functions of large BPS operators as recalled in [Figure 6.1a](#). The octagon is also the fundamental building block for these correlators beyond the planar limit [\[4\]](#). In [\[3\]](#) the octagon was bootstrapped providing an all loop weak coupling perturbative expansion for this object and in [\[140\]](#) a beautiful finite coupling representation for it as an infinite dimensional Pfaffian was provided. In this small note we study the octagon at strong coupling.

Our study is split in two parts: the derivation of the strong coupling result and its analysis.

The derivation actually follows the clustering analysis of Komatsu, Kostov, Serban, and Jiang [\[29\]](#) almost verbatim. There it was explained how to re-sum the so-called bottom wrapping in a three point function of one non-BPS operators and two BPS operators as illustrated in [Figure 6.2a](#). In the octagon also glue together two hexagons but for the purpose of computing a four point function of four BPS operators as illustrated in [Figure 6.2b](#). Both sums involve sums over mirror particles containing bosons and fermions. In the three-point function case this sum is weighted by the transfer matrix of the non-BPS operator which accounts for the interaction of these particles with the mirror particles which break supersymmetry and thus leads to a non-trivial result. In the octagon case

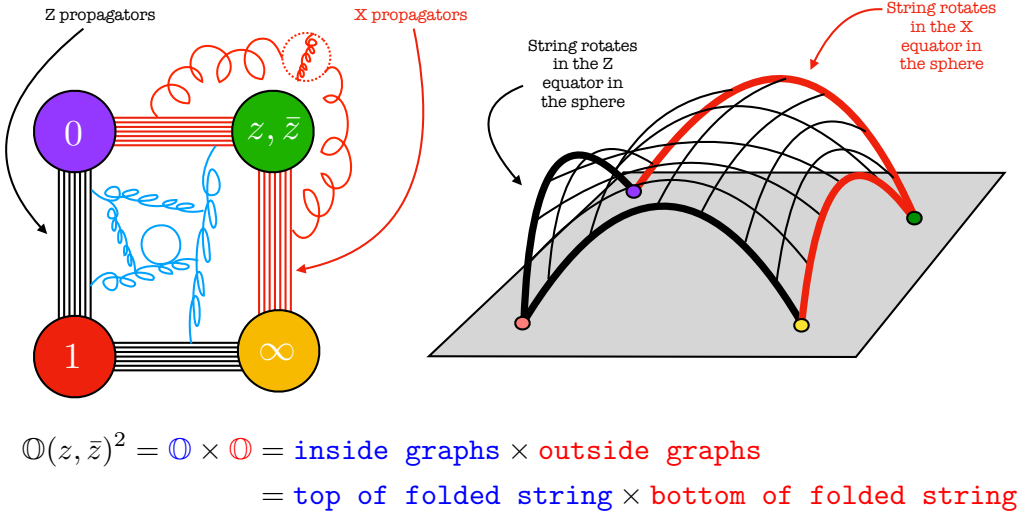


Figure 6.1: We work here with the so-called *simplest* correlator introduced in [2]. Two operators are BPS primaries made out of only Z or only X fields respectively while the other two are BPS descendants composed of both \bar{Z} and \bar{X} so that at tree level there is a single square frame diagram describing this correlator. At loop level, for large operators, the inside and outside decouple. In string theory language the correlator is described by a folded string ending on some spinning geodesics [4]; the top and bottom folds decoupling is the string counterpart of the inside/outside gauge theory decoupling.

the sum is weighted by the geometry of the four point function encoded in the rotation of one of the hexagons leading to character-like Boltzman weights which also break supersymmetry and thus lead to a non-trivial result. Technically it is trivial to spot and replace the transfer matrices by the characters and that is why we can recycle the analysis of [29] rather efficiently. Furthermore, important in [29] was that the momenta of mirror particles was constrained to be small, of order $1/\sqrt{\lambda}$ because they show up multiplied by the length of the bottom bridge which was of order $\sqrt{\lambda}$. This turns out to be exactly the same kinematical region we need in the octagon since here we weight the mirror particles by their energy multiplied by (logarithms of) the space-time cross-ratios. The later is obviously of order 1 and the mirror energy is of order 1 precisely when the mirror momenta is of order $1/\sqrt{\lambda}$ so all in all, the kinematical region is precisely as in [29].

Having realized this, the derivation exercise becomes rather straightforward and is presented in Section 6.3. The reader might want to skip directly to the final result, equation (6.11) below. We observe a nice exponentiation as

$$\mathbb{O}(z, \bar{z}|\lambda) \simeq e^{-\sqrt{\lambda} \mathbb{A}(z, \bar{z})} \quad (6.1)$$

As explained in [4], \mathbb{A} should be the minimal area of a string ending on four BMN geodesics in AdS *and* rotating in the sphere as sketched in Figure 6.1b. What makes this minimal

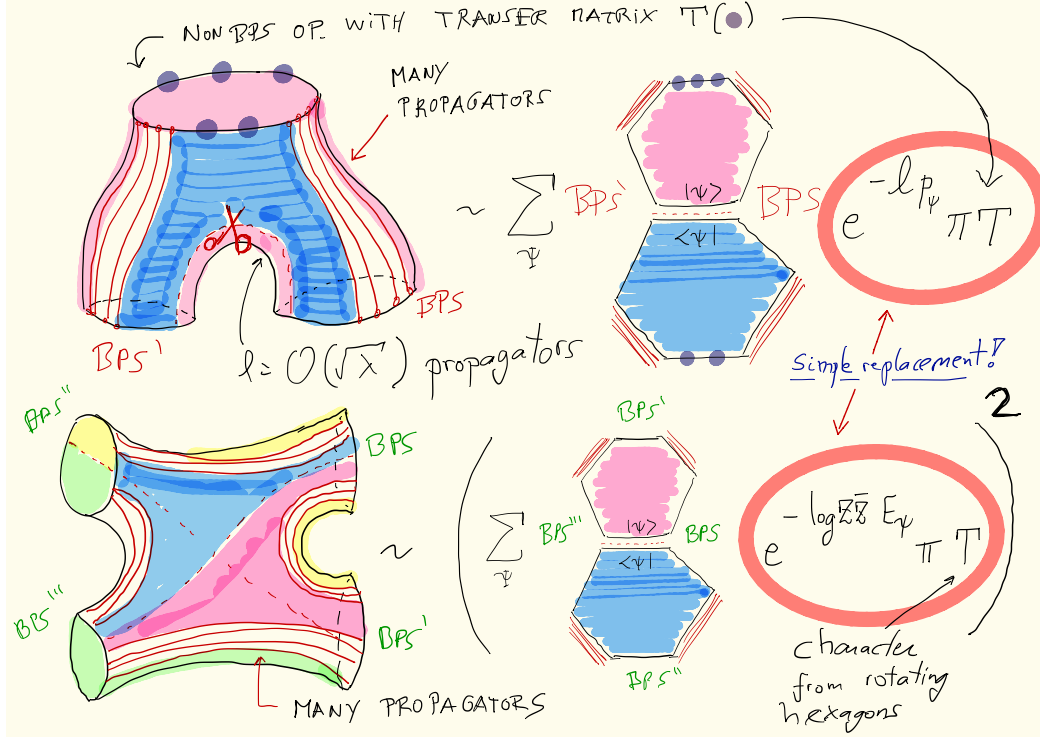


Figure 6.2: (a) Top: Three point function wrapping corrections re-summed in [29]. (b) Bottom: Virtual corrections for the simplest four point function = octagon². We see that they exhibit strong similarities: In the top we have a transfer matrix associated to the non-BPS operator in the three-point function; in the bottom we have a character associated to the cross-ratios of the correlation function. Under a simple replacement we can thus re-use the clustering analysis of [29] to derive the strong coupling octagon representation, see final expression (6.11) below.

area computation quite non-trivial is that the surface does not just move in AdS but also rotates in the sphere. Still, the form of \mathbb{A} clearly indicates that some Y-system like technology should be possible to develop to directly compute this minimal area at strong coupling starting from the string sigma model. It would be very interesting to perform this exercise.

In [Section 6.4](#), we analyse this result. We note that the area \mathbb{A} is real and positive once we start in the Euclidean regime where

$$z, \bar{z} = e^{\varphi \pm i\phi} \quad (6.2)$$

with φ and ϕ both real and we explore what happens as we analytically continue the cross-ratios to various other interesting kinematical regimes such as the Lorentzian regime and various OPE like limits. We also make contact with [\[4\]](#) and explore the consequences of these results for the full non-planar expansion of the correlator of four large BPS operators.

6.3 Derivation

As explained in the introduction, we can immediately recycle the results of [\[29\]](#) with appropriate replacements of their non-BPS transfer matrices by our characters. Simple comparison of their starting point with our octagon infinite sum representation indicates that we should take

$$T_a = \underbrace{e^{-a\varphi \frac{i u}{\sqrt{4g^2 - u^2}}}}_{(z\bar{z}) \text{ mirror energy}} \underbrace{X \sin(a\phi)}_{\text{character}}, \quad X \equiv \underbrace{\frac{4 \sinh\left(\frac{\varphi}{2} + \frac{i\phi}{2}\right) \sinh\left(\frac{\varphi}{2} - \frac{i\phi}{2}\right)}{2i(1-z)(1-\bar{z})}}_{a \text{ independent part of character}} \sin(\phi) \quad (6.3)$$

and plug it into the final strong coupling expression (5.49) and (5.43) in [\[29\]](#),

$$\log \mathbb{O} \simeq \int_{-2g}^{+2g} \frac{du}{2\pi} \sum_{n=1}^{\infty} \frac{1}{n} \sum_{\{n_a\}} (-1)^{(K-1)} (K-1)! \prod_a \frac{(T_a)^{n_a}}{n_a!}, \quad (6.4)$$

where the sum over the positive mode numbers n_a is constrained as $\sum_a a n_a = n$ and where K is defined as $K \equiv \sum_a n_a$. What follows is a straightforward simplification of this expression. The reader might want to jump to the final simplified result ([6.11](#)).

The goal is to factorize the integrand in a way that we can decouple the sum over mode numbers into independent sums which we can then perform. For instance, to factorize the factorial factor we simply write $(K-1)! = \int dt e^{-t} t^{K-1}$ so that $K = \sum_a n_a$ appears in exponents and thus breaks apart into a product of factors for the various mode numbers. Next we want to cancel the $1/n$ factor in (6.4) which is easy by a simple integration by parts. For that we note that the rapidity u dependence only arises through the exponential factor in T_a ; using the definition of n we can take

it out of the n sum completely and write (here we assume $\text{Re}(\varphi) < 0$ otherwise we should pick an opposite shift in (6.6))

$$\begin{aligned} \frac{1}{n} \int_{-2g}^{2g} du e^{-in\varphi u/\sqrt{4g^2-u^2}} &= \frac{2g}{n} \int_{-\infty}^{\infty} d\theta \frac{d \tanh(\theta)}{d\theta} e^{-in\varphi \sinh(\theta)} & u = 2g \tanh(\theta) \\ &= 2gi\varphi \int_{-\infty}^{\infty} d\theta \sinh(\theta) e^{-in\varphi \sinh(\theta)} & \text{integration by parts} \end{aligned} \quad (6.5)$$

$$= -2g\varphi \int_{-\infty}^{\infty} d\theta \cosh(\theta) e^{n\varphi \cosh(\theta)} \quad \theta \rightarrow \theta + i\pi/2 \text{ shift} \quad (6.6)$$

to finally obtain the desired factorization

$$\log \mathbb{O} \simeq \frac{g}{\pi} \varphi \int_{-\infty}^{\infty} d\theta \cosh(\theta) \int_0^{\infty} \frac{dt}{t} e^{-t} \sum_{n=1}^{\infty} \sum_{\{n_a\}} \prod_a \frac{(-Xt \sin(a\phi) e^{a\varphi \cosh(\theta)})^{n_a}}{n_a!}, \quad (6.7)$$

where $n = \sum a n_a$. Adding and subtracting a $n = 0$ term (corresponding to all $n_a = 0$) we get a final factorization into *unconstrained* mode numbers as

$$\log \mathbb{O} \simeq \frac{g}{\pi} \varphi \int_{-\infty}^{\infty} d\theta \cosh(\theta) \int_0^{\infty} \frac{dt}{t} e^{-t} \left[\prod_{a=1}^{\infty} \sum_{n_a=0}^{\infty} \frac{(-Xt \sin(a\phi) e^{a\varphi \cosh(\theta)})^{n_a}}{n_a!} - 1 \right], \quad (6.8)$$

We can now sum over the mode numbers

$$\log \mathbb{O} \simeq \frac{g}{\pi} \varphi \int_{-\infty}^{\infty} d\theta \cosh(\theta) \int_0^{\infty} \frac{dt}{t} e^{-t} \left[e^{-\sum_{a=1}^{\infty} t X \sin(a\phi) e^{a\varphi \cosh(\theta)}} - 1 \right], \quad (6.9)$$

The sum over a can also be done leading to

$$\log \mathbb{O} \simeq \frac{g}{\pi} \varphi \int_{-\infty}^{\infty} d\theta \cosh(\theta) \int_0^{\infty} \frac{dt}{t} e^{-t} \left[e^{-tY(\theta)} - 1 \right], \quad (6.10)$$

where $Y(\theta)$ is given by (6.12) below. Finally, the integral over t yields $-\log(1+Y)$ and so we obtain (6.11) once we recall the relation to the 't Hooft coupling $g = \sqrt{\lambda}/4\pi$.

In sum, we find

$$\log \mathbb{O} \simeq -\frac{\sqrt{\lambda}}{2\pi} \int_{-\infty}^{\infty} \frac{d\theta}{2\pi} \varphi \cosh(\theta) \log(1+Y(\theta)), \quad (6.11)$$

where

$$Y(\theta) = -\frac{\sin\left(\frac{\phi}{2} + i\frac{\varphi}{2}\right) \sin\left(\frac{\phi}{2} - i\frac{\varphi}{2}\right)}{\sin\left(\frac{\phi}{2} + i\frac{\varphi}{2} \cosh(\theta)\right) \sin\left(\frac{\phi}{2} - i\frac{\varphi}{2} \cosh(\theta)\right)}. \quad (6.12)$$

We derived this result from the octagon. Would be very nice to derive it from the string world-sheet Tthis TBA-like result is obviously very reminiscent of the sort of expressions coming out from exploring the classical string integrability. Note in particular that

$$1+Y = \frac{\sinh\left(\frac{\varphi}{2} - \frac{\varphi}{2} \cosh(\theta)\right) \sinh\left(\frac{\varphi}{2} + \frac{\varphi}{2} \cosh(\theta)\right)}{\sinh\left(\frac{i\phi}{2} - \frac{\varphi}{2} \cosh(\theta)\right) \sinh\left(\frac{i\phi}{2} + \frac{\varphi}{2} \cosh(\theta)\right)} \quad (6.13)$$

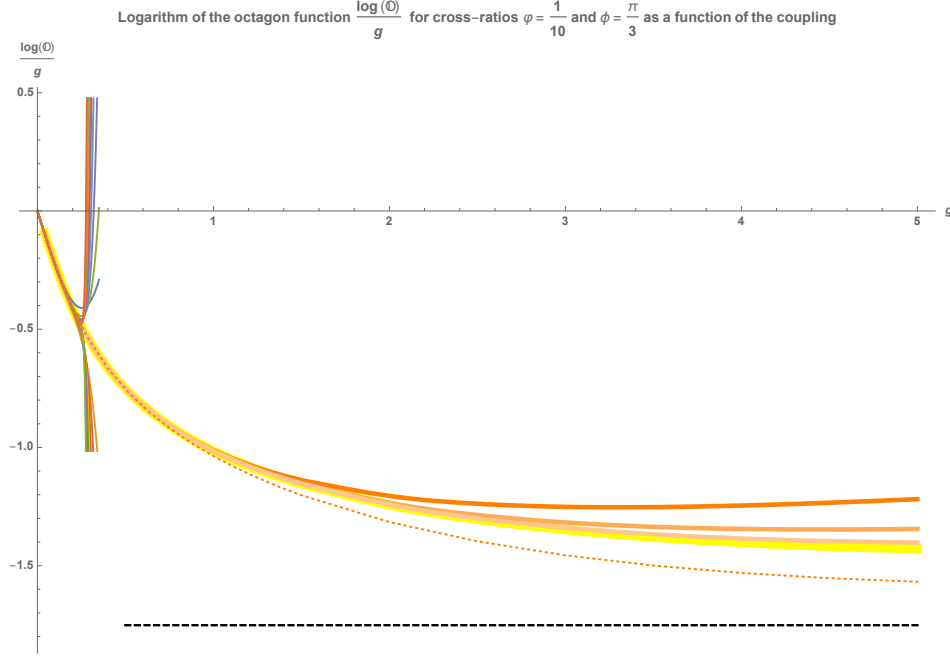


Figure 6.3: The thin lines which go wild as we reach the radius of convergence at $g = 1/4$ are the perturbative results, from two loops all the way to 20 loops. The thicker lines from darker orange to yellow are the numerical evaluation of the determinant representation of [140]. It nicely agrees with the perturbative representation and continues it beyond its radius of convergence. To evaluate the determinant we truncated the semi-infinite matrix to sizes $N = 10, 15, 20, 25$ with the yellow line corresponding to the largest size; clearly it becomes more and more important to consider larger matrices at strong coupling. The dashed orange line represents an extrapolation of these results towards infinite matrices (using the results from $N = 2$ to $N = 25$ and a simple fit $a + b/N$). Finally the black horizontal dashed line is the strong coupling prediction in (6.11). (In this plot we have euclidean cross-ratios $\varphi = 1/10, \phi = \pi/3$.)

takes a very nice factorized form which allows us to nicely split the putative area in (6.11); perhaps one contribution will come from the *AdS* part and another from the sphere.

In Figure 6.3, we compare the strong coupling result to the finite coupling representation of the octagon recently worked out in [140]. It looks good but it would be very nice to work out the one loop prefactor in (6.1) as well as improve the determinant evaluation at strong coupling to perform a much more impressive and conclusive comparison. Furthermore, if we could compute the one loop prefactor from the octagon representation, it would provide us with yet another powerful point of data to try to reproduce from the string sigma model.

Note also that the result was derived for real $\phi \in [0, 2\pi]$ and real $\varphi < 0$ (see shift (6.6)). This translates into $\bar{z} = z^*$ and $|z|, |\bar{z}| < 1$. Of course, we can (and will) move away and study any range of parameters – both real and complex – but we need to carefully analytically continue the result starting from this safe starting point. This is particularly obvious even if we remain in the fully Euclidean region where ϕ and φ are both real. The

Y -function in (6.12) is *even* under $\varphi \rightarrow -\varphi$ but because of the φ outside the log in the area (6.11), the integrand is odd and thus we would naively guess that the full result is *odd*. That is wrong. The full area is *even*, nicely realizing the $z \rightarrow 1/z$ symmetry of the octagon. To see that, however, it is a bit non-trivial. It turns out that as we rotate from $\varphi < 0$ to $\varphi > 0$ infinitely many singularities hit the integration contour which therefore needs to be rearranged dramatically. In the end the net result is to simply produce an additional minus sign required to convert the *naive odd* guess into the *correct even* result.

i

6.4 Analysis

In the Euclidean regime the two cross-ratios are complex conjugate to each other and therefore φ and ϕ in (6.2) are real. Then

$$\log \mathbb{O} \simeq -\frac{\sqrt{\lambda}}{2\pi} \int_{-\infty}^{\infty} \frac{d\theta}{2\pi} \varphi \cosh(\theta) \log \left[1 - \frac{\sin\left(\frac{\phi}{2} + i\frac{\varphi}{2}\right) \sin\left(\frac{\phi}{2} - i\frac{\varphi}{2}\right)}{\sin\left(\frac{\phi}{2} + i\frac{\varphi}{2} \cosh(\theta)\right) \sin\left(\frac{\phi}{2} - i\frac{\varphi}{2} \cosh(\theta)\right)} \right], \quad (6.14)$$

is manifestly real. The logarithm is negative and so is φ and thus the full integrated right hand side is negative. It is also manifestly periodic in ϕ leading to a single valued expression in the Euclidean regime as expected, see figure 6.4. Since it is multiplied by a large string tension $\sqrt{\lambda}$ we see that in the Euclidean regime the octagon is exponentially small and thus

$$\mathbb{O} \rightarrow 0 \quad (6.15)$$

as $\lambda \rightarrow \infty$. This has nice implications if we consider the double scaling limit analysed in Chapter 7. Since the minimal area configuration leads to a vanishing result, the full non-planar correlator in the Euclidean regime reduces to those BMN-like configurations where the string worldsheet degenerates into various point like geodesics. Such configurations first show up at genus 1. All in all, these BMN configurations resum into the explicit expression (??).

The octagon expression (6.14) also exhibits very rich behavior in various interesting kinematical regimes as we will now explore. To explore these limits, it is useful to derive two mathematical formulae for our expression:

$$\log \mathbb{O} \simeq -\frac{\sqrt{\lambda}}{4\pi^{\frac{3}{2}}} \sqrt{\log\left(\frac{1}{z\bar{z}}\right)} \left(\text{Li}_{\frac{3}{2}}(1) + \text{Li}_{\frac{3}{2}}(z\bar{z}) - \text{Li}_{\frac{3}{2}}(z) - \text{Li}_{\frac{3}{2}}(\bar{z}) \right) \quad \text{if} \quad \begin{array}{l} z \simeq 0 \text{ or } 1 \\ \text{or} \\ \bar{z} \simeq 0 \text{ or } 1 \end{array}, \quad (\text{I})$$

valid in the Euclidean sheet with $|z\bar{z}| \leq 1$ and

$$\log \mathbb{O} \simeq \frac{\sqrt{\lambda}}{8\pi^2} \frac{\log(z/\bar{z})}{2i} \left(2\pi - \frac{\log(z/\bar{z})}{2i} \right) \quad \text{if} \quad |\log(z/\bar{z})/\log(z\bar{z})| \gg 1. \quad (\text{II})$$

Here are the sketches of the corresponding derivations:

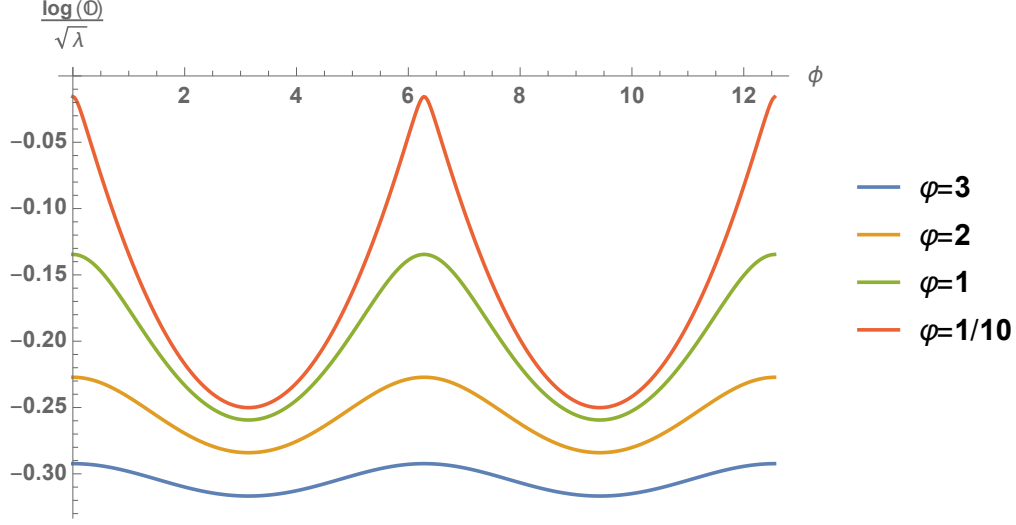


Figure 6.4: In the Euclidean regime the area is single valued in the physical sheet, i.e. it is periodic in the angle ϕ . As a function of this angle, we see that it develops kinks as $\varphi \rightarrow 0$ and approaches a constant as $\varphi \rightarrow \infty$.

- (I) The kinematical limit in (I) is dominated by small θ . In order to analyze limits of z or \bar{z} individually we write the Y -function as:

$$Y = -\frac{\sinh\left(\frac{1}{2}\log z\right) \sinh\left(\frac{1}{2}\log \bar{z}\right)}{\sinh\left(\frac{1}{2}\log z + \frac{1}{2}\sinh^2\left(\frac{\theta}{2}\right)\log(z\bar{z})\right) \sinh\left(\frac{1}{2}\log \bar{z} + \frac{1}{2}\sinh^2\left(\frac{\theta}{2}\right)\log(z\bar{z})\right)}. \quad (6.16)$$

By inspecting (6.16) we recognize that when a cross ratio z or \bar{z} approaches 0 or 1 then the Y -function (6.16) approaches -1 in the region of very small rapidity. It is thus this region which therefore dominates the integral in (6.11) so that the integrand

$$\cosh(\theta) \log(1 + Y) = \cosh(\theta) \log \frac{\left(1 - e^{\log(z\bar{z}) \sinh^2(\frac{\theta}{2})}\right) \left(1 - z\bar{z} e^{\log(z\bar{z}) \sinh^2(\frac{\theta}{2})}\right)}{\left(1 - z e^{\log(z\bar{z}) \sinh^2(\frac{\theta}{2})}\right) \left(1 - \bar{z} e^{\log(z\bar{z}) \sinh^2(\frac{\theta}{2})}\right)} \quad (6.17)$$

can be dramatically simplified by expanding the $\sinh(\theta/2) \simeq \theta/2$ and $\cosh(\theta/2) \simeq 1$ and using

$$\int_{-\infty}^{\infty} d\theta \log\left(1 - x e^{-y\theta^2}\right) = -\sqrt{\pi/y} \text{Li}_{\frac{3}{2}}(x) \quad (6.18)$$

to establish (I). From a thermodynamic Bethe ansatz context, these limits resemble non-relativistic limits where particles have small rapidities.

- (II) The kinematical limit in (II) is dominated by large θ . For example, once possibility to reaching this limit is by taking $\log(z\bar{z}) \rightarrow 0$ so we see that all exponents in (6.17) can be effectively set to zero *unless* θ is huge, of order $\log\log(z\bar{z})$. Furthermore, the full expression is multiplied by $\varphi = \log(z\bar{z})/2$ and thus vanishes unless θ is huge indeed. So we can freely replace all hyperbolic functions by their large θ single exponential. Once that is done, it suffices to use

$$2 \int_{-\infty}^{\infty} d\theta \frac{y}{2} e^{\theta} \log\left(1 - x e^{-y e^{\theta}/4}\right) = -4 \text{Li}_2(x), \quad (6.19)$$

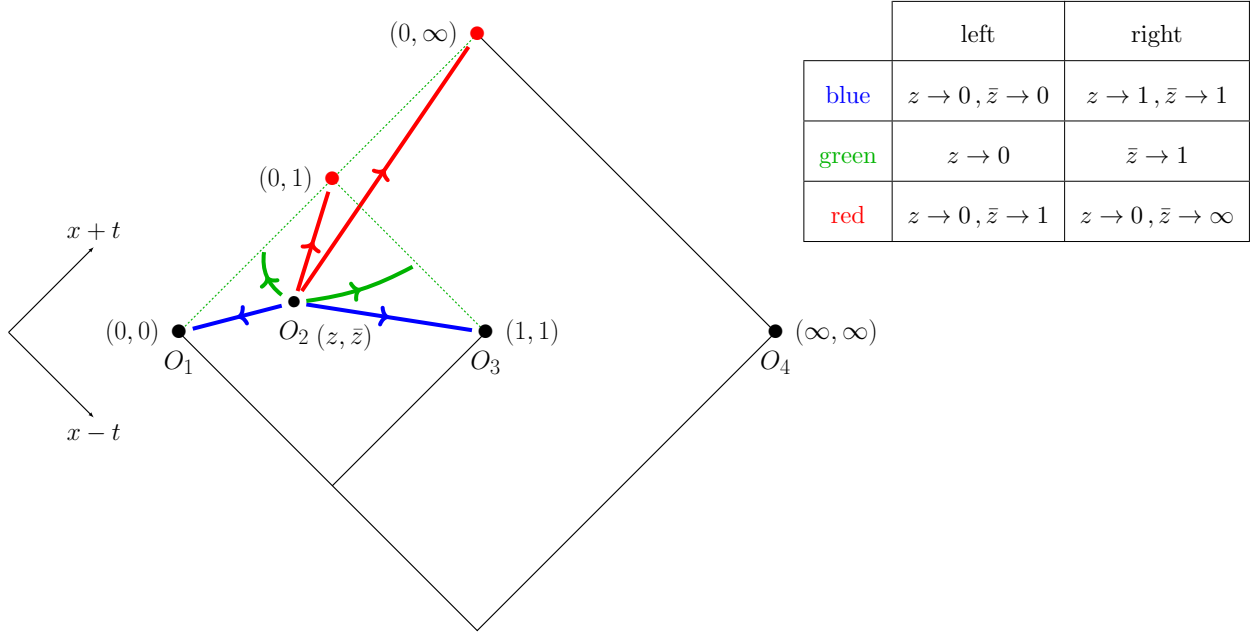


Figure 6.5: Poincare patch in light-cone coordinates with operators O_2 at (z, \bar{z}) and O_1, O_3, O_4 in canonical positions. OPE limits are obtained when O_2 approaches any of the corners or edges of the dashed squares. We indicate in blue the Euclidean or space-like OPEs, in green the single light-like OPEs of and in red the double light-like OPEs

to evaluate all resulting integrals and thus get that the area is proportional to $\text{Li}_2(1) + \text{Li}_2(z\bar{z}) - \text{Li}_2(z) - \text{Li}_2(\bar{z})$. Expanding for $\log(z\bar{z}) \rightarrow 0$ (i.e. for $z \rightarrow 1/\bar{z}$) does simplify this expression into (II). Now, as written in (II) we could also take other limits such as $\log(z/\bar{z}) \rightarrow \infty$; they would indeed be again be dominated by large θ and, again, expanding the Li_2 expression in this other limit does leads once more to the same right hand side of (II). From a thermodynamic Bethe ansatz point of view, these manipulations go by the name of high-temperature analysis, dominated by very energetic particles with very large rapidities.

6.4.1 OPE Limits

Armed with (II) and (I) we can now straightforwardly explore all the various interesting OPE limits summarized in figure 6.5. They can be Euclidean OPE's (if two points approach each other), light-like OPE (if two points become null separated) or double-light-like OPE limits (if the four points approach a null square). For each such limit there is a further choice of who is colliding (or becoming null separated) since in our correlator points x_i and x_{i+1} are connected by an edge of our large R-charge frame (see figure 6.1) and therefore in a very different footing from x_i and x_{i+2} who are non-neighbouring cusps in the square. This important difference is illustrated in an example in figure 6.6. So all in all, there are six interesting different limits we can take as summarized 6.5.

We therefore find that $-(\log \odot)/\sqrt{\lambda} \equiv \mathbb{A}$ is approximately given by the following expressions in the various limits:

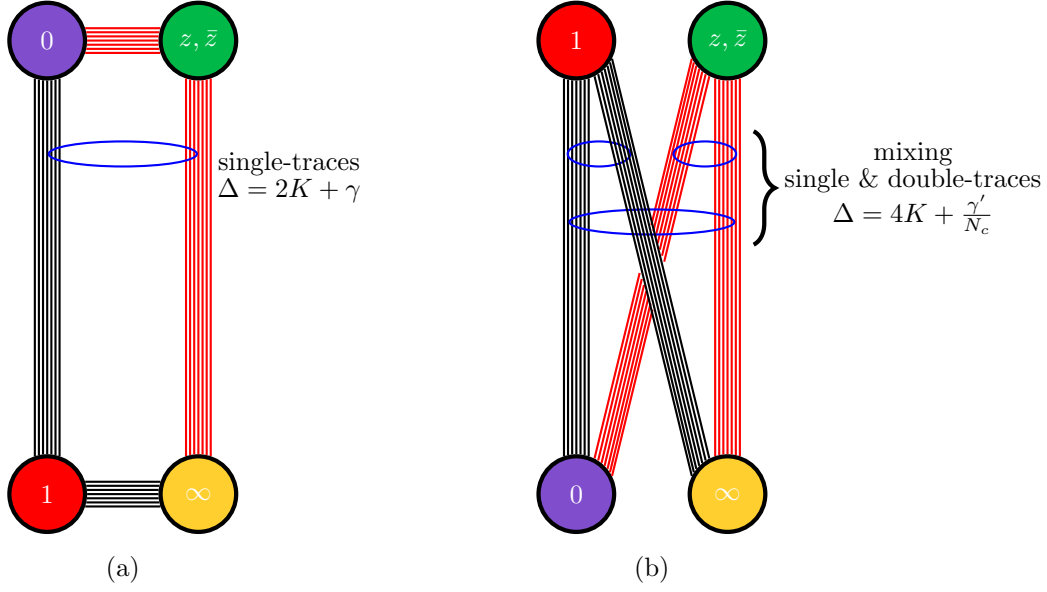


Figure 6.6: (a) The OPE $z, \bar{z} \rightarrow \infty$ or $z, \bar{z} \rightarrow 0$ is controlled by large single trace operators. (b) The other OPE limit connecting diagonals of the square, that is $z, \bar{z} \rightarrow 1$ is dominated by double traces. The area will indeed behave strikingly differently in both limits.

	$z \rightarrow 0$	$z \rightarrow 1$
$\bar{z} \rightarrow 0$	Euclidean OPE ★ $4\pi^{3/2}\mathbb{A} \simeq \zeta(3/2)\sqrt{-\log(z\bar{z})}$	Equivalent to $z \rightarrow 0, \bar{z} \rightarrow 1$
\bar{z} finite	Light-line OPE ★ $4\pi^{3/2}\mathbb{A} \simeq \sqrt{\log \frac{1}{z\bar{z}}} \left(\zeta\left(\frac{3}{2}\right) - \text{Li}_{\frac{3}{2}}(\bar{z}) \right)$	Light-like OPE * $2\pi\mathbb{A} \simeq \sqrt{1-z}\sqrt{-\log \bar{z}}$
$\bar{z} \rightarrow 1$	Double Light-like OPE $2\pi\mathbb{A} \simeq \sqrt{1-\bar{z}}\sqrt{-\log z}$	Euclidean OPE * $2\pi\mathbb{A} \simeq \sqrt{1-\bar{z}}\sqrt{1-z}$
$\bar{z} \rightarrow \infty$	Double Light-line OPE ★ $8\pi^2\mathbb{A} \simeq \phi(2\pi - \phi), \quad \phi = \frac{\log(z/\bar{z})}{2i}$	Equivalent to $z \rightarrow 1, \bar{z} \rightarrow 0$

A few comments

- Some areas are very large (identified with ★), some are very small (identified with *), and some can be either. The large areas are the ones where the points colliding or becoming null separated are neighbours in the square while the vanishingly small area are those where the points colliding or becoming null separated are non-neighbouring cusps in the square. This is in nice agreement with the intuition that the first is a single trace OPE channel while the former ought to be dominated by double trace, see figure 6.6. In particular, when the area is very large we can extract effective spin and dimension of the exchanged operator as those are dominated by some saddle point effective operator. When the area vanishes, instead, the prefactor multiplying the classical area would become important; would be very interesting to study this

prefactor, at least in these limits.¹

- Some limits arise as particular cases of (I); others of (II). For example, the first line is a specialization of (I) while the last line follows from (II). Some, like the Euclidean limit $\bar{z}, z \rightarrow 1$ can be reached as particular cases of both (I) or (II).
- Most limits commute with each other. For example, from the second line we can further specialize to the elements in the first and third lines. One exception is the limit where $z \rightarrow 0$ and $\bar{z} \rightarrow \infty$ with their product held fixed. This leads to the fourth line which is not a trivial expansion of the second line at large \bar{z} . So in this case the order of limits matters.
- The Euclidean OPE limit $z, \bar{z} \rightarrow 1$ corresponds to $\varphi \rightarrow 0$ and $\phi \rightarrow 0$. If $\varphi \rightarrow 0$ then we are under the conditions of (II) even before taking any limit on ϕ . We hence obtain, when $\varphi \rightarrow 0$,

$$\log \mathbb{O} \simeq -\frac{\sqrt{\lambda}}{8\pi^2} \tilde{\phi} (2\pi - \tilde{\phi}). \quad (6.20)$$

Here $\tilde{\phi} = \phi \bmod 2\pi$ since the derivation implicitly assumes that $\phi = \frac{1}{2i} \log(z/\bar{z})$ is defined in the principal sheet to be between 0 and 2π . Outside this range the result should be periodized to match with the manifestly periodic function (6.14) in the Euclidean regime, see figure 6.4. This weaker condition $z\bar{z} \rightarrow 1$ would show up, for example, as soon as the fourth and third points are equidistant from point 1 which is clearly not an OPE limit of any kind. It is still nice that the area can be computed already in this more general configuration. The strict Euclidean OPE limit corresponds to $z, \bar{z} \rightarrow 1$ and not just $z\bar{z} \rightarrow 1$ and leads to the corresponding expression in the table.

- The very last limit, with $z \rightarrow 0$ and $\bar{z} \rightarrow \infty$ was very important in bootstrapping the octagon to all loops in Chapter 5.

¹We were told of very interesting very closely related unpublished results in this regard by Benjamin Basso whom we thank for enlightening discussions on the physics of this OPE channel and its relation to (the singularities of) extremal three-point functions.

Chapter 7

Non-planar

7.1 Summary of the chapter

We explain how the 't Hooft expansion of correlators of half-BPS operators can be re-summed in a large-charge limit in $\mathcal{N} = 4$ super Yang–Mills theory. The full correlator in the limit is given by a non-trivial function of two variables: One variable is the charge of the BPS operators divided by the square root of the number N_c of colors; the other variable is the \mathbb{O} that contains all the 't Hooft coupling and spacetime dependence. At each genus g in the large N_c expansion, this function is a polynomial of degree $2g + 2$ in the octagon. We find several dual matrix model representations of the correlators in the large-charge limit. Amusingly, the number of colors in these matrix models is formally taken to zero in the relevant limit.

7.2 Introduction

In this work, we will consider correlation functions of single-trace half-BPS operators in $\mathcal{N} = 4$ super Yang–Mills theory. Each of these operators creates a closed string state, so these correlation functions describe closed-string scattering in $\text{AdS}_5 \times S^5$.

We will focus on four-point correlation functions in an interesting limit of very large BPS operators with carefully chosen polarizations, where the closed string scattering process factorizes into several copies of an off-shell open string partition function \mathbb{O} that was determined exactly in [2, 3] at any value of the 't Hooft coupling and further simplified into an infinite determinant representation in [140].

The dimensions of the operators we will consider scale with the rank of the $U(N_c)$ gauge group as $\sqrt{N_c}$, reminiscent of inspiring earlier studies [141, 142, 143, 144] in the plane-wave Berenstein–Maldacena–Nastase (BMN) limit [145]. The motivation for this particular limit is similar to the one considered in those works: It will allow us to re-sum the large N_c 't Hooft expansion. We now have a much stronger control over the 't Hooft

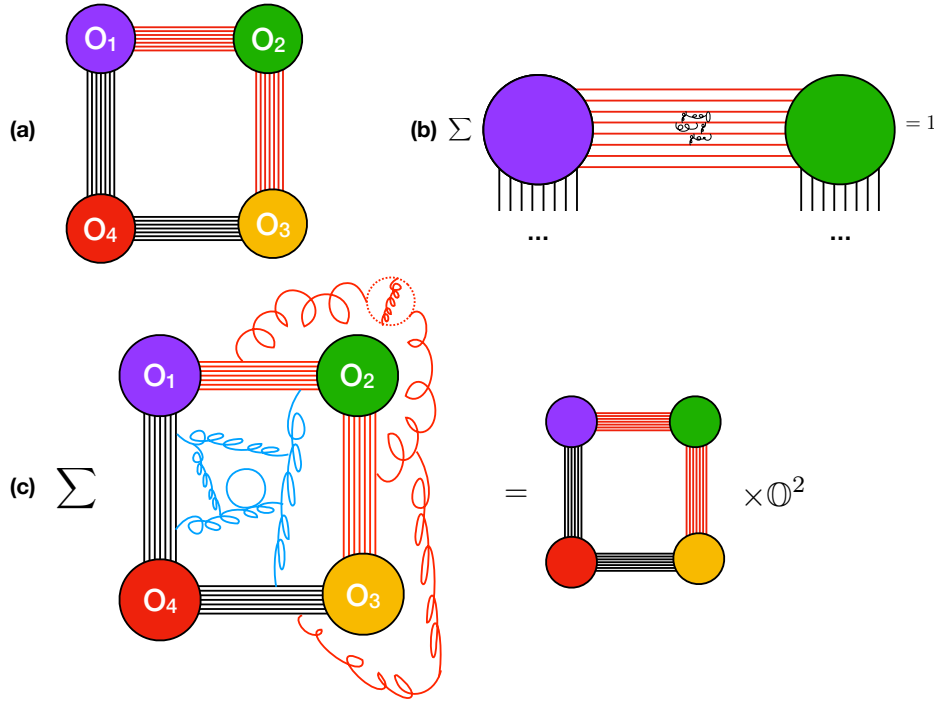


Figure 7.1: Large cyclic operators at genus zero. (a) The tree-level result is given by a single Feynman graph of rectangular form. For large operators, this rectangle creates a big frame. (b) The frame, when big, does not receive loop corrections because of supersymmetry. Indeed these loop corrections are indistinguishable from those arising in the two-point function of BPS operators, a protected quantity. (c) The inside and the outside of the frame, on the other hand, are loop corrected. The sum of all quantum corrections to the inside (or outside) define a function \mathbb{O} of the 't Hooft coupling and of the four-point cross ratio.

coupling behavior due to integrability and bootstrap techniques that were not yet available at the time, so it seems rather timely to revive those explorations in light of these newer technologies.

A key difference compared to the earlier BMN-related works [141, 142, 143, 144] is that in those studies there was typically a single R-charge that was taken to be large, while for the present work it is crucial that the operators correspond to closed strings rotating in different S^5 equators. To be precise, we will take two operators to be two *different* BMN highest-weight states

$$\mathcal{O}_2 = \text{tr}(\mathbf{X}^{2k})(z), \quad \mathcal{O}_4 = \text{tr}(Z^{2k})(\infty), \quad (7.1)$$

and two other operators to be two *equal* BMN descendants

$$\mathcal{O}_1 = \text{tr}(\bar{Z}^k \bar{\mathbf{X}}^k)(0) + \text{permutations}, \quad \mathcal{O}_3 = \text{tr}(\bar{Z}^k \bar{\mathbf{X}}^k)(1) + \text{permutations}, \quad (7.2)$$

where X and Z are two complex scalars in $\mathcal{N} = 4$. This choice of two highest-weight states

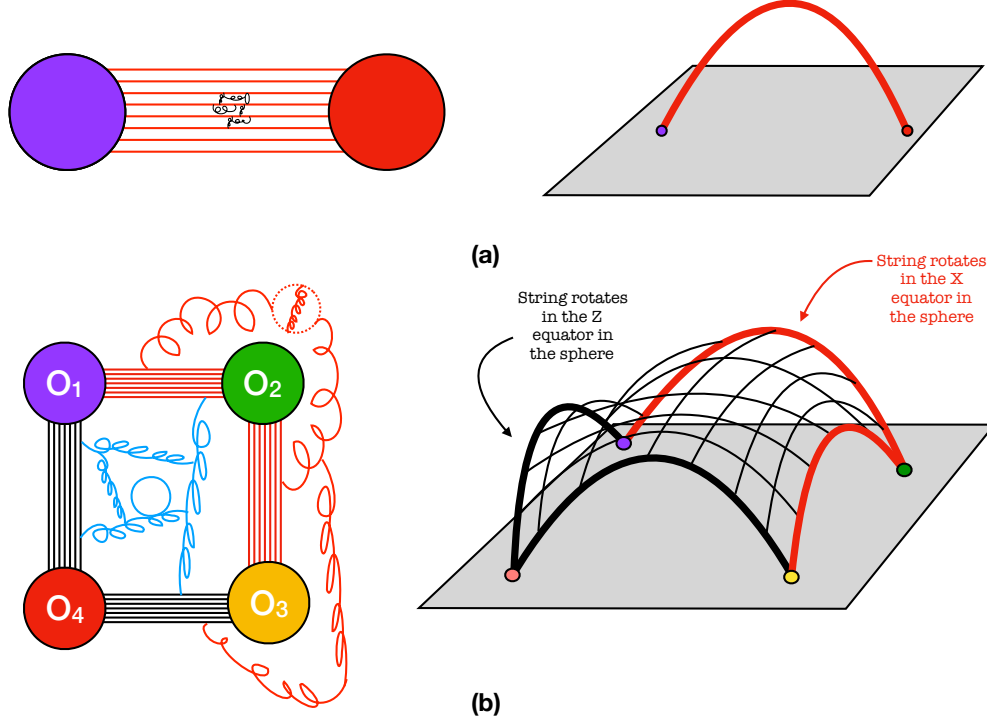


Figure 7.2: Each bundle of propagators in the field theory can be thought of as a very heavy BMN string geodesic which is protected by supersymmetry. The octagon is the sum of all Feynman diagrams inside (or outside) the tree level frame or, equivalently, the top (or bottom) of the folded string stretching between four consecutive geodesics. At genus zero, the folded string has a top and bottom and hence the result is given by \mathbb{O}^2 in agreement with the field theory result.

and two BMN descendents might seem asymmetric and unorthodox but is actually quite important, both technically and physically.

The technical simplification can already be seen at tree level in the planar limit: Because of R-charge conservation, there is only a single Feynman diagram computing the four-point correlation function! The correlator is simply given by a product of $4k$ propagators, with k parallel propagators connecting each pair of consecutive operators \mathcal{O}_i and \mathcal{O}_{i+1} , thus drawing a square frame as depicted in Figure 7.1(a).

Beyond tree level – but still at genus zero – we decorate this correlator by all possible Feynman loops. The diagrams inside individual propagator bundles connecting two operators – as depicted in Figure 7.1(b) – cancel out by supersymmetry, so they do not correct the correlator. After all, those diagrams do not *know* they belong to a four-point function rather than a protected two-point function of BPS operators. The diagrams inside the square – represented in Figure 7.1(c) – do probe all four operators and hence lead to a non-trivial function \mathbb{O} that depends on the 't Hooft coupling λ and on the conformal cross ratios formed by the four operators. This function \mathbb{O} was studied in detail in [2, 3]. The diagrams outside the square contribute by the same amount as the diagrams inside, hence

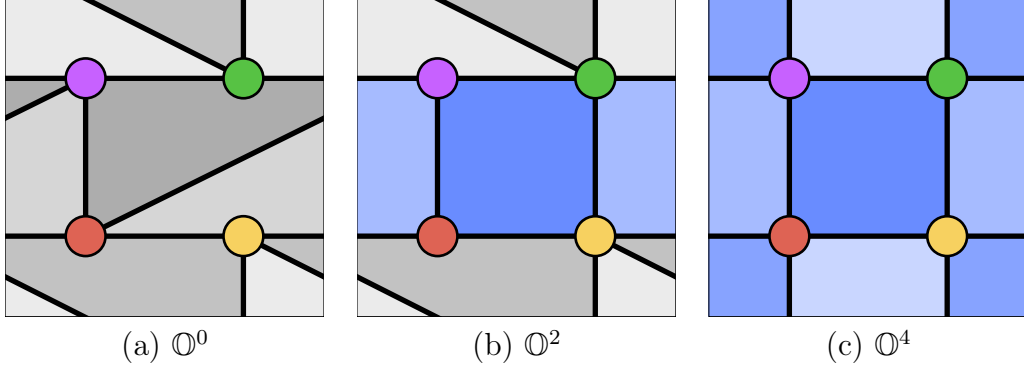


Figure 7.3: Four operators (circles) are inserted on a torus (the top and bottom sides as well as the left and right sides of the square are identified). Wick contractions organize into *skeleton graphs*, where each edge (black line) is a bundle of parallel propagators. For our choice of operators, all faces of all skeleton graphs are octagons. Shown in shades of gray are octagons that touch only two or three of the operators, these are protected by supersymmetry. Octagons that touch all four operators (blue shades) are non-trivial functions of the 't Hooft coupling and conformal cross ratios.

the full genus-zero result is simply given by (throughout this work, g denotes the genus)

$$\langle \mathcal{O}_1 \dots \mathcal{O}_4 \rangle_{g=0} = \langle \mathcal{O}_1 \dots \mathcal{O}_4 \rangle_{\lambda=0, g=0} \times \mathbb{O}^2. \quad (7.3)$$

Note that if it were not for large k , the decoupling between outside and inside would be absent. Indeed, for any finite k and large enough loop order, diagrams can communicate all the way from the inside to the outside.¹

In dual string theory terms, each bundle of propagators connecting consecutive BPS operators can be thought of as a heavy geodesic connecting points x_i and x_{i+1} on the AdS boundary, as represented in Figure 7.2(a). Because there are so many propagators k in each bundle, these geodesics are very heavy and will not move away from their classical configuration. The four classical geodesics will be connected by a folded string, as depicted in Figure 7.2(b). The fold lines are given by the heavy geodesics, which effectively decouple the top and bottom of the folded string. The two sides of the folded string are the string counterpart to the gauge-theory Feynman diagrams inside and outside of the square. In contrast to the heavy geodesics, they do vibrate quantum mechanically, each of them thus defining a full-fledged open string partition function² – this open string partition function is the string definition of the function \mathbb{O} .

¹In the language of hexagonalization [6, 146, 7, 147, 148], the two faces decouple because mirror-particle propagation across large propagator bundles is suppressed.

²The boundary conditions for this open string partition function say that the string should end on the BMN classical geodesics in the bulk. This is somewhat unusual – typically the boundary conditions are such that the worldsheet ends at the boundary of AdS. To properly define the boundary conditions for this open string partition function, we also need to specify how the four classical geodesics rotate in the sphere. There are k units of R-charge of type X (Z) connecting \mathcal{O}_2 (\mathcal{O}_4) with its cyclic neighbours, so the geodesics emanating from operator \mathcal{O}_2 (\mathcal{O}_4) rotate in the $X\bar{X}$ ($Z\bar{Z}$) equator of S^5 with k units

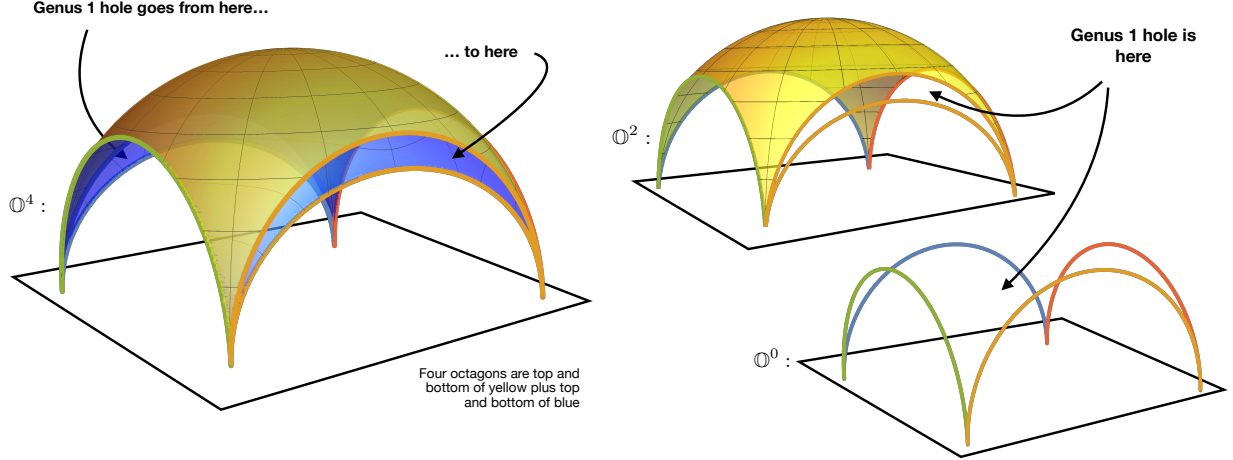


Figure 7.4: AdS embeddings of the three graphs in Figure 7.3. Each edge in Figure 7.3 represents a bundle of $\mathcal{O}(\sqrt{N_c})$ propagators, and therefore becomes a heavy BMN geodesic connecting two operators. These geodesics are folds of the worldsheet that connect adjacent octagons. The BPS octagons have no extent in AdS, they curl up along the BMN geodesics. The non-BPS octagons are extended objects that touch all four operators.

This concludes the genus-zero considerations. This chapter's main focus is on the higher-genus picture. We will explain the general structure of the correlator in detail in the next section. The upshot is that (i) the leading term in the large- k limit at fixed genus g is proportional to k^{4g} , and (ii) we can stack from zero to $2g + 2$ folded strings on top of each other to construct a genus- g surface.³ Since each fold joins two open strings, the number of open string surfaces ought to be even, and thus the full correlation function, i.e. the full closed-string partition function – in the limit of large k – will be simply given by a polynomial P_{g+1} of degree $g + 1$ in the square of the open string partition function \mathbb{O} ,⁴

$$\langle \mathcal{O}_1 \dots \mathcal{O}_4 \rangle = \langle \mathcal{O}_1 \dots \mathcal{O}_4 \rangle_{\lambda=0, g=0} \times \left[\mathbb{O}^2 + \frac{k^4}{N_c^2} P_2(\mathbb{O}^2) + \frac{k^8}{N_c^4} P_3(\mathbb{O}^2) + \dots \right]. \quad (7.4)$$

Resumming the full large N_c expansion, at any value of the 't Hooft coupling, thus amounts to finding the function of two variables

$$\mathcal{A}(\zeta, \mathbb{O}) \equiv \lim_{N_c \rightarrow \infty} \frac{\langle \mathcal{O}_1 \dots \mathcal{O}_4 \rangle}{\langle \mathcal{O}_1 \dots \mathcal{O}_4 \rangle_{\lambda=0, g=0}} \Big|_{k=\zeta\sqrt{N_c}}. \quad (7.5)$$

of angular momentum, see Figure 7.1(a). The full open string will thus interpolate between these two different BMN geodesic behaviors. At large 't Hooft coupling, the open string surfaces become classical, and the open partition function should be given by the area of a minimal surface ending on the four BMN geodesics. Reference [149] is an inspiring related paper where a slightly different class of folded strings were considered, corresponding to null squares with further movement in the sphere.

³For example, if we remove the folded string from Figure 7.2(b), we are left with the four geodesics with a hole in the middle – a genus 1 surface, see Figure 7.4.

⁴The dots in this formula contain higher-genus terms, but also, for each genus, including the terms presented here, smaller powers of k , subleading in the large k limit we are interested in.

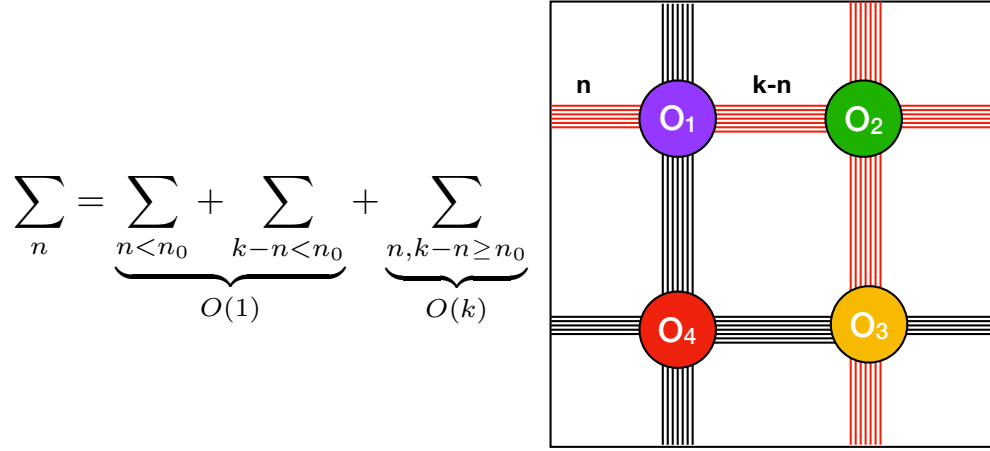


Figure 7.5: Octopus principle. Configurations where some available propagator bundles are not massively occupied are strongly suppressed in the large charge limit. All skeleton graphs are thus maximal graphs, where no further propagator bundle can be added without increasing the genus at hand.

Note that this correlation function \mathcal{A} depends very non-trivially on the conformal cross ratios and on the 't Hooft coupling of the theory through the octagon function \mathbb{O} computed in [2, 3]. The main result of this chapter is a representation of the function \mathcal{A} and of the associated polynomials P_{g+1} in (7.4) in terms of a matrix model, where the octagon function \mathbb{O} enters as an effective quartic coupling.

7.3 A Matrix Model for Large Operators

The basis of our computation is the (planar and non-planar) hexagonalization prescription for correlation functions [6, 146, 7, 147, 148]. The starting point of that prescription is a sum over all Wick contractions of the free gauge theory. We organize this sum by first summing over “skeleton graphs” of the desired genus. Each edge in a skeleton graph represents a bundle of one or more parallel propagators.⁵ For each skeleton graph, we then sum over all possible ways of distributing propagators on the edges of the graph (that are compatible with the charges of the operators).

We saw in the introduction that, for our choice of operators, there is only a single skeleton graph at genus zero. At higher genus, there are several contributing diagrams. For example, the top row of Figure 7.3 shows three different genus-one graphs contributing to the four-point correlation function of our operators (7.1), (7.2). The key observation illustrated by these examples is the following: For large operators, at any genus order,

⁵Because they represent Wick contractions of single-trace operators, the incident edges at each vertex (operator) have a well-defined cyclic ordering. Graphs with this property are called *ribbon graphs* (or fat graphs). See Appendix G.1 for more details.

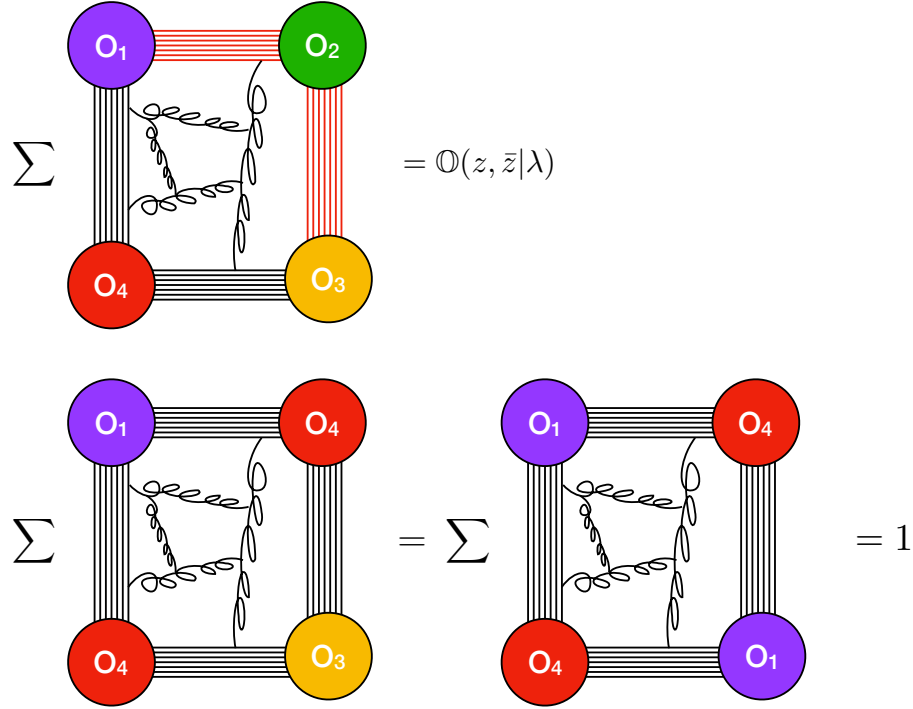


Figure 7.6: The three types of squares all large- k skeleton graphs are made of, see (7.7). Squares can connect all four operators (top figure), and all such squares equal the non-trivial function \mathbb{O} of the 't Hooft coupling λ and the cross ratios parametrized by z and \bar{z} . Squares may also only connect three operators (bottom left) or two operators (bottom right), such squares are protected by supersymmetry and hence do not receive loop corrections.

all skeleton graphs that contribute are *quadrangulations*, i.e. all faces of these graphs are quadrangles. This is because of what we call *the octopus principle*. It comes about because we have to distribute a large number of propagators on the edges of the skeleton graphs. For example, consider the k propagators connecting operators \mathcal{O}_1 and \mathcal{O}_2 in Figure 7.5. In this case, operators \mathcal{O}_1 and \mathcal{O}_2 are connected by two bridges, and we have to sum over all ways of distributing k propagators on these two bridges. For large k , the overwhelming number of terms will have $\mathcal{O}(k)$ propagators on both bridges, and the sum of these terms will produce a factor k . The sum of all terms where any of the bridges is populated by only a finite number of propagators is finite, and thus suppressed in the large- k limit. Hence we immediately see that all propagator bundles want to be heavily populated, evoking the picture of an octopus who wants to spread its tentacles over all possible cycles of the Riemann surface. More generally, if there are n edges connecting two operators, we have to sum over the number k_i of propagators on each edge i , with the constraint that $\sum_i k_i = k$. This sum expands to

$$\sum_{\substack{k_1, \dots, k_n \\ k_1 + \dots + k_n = k}} = \frac{k^{n-1}}{(n-1)!} + \mathcal{O}(k^{n-2}), \quad (7.6)$$

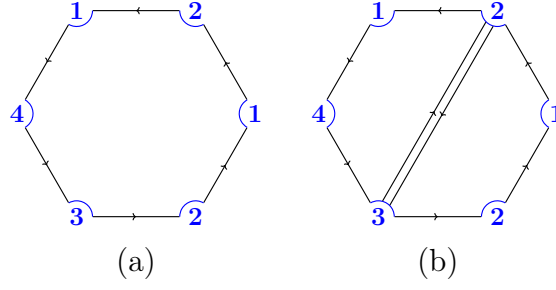


Figure 7.7: All bigger polygons, such as the hexagon shown in (a), can be split into squares by adding further bridges, as shown in (b). Adding such bridges does not increase the genus of the surrounding graph.

and the leading term only receives contributions from configurations where all $k_i = \mathcal{O}(k)$. This has two consequences: At large k , (i) all edges of all skeleton graphs are occupied by $\mathcal{O}(k)$ propagators, and (ii) only graphs where the total number of edges between all operators is maximal will contribute. All terms that violate any of these two conditions will only contribute at subleading orders in large k . At every fixed genus, we will call graphs whose total number of edges is maximal *maximal graphs*. As will be seen below, the number of edges in a maximal graph of genus g is equal to $4g + 4$. Hence the contribution at each genus g comes with an additional k^4 enhancement compared to the genus $g - 1$ contribution. This explains the powers of k in the series (7.4).⁶ This is also why the double-scaling limit $k \sim \sqrt{N_c}$ is precisely the regime that we probe when re-summing that expansion.

We conclude that at large k , the dominating graphs are the so-called maximal graphs, to which no extra propagator bundles can be added without increasing the genus. In such graphs, all faces are bounded by as few edges as possible. For our operator polarizations (7.1), (7.2), the irreducible faces are squares, and hence all maximal graphs are quadrangulations. More precisely, since each operator \mathcal{O}_i can only connect to operators $\mathcal{O}_{i\pm 1}$, all faces of all large- k skeleton graphs must be of one of the following three types:

$$\begin{aligned} \mathbb{O} &= \text{square}[\mathcal{O}_i - \mathcal{O}_{i+1} - \mathcal{O}_{i+2} - \mathcal{O}_{i+3}] = \text{square}[\mathcal{O}_i - \mathcal{O}_{i-1} - \mathcal{O}_{i-2} - \mathcal{O}_{i-3}], \\ 1 &= \mathbb{O}_{\text{BPS}} = \text{square}[\mathcal{O}_i - \mathcal{O}_{i+1} - \mathcal{O}_i - \mathcal{O}_{i+1}] = \text{square}[\mathcal{O}_i - \mathcal{O}_{i-1} - \mathcal{O}_i - \mathcal{O}_{i-1}], \\ 1 &= \mathbb{O}'_{\text{BPS}} = \text{square}[\mathcal{O}_i - \mathcal{O}_{i+1} - \mathcal{O}_{i+2} - \mathcal{O}_{i+1}] = \text{square}[\mathcal{O}_i - \mathcal{O}_{i-1} - \mathcal{O}_{i-2} - \mathcal{O}_{i-1}], \end{aligned} \quad (7.7)$$

as illustrated in Figure 7.6. All bigger polygons can always be split into squares by adding further bridges without increasing the genus, as illustrated in Figure 7.7. Note that we cannot break the squares into triangles, since each operator \mathcal{O}_i can only connect to operators $\mathcal{O}_{i\pm 1}$. The squares in the last two lines of (7.7) only contain at most three different

⁶For a more detailed discussion of this octopus principle (unbaptized until now) see the discussions around equation (6) in [147] or equation (6.10) in [148]. This phenomenon was actually encountered long before, in the times of the BMN explorations; see most notably the discussion on pages 5 and 6 in [141], where it was already identified that the large-charge limit would project out skinny handles in the genus expansion. As mentioned in the introduction, the key difference compared to those earlier BMN works is that here several R-charge directions are taken to be large, and that only now we can take advantage of the great control over the 't Hooft coupling, as fully captured by the function \mathbb{O} .

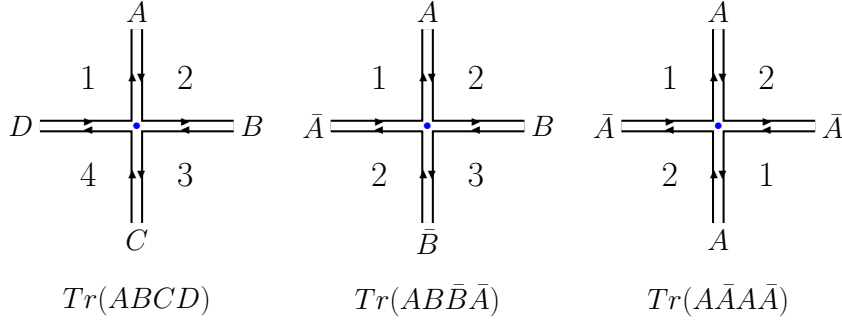


Figure 7.8: Matrix model vertices. Each is the dual counterpart of the corresponding three square types represented in Figure 7.6.

BPS operators and are thus protected by supersymmetry and simply give 1. The square in the first line is the non-trivial function \mathbb{O} that appeared already at genus zero.

To summarize, all graphs that contribute at genus g in the large- k limit are quadrangulations of a genus- g surface, such that all faces are squares of the types (7.7). By Euler counting we have

$$2 - 2g = (V = 4) + (F = n) - (E = 4n/2) = 4 - n, \quad (7.8)$$

so that at genus g , all graphs contain a total of $n = 2g + 2$ squares and twice as many edges. Indeed, our single genus-zero skeleton graph was simply given by two squares, as explained in the previous section. In the three genus-one examples of Figure 7.3, we have four squares.⁷ It is also simple to see that the number of non-BPS squares \mathbb{O} in each graph ought to be even.⁸ Therefore, we conclude that at each fixed genus g , all contributions sum to a polynomial P_{g+1} in \mathbb{O}^2 of degree $g+1$, thus leading to (7.4). Finding these polynomials is tantamount to counting quadrangulations.

In order to count quadrangulations of surfaces of genus g with 4 vertices (punctures) and $2g + 2$ squares, we introduce a matrix model.⁹ The matrix model naturally describes the duals of the skeleton graphs, where each of the $2g + 2$ original square faces becomes a quartic vertex, and where the original 4 vertex operators $\mathcal{O}_1, \dots, \mathcal{O}_4$ become four faces of the dual graph. Each bridge connecting operators \mathcal{O}_i with \mathcal{O}_{i+1} is now pierced by a propagator of the dual graph; since there are four types of bridges $\mathcal{O}_i - \mathcal{O}_{i+1}$, we will have four complex matrices, one for each such original bridge type. See Figure 7.8 for the vertices and Figure 7.9 for example graphs with their duals. There are 10 different square

⁷As indicated by the colors, the diagram in Figure 7.3(a) contains only BPS squares, the diagram in Figure 7.3(b) contains two copies of the non-BPS square \mathbb{O} (and two BPS squares), and the diagram in Figure 7.3(c) contains four copies of the non-BPS square \mathbb{O} .

⁸The non-BPS square is bounded by four different types of edges, while the perimeter of the other two types of squares is formed by even numbers of edges of the same type, as can be seen in Figure 7.6. Since each square is glued to another square along an identical type of edge, the surface can only close if the number of non-BPS squares is even.

⁹Two beautiful matrix model reviews are [150, 151].

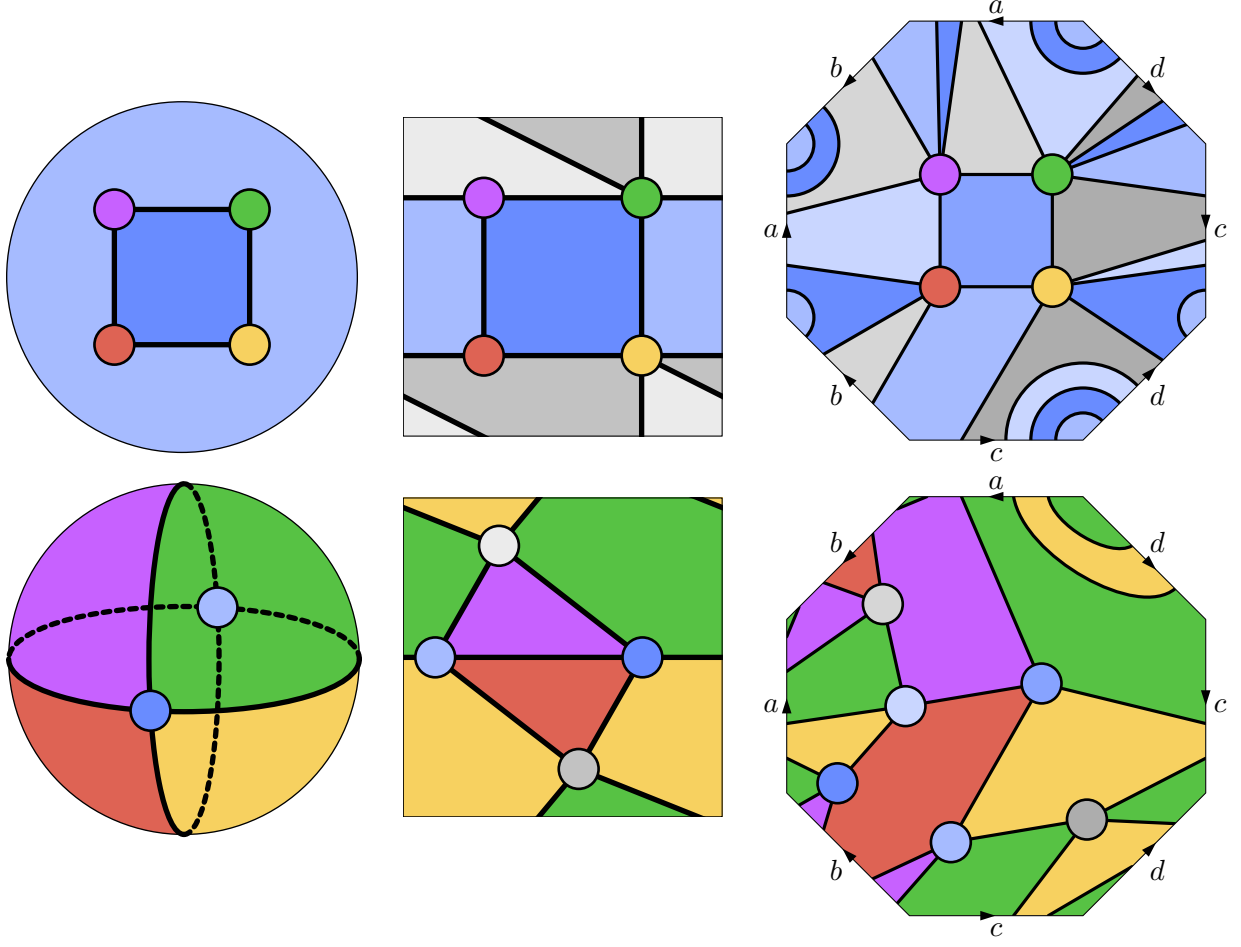


Figure 7.9: Example graphs at genus $g = 0, 1, 2$ (top) with their duals (bottom). In the top row we have four vertices (the BPS operators) and $2g + 2$ faces (the squares). In the bottom row we have four faces (the BPS operators) and $2g + 2$ quartic vertices (the squares).

faces in (7.7), and so there will be 10 different vertices in the matrix model. All in all, the partition function of our matrix model is

$$Z \equiv \int [\mathcal{D}A][\mathcal{D}B][\mathcal{D}C][\mathcal{D}D] \exp(-S_{\text{kin}}[A, B, C, D] + S_{\text{int}}[A, B, C, D]) , \quad (7.9)$$

with the kinetic action term

$$S_{\text{kin}} = \text{tr} \left[\frac{A\bar{A}}{k_1} + \frac{B\bar{B}}{k_2} + \frac{C\bar{C}}{k_3} + \frac{D\bar{D}}{k_4} \right] \quad (7.10)$$

and the interaction term

$$S_{\text{int}} = \mathbb{O}\text{tr} (ABCD) + \mathbb{O}\text{tr} (\bar{D}\bar{C}\bar{B}\bar{A}) \quad (7.11) \\ + \text{tr} \left[\frac{(A\bar{A})^2 + (B\bar{B})^2 + (C\bar{C})^2 + (D\bar{D})^2}{2} + AB\bar{B}\bar{A} + BC\bar{C}\bar{B} + CD\bar{D}\bar{C} + DA\bar{A}\bar{D} \right] .$$

The interaction part consists of two non-BPS vertices in the first line (the duals of the non-BPS squares, which therefore come with a factor \mathbb{O}), and eight BPS vertices (which come with a factor of 1 since they are BPS) in the second line.

In the kinetic term, we have introduced parameters k_i , $i = 1, \dots, 4$ as a means of counting the number of propagator bundles connecting \mathcal{O}_i and \mathcal{O}_{i+1} in each skeleton graph by simply reading off the corresponding power of k_i . This is quite important, because we have to dress each quadrangulation by four factors of the type (7.6), one for each type of connection. Keeping track of the numbers of different types of edges individually also allows us to calculate the correlator of a more general and considerably richer set of operators (the sum over permutations for \mathcal{O}_1 and \mathcal{O}_3 is implicit)

$$\mathcal{O}_1 = \text{tr}(\bar{Z}^{k_4} \bar{X}^{k_1}), \quad \mathcal{O}_2 = \text{tr}(X^{k_1+k_2}), \quad \mathcal{O}_3 = \text{tr}(\bar{Z}^{k_3} \bar{X}^{k_2}), \quad \mathcal{O}_4 = \text{tr}(Z^{k_3+k_4}). \quad (7.12)$$

At genus zero, there is again a single graph contributing to the correlator, and it is again a nice rectangle frame as in Figure 7.1(a). The difference is that now there are k_i propagators connecting \mathcal{O}_i and \mathcal{O}_{i+1} . The limit of large charges now amounts to taking all the k_i to be of order $\sqrt{N_c}$. At genus zero, for example, we have

$$\langle \mathcal{O}_1 \dots \mathcal{O}_4 \rangle_{g=0} = \frac{\mathbb{O}^2}{(x_1 - x_2)^{2k_1} (x_2 - x_3)^{2k_2} (x_3 - x_4)^{2k_3} (x_4 - x_1)^{2k_4}}. \quad (7.13)$$

At higher genus, in the large charge limit and with $\zeta_i \equiv k_i / \sqrt{N_c}$,

$$\frac{\langle \mathcal{O}_1 \dots \mathcal{O}_4 \rangle}{\langle \mathcal{O}_1 \dots \mathcal{O}_4 \rangle_{\lambda=0, g=0}} \xrightarrow{k_i \sim \sqrt{N_c}} \sum_{g=0}^{\infty} \frac{P_{4g|g+1}(k_1, k_2, k_3, k_4, \mathbb{O}^2)}{N_c^{2g}} \equiv \mathcal{A}(\zeta_1, \zeta_2, \zeta_3, \zeta_4, \mathbb{O}), \quad (7.14)$$

where $P_{4g|g+1}$ are polynomials of degree $g+1$ in \mathbb{O}^2 whose coefficients are *homogeneous* polynomials of degree $4g$ in the four k_i . When all k_i are equal, then

$$P_{4g|g+1}(k_i | \mathbb{O}^2) \xrightarrow{k_i \rightarrow k} k^{4g} P_{g+1}(\mathbb{O}^2), \quad (7.15)$$

and we get back to our previous correlator (7.4).

To obtain the full correlator (7.14) at genus g from the matrix model (7.9), we bring down $2g+2$ vertices, pick the N^4 coefficient¹⁰ (since we are after a four-point correlation function, which in terms of the dual matrix model means that we are interested in graphs with four faces), and focus on those contributions where all k_j appear. That last condition is due to R-charge conservation, which implies that all types of bridges between operators \mathcal{O}_i and \mathcal{O}_{i+1} must appear. We thus discard any monomials such as $k_1^2 k_2^2$ which do not contain all k_i . All in all, the term that we are interested in is

$$Z = \dots + N^4 k_1 k_2 k_3 k_4 \left(\mathcal{Z} \equiv \sum_{g=0}^{\infty} \tilde{P}_{4g|g+1}(k_1, k_2, k_3, k_4 | \mathbb{O}^2) \right) + \dots \quad (7.16)$$

¹⁰The matrix model comes with its own number of colors N , which we use to identify numbers of faces and genus, as illustrated in the example (7.16). As usual with such graph dualities, N is not to be identified with the N_c of $\mathcal{N} = 4$ SYM, see e.g. [152]. In fact, we will soon explain that it is often convenient to introduce rectangular matrices with sizes $N_i \times N_{i+1}$ in the matrix model language, to better keep track of the different faces in the matrix model, i.e. the different operators in the original picture.

These tilded polynomials $\tilde{P}_{4g|g+1}$ count our quadrangulations, and are thus *almost* the polynomials arising in the correlator (7.14). To get precisely those, however, we also need to include the combinatorial factors (7.6). Since we strip out an overall k_1, \dots, k_4 factor in defining the reduced partition function \mathcal{Z} , we finally conclude that

$$P_{4g|g+1}(k_1, k_2, k_3, k_4 | \mathbb{O}^2) = \tilde{P}_{4g|g+1}(k_1, k_2, k_3, k_4 | \mathbb{O}^2) \Big|_{k_1^{n_1} \dots k_4^{n_4}} \rightarrow \frac{k_1^{n_1} \dots k_4^{n_4}}{n_1! \dots n_4!}. \quad (7.17)$$

or equivalently

$$\mathcal{A}(\zeta_1, \zeta_2, \zeta_3, \zeta_4, \mathbb{O}) = \mathcal{Z} \Big|_{k_i^n \rightarrow \zeta_i^n / n!} \quad (7.18)$$

for the full correlator at any genus and any coupling.¹¹ This is our main result.

As a trivial check, consider genus zero. We need to bring down $2g + 2 = 2$ vertices, i. e. we consider terms in the expansion of $\exp(-S_{\text{int}})$ that are of degree 2 in the interaction vertices. If we bring down two vertices from the second line in (7.11), we see right away that we either get more than four faces (from $\langle \text{tr}(AB\bar{B}\bar{A}) \text{tr}(CD\bar{D}\bar{C}) \rangle$ for example) *or* we generate terms which do not contain all k_i 's (from $\langle \text{tr}(A\bar{A})^2 \text{tr}(B\bar{B})^2 \rangle$ for example). Bringing down an odd number of vertices from the first line in (7.11) gives a zero result by charge conservation. So we are left with the possibility of bringing down two non-BPS vertices from the first line. This leads to

$$\mathbb{O}^2 \langle \text{tr}(ABCD) \text{tr}(\bar{D}\bar{C}\bar{B}\bar{A}) \rangle = N^4 k_1 k_2 k_3 k_4 \mathbb{O}^2, \quad (7.19)$$

recognizing precisely the genus zero result in (7.13).

Bringing down further octagon vertices from $\exp(-S_{\text{int}})$, we generate all the above-mentioned polynomials \tilde{P} and thus their transformed partners P , which enter the four-point correlation function (7.14). We managed to compute the general polynomials $P_{4g|g+1}$ up to genus $g = 4$. As we saw above, the genus-zero polynomial is simply $P_{0|1} = \mathbb{O}^2$. At genus one, we find

$$P_{4|2} = k_1 k_2 k_3 k_4 \left[1 + \mathbb{O}^2 \frac{\sum_{j=1}^4 [(k_j + k_{j+1})^4 - k_j^4] + 12(k_1 k_2 + k_3 k_4)(k_1 k_4 + k_2 k_3)}{24 k_1 k_2 k_3 k_4} + \frac{\mathbb{O}^4}{2} \right].$$

The polynomials for $g = 2, 3, 4$ are attached in the file For equal charges, $k_i \equiv k$, the polynomials $P_{4g|g+1}$ reduce to k^{4g} times a polynomial P_{g+1} in \mathbb{O} with rational coefficients, see (7.15). The resulting correlator \mathcal{A} is quoted in (8.6) below. We have cross-checked the polynomials $P_{4g|g+1}$ obtained from the matrix model against an explicit construction of all contributing skeleton graphs up to genus three, see Appendix G.1.

Let us make three comments. The first one is that we are extracting the term with 4 faces, proportional to N^4 . This is actually the *smallest* power of N arising in the perturbative expansion if we keep only terms containing all four k_i , as we are instructed to do. (It would be the next-to-smallest if we lift the latter restriction.) This is in stark contrast

¹¹Obviously, the replacement $k_i^n \rightarrow \zeta_i^n / n!$ should only be made after expanding \mathcal{Z} .

with the usual large- N expansion, where the leading terms carry the largest powers of N . So the limit we are interested in is a sort of $N \rightarrow 0$ limit of the matrix model.

In vector models, the limit of small number of colors is a very interesting one, related to polymers and other such fascinating combinatorics. Another interesting instance of such limits shows up in the study of entanglement entropy and quenches disorder, where one often uses the replica trick to study the n copies of a given system in the formal $n \rightarrow 0$ limit. This is done to generate logarithms (of a density matrix or partition function) that were originally absent through the identity $\lim_{n \rightarrow 0} (x^n - 1)/n = \log(x)$. Sometimes the coupling between the various copies is encoded in a matrix, see e.g. [154]. In those cases, we are also interested in a formal limit where the matrix size goes to zero. Such matrices, present most notably in spin-glass studies, have extremely rich dynamics. In matrix model theory, dualities between $N \rightarrow \infty$ and $\tilde{N} \rightarrow 0$ limits have in fact been found before, in the context of the theory of intersection numbers of moduli spaces of curves, see [155, 156, 157].¹² As we will see below, the $N \rightarrow 0$ limit will show up again and again in several simplified matrix model combinatorics in very amusing ways. It would be interesting to find a nice statistical mechanics application of this zero-color limit.

A second small comment is that we can consider rectangular matrices [159], where matrix A has dimensions $N_1 \times N_2$, matrix B has dimensions $N_2 \times N_3$, and so on. Then N^4 would be replaced by $N_1 N_2 N_3 N_4$, identifying precisely the four faces corresponding to the four distinct operators. The terms containing this factor automatically contain all k_i , so using rectangular matrices would allow us to condense the instructions above into simply

$$\mathcal{Z}(k_i) = \frac{1}{k_1 k_2 k_3 k_4} \lim_{N_i \rightarrow 0} \frac{\partial}{\partial N_1} \frac{\partial}{\partial N_2} \frac{\partial}{\partial N_3} \frac{\partial}{\partial N_4} Z(N_i, k_i). \quad (7.20)$$

This highlights once more the limit of small number of colors we are interested in.

The last comment pertains to the combinatorial replacement in (7.17). In effect, by introducing an extra $1/n!$ for each coupling k_i^n , we are Borel transforming our matrix model perturbative expansion. Interestingly, it renders the partition function expansion finite, as we will see explicitly below. Namely, the transformation removes the usual $(2g)!$ divergence that is due to the proliferation of graphs at higher genus [160], and thus leads to a fully convergent expansion. While getting rid of divergences might be seen as a feature, losing the D-brane physics they encode is bit of a bug. This is presumably related to the fact that although we are resumming a 't Hooft expansion, we are not generating arbitrarily complicated multi-string intermediate states. The large-charge limit projects onto folded strings, BMN strings and copies thereof, eliminating non-perturbative effects arising from the more complicated multi-string states which the D-branes source. It would be fascinating to slowly decrease the size of our BPS operators to move away from our fully convergent limit and carefully isolate these novel effects in a controllable way.

¹²Another reference which mentions this limit and dubs it as the anti-planar limit is [158].

7.4 Matrix Model Simplification and Limits

Ideally, we would like to determine the full correlation function $\mathcal{A}(\zeta_1, \zeta_2, \zeta_3, \zeta_4, \mathbb{O})$ by solving the matrix model (7.9). That would be equivalent to computing the polynomials $P_{4g|g+1}$ to all genus, which we have not succeeded thus far. What we *did* manage to do is to simplify this matrix model problem into an equivalent matrix model problem where we have two hermitian matrices $\mathbb{M}_1, \mathbb{M}_2$ and two complex matrices \mathbb{X}, \mathbb{Y} , with a non-diagonal propagator between \mathbb{X} and \mathbb{Y} equal to the octagon function \mathbb{O} , so that

$$\langle F \rangle \equiv \int [\mathcal{D}\mathbb{M}_1][\mathcal{D}\mathbb{M}_2][\mathcal{D}\mathbb{X}][\mathcal{D}\mathbb{Y}] F \exp \left[-\frac{1}{2} \text{tr } \mathbb{M}_1^2 - \frac{1}{2} \text{tr } \mathbb{M}_2^2 - \text{tr } \begin{pmatrix} \mathbb{X} & \mathbb{Y} \end{pmatrix} \begin{pmatrix} 1 & \mathbb{O} \\ \mathbb{O} & 1 \end{pmatrix}^{-1} \begin{pmatrix} \bar{\mathbb{X}} \\ \bar{\mathbb{Y}} \end{pmatrix} \right]. \quad (7.21)$$

Then we have the rather compact expression

$$\mathcal{Z} = \frac{\left\langle \text{tr } \log \left(\mathbb{I} - \frac{k_2}{\mathbb{I} - k_2 \mathbb{M}_2} \bar{\mathbb{X}} \frac{k_1}{\mathbb{I} - k_1 \mathbb{M}_1} \mathbb{X} \right) \text{tr } \log \left(\mathbb{I} - \frac{k_3}{\mathbb{I} - k_3 \mathbb{M}_2} \bar{\mathbb{Y}} \frac{k_4}{\mathbb{I} - k_4 \mathbb{M}_1} \mathbb{Y} \right) \right\rangle_{\text{two faces}}}{k_1 k_2 k_3 k_4} \quad (7.22)$$

for the reduced partition function, from which we can readily extract the correlator via (7.18). When expanding the logarithms in powers of k , we can drop all terms whose total power is not a multiple of four, since the latter are the terms that correspond to an even number of octagons as required (at genus g we keep $4g + 4$ powers of k). We also extract the coefficient of N^2 , which is the smallest power of N on the right hand side. So again, in this alternative matrix model formulation, we are after the $N \rightarrow 0$ limit. As a check, we can expand to leading order in k to get

$$\mathcal{Z} = \langle \text{tr } (\bar{\mathbb{X}} \mathbb{X}) \text{tr } (\bar{\mathbb{Y}} \mathbb{Y}) \rangle_{\text{two faces}} + \mathcal{O}(k^4), \quad (7.23)$$

which evaluates to \mathbb{O}^2 , since Wick contracting complex fields of the same type would lead to four faces, and since each off-diagonal propagator equals \mathbb{O} . This is exactly what we expect at genus zero.

The derivation of (7.22) follows the graphical manipulations in Appendix G.3.2. Technically, we open up all quartic vertices in (7.11) into pairs of cubic vertices using auxiliary fields as detailed in Appendix G.3.4. If done carefully, the resulting action is Gaussian in the original four complex matrices. Integrating them out then leads to (7.22). In particular, the logarithms arise from the complex matrix identity

$$\int [\mathcal{D}\mathbb{A}] e^{-\text{tr } (\mathbb{A} \cdot \mathbb{Q} \cdot \bar{\mathbb{A}})} = (\det \mathbb{Q})^{-N}. \quad (7.24)$$

It is particularly nice that in these integrations we explicitly generate two such factors which automatically produce two factors of N . That is why in (7.22) we extract two faces only rather than four as in the original representation with four complex matrices. Technically, this renders the representation (7.22) quite powerful. Besides, there are less degrees of freedom as we went from four complex matrices to two complex and two hermitian.

More physically, we started with a matrix model with four complex matrices corresponding to the four types of consecutive propagators in our large cyclic operators. The four-point function of these four cyclic operators was mapped to a dual correlation function with four faces in the dual matrix model with matrices A, B, C, D . The two-point function with two faces in (7.22) is thus a hybrid representation, where two of the four operators are represented as vertices and the other two as faces, see Figure G.15. See [161, 152], and also the very inspiring talk [162] for very similar (and often more general) dynamical graph dualities obtained by integrating-in and -out matrix fields.

In practice, we compute (7.22) by expanding out the expression to any desired monomial in the k_i and then performing the various free Wick contractions. We found it particularly convenient to Wick contract the complex matrices first and the hermitian matrices at the end. Once \mathbb{X} and \mathbb{Y} are integrated out, because of the alternating pattern in (7.22) it is easy to see that we generate products of traces containing either $U_{k_1}(\mathbb{M}_1)$ and $U_{k_4}(\mathbb{M}_1)$ or $U_{k_2}(\mathbb{M}_2)$ and $U_{k_3}(\mathbb{M}_2)$, but never both (here $U_k(M) \equiv k/(\mathbb{I} - kM)$). Expanding further the U_k in terms of the fundamental Hermitian fields we conclude that our full reduced partition function is given by a sum of factorized one-matrix correlators,

$$\mathcal{Z} = \sum_{g=0}^{\infty} \sum_{n_1, \dots, n'_{M'}} \mathbb{C}_{n_1, \dots, n'_{M'}}^{(g)} \times \langle \text{tr}(\mathbb{M}_1^{n_1}) \dots \text{tr}(\mathbb{M}_1^{n_M}) \rangle_{\text{one face}} \times \langle \text{tr}(\mathbb{M}_2^{n'_1}) \dots \text{tr}(\mathbb{M}_2^{n'_{M'}}) \rangle_{\text{one face}}. \quad (7.25)$$

In this sum, $n_1 + \dots + n_M + n'_1 + \dots + n'_{M'} \leq 4g$, and the combinatorial factors $\mathbb{C}^{(g)}$ arising from integrating out the complex matrices \mathbb{X} and \mathbb{Y} are *homogeneous* polynomials of degree $4g$ in the k_j , with coefficients that are polynomials in \mathbb{O}^2 of maximally degree $g + 1$.¹³ Importantly, note that because of the factorization in (7.25), each Hermitian correlator now has to be restricted to a *single* face, which is quite a bit simpler than the previous two-face problem in (7.22), which in turn was a considerable simplification over the initial four-face problem in (7.9).¹⁴

In fact, the one-face problem was solved already in the first days of matrix models, see e.g. the discussion below equation (9) in [163], from which we readily get the generating

¹³Note in particular that we can have $M = 1$ and $n_1 = 0$, so that the first term in (7.25) would just give $\langle \text{tr}(\mathbb{I}) = N \rangle_{\text{one face}} = 1$.

¹⁴Up to genus 1, using the notation $\langle \dots \rangle_1 \equiv \langle \dots \rangle_{\text{one face}}$, we have

$$\begin{aligned} \mathcal{Z} &= \mathbb{O}^2 \langle \text{tr}(\mathbb{I}) \rangle_1^2 + \mathbb{O}^4 k_1 k_2 k_3 k_4 \langle \text{tr}(\mathbb{I}) \rangle_1^2 + k_1 k_2 k_3 k_4 \langle \text{tr}(\mathbb{M}_1)^2 \rangle_1 \langle \text{tr}(\mathbb{M}_2)^2 \rangle_1 + \mathbb{O}^2 \left(\frac{(k_1 + k_4)^4}{24} \langle \text{tr}(\mathbb{M}_1^4) \rangle_1 \langle \text{tr}(\mathbb{I}) \rangle_1 \right. \\ &\quad \left. + \frac{k_1^2 k_2^2}{4} \langle \text{tr}(\mathbb{I}) \rangle_1^2 + \frac{k_1^3 k_2 + 3k_1^2 k_2 k_4 + 3k_1 k_3 k_4^2 + k_3 k_4^3}{6} \langle \text{tr}(\mathbb{M}_1)^2 \rangle_1 \langle \text{tr}(\mathbb{I}) \rangle_1 + \frac{k_1 \leftrightarrow k_3}{k_2 \leftrightarrow k_4} \frac{\mathbb{M}_1 \leftrightarrow \mathbb{M}_2}{\mathbb{M}_1 \leftrightarrow \mathbb{M}_2} \right) + \dots \\ &= \left(1 + \frac{1}{2} \mathbb{O}^4 \right) \prod_{i=1}^4 k_i + \mathbb{O}^2 \left(1 + \sum_{i=1}^4 k_i^4 + k_i^3 k_{i+1} + k_i k_{i+1}^3 + k_i^2 k_{i+1}^2 + k_i k_{i+1}^2 k_{i+2} \right) + \dots \\ \Rightarrow \mathcal{A} &= \left(1 + \frac{1}{2} \mathbb{O}^4 \right) \prod_{i=1}^4 \frac{\zeta_i}{1!} + \mathbb{O}^2 \left(1 + \sum_{i=1}^4 \frac{\zeta_i^4}{4!} + \frac{\zeta_i^3 \zeta_{i+1}}{3! 1!} + \frac{\zeta_i \zeta_{i+1}^3}{1! 3!} + \frac{\zeta_i^2 \zeta_{i+1}^2}{2! 2!} + \frac{\zeta_i \zeta_{i+1}^2 \zeta_{i+2}}{1! 2! 1!} \right) + \dots \end{aligned}$$

function of all these multi-trace Hermitian matrix model single-face expectation values as

$$\begin{aligned} & \left\langle \exp \sum_{n=1}^{\infty} t_n \text{tr} (\mathbb{M}^n) \right\rangle_{\text{one face}} \\ &= \sum_{j=1}^{\infty} \sum_{k=0}^{j-1} \frac{(2k+1)!!(2j-2k-3)!!}{2j(-1)^k} \left(\frac{j-2k-1}{k+1/2} \sum_{r=0}^{2k} \bar{p}_r p_{2j-r} - \bar{p}_{2k+1} p_{2j-2k-1} \right), \end{aligned} \quad (7.26)$$

where p_r, \bar{p}_r are defined via the Schur polynomial identities

$$\sum_{n=0}^{\infty} p_n z^n \equiv \exp \left(\sum_{n=1}^{\infty} z^n t_n \right) \quad \text{and} \quad \sum_{n=0}^{\infty} \bar{p}_n z^n \equiv \exp \left(- \sum_{n=1}^{\infty} z^n t_n \right). \quad (7.27)$$

Another beautiful representation follows from the single-face limit of [164], which gives

$$\left\langle \exp \sum_{n=1}^{\infty} t_n (\mathbb{M}^n) \right\rangle_{\text{one face}} = \left(\exp \sum_{a,b=0}^{\infty} \overbrace{ab t_a t_b \frac{\partial}{\partial t_{a+b-2}}}^{\text{splitting}} + \overbrace{(a+b+2) t_{a+b+2} \frac{\partial}{\partial t_a} \frac{\partial}{\partial t_b}}^{\text{joining}} \right) t_0, \quad (7.28)$$

where the differential operator can be thought of as implementing fusion and fission of the various traces as one Wick-contracts all these correlators, see Figure 7.10. For general N , we would replace the t_0 at the end by $e^{N t_0}$, and the N^F coefficient in the final expansion would compute the F -face result; it is quite a huge simplification to simply linearize this exponent to get a single face in (7.28), as needed for our problem.¹⁵

We could also try to integrate out the Hermitian matrices first.¹⁶

This concludes the general description of our matrix model, and how we dealt with it in practice to produce higher-genus predictions. Next, we focus on interesting simplifying limits. There are at least three obvious interesting limits where our correlator should simplify:

$$(\mathbf{A}) \circlearrowleft \rightarrow 1, \quad (\mathbf{B}) \circlearrowleft \rightarrow 0, \quad (\mathbf{C}) \circlearrowleft \rightarrow \infty. \quad (7.29)$$

¹⁵We also found, experimentally, yet another beautiful and even more compact representation for these single-face correlators:

$$\left\langle \prod_{a=1}^n \text{tr} (e^{t_a \mathbb{M}} - \mathbb{I}) \right\rangle_{\text{one face}} = \frac{1}{T^2} \prod_{a=1}^n 2 \sinh \left(\frac{t_a T}{2} \right), \quad T \equiv \sum_{b=1}^n t_b,$$

see also Appendix G.4.1 for a multi-hermitian matrix generalization. In fact, this representation has been found before in the context of intersection theory on moduli spaces [156].

¹⁶In this regard, note that when we set all couplings $k_j \equiv k$ equal, then we can rescale the matrices $\mathbb{X} \rightarrow \sqrt{1-k\mathbb{M}_1} \mathbb{X} \sqrt{1-k\mathbb{M}_2}$, and similarly for \mathbb{Y} , to get rid of all Hermitian matrices in the logarithms in (7.22), and put them in new Yukawa-like interactions upstairs, linear in both \mathbb{M}_1 and \mathbb{M}_2 (because the square roots nicely combine when the couplings k_j are equal). Then we could use the tricks of [165] to integrate out the Hermitian matrices and generate some new logarithmic potentials for the remaining two complex matrices. The problem is that by setting all couplings to be the same, we naively lose the possibility of Borel resumming w.r.t. each individual coupling, as needed to get our correlator in (7.18). It would be very nice to overcome this obstacle.

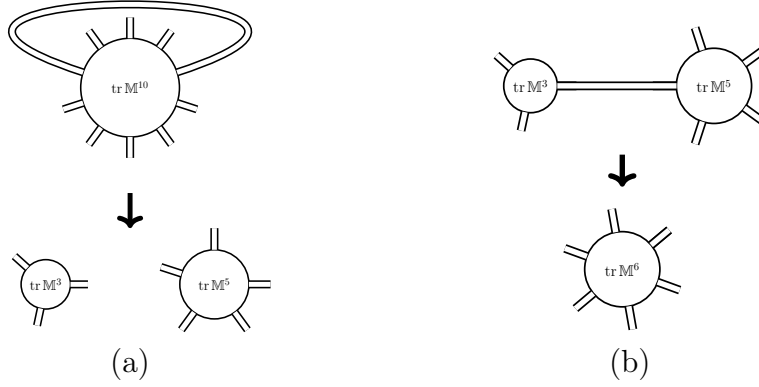


Figure 7.10: (a) Splitting and (b) joining of traces represented as differential operators in (7.28).

The first corresponds to $\lambda = 0$ or tree level (but all genus orders). The other limits are more interesting [119]. The second shows up, for example, at strong coupling, and also in interesting null limits at finite coupling. The last one would be realized for instance in the so-called bulk-point limit [22].

7.4.1 Small Octagon Limit, $\mathbb{O} \rightarrow 0$

In the small octagon limit where $\mathbb{O} \rightarrow 0$, we are left with the eight BPS square vertices in the second line of (7.11), all with the same weight = 1. Now, there is another setup where we would have encountered these, and only these, type of vertices, namely if we were to study extremal correlators in the double-scaling limit of [141, 142, 143, 144] using quadrangulations. There, we know how to solve the original problem directly, using single-matrix model technology, and the results found for these correlators are basically given by products of $\sinh(\omega_{ij} J_i J_j)$ factors times some simple rational function, where J_i are the charges of the involved operators, and the frequencies ω_{ij} are pure numbers. We cannot directly apply the very same techniques to our case, since we are now dealing with several complex matrices. Instead, we guessed that the result ought to take a similar form. We made an ansatz with a number of \sinh factors and fixed the various frequencies and prefactors by matching with the first few terms of our matrix-model perturbative expansion. Then we computed a few more orders to cross-check the validity of this guess up to genus six. It all works out beautifully, and the result turns out to be remarkably simple:

$$\mathcal{A}(\zeta_1, \zeta_2, \zeta_3, \zeta_4 | \mathbb{O} = 0) = \prod_{i=1}^4 \frac{\sinh\left(\frac{1}{2} \zeta_i (\zeta_{i-1} + \zeta_i + \zeta_{i+1})\right)}{\frac{1}{2} (\zeta_{i-1} + \zeta_i + \zeta_{i+1})}. \quad (7.30)$$

In fact, we did a bit more than this: We considered a generalized matrix model, where each of the eight BPS vertices is dressed with an arbitrary coefficient, and guessed the general form of the resulting “twisted” correlator following the same strategy, see Appendix G.3.4. We also studied these generalized BPS quadrangulations for n -point extremal correlators

in [Appendix G.4.1](#), and for a setup where n operators are cyclically connected (the correlator discussed here is the $n = 4$ case of that) in [Appendix G.4.2](#).

It would be very interesting to find a first-principle honest derivation of (7.30), starting from (7.9) or (7.21). It might very well elucidate powerful tricks which we may hope to use in the general case, where the octagon vertex is inserted back.

It is important to stress that the result (7.30) is very non-perturbative, although it has no coupling dependence in it. Note in particular that setting $\mathbb{O} \rightarrow 0$ is not the same as setting the coupling to zero, which is instead $\mathbb{O} \rightarrow 1$. When $\mathbb{O} \rightarrow 0$, the various loop corrections must work hard to completely cancel the tree-level result $\mathbb{O} = 1$. For example, at genus zero and tree level, the correlator is equal to 1, but it becomes \mathbb{O}^2 at non-zero coupling. So when $\mathbb{O} \rightarrow 0$, the full genus zero result is washed out non-perturbatively. In string terms, the BPS vertices describe point-like string configurations, while \mathbb{O} describes a large folded string. When the string tension is very large, the BPS configurations with no area survive, while the big extended strings are suppressed. Recall that the planar result consists of just two copies of a big folded string glued together. Interestingly, this contribution gets suppressed for $\mathbb{O} \rightarrow 0$. At genus one, we start having configurations that are free of folded strings and those should survive. Indeed, the genus expansion of (7.30) starts at genus one:

$$\begin{aligned} \frac{\mathcal{A}}{k_1 k_2 k_3 k_4} &= 0 \times N_c^0 + \frac{1}{N_c^2} + \frac{1}{N_c^4} \frac{1}{24} \sum_{j=1}^4 k_j^2 (k_{j-1} + k_j + k_{j+1})^2 \\ &+ \frac{1}{N_c^6} \frac{1}{1152} \sum_{i=1}^4 \sum_{j=1}^4 \left(1 - \frac{2}{5} \delta_{i,j}\right) k_i^2 k_j^2 (k_{i-1} + k_i + k_{i+1})^2 (k_{j-1} + k_j + k_{j+1})^2 \\ &+ \mathcal{O}(1/N_c^8) \end{aligned} \quad (7.31)$$

It would be cute if we could understand the numbers in this expansion directly from string theory by carefully counting these degenerate string configurations. A good starting point could be [166], where degenerate point-like string configurations for two- and three- point functions were analyzed, see also [167]. It would be interesting to generalize them to our BPS squares, and to understand how those can be put together purely in string terms.

7.4.2 Large Octagon Limit, $\mathbb{O} \rightarrow \infty$

Another interesting limit is the regime where the octagon \mathbb{O} becomes very large. In this case, only the maximal power of \mathbb{O} survives at each order in the genus expansion, which is \mathbb{O}^{2g+2} . In other words, we only use the two non-BPS squares in our quadrangulations, and set all BPS squares to zero. This dramatically simplifies the representation (7.22) to

$$\mathcal{Z} = \sum_{n=1}^{\infty} \frac{(k_1 k_2 k_3 k_4)^{n-1} \mathbb{O}^{2n}}{n^2} \langle \text{tr} ((\mathbb{X}\mathbb{Y})^n) \text{tr} ((\bar{\mathbb{X}}\bar{\mathbb{Y}})^n) \rangle_{\text{two faces}}, \quad (7.32)$$

where \mathbb{X} and \mathbb{Y} here are complex matrices with diagonal propagator normalized to 1, i.e. with kinetic term simply given by $-\text{tr}(\mathbb{X}\mathbb{X}) - \text{tr}(\mathbb{Y}\mathbb{Y})$. To arrive at this expression, we notice that (i) we can set to zero all \mathbb{M}_j matrices, since they describe BPS quadrangulations, and (ii) we only keep the off-diagonal Wick contractions between the complex matrices in (7.22), since those generate octagons, while self-contractions do not. Since we are only off-diagonally contracting \mathbb{X} with $\bar{\mathbb{Y}}$ and \mathbb{Y} with $\bar{\mathbb{X}}$, we can swap $\bar{\mathbb{Y}}$ and $\bar{\mathbb{X}}$ and replace the off-diagonal by a purely diagonal propagator equal to \mathbb{O} for the matrices \mathbb{X} and \mathbb{Y} . Finally, we can rescale the propagator to 1 by taking all factors of \mathbb{O} out of the correlator. In this way, upon expanding the logarithms, we obtain (7.32).

The representation (7.32) immediately leads to a very compact expression for our correlator in the large octagon limit, since the dependence on k is explicit, and thus the Borel-transform procedure can be done straightforwardly, yielding

$$\mathcal{A} = \frac{1}{\zeta_1 \zeta_2 \zeta_3 \zeta_4} \sum_{n=1}^{\infty} \frac{(\zeta_1 \zeta_2 \zeta_3 \zeta_4 \mathbb{O}^2)^n}{n^2 (\textcolor{red}{n} - 1)!^4} \langle \text{tr}((\mathbb{X}\mathbb{Y})^n) \text{tr}((\bar{\mathbb{X}}\bar{\mathbb{Y}})^n) \rangle_{\text{two faces}}. \quad (7.33)$$

The two-point function in this expression can be evaluated analytically at any N , that is for any number of faces, starting from its single-complex-matrix counterpart

$$\langle \text{tr}(\mathbb{X}^n) \text{tr}(\bar{\mathbb{X}}^n) \rangle = \sum_{k=1}^n \prod_{i=1}^k (i + N - 1) \prod_{m=1}^{n-k} (N - m). \quad (7.34)$$

This expression is derived by decomposing each trace into characters of hook representations (generating one sum per trace) and then using character two-point function orthogonality, thus killing one of the two sums. See for instance formula (B.2) in [143]. The final sum over hooks is (7.34). We want the same expression with $\mathbb{X} \rightarrow \mathbb{X}\mathbb{Y}$. To find it, we proceed as for the single-matrix case, except that we use so-called fission relations to open up characters $\chi_\lambda(\mathbb{X}\mathbb{Y})$ into $\chi_\lambda(\mathbb{X})\chi_\lambda(\mathbb{Y})$ upon doing the relative matrix angle integral between the two matrices. Each character thus splits into two, so the representation (7.34) ends up being modified to

$$\langle \text{tr}((\mathbb{X}\mathbb{Y})^n) \text{tr}((\bar{\mathbb{X}}\bar{\mathbb{Y}})^n) \rangle = \sum_{k=1}^n \left(\prod_{i=1}^k (i + N - 1) \prod_{m=1}^{n-k} (N - m) \right)^{\textcolor{red}{2}}. \quad (7.35)$$

We can now simply expand the summand at small N to read off the leading $N \rightarrow 0$ term, which is precisely the required two-face contribution. Plugging that into (7.33), we obtain our full correlator

$$\mathcal{A} = \frac{1}{\zeta_1 \zeta_2 \zeta_3 \zeta_4} \sum_{g=0}^{\infty} \frac{(\zeta_1 \zeta_2 \zeta_3 \zeta_4 \mathbb{O}^2)^{g+1}}{(g+1)^2 g!^4} \sum_{m=0}^g m!^2 (g-m)!^2. \quad (7.36)$$

We can re-sum this expression into¹⁷

$$\mathcal{A} = \mathbb{O}^2 \int_0^1 ds \int_0^1 dt \left[\frac{st}{s+t-1} I_0(2\sqrt{st}\omega) - \frac{(1-s)(1-t)}{s+t-1} I_0(2\sqrt{(1-s)(1-t)}\omega) \right], \quad (7.37)$$

where $\omega = \zeta_1 \zeta_2 \zeta_3 \zeta_4 \mathbb{O}^2$, and where I_0 is the modified Bessel function of the first kind. Note that this expression is valid for \mathbb{O} large, k_j large, N_c large, but $\omega = k_1 k_2 k_3 k_4 \mathbb{O}^2 / N_c^2$ can be either large or not, it depends on how these limits are taken. In particular we find

$$\mathcal{A} \simeq \frac{1}{\zeta_1 \zeta_2 \zeta_3 \zeta_4} \times \begin{cases} \omega + O(\omega^2) & \omega \ll 1, \\ \frac{e^{2\sqrt{\omega}}}{\sqrt{\pi} \omega^{1/4}} & \omega \gg 1. \end{cases} \quad (7.38)$$

As mentioned above, in the two-point function representation (7.22), each of the two logarithms represents one of the large cyclic operators, and the two faces encode the remaining two operators. This is how this matrix model representation encodes our original four-point correlator. There are other representations of this fully non-BPS result, which are instructive in their own right, such as the original matrix model where the four operators are faces, and also two new representations in Appendix G.3.3: A one-point function with three faces, and a three-point function with one face, see (G.25). In all these matrix model representations, we are after the leading term in the $N \rightarrow 0$ limit.

Finally, let us stress once more the very important effect of the Borel $1/g!$ arising from the large operator combinatorics. It is the four $1/g!$ factors in (7.36) that are responsible for the very nice convergence of this expression. Indeed,

$$\sum_{m=0}^g m!^2 (g-m)!^2 \simeq 2(g!)^2 \simeq \sqrt{4\pi g} 4^{-g} (2g)! \quad \text{for } g \gg 1, \quad (7.39)$$

exhibiting the usual large-genus behavior expected in such string/matrix theories [160]. This growth would otherwise render the matrix model perturbative expansion asymptotic, with missing non-perturbative effects hinting at the physics of D-branes, see above. Because of the extra combinatorial factors in (7.36) we obtain instead a perfectly convergent expression (7.37) with asymptotic behavior (7.38).

7.4.3 Free Octagon Limit, $\mathbb{O} \rightarrow 1$

Having analyzed the very non-perturbative $\mathbb{O} \rightarrow 0$ and $\mathbb{O} \rightarrow \infty$ limits, we turn to what should naively be a much simpler limit: The free octagon limit, where $\mathbb{O} \rightarrow 1$. In this case,

¹⁷The two terms in the integrand can be combined to the simpler expression $2stI_0(2\sqrt{st}\omega)/(s+t-1)$. However, the integration of the small- ω expansion of this expression is badly defined, whereas after expanding the integrand in (7.37), the integration directly gives (7.36).

the diagonal and off-diagonal propagators of the complex matrices in (7.22) are identical. Hence the matrices \mathbb{X} and \mathbb{Y} can be identified, thus leading to a simpler matrix model representation with a single complex matrix \mathbb{X} and two Hermitian matrices \mathbb{M}_1 and \mathbb{M}_2 , with partition function

$$\mathcal{Z} = \frac{\left\langle \text{tr} \log \left(\mathbb{I} - \frac{k_2}{\mathbb{I} - k_2 \mathbb{M}_2} \bar{\mathbb{X}} \frac{k_1}{\mathbb{I} - k_1 \mathbb{M}_1} \mathbb{X} \right) \text{tr} \log \left(\mathbb{I} - \frac{k_3}{\mathbb{I} - k_3 \mathbb{M}_2} \bar{\mathbb{X}} \frac{k_4}{\mathbb{I} - k_4 \mathbb{M}_1} \mathbb{X} \right) \right\rangle_{\text{two faces, } k^{4m}}}{k_1 k_2 k_3 k_4}, \quad (7.40)$$

where

$$\langle F \rangle \equiv \int [\mathcal{D}\mathbb{M}_1][\mathcal{D}\mathbb{M}_2][\mathcal{D}\mathbb{X}] F \exp \left[\frac{1}{2} \text{tr} \mathbb{M}_1^2 + \frac{1}{2} \text{tr} \mathbb{M}_2^2 + \text{tr} \mathbb{X} \bar{\mathbb{X}} \right]. \quad (7.41)$$

Once Borel transformed, this matrix model partition function computes the tree level correlator ($\lambda = 0$) of the operators (7.12) at any genus order in the double-scaling limit where $k_j/\sqrt{N_c}$ is held fixed with k_j and N_c both taken to infinity. As before, it is easy to expand this correlator to very high genus order. However, compared to the previous cases, we were not able to either derive or guess the all-genus expansion. It would be very interesting to find the proper matrix model technology allowing us to compute the expectation value (7.40) in this amusing $N \rightarrow 0$ limit where the two-face contribution dominates.

Perhaps we could even expect more, and actually compute the correlator for any N_c in this free theory limit. Note that the space-time dependence at tree level is completely fixed by R-charge conservation and thus factors out, as there must be exactly k_i propagators connecting each two consecutive operators. The free-theory all-genus correlator is thus given by a matrix model of two complex matrices that are simply the complex scalars Z and X in $\mathcal{N} = 4$ SYM. Perhaps this model can be solved using two-matrix model techniques following e. g. [170, 171].

A related observation stemming from the absence of any non-trivial space-time dependence at tree level, and from the fact that complex fields cannot self-contract, is that the free-theory correlator can also be thought of as a two-point function of a *holomorphic* double-trace operator $\mathcal{O} = \text{tr} (X^{k_1+k_2}) \text{tr} (Z^{k_3+k_4})$ with an *anti-holomorphic* double trace operator $\mathcal{O}' = \text{tr} (\bar{Z}^{k_4} \bar{X}^{k_1}) \text{tr} (\bar{Z}^{k_3} \bar{X}^{k_2})$. If we could decompose these operators into restricted Schur polynomials as in [172], we could exploit their orthogonality to evaluate the free correlator at finite N_c and k_i .

Another final option would be to try to compute the free correlator for many more values of k_i and N_c , observe a pattern and guess the full result.

Chapter 8

Conclusions

In this thesis we have seen how to reconstruct a family of four-point correlators in planar $\mathcal{N} = 4$ SYM from the knowledge of more elementary data. We have used two different ways of decomposing the correlators, see [Figure 8.1](#), both valid non-perturbatively in the 't Hooft coupling λ . The first one corresponds to the standard operator product expansion OPE of CFTs. The second consists on tessellations of the string worldsheet that appears as an effective description of this observable in the 't Hooft limit ($N_c \rightarrow \infty$ and λ fixed). This latter is dubbed hexagonalization due to the hexagonal patches we obtain after “cutting” the worldsheet.

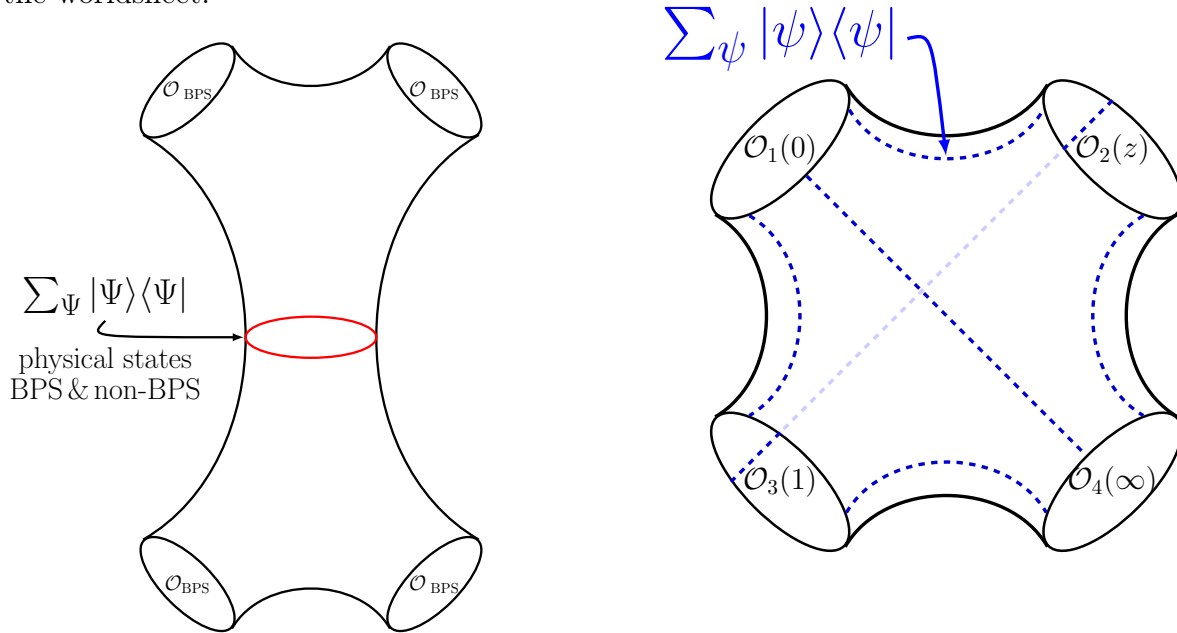


Figure 8.1: Two ways of decomposing planar correlators in $\mathcal{N} = 4$ SYM.

Thanks to the integrability of planar $\mathcal{N} = 4$ SYM we have access to the simpler building blocks of these two decompositions at finite coupling! In the OPE decomposition (see [Chapter 3](#)) these are the scaling dimensions (see [Chapter 1](#)) and structure constants

(see [Chapter 2](#)) of single-trace operators¹ and in hexagonalization these are the hexagon form factors (see [Chapter 4](#)).

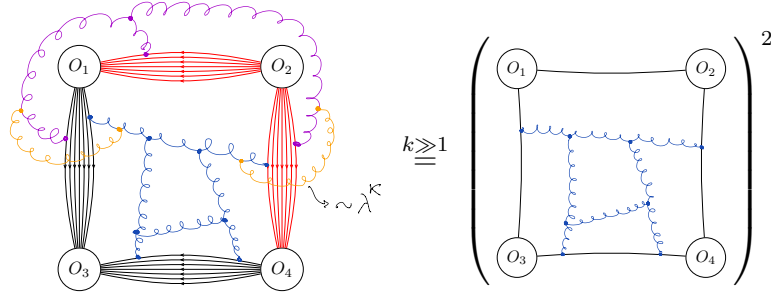


Figure 8.2: Diagrammatic representation of the factorisation of the *simplest* correlator

The simplest (\mathbb{S}) of the four point functions we have constructed in this thesis is given by:²

$$\mathbb{S} = \frac{\langle \text{tr} (\bar{\mathbf{Z}}^k \bar{\mathbf{X}}^k)(0) \text{tr} (\mathbf{X}^{2k})(z) \text{tr} (\bar{\mathbf{X}}^k \bar{\mathbf{Z}}^k)(1) \text{tr} (\mathbf{Z}^{2k})(\infty) \rangle}{\text{same at } \lambda = 0 \text{ and genus} = 0} \quad (8.1)$$

As shown diagrammatically in [Figure 8.2](#), in the planar limit, this *simplest* correlator factorises into two identical copies. To make this manifest we introduced the function \mathbb{O} that we dubbed the octagon:

$$\mathbb{S}_{\text{planar}} = \mathbb{O}(z, \bar{z}|\lambda)^2 \quad (8.2)$$

By performing the OPE and hexagon reconstructions first formally as infinite series at finite coupling and then more explicitly up to nine loops ($\lambda \rightarrow 0$), we have learned about various kinematical properties of \mathbb{O} and the class of four-point functions we studied. Gathering this data we have been able to set up a bootstrap problem for the four-point function (8.2) and by solving it we have obtained one of the main results in this thesis. In this unitary 4D conformal gauge theory, we provide a result at all loops in the 't Hooft coupling for a four-point correlator with very non-trivial spacetime dependence (see [Chapter 5](#)). In short, we identified the explicit basis of functions that appear at each loop order and fixed their relative coefficients by assuming certain kinematical properties hold at all loop orders, based on the evidence that they hold up to nine loops.

We were also able to take the strong coupling limit of our formal finite coupling infinite series and re-sum it (see [Chapter 6](#)). Our result takes the expected form of correlators of operators \mathcal{O}_i in a strongly coupled holographic CFT dual to classical strings in AdS:

$$\lim_{\lambda \rightarrow \infty} (\mathbb{S}_{\text{planar}} = \mathbb{O}^2) \simeq e^{-\sqrt{\lambda} A_{\text{min}}(z, \bar{z})}. \quad (8.3)$$

¹We consider an OPE channel where only single-trace exchanged operators are favoured, so double-trace exchanged can be disregarded. This is due to our choice of R-charge polarizations for the external operators in our four-point functions.

²A sum over permutations is implicit for the operators with two scalars $\text{tr} (\bar{\mathbf{Z}}^k \bar{\mathbf{X}}^k)$, such that they are $\frac{1}{2}$ -BPS.

We obtained an explicit result for the positive function A_{min} which in the string theory side should correspond to the minimal area of the classical string worldsheet that extends from the four positions of \mathcal{O}_i at the boundary into the bulk of AdS. We also studied various OPE limits of this expression.

Furthermore we were also able to go beyond the strict 't Hooft limit by taking instead a double scaling (DS) limit (see [Chapter 7](#)). This is obtained by taking the dimensions k to scale as $\sqrt{N_c}$. In this DS limit the effective genus counting parameter is $\zeta = \frac{k}{\sqrt{N_c}}$. We found the Taylor expansion in ζ up to genus four:

$$\begin{aligned} \mathbb{S}_{DS} = & \mathbb{O}^2 + \zeta^4 \left(1 + \frac{9}{2}\mathbb{O}^2 + \frac{1}{2}\mathbb{O}^4 \right) \\ & + \zeta^8 \left(\frac{3}{2} + \frac{607}{80}\mathbb{O}^2 + \frac{97}{36}\mathbb{O}^4 + \frac{1}{16}\mathbb{O}^6 \right) \\ & + \zeta^{12} \left(\frac{81}{80} + \frac{7321}{1120}\mathbb{O}^2 + \frac{953}{216}\mathbb{O}^4 + \frac{5689}{12960}\mathbb{O}^6 + \frac{5}{1296}\mathbb{O}^8 \right) \\ & + \zeta^{16} \left(\frac{459}{1120} + \frac{75553}{22400}\mathbb{O}^2 + \frac{44971}{12600}\mathbb{O}^4 + \frac{5587171}{7257600}\mathbb{O}^6 + \frac{2903}{86400}\mathbb{O}^8 + \frac{31}{207360}\mathbb{O}^{10} \right) \\ & + \mathcal{O}(\zeta^{20}). \end{aligned} \tag{8.4}$$

The reason for this structure is a nice decoupling of the large N_c expansion combinatorics – which are encoded in the dependence of \mathbb{S}_{DS} on the effective coupling ζ and on the octagon function \mathbb{O} – and the finite 't Hooft coupling dynamics and conformal field theory geometry – which enter through the octagon function alone as $\mathbb{O} = \mathbb{O}(z, \bar{z}|\lambda)$. We attacked the combinatorial problem by using a matrix model which effectively counts the quadrangulations³ of the worldsheet for all genera. Through its vertices this matrix model distinguishes between the protected squares and non-protected squares i.e. \mathbb{O} . We were not able to solve this model in full generality but found simple all-genus re-summed expressions in some limits.

We found for instance that as $\mathbb{O} \rightarrow 0$, the correlator simplifies to

$$\mathbb{S}_{DS} = \left(\frac{\sinh(\frac{3}{2}\zeta^2)}{\frac{3}{2}\zeta} \right)^4, \tag{8.5}$$

while as $\mathbb{O} \gg 1$, we obtain instead

$$\mathbb{S}_{DS} = \mathbb{O}^2 \int_0^1 dt \int_0^1 ds \left[\frac{ts}{t+s-1} I_0(2\sqrt{ts}\zeta^2\mathbb{O}) - \frac{(1-t)(1-s)}{t+s-1} I_0(2\sqrt{(1-t)(1-s)}\zeta^2\mathbb{O}) \right]. \tag{8.6}$$

where I_0 is the Bessel function.

While this latter limit is still under investigation, we already know the former limit can be obtained at strong coupling. In [\(8.3\)](#) the overall negative exponent is multiplied by a large string tension $\sqrt{\lambda}$ making the octagon exponentially small

$$\mathbb{O} \rightarrow 0 \tag{8.7}$$

³Remember our octagons are squares when considering only the mirror edges

as $\lambda \rightarrow \infty$. Since the minimal area configuration leads to a vanishing result, the full non-planar correlator in the Euclidean regime reduces to those BMN-like configurations where the string worldsheet degenerates into various point like geodesics. Such configurations first show up at genus 1.

These are our main results. We should emphasise that it is rare to have access to a full fledged four point function at all loops or at strong coupling. The result exhibits a plethora of interesting limits, some of which we have explored in this thesis and some others are still under investigation. It would be very nice to address these at finite coupling, perhaps making use of the recent determinant representation [140] for \mathbb{O} .

It would be formidable to exploit the non-perturbative nature of hexagonalization to study other regimes of the coupling λ and the external dimension k , see figure 8.3.

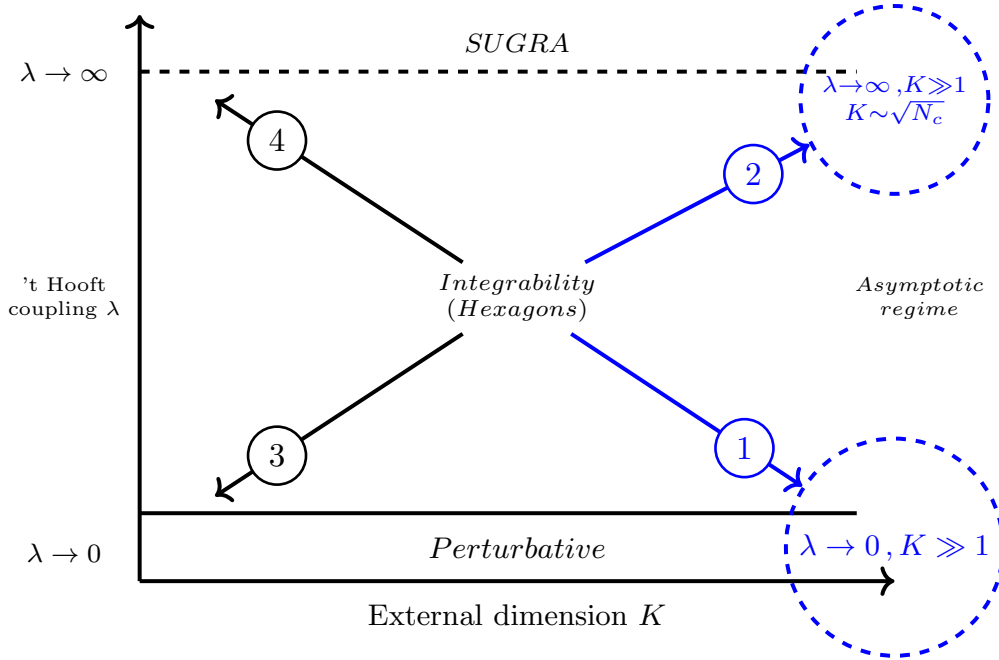


Figure 8.3: Parameter space of planar $\mathcal{N} = 4$ SYM in terms of the coupling λ and the scaling dimension k of the external $\frac{1}{2}$ -BPS operators. We highlight in blue the regions we explored in this thesis.

1. This regime is studied in this thesis and constitutes the most accessible corner of Figure 8.3 for hexagonalization. One could still try to extend this work for generic polarisations for which other mirror contributions are needed.
2. This regime, also studied here, corresponds to $\lambda \rightarrow \infty$ and $k \rightarrow \infty$ as $k \sim \sqrt{N_c}$ such that the dual states in AdS are classical strings.

It would be very interesting to compute A_{min} in (8.3) directly from string theory. It should be a nice minimal area. It would be even more interesting to compute the one

loop prefactor multiplying the exponential, both from the integrability representation for the octagon and from string theory. Together with the area, the prefactor should provide insights about the finite coupling nature of this object.

3. This is the weak coupling regime for finite small k and was addressed at one loop in the original hexagonalization paper [6]. Although the weak coupling limit keeps the number of contributions finite at a given loop order, some of these contributions are very hard to tackle due to their complicated matrix parts. These complications already start at two loops.

In the spirit of Chapter 5, we consider it important to understand which bootstrap conditions we should include to address the case of generic R -charge polarisations and ultimately operators of arbitrary or short scaling dimension. At weak coupling there is a vast list of results, obtained using bootstrap ideas, for the integrands of these correlators [128, 129, 130, 131, 132, 133]. It would be nice to be able to go from the integrand to explicit functions as the ones presented in this thesis.

4. This is the regime with $\lambda \rightarrow \infty$ for arbitrary k and is known to be described by supergravity in the bulk dual. Recently, bootstrap methods in Mellin space [134, 135] and the analytic conformal bootstrap [136, 137, 139, 138] have proved fruitful here. Yet from the point of view of hexagonalization seems to be the hardest regime to access as there is no truncation in the number of mirror states. It would be interesting to reproduce these known results and study how the decoupling of non-protected single traces in the OPE becomes apparent in hexagonalization.
5. This is the non-planar regime and extends as a third dimension perpendicular to the plane of Figure 8.3 which stands for $N_c \rightarrow \infty$. Concerning our double scaling limit it would be interesting to find the full resummed \mathbb{S}_{DS} that interpolates between (8.5) and (8.6), reproducing (8.4) in the 't Hooft expansion. Obtaining one more simplifying point of data, such as the free correlator⁴ $\mathbb{O} \rightarrow 1$, might provide us with some inspired guess.

In regard to more generic short operators hexagonalization has been extended to include tessellations of higher genus surfaces to compute non-planar corrections [98, 99].

Another direction would be to extend the strategies presented here to compute polarized higher-point functions. The situation for these correlators is not as simple since the number of bridges is bigger and our choices of external R -charge polarizations are limited to the three complex scalars in $\mathcal{N} = 4$ SYM. Hence it is harder to achieve optimal simplifications such as factorization of the correlators into octagons. The best one can do is to obtain a factorization into higher polygons as shown in Figure 8.4 for polarized five-point and six-point functions (but not more).

⁴Surprisingly or not the DS limit of the free correlator is harder to find using our matrix model. The reason being that the limit $\mathbb{O} \rightarrow 1$ makes all quadrangulations count, while the other limits $\mathbb{O} \rightarrow 0$ and $\mathbb{O} \rightarrow \infty$ only favour a smaller subset of quadrangulations.

We may be able to bootstrap these higher polygons if they satisfy a version of Steinmann relations. If such is the case, finding a basis similar to (5.10) or the Steinmann functions that appear in the context of the S-matrix [126, 127], would be of relevance to find the loop corrections of these correlators.

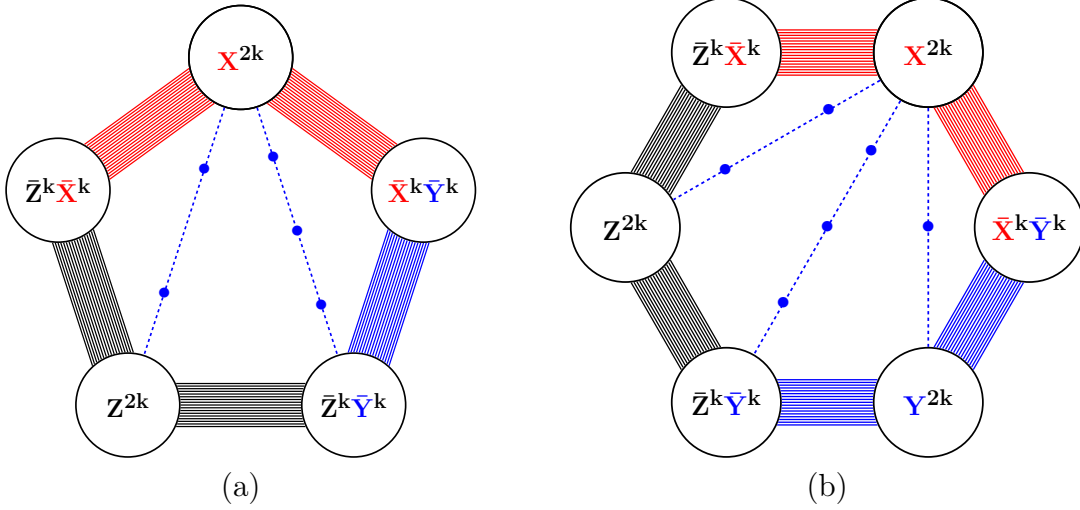


Figure 8.4: The *simplest* (a) five-point and (b) six-point functions. We make full use of the three complex scalars to adjust the external polarizations. For large charges $k \gg 1$ the planar correlators are given by the product of two decagons and two dodecagons respectively. The dodecagon is obtained by gluing four hexagons including complicated multi-particle strings on bridges of zero length.

What happens to these higher cyclic correlators in the double scaling limit? Although we have non-BPS pentagons or hexagons (i.e. decagons or dodecagons in Figure 8.4) the combinatorics of DS is dominated by the BPS quadrangulations, which we found in Appendix G.4.2. Explicitly, we find

$$\frac{G_5^{\text{DS}}}{G_{5,\text{free,planar}}^{\text{DS}}} = \left(\frac{\sinh(\frac{3}{2}\zeta^2)}{\frac{3}{2}\zeta} \right)^5, \quad \frac{G_6^{\text{DS}}}{G_{6,\text{free,planar}}^{\text{DS}}} = \left(\frac{\sinh(\frac{3}{2}\zeta^2)}{\frac{3}{2}\zeta} \right)^6. \quad (8.8)$$

Of course, we could look for subleading corrections to the double-scaling limit where interesting coupling dependence would show up. This would be particularly interesting for the six-point case, since we expect the dodecagon – being akin to a four-dimensional six-point function – to probe the genuine bulk-point singularity in four dimensions [22].

Everything so far was about very large operators. Can we go beyond the large-operator limit and construct a dual matrix model formulation of $\mathcal{N} = 4$ SYM, with hexagons as vertex building blocks describing any correlation function at any genus and any coupling? In a way, it would be a concrete gauge theory realisation of the very inspiring proposal [176].

Finally, the separation of combinatorics and dynamics for our four-point functions relies on nothing but a little bit of supersymmetry, on the large N_c limit, and on having large R -charges to play with. We should therefore be able to find correlators that factorised into

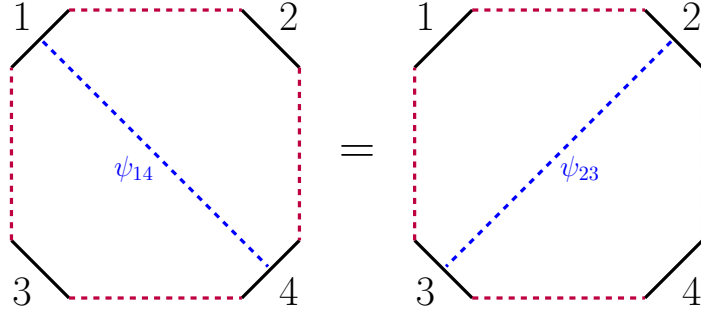


Figure 8.5: Flipping symmetry of the octagon.

octagons in other gauge theories with less supersymmetry. Then we may be able to perform large N_c resummations as the one presented here. However, the situation is certainly more challenging to find the octagon itself even if a worldsheet description is available. If this latter is not integrable then it is harder to have access to the mirror spectrum necessary to construct the octagon. Nevertheless the symmetry of the octagon represented in [Figure 8.5](#) may be of great aid to find this spectrum, in the same way the crossing equation of the four-point function constrains the conformal data.

Bibliography

- [1] B. Basso, F. Coronado, S. Komatsu, H. T. Lam, P. Vieira and D. l. Zhong, “Asymptotic Four Point Functions,” arXiv:1701.04462 [hep-th].
- [2] F. Coronado, “Perturbative four-point functions in planar $\mathcal{N} = 4$ SYM from hexagonalization,” JHEP **1901**, 056 (2019) [arXiv:1811.00467 [hep-th]].
- [3] F. Coronado, “Bootstrapping the simplest correlator in planar $\mathcal{N} = 4$ SYM at all loops,” arXiv:1811.03282 [hep-th].
- [4] T. Bargheer, F. Coronado and P. Vieira, “Octagons I: Combinatorics and Non-Planar Resummations,” arXiv:1904.00965 [hep-th].
- [5] B. Basso, S. Komatsu and P. Vieira, “Structure Constants and Integrable Bootstrap in Planar N=4 SYM Theory,” arXiv:1505.06745 [hep-th].
- [6] T. Fleury and S. Komatsu, “Hexagonalization of Correlation Functions,” JHEP **1701**, 130 (2017) [arXiv:1611.05577 [hep-th]].
- [7] T. Fleury and S. Komatsu, “Hexagonalization of Correlation Functions II: Two-Particle Contributions,” JHEP **1802**, 177 (2018) [arXiv:1711.05327 [hep-th]].
- [8] S. Komatsu, “Lectures on Three-point Functions in N=4 Supersymmetric Yang-Mills Theory,” arXiv:1710.03853 [hep-th].
- [9] J. Escobedo, N. Gromov, A. Sever and P. Vieira, “Tailoring Three-Point Functions and Integrability,” JHEP **1109**, 028 (2011) [arXiv:1012.2475 [hep-th]].
- [10] P. Vieira and T. Wang, “Tailoring Non-Compact Spin Chains,” JHEP **1410**, 35 (2014) [arXiv:1311.6404 [hep-th]].
- [11] J. Caetano and T. Fleury, “Three-point functions and $\mathfrak{su}(1|1)$ spin chains,” JHEP **1409**, 173 (2014) [arXiv:1404.4128 [hep-th]].
- [12] A. L. Fitzpatrick, J. Kaplan, D. Poland and D. Simmons-Duffin, “The Analytic Bootstrap and AdS Superhorizon Locality,” JHEP **1312**, 004 (2013) [arXiv:1212.3616 [hep-th]].

- [13] L. F. Alday and A. Zhiboedov, “An Algebraic Approach to the Analytic Bootstrap,” JHEP **1704**, 157 (2017) [arXiv:1510.08091 [hep-th]].
- [14] D. Simmons-Duffin, JHEP **1703**, 086 (2017) [arXiv:1612.08471 [hep-th]].
- [15] R. Rattazzi, V. S. Rychkov, E. Tonni and A. Vichi, “Bounding scalar operator dimensions in 4D CFT,” JHEP **0812**, 031 (2008) [arXiv:0807.0004 [hep-th]].
- [16] S. El-Showk, M. F. Paulos, D. Poland, S. Rychkov, D. Simmons-Duffin and A. Vichi, “Solving the 3D Ising Model with the Conformal Bootstrap,” Phys. Rev. D **86**, 025022 (2012) [arXiv:1203.6064 [hep-th]].
- [17] F. Gliozzi, “More constraining conformal bootstrap,” Phys. Rev. Lett. **111**, 161602 (2013) [arXiv:1307.3111 [hep-th]].
- [18] C. Beem, L. Rastelli and B. C. van Rees, “The $\mathcal{N} = 4$ Superconformal Bootstrap,” Phys. Rev. Lett. **111**, 071601 (2013) [arXiv:1304.1803 [hep-th]].
- [19] F. Aprile, J. M. Drummond, P. Heslop and H. Paul, “Unmixing Supergravity,” JHEP **1802**, 133 (2018) [arXiv:1706.08456 [hep-th]].
- [20] F. Aprile, J. Drummond, P. Heslop and H. Paul, “Double-trace spectrum of $N = 4$ supersymmetric Yang-Mills theory at strong coupling,” Phys. Rev. D **98**, no. 12, 126008 (2018) [arXiv:1802.06889 [hep-th]].
- [21] L. F. Alday and A. Bissi, “Higher-spin correlators,” JHEP **1310**, 202 (2013) [arXiv:1305.4604 [hep-th]].
- [22] J. Maldacena, D. Simmons-Duffin and A. Zhiboedov, “Looking for a bulk point,” JHEP **1701**, 013 (2017) [arXiv:1509.03612 [hep-th]].
- [23] M. S. Costa, V. Goncalves and J. Penedones, “Conformal Regge theory,” JHEP **1212**, 091 (2012) [arXiv:1209.4355 [hep-th]].
- [24] L. F. Alday, B. Eden, G. P. Korchemsky, J. Maldacena and E. Sokatchev, “From correlation functions to Wilson loops,” JHEP **1109**, 123 (2011) doi:10.1007/JHEP09(2011)123 [arXiv:1007.3243 [hep-th]].
- [25] N. Beisert *et al.*, “Review of AdS/CFT Integrability: An Overview,” Lett. Math. Phys. **99**, 3 (2012) [arXiv:1012.3982 [hep-th]].
- [26] J. M. Maldacena, “The Large N limit of superconformal field theories and supergravity,” Int. J. Theor. Phys. **38**, 1113 (1999) [Adv. Theor. Math. Phys. **2**, 231 (1998)] [hep-th/9711200].
- [27] O. Aharony, S. S. Gubser, J. M. Maldacena, H. Ooguri and Y. Oz, “Large N field theories, string theory and gravity,” Phys. Rept. **323**, 183 (2000) [hep-th/9905111].

- [28] G. 't Hooft, “A Planar Diagram Theory for Strong Interactions,” Nucl. Phys. B **72**, 461 (1974).
- [29] Y. Jiang, S. Komatsu, I. Kostov and D. Serban, “Clustering and the Three-Point Function,” J. Phys. A **49**, no. 45, 454003 (2016) [arXiv:1604.03575 [hep-th]].
- [30] J. A. Minahan and K. Zarembo, “The Bethe ansatz for N=4 superYang-Mills,” JHEP **0303**, 013 (2003) [hep-th/0212208].
- [31] N. Beisert, “The complete one loop dilatation operator of N=4 superYang-Mills theory,” Nucl. Phys. B **676**, 3 (2004) [hep-th/0307015].
- [32] N. Beisert and M. Staudacher, “The N=4 SYM integrable super spin chain,” Nucl. Phys. B **670**, 439 (2003) [hep-th/0307042].
- [33] H. Bethe, Z. Phys. **71**, 205 (1931).
- [34] L. D. Faddeev, “How algebraic Bethe ansatz works for integrable model,” hep-th/9605187.
- [35] N. Beisert and M. Staudacher, “Long-range $\mathfrak{psu}(2,2|4)$ Bethe Ansatzes for gauge theory and strings,” Nucl. Phys. B **727**, 1 (2005) [hep-th/0504190].
- [36] N. Beisert, B. Eden and M. Staudacher, “Transcendentality and Crossing,” J. Stat. Mech. **0701**, P01021 (2007) doi:10.1088/1742-5468/2007/01/P01021 [hep-th/0610251].
- [37] J. L. Cardy, O. A. Castro-Alvaredo and B. Doyon, “Form factors of branch-point twist fields in quantum integrable models and entanglement entropy,” J. Statist. Phys. **130**, 129 (2008) [arXiv:0706.3384 [hep-th]].
- [38] T. Bargheer, “Four-Point Functions with a Twist,” J. Phys. A **51**, no. 3, 035401 (2018) [arXiv:1701.04424 [hep-th]].
- [39] G. P. Korchemsky, “On level crossing in conformal field theories,” JHEP **1603**, 212 (2016) [arXiv:1512.05362 [hep-th]].
- [40] B. Basso, V. Goncalves, S. Komatsu and P. Vieira, “Gluing Hexagons at Three Loops,” Nucl. Phys. B **907**, 695 (2016) [arXiv:1510.01683 [hep-th]].
- [41] N. Gromov, V. Kazakov and P. Vieira, “Exact Spectrum of Anomalous Dimensions of Planar N=4 Supersymmetric Yang-Mills Theory,” Phys. Rev. Lett. **103** (2009) 131601 [arXiv:0901.3753 [hep-th]]. • A. Cavaglia, D. Fioravanti and R. Tateo, “Extended Y-system for the AdS_5/CFT_4 correspondence,” Nucl. Phys. B **843** (2011) 302 [arXiv:1005.3016 [hep-th]].

- [42] D. Bombardelli, D. Fioravanti and R. Tateo, “Thermodynamic Bethe Ansatz for planar AdS/CFT: A Proposal,” *J. Phys. A* **42** (2009) 375401 [arXiv:0902.3930 [hep-th]]. • N. Gromov, V. Kazakov, A. Kozak and P. Vieira, “Exact Spectrum of Anomalous Dimensions of Planar $N = 4$ Supersymmetric Yang-Mills Theory: TBA and excited states,” *Lett. Math. Phys.* **91** (2010) 265 [arXiv:0902.4458 [hep-th]]. • G. Arutyunov and S. Frolov, “Thermodynamic Bethe Ansatz for the $\text{AdS}(5) \times \text{S}(5)$ Mirror Model,” *JHEP* **0905** (2009) 068 [arXiv:0903.0141 [hep-th]].
- [43] N. Gromov, V. Kazakov, S. Leurent and D. Volin, “Solving the AdS/CFT Y-system,” *JHEP* **1207** (2012) 023 [arXiv:1110.0562 [hep-th]].
- [44] N. Gromov, V. Kazakov, S. Leurent and D. Volin, “Quantum spectral curve for arbitrary state/operator in $\text{AdS}_5/\text{CFT}_4$,” *JHEP* **1509**, 187 (2015) [arXiv:1405.4857 [hep-th]].
- [45] N. Drukker and J. Plefka, “Superprotected n-point correlation functions of local operators in $N=4$ super Yang-Mills,” *JHEP* **0904** (2009) 052 [arXiv:0901.3653 [hep-th]].
- [46] N. Beisert, “The Dilatation operator of $N=4$ super Yang-Mills theory and integrability,” *Phys. Rept.* **405**, 1 (2004) [hep-th/0407277].
- [47] D. Serban, “Integrability and the AdS/CFT correspondence,” *J. Phys. A* **44**, 124001 (2011) [arXiv:1003.4214 [hep-th]].
- [48] B. Basso, V. Goncalves and S. Komatsu, “Structure constants at wrapping order,” to appear.
- [49] N. Beisert, “The Analytic Bethe Ansatz for a Chain with Centrally Extended $\text{su}(2|2)$ Symmetry,” *J. Stat. Mech.* **0701** (2007) P01017 [nlin/0610017 [nlin.SI]].
- [50] Y. Jiang, I. Kostov, A. Petrovskii and D. Serban, “String Bits and the Spin Vertex,” *Nucl. Phys. B* **897**, 374 (2015) [arXiv:1410.8860 [hep-th]]. • Y. Kazama, S. Komatsu and T. Nishimura, “Novel construction and the monodromy relation for three-point functions at weak coupling,” *JHEP* **1501**, 095 (2015) [arXiv:1410.8533 [hep-th]].
- [51] F. A. Dolan, M. Nirschl and H. Osborn, “Conjectures for large N superconformal $N=4$ chiral primary four point functions,” *Nucl. Phys. B* **749**, 109 (2006) [hep-th/0601148].
- [52] See e.g. P. Vieira’s Mathematica notebook at the Nordita Integrability School in 2014 <https://www.nordita.org/~zaremba/Nordita2014/program.html>
- [53] R. I. Nepomechie and C. Wang, “Twisting singular solutions of Bethe’s equations,” *J. Phys. A* **47**, no. 50, 505004 (2014) [arXiv:1409.7382 [math-ph]].
- [54] G. Arutyunov, S. Frolov and A. Sfondrini, “Exceptional Operators in $N=4$ super Yang-Mills,” *JHEP* **1209**, 006 (2012) [arXiv:1205.6660 [hep-th]].

- [55] W. Hao, R. I. Nepomechie and A. J. Sommes, “Completeness of solutions of Bethe’s equations,” *Phys. Rev. E* **88**, no. 5, 052113 (2013) [arXiv:1308.4645 [math-ph]].
- [56] C. Marboe and D. Volin, “Fast analytic solver of rational Bethe equations,” arXiv:1608.06504 [math-ph].
- [57] C. Marboe and D. Volin, “The full spectrum of $\text{AdS}_5/\text{CFT}_4$ I: Representation theory and one-loop Q-system,” arXiv:1701.03704.
- [58] B. Eden, C. Schubert and E. Sokatchev, “Three loop four point correlator in $N=4$ SYM,” *Phys. Lett. B* **482**, 309 (2000) [hep-th/0003096]. • G. Arutyunov, F. A. Dolan, H. Osborn and E. Sokatchev, “Correlation functions and massive Kaluza-Klein modes in the AdS / CFT correspondence,” *Nucl. Phys. B* **665**, 273 (2003) [hep-th/0212116]. • G. Arutyunov and E. Sokatchev, “On a large N degeneracy in $N=4$ SYM and the AdS / CFT correspondence,” *Nucl. Phys. B* **663**, 163 (2003) [hep-th/0301058]. • G. Arutyunov, S. Penati, A. Santambrogio and E. Sokatchev, “Four point correlators of BPS operators in $N=4$ SYM at order g^{*4} ,” *Nucl. Phys. B* **670**, 103 (2003) [hep-th/0305060].
- [59] D. Chicherin, J. Drummond, P. Heslop and E. Sokatchev, “All three-loop four-point correlators of half-BPS operators in planar $N=4$ SYM,” arXiv:1512.02926 [hep-th].
- [60] B. Eden, P. Heslop, G. P. Korchemsky and E. Sokatchev, “Hidden symmetry of four-point correlation functions and amplitudes in $N=4$ SYM,” *Nucl. Phys. B* **862**, 193 (2012) [arXiv:1108.3557 [hep-th]]. • B. Eden, P. Heslop, G. P. Korchemsky and E. Sokatchev, “Constructing the correlation function of four stress-tensor multiplets and the four-particle amplitude in $N=4$ SYM,” *Nucl. Phys. B* **862**, 450 (2012) [arXiv:1201.5329 [hep-th]]. • R. G. Ambrosio, B. Eden, T. Goddard, P. Heslop and C. Taylor, “Local integrands for the five-point amplitude in planar $N=4$ SYM up to five loops,” *JHEP* **1501**, 116 (2015) [arXiv:1312.1163 [hep-th]]. • V. Goncalves, “Extracting OPE coefficient of Konishi at four loops,” arXiv:1607.02195 [hep-th]. • B. Eden and F. Paul, “Half-BPS half-BPS twist two at four loops in $N=4$ SYM,” arXiv:1608.04222 [hep-th].
- [61] B. Eden and A. Sfondrini, “Three-point functions in $\mathcal{N} = 4$ SYM: the hexagon proposal at three loops,” arXiv:1510.01242 [hep-th].
- [62] F. Cachazo, S. He and E. Y. Yuan, “Scattering of Massless Particles in Arbitrary Dimensions,” *Phys. Rev. Lett.* **113** (2014) no.17, 171601 [arXiv:1307.2199 [hep-th]].
- [63] C. Cardona and C. Kalousios, “Elimination and recursions in the scattering equations,” *Phys. Lett. B* **756** (2016) 180 [arXiv:1511.05915 [hep-th]]. • M. Zlotnikov, “Polynomial reduction and evaluation of tree- and loop-level CHY amplitudes,” *JHEP* **1608** (2016) 143 [arXiv:1605.08758 [hep-th]].
- [64] J. Caetano and J. Escobedo, “On four-point functions and integrability in $N=4$ SYM: from weak to strong coupling,” *JHEP* **1109**, 080 (2011) [arXiv:1107.5580 [hep-th]].

- [65] B. Eden and A. Sfondrini, “Tessellating cushions: four-point functions in $N=4$ SYM,” arXiv:1611.05436 [hep-th].
- [66] M. Nirschl and H. Osborn, “Superconformal Ward identities and their solution,” Nucl. Phys. B **711** (2005) 409 [hep-th/0407060].
- [67] F. A. Dolan, L. Gallot and E. Sokatchev, “On four-point functions of $1/2$ -BPS operators in general dimensions,” JHEP **0409** (2004) 056 [hep-th/0405180].
- [68] F. A. Dolan and H. Osborn, “Conformal partial wave expansions for $N=4$ chiral four point functions,” Annals Phys. **321** (2006) 581 [hep-th/0412335].
- [69] A. Bissi and T. Lukowski, “Revisiting $\mathcal{N} = 4$ superconformal blocks,” JHEP **1602** (2016) 115 [arXiv:1508.02391 [hep-th]].
- [70] F. A. Dolan and H. Osborn, “Conformal partial waves and the operator product expansion,” Nucl. Phys. B **678** (2004) 491 [hep-th/0309180].
- [71] F. A. Dolan and H. Osborn, “Superconformal symmetry, correlation functions and the operator product expansion,” Nucl. Phys. B **629** (2002) 3 [hep-th/0112251].
- [72] F. A. Dolan and H. Osborn, “Conformal four point functions and the operator product expansion,” Nucl. Phys. B **599** (2001) 459 [hep-th/0011040].
- [73] S. Okada. "An elliptic generalization of Schur's Pfaffian identity." Advances in Mathematics 204.2 (2006): 530-538. arXiv:math/0412038
- [74] E. Rains, “Correlation functions for symmetrized increasing subsequences,” arXiv:math/0006097
- [75] Y. Jiang, S. Komatsu, I. Kostov and D. Serban, “Clustering and the Three-Point Function,” J. Phys. A **49**, no. 45, 454003 (2016) [arXiv:1604.03575 [hep-th]].
- [76] J. A. Minahan and K. Zarembo, “The Bethe ansatz for $N=4$ superYang-Mills,” JHEP **0303**, 013 (2003) [hep-th/0212208].
- [77] N.A. Slavnov, “The algebraic Bethe ansatz and quantum integrable systems,” Russ. Math. Surv. 62 (2007) 727-766.
- [78] M. Wheeler, “Scalar products in generalized models with $SU(3)$ -symmetry,” Commun. Math. Phys. **327**, 737 (2014) [arXiv:1204.2089 [math-ph]].
- [79] O. Foda, Y. Jiang, I. Kostov and D. Serban, “A tree-level 3-point function in the $su(3)$ -sector of planar $N=4$ SYM,” JHEP **1310**, 138 (2013) [arXiv:1302.3539 [hep-th]].
- [80] A. Bissi, G. Grignani and A. V. Zayakin, “The $SO(6)$ Scalar Product and Three-Point Functions from Integrability,” arXiv:1208.0100 [hep-th].

- [81] H. J. de Vega and M. Karowski, “Exact Bethe Ansatz Solution of $O(2n)$ Symmetric Theories,” Nucl. Phys. B **280**, 225 (1987).
- [82] C. Meneghelli, *unpublished*.
- [83] L. D. Faddeev, “How algebraic Bethe ansatz works for integrable model,” hep-th/9605187.
- [84] N. Beisert, “The $SU(2|2)$ dynamic S-matrix,” Adv. Theor. Math. Phys. **12** (2008) 948 [hep-th/0511082].
- [85] M. de Leeuw, “Coordinate Bethe Ansatz for the String S-Matrix,” J. Phys. A **40**, 14413 (2007) [arXiv:0705.2369 [hep-th]].
- [86] B. Pozsgay and G. Takacs, “Form-factors in finite volume I: Form-factor bootstrap and truncated conformal space,” Nucl. Phys. B **788**, 167 (2008) [arXiv:0706.1445 [hep-th]].
- [87] B. Pozsgay and G. Takacs, “Form factors in finite volume. II. Disconnected terms and finite temperature correlators,” Nucl. Phys. B **788**, 209 (2008) [arXiv:0706.3605 [hep-th]].
- [88] B. Eden and A. Sfondrini, “Tessellating cushions: four-point functions in $\mathcal{N} = 4$ SYM,” JHEP **1710**, 098 (2017) [arXiv:1611.05436 [hep-th]].
- [89] C. Marboe and D. Volin, “Fast analytic solver of rational Bethe equations,” arXiv:1608.06504 [math-ph].
- [90] C. Marboe and D. Volin, “The full spectrum of AdS5/CFT4 I: Representation theory and one-loop Q-system,” J. Phys. A **51**, no. 16, 165401 (2018) [arXiv:1701.03704 [hep-th]].
- [91] N. Beisert, “The $SU(2|2)$ dynamic S-matrix,” Adv. Theor. Math. Phys. **12**, 945 (2008) [hep-th/0511082].
- [92] G. Arutyunov, M. de Leeuw and A. Torrielli, “The Bound State S-Matrix for AdS(5) x S**5 Superstring,” Nucl. Phys. B **819**, 319 (2009) [arXiv:0902.0183 [hep-th]].
- [93] R. I. Nepomechie and F. Ravanini, “Completeness of the Bethe ansatz solution of the open XXZ chain with nondiagonal boundary terms,” J. Phys. A **36**, 11391 (2003) [hep-th/0307095].
- [94] G. Albertini, S. Dasmahapatra, and B. M. McCoy, “Spectrum and completeness of the integrable three state Potts model: A Finite size study,” *Int.J.Mod.Phys.A* **07** (Suppl. 1A) (1992) 1–53.
- [95] B. Basso and L. J. Dixon, “Gluing Ladder Feynman Diagrams into Fishnets,” Phys. Rev. Lett. **119**, no. 7, 071601 (2017) [arXiv:1705.03545 [hep-th]].

- [96] N. Beisert, “Review of AdS/CFT Integrability, Chapter VI.1: Superconformal Symmetry,” *Lett. Math. Phys.* **99**, 529 (2012) [arXiv:1012.4004 [hep-th]].
- [97] B. Eden, Y. Jiang, D. le Plat and A. Sfondrini, “Colour-dressed hexagon tessellations for correlation functions and non-planar corrections,” *JHEP* **1802**, 170 (2018) [arXiv:1710.10212 [hep-th]].
- [98] T. Bargheer, J. Caetano, T. Fleury, S. Komatsu and P. Vieira, “Handling Handles I: Nonplanar Integrability,” arXiv:1711.05326 [hep-th].
- [99] T. Bargheer, J. Caetano, T. Fleury, S. Komatsu and P. Vieira, “Handling Handles II: Stratification and Data Analysis,” arXiv:1809.09145 [hep-th].
- [100] M. Hogervorst and S. Rychkov, “Radial Coordinates for Conformal Blocks,” *Phys. Rev. D* **87**, 106004 (2013) [arXiv:1303.1111 [hep-th]].
- [101] D. Chicherin, J. Drummond, P. Heslop and E. Sokatchev, “All three-loop four-point correlators of half-BPS operators in planar $\mathcal{N} = 4$ SYM,” *JHEP* **1608**, 053 (2016) [arXiv:1512.02926 [hep-th]].
- [102] D. Chicherin, A. Georgoudis, V. Gonçalves and R. Pereira, “All five-loop planar four-point functions of half-BPS operators in $\mathcal{N} = 4$ SYM,” arXiv:1809.00551 [hep-th].
- [103] J. L. Bourjaily, P. Heslop and V. V. Tran, “Amplitudes and Correlators to Ten Loops Using Simple, Graphical Bootstraps,” *JHEP* **1611**, 125 (2016) [arXiv:1609.00007 [hep-th]].
- [104] See e.g. P. Vieira’s Mathematica notebook at the Nordita Integrability School in 2014 <https://www.nordita.org/~zaremba/Nordita2014/program.html>
- [105] N. Beisert and B. I. Zwiebel, “On Symmetry Enhancement in the $\text{psu}(1,1|2)$ Sector of $\mathcal{N}=4$ SYM,” *JHEP* **0710**, 031 (2007) [arXiv:0707.1031 [hep-th]].
- [106] D. J. Broadhurst and A. I. Davydychev, “Exponential suppression with four legs and an infinity of loops,” *Nucl. Phys. Proc. Suppl.* **205-206**, 326 (2010) [arXiv:1007.0237 [hep-th]].
- [107] S. Caron-Huot, L. J. Dixon, M. von Hippel, A. J. McLeod and G. Papathanasiou, “The Double Pentagonal Integral to All Orders,” *JHEP* **1807**, 170 (2018) [arXiv:1806.01361 [hep-th]].
- [108] N. I. Usyukina and A. I. Davydychev, “Exact results for three and four point ladder diagrams with an arbitrary number of rungs,” *Phys. Lett. B* **305**, 136 (1993).
- [109] F. Coronado, Bootstrapping the *simplest* four-point function in planar $\mathcal{N} = 4$ SYM, to appear soon.
- [110] T. Bargheer, F. Coronado and P. Vieira, Large-Charge Non-Planar Correlators from Octagons, to appear.

- [111] T. Bargheer, F. Coronado, V. Gonçalves and P. Vieira, work in progress.
- [112] B. Eden and A. Sfondrini, arXiv:1611.05436 [hep-th].
- [113] B. Eden, Y. Jiang, D. le Plat and A. Sfondrini, JHEP **1802**, 170 (2018) [arXiv:1710.10212 [hep-th]].
- [114] T. Bargheer, J. Caetano, T. Fleury, S. Komatsu and P. Vieira, arXiv:1711.05326 [hep-th].
- [115] T. Bargheer, J. Caetano, T. Fleury, S. Komatsu and P. Vieira, arXiv:1809.09145 [hep-th].
- [116] F. Coronado, arXiv:1811.00467 [hep-th].
- [117] N. I. Usyukina and A. I. Davydychev, Phys. Lett. B **305**, 136 (1993).
- [118] Private communication with Benjamin Basso
- [119] T. Bargheer, F. Coronado, V. Gonçalves and P. Vieira, work in progress.
- [120] L. F. Alday, B. Eden, G. P. Korchemsky, J. Maldacena and E. Sokatchev, JHEP **1109**, 123 (2011) [arXiv:1007.3243 [hep-th]].
- [121] B. Basso and L. J. Dixon, Phys. Rev. Lett. **119**, no. 7, 071601 (2017) [arXiv:1705.03545 [hep-th]].
- [122] L. F. Alday and A. Bissi, JHEP **1310**, 202 (2013) [arXiv:1305.4604 [hep-th]].
- [123] L. F. Alday and A. Bissi, JHEP **1712**, 118 (2017) [arXiv:1603.05150 [hep-th]].
- [124] Ö. Gürdoğan and V. Kazakov, Phys. Rev. Lett. **117** (2016) 201602; addendum: Phys. Rev. Lett. **117** (2016) 259903 [arXiv:1512.06704 [hep-th]].
- [125] N. Gromov, V. Kazakov and G. Korchemsky, arXiv:1808.02688 [hep-th].
- [126] S. Caron-Huot, L. J. Dixon, A. McLeod and M. von Hippel, Phys. Rev. Lett. **117**, no. 24, 241601 (2016) [arXiv:1609.00669 [hep-th]].
- [127] L. J. Dixon, J. Drummond, T. Harrington, A. J. McLeod, G. Papathanasiou and M. Spradlin, JHEP **1702**, 137 (2017) [arXiv:1612.08976 [hep-th]].
- [128] D. Chicherin, R. Doobary, B. Eden, P. Heslop, G. P. Korchemsky, L. Mason and E. Sokatchev, JHEP **1506**, 198 (2015) [arXiv:1412.8718 [hep-th]].
- [129] G. P. Korchemsky and E. Sokatchev, JHEP **1512**, 133 (2015) [arXiv:1504.07904 [hep-th]].
- [130] D. Chicherin, R. Doobary, B. Eden, P. Heslop, G. P. Korchemsky and E. Sokatchev, JHEP **1603**, 031 (2016) [arXiv:1506.04983 [hep-th]].

- [131] D. Chicherin, J. Drummond, P. Heslop and E. Sokatchev, JHEP **1608**, 053 (2016) [arXiv:1512.02926 [hep-th]].
- [132] J. L. Bourjaily, P. Heslop and V. V. Tran, JHEP **1611**, 125 (2016) [arXiv:1609.00007 [hep-th]].
- [133] D. Chicherin, A. Georgoudis, V. Gonçalves and R. Pereira, arXiv:1809.00551 [hep-th].
- [134] L. Rastelli and X. Zhou, Phys. Rev. Lett. **118**, no. 9, 091602 (2017) [arXiv:1608.06624 [hep-th]].
- [135] L. Rastelli and X. Zhou, JHEP **1804**, 014 (2018) [arXiv:1710.05923 [hep-th]].
- [136] L. F. Alday and A. Bissi, Phys. Rev. Lett. **119**, no. 17, 171601 (2017) [arXiv:1706.02388 [hep-th]].
- [137] L. F. Alday and S. Caron-Huot, arXiv:1711.02031 [hep-th].
- [138] S. Caron-Huot and A. K. Trinh, arXiv:1809.09173 [hep-th].
- [139] L. F. Alday, A. Bissi and E. Perlmutter, arXiv:1809.10670 [hep-th].
- [140] I. Kostov, V. B. Petkova and D. Serban, “Determinant formula for the octagon form factor in $\mathcal{N}=4$ SYM,” arXiv:1903.05038 [hep-th].
- [141] C. Kristjansen, J. Plefka, G. W. Semenoff and M. Staudacher, “A New double scaling limit of $N=4$ superYang-Mills theory and PP wave strings,” Nucl. Phys. B **643**, 3 (2002) [hep-th/0205033].
- [142] N. R. Constable, D. Z. Freedman, M. Headrick, S. Minwalla, L. Motl, A. Postnikov and W. Skiba, “PP wave string interactions from perturbative Yang-Mills theory,” JHEP **0207**, 017 (2002) [hep-th/0205089].
- [143] N. Beisert, C. Kristjansen, J. Plefka, G. W. Semenoff and M. Staudacher, “BMN correlators and operator mixing in $N=4$ superYang-Mills theory,” Nucl. Phys. B **650**, 125 (2003) [hep-th/0208178].
- [144] N. R. Constable, D. Z. Freedman, M. Headrick and S. Minwalla, “Operator mixing and the BMN correspondence,” JHEP **0210**, 068 (2002) [hep-th/0209002].
- [145] D. E. Berenstein, J. M. Maldacena and H. S. Nastase, “Strings in flat space and pp waves from $N=4$ superYang-Mills,” JHEP **0204**, 013 (2002) [hep-th/0202021].
- [146] B. Eden and A. Sfondrini, “Tessellating cushions: four-point functions in $\mathcal{N} = 4$ SYM,” JHEP **1710**, 098 (2017) [arXiv:1611.05436 [hep-th]].
- [147] T. Bargheer, J. Caetano, T. Fleury, S. Komatsu and P. Vieira, “Handling Handles: Nonplanar Integrability in $\mathcal{N} = 4$ Supersymmetric Yang-Mills Theory,” Phys. Rev. Lett. **121**, no. 23, 231602 (2018) [arXiv:1711.05326 [hep-th]].

- [148] T. Bargheer, J. Caetano, T. Fleury, S. Komatsu and P. Vieira, “Handling handles. Part II. Stratification and data analysis,” JHEP **1811**, 095 (2018) [JHEP **2018**, 095 (2020)] [arXiv:1809.09145 [hep-th]].
- [149] H. Dorn, N. Drukker, G. Jorjadze and C. Kalousios, “Space-like minimal surfaces in AdS \times S,” JHEP **1004**, 004 (2010) [arXiv:0912.3829 [hep-th]].
- [150] V. A. Kazakov, “Solvable matrix models,” hep-th/0003064.
- [151] A. Zvonkin, "Matrix integrals and map enumeration: An accessible introduction", Mathematical and Computer Modelling 26, 281 (1997).
- [152] T. W. Brown, “Complex matrix model duality,” Phys. Rev. D **83**, 085002 (2011) [arXiv:1009.0674 [hep-th]].
- [153] P. G. de Gennes, “Exponents for the excluded volume problem as derived by the Wilson method,” Phys. Lett. A **38**, 339 (1972).
- [154] D. Sherrington and S. Kirkpatrick, “Solvable Model of a Spin-Glass,” Phys. Rev. Lett. **35**, 1792 (1975).
- [155] E. Brezin and S. Hikami, “Vertices from replica in a random matrix theory,” J. Phys. A **40**, 3545 (2007) [arXiv:0704.2044 [math-ph]].
- [156] E. Brezin and S. Hikami, “Intersection theory from duality and replica,” Commun. Math. Phys. **283**, 507 (2008) [arXiv:0708.2210 [hep-th]].
- [157] E. Brezin and S. Hikami, “Duality and replicas for a unitary matrix model,” JHEP **1007**, 067 (2010) [arXiv:1005.4730 [hep-th]].
- [158] S. Bellucci and C. Sochichiu, “On matrix models for anomalous dimensions of super Yang-Mills theory,” Nucl. Phys. B **726**, 233 (2005) [hep-th/0410010].
- [159] P. Di Francesco, “Rectangular matrix models and combinatorics of colored graphs,” Nucl. Phys. B **648**, 461 (2003) [cond-mat/0208037].
- [160] J. Polchinski, “Combinatorics of boundaries in string theory,” Phys. Rev. D **50**, R6041 (1994) [hep-th/9407031].
- [161] J. M. Maldacena, G. W. Moore, N. Seiberg and D. Shih, “Exact vs. semiclassical target space of the minimal string,” JHEP **0410**, 020 (2004) [hep-th/0408039].
- [162] Gopakumar, R. Open-Closed-Open String Duality - 2010. talk at the Johannesburg workshop: “Correlation Functions and the AdS/CFT Correspondence” (April 27).
- [163] P. Di Francesco and C. Itzykson, “A Generating function for fatgraphs,” Ann. Inst. H. Poincaré Phys. Theor. **59**, 117 (1993) [hep-th/9212108].

- [164] A. Mironov and A. Morozov, “On the complete perturbative solution of one-matrix models,” *Phys. Lett. B* **771**, 503 (2017) [arXiv:1705.00976 [hep-th]].
- [165] I. K. Kostov, “ $O(n)$ Vector Model on a Planar Random Lattice: Spectrum of Anomalous Dimensions,” *Mod. Phys. Lett. A* **4**, 217 (1989).
- [166] R. A. Janik, P. Surowka and A. Wereszczynski, “On correlation functions of operators dual to classical spinning string states,” *JHEP* **1005**, 030 (2010) [arXiv:1002.4613 [hep-th]].
- [167] J. A. Minahan, “Holographic three-point functions for short operators,” *JHEP* **1207**, 187 (2012) [arXiv:1206.3129 [hep-th]].
- [168] I. K. Kostov and M. Staudacher, “Two-dimensional chiral matrix models and string theories,” *Phys. Lett. B* **394**, 75 (1997) [hep-th/9611011].
- [169] V. A. Kazakov, M. Staudacher and T. Wynter, “Character expansion methods for matrix models of dually weighted graphs,” *Commun. Math. Phys.* **177**, 451 (1996) [hep-th/9502132].
- [170] V. A. Kazakov, M. Staudacher and T. Wynter, “Almost flat planar diagrams,” *Commun. Math. Phys.* **179**, 235 (1996) [hep-th/9506174].
- [171] V. A. Kazakov, M. Staudacher and T. Wynter, “Exact solution of discrete two-dimensional R^{*2} gravity,” *Nucl. Phys. B* **471**, 309 (1996) [hep-th/9601069].
- [172] S. Corley, A. Jevicki and S. Ramgoolam, “Exact correlators of giant gravitons from dual $N=4$ SYM theory,” *Adv. Theor. Math. Phys.* **5**, 809 (2002) [hep-th/0111222].
- [173] B. Basso and L. J. Dixon, “Gluing Ladder Feynman Diagrams into Fishnets,” *Phys. Rev. Lett.* **119**, no. 7, 071601 (2017) [arXiv:1705.03545 [hep-th]].
- [174] N. Berkovits, “Sketching a Proof of the Maldacena Conjecture at Small Radius,” arXiv:1903.08264 [hep-th].
- [175] N. Gromov and A. Sever, “The Holographic Fishchain,” arXiv:1903.10508 [hep-th].
- [176] V. A. Kazakov, “Field theory as a matrix model,” *Nucl. Phys. B* **587**, 645 (2000) [hep-th/0003065].
- [177] A. Hatcher, “On triangulations of surfaces” , *Topology and its Applications* **40**, 189 (1991).
- [178] J. Harer and D. Zagier, “The Euler characteristic of the moduli space of curves”, *Invent. Math.* **85**, 457 (1986).

Appendix A

All-loop Beisert-Staudacher equations

$$1 = \prod_{j=1}^{K^{(2)}} \frac{v_k^{(3)} - v_j^{(2)} + \frac{i}{2}}{v_k^{(3)} - v_j^{(2)} - \frac{i}{2}} \prod_{j=1}^K \frac{1 - \frac{1}{x(v_k^{(3)})x^+(u_j)}}{1 - \frac{1}{x(v_k^{(3)})x^-(u_j)}} \quad (\text{A.1})$$

$$1 = \prod_{j=1}^{K^{(1)}} \frac{v_k^{(2)} - v_j^{(1)} + \frac{i}{2}}{v_k^{(2)} - v_j^{(1)} - \frac{i}{2}} \prod_{\substack{j=1 \\ j \neq k}}^{K^{(2)}} \frac{v_k^{(2)} - v_j^{(2)} - i}{v_k^{(2)} - v_j^{(2)} + i} \prod_{j=1}^{K^{(3)}} \frac{v_k^{(2)} - v_j^{(3)} + \frac{i}{2}}{v_k^{(2)} - v_j^{(3)} - \frac{i}{2}} \quad (\text{A.2})$$

$$1 = \prod_{j=1}^K \frac{x(v_k^{(1)}) - x^-(u_k)}{x(v_k^{(1)}) - x^+(u_k)} \prod_{j=1}^{K^{(2)}} \frac{v_k^{(1)} - v_j^{(2)} - \frac{i}{2}}{v_k^{(1)} - v_j^{(2)} + \frac{i}{2}} \quad (\text{A.3})$$

$$1 = \left(\frac{x^+(u_k)}{x^-(u_k)} \right)^L \prod_{\substack{j=1 \\ j \neq k}}^K \left(\frac{x^+(u_k) - x^-(u_j)}{x^-(u_k) - x^+(u_j)} \frac{1 - \frac{1}{x^-(u_k)x^+(u_j)}}{1 - \frac{1}{x^+(u_k)x^-(u_j)}} \frac{1}{\sigma^2(u_k, u_j)} \right) \\ \times \prod_{j=1}^{K^{(1)}} \frac{x^-(u_k) - x(v^{(1)})}{x^+(u_k) - x(v^{(1)})} \prod_{j=1}^{K^{(3)}} \frac{1 - \frac{1}{x^-(u_k)x(v_j^{(3)})}}{1 - \frac{1}{x^+(u_k)x(v_j^{(3)})}} \prod_{j=1}^{\tilde{K}^{(1)}} \frac{x^-(u_k) - x(w^{(1)})}{x^+(u_k) - x(w^{(1)})} \prod_{j=1}^{\tilde{K}^{(3)}} \frac{1 - \frac{1}{x^-(u_k)x(w_j^{(3)})}}{1 - \frac{1}{x^+(u_k)x(w_j^{(3)})}} \quad (\text{A.4})$$

$$1 = \prod_{j=1}^K \frac{x(w_k^{(1)}) - x^-(u_k)}{x(w_k^{(1)}) - x^+(u_k)} \prod_{j=1}^{\tilde{K}^{(2)}} \frac{w_k^{(1)} - w_j^{(2)} - \frac{i}{2}}{w_k^{(1)} - w_j^{(2)} + \frac{i}{2}} \quad (\text{A.5})$$

$$1 = \prod_{j=1}^{\tilde{K}^{(1)}} \frac{w_k^{(2)} - w_j^{(1)} + \frac{i}{2}}{w_k^{(2)} - w_j^{(1)} - \frac{i}{2}} \prod_{\substack{j=1 \\ j \neq k}}^{\tilde{K}^{(2)}} \frac{w_k^{(2)} - w_j^{(2)} - i}{w_k^{(2)} - w_j^{(2)} + i} \prod_{j=1}^{\tilde{K}^{(3)}} \frac{w_k^{(2)} - w_j^{(3)} + \frac{i}{2}}{w_k^{(2)} - w_j^{(3)} - \frac{i}{2}} \quad (\text{A.6})$$

$$1 = \prod_{j=1}^{\tilde{K}^{(2)}} \frac{w_k^{(3)} - w_j^{(2)} + \frac{i}{2}}{w_k^{(3)} - w_j^{(2)} - \frac{i}{2}} \prod_{j=1}^K \frac{1 - \frac{1}{x(w_k^{(3)})x^+(u_j)}}{1 - \frac{1}{x(w_k^{(3)})x^-(u_j)}} \quad (\text{A.7})$$

$$1 = \prod_{j=1}^K \frac{x^+(u_j)}{x^-(u_j)} \quad (\text{A.8})$$

Appendix B

The $\mathfrak{so}(6)$ Structure Constant at Tree Level

In this appendix we compute the tree-level three point function of operators in the $\mathfrak{so}(6)$ sector of planar $N = 4$ SYM. We focus on the case of two $\frac{1}{2}$ -BPS operators and one non-BPS single-trace operators:

$$\mathcal{O}_1 = Tr(\tilde{Z}^{L_1}), \quad \mathcal{O}_2 = Tr(\bar{Z}^{L_2}), \quad \mathcal{O}_3 = Tr(\underbrace{Z\bar{Z}X\bar{X}\cdots}_L) + \cdots \quad (\text{B.1})$$

The protected operators are given by the BMN vacua spanned by the elementary field \bar{Z} and by the rotated field $\tilde{Z} \equiv Z + \bar{Z} + X - \bar{X}$. The non-protected operator is given by an eigenstate of the one-loop dilatation operator. Such operator can be obtained by diagonalizing the Hamiltonian of the dual integrable spin chain [76], using the Algebraic Bethe Ansatz (ABA). We develop on such construction in section B.3.

This three point function can be computed by Wick contractions as shown in figure B.1. Following the tailoring procedure, introduced for the $\mathfrak{su}(2)$ sector in [9], we can express the wick contractions as scalar products of spin chain states dual to the single trace operators. In our configuration – dubbed the reservoir picture in [5] – we have two trivial bridges which only feature propagators of the type $Z\text{-}\bar{Z}$ (blue lines). The only non-trivial wick contraction comes therefore from the bridge $l = (L + L_1 - L_2)/2$ between operators \mathcal{O}_1 and \mathcal{O}_3 and is given by the spin chain scalar product¹

$$\mathcal{C}_{123} = \langle \tilde{Z}^l | \Psi_l \rangle \quad (\text{B.2})$$

where Ψ_l is a sub-chain of length l in the cyclic spin chain state Ψ , dual to the single trace operator i.e. $\mathcal{O}_3 \equiv |\Psi\rangle$. In this way the computation of the tree level three-point function is reduced to finding an inner product of states in the dual $\mathfrak{so}(6)$ spin chain. In the $\mathfrak{su}(2)$ sector the relevant scalar product was computed with ABA techniques [9],

¹This renders an unnormalized structure constant. The normalized version includes the norms of the three operators involved

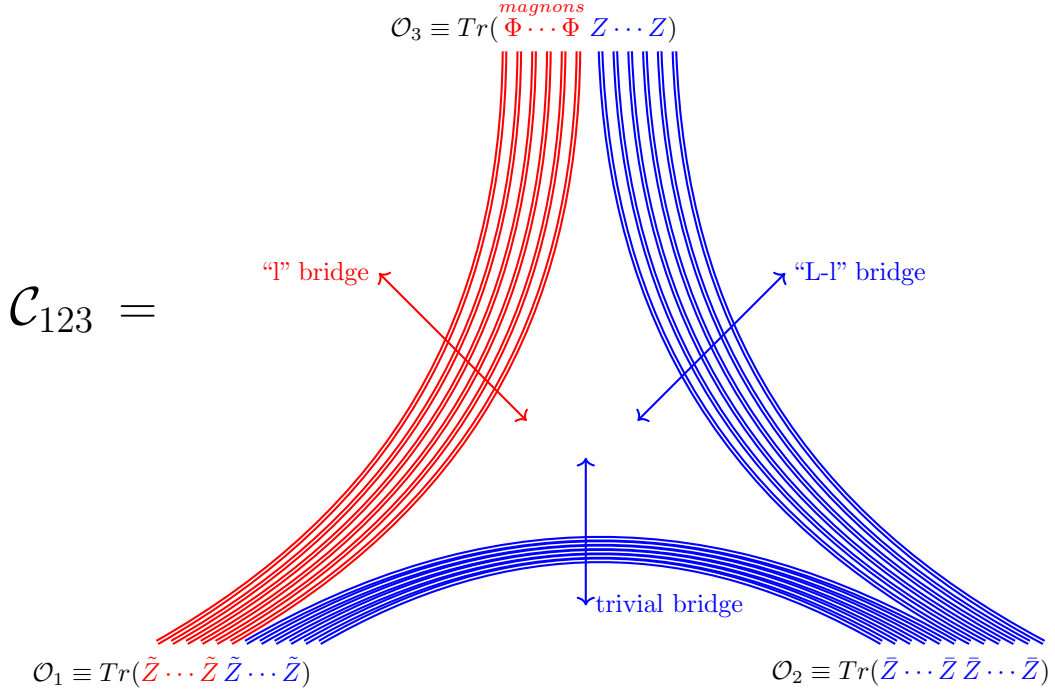


Figure B.1: Wick contraction for planar tree level structure constant $\mathcal{C}_{\mathcal{O}_1 \mathcal{O}_2 \mathcal{O}_3}$

obtaining sum formulas or more compact determinant expressions for some special cases, see [77] for a review. In [78] $\mathfrak{su}(3)$ scalar products were computed and used in [79] for the computation of structure constants in this sector. While for the $\mathfrak{so}(6)$ spin chain there are no available formulas for the scalar products² in the literature. One of the obstacles being the complexity of the ABA for $\mathfrak{so}(2n)$ models [81]. To overcome this problem we construct an alternative version³ of the $\mathfrak{so}(6)$ ABA which allows for a simpler approach to the computation of scalar products⁴. In particular we use this machinery to find the scalar product (B.2) as a sum formula. This result makes direct contact with the conjecture (2.56), restricted to $\mathfrak{so}(6)$ at tree level, showing the structure of a sum over partitions and a matrix part depending on the nested levels of the Bethe Ansatz. It would be interesting to generalize this Bethe Ansatz to address operators in the full sector $\mathfrak{psu}(2, 2|4)$ and reproduce the conjecture (2.56) at tree level.

The rest of this appendix is organized as follows: in section B.1 we introduce the $\mathfrak{so}(6)$ integrable spin chain, the corresponding transfer matrix, as well as some notation. In section B.2 we present a novel $\mathfrak{so}(6)$ vertex model, specifying the Boltzmann weights and the way to extract the Bethe states from the lattice. In section B.3 we develop a $\mathfrak{so}(6)$ ABA for the diagonalization of the spin chain Hamiltonian and transfer matrix. In section B.4 we present the Yang-Baxter algebra, showing how to use it to derive the so called wanted and unwanted terms of the ABA. In section B.5 we present the coordinate Bethe

²An attempt to conjecture the $\mathfrak{so}(6)$ scalar product, based on the results for $\mathfrak{su}(2)$, was given in [80]

³ $\mathfrak{so}(6)$ is special due to its isomorphism with $\mathfrak{su}(4)$

⁴A very similar approach was developed independently by Carlo Meneghelli [82].

Ansatz (CBA) which can be derived from our ABA and vertex model. Finally, in section B.6 we put in used the Yang-Baxter algebra to compute the tree level structure constant given by the scalar product (B.2). We show how to simplify the result to obtain the $\mathfrak{so}(6)$ tree-level analog of the conjecture (2.56).

B.1 The $\mathfrak{so}(6)$ spin chain

To obtain a basis of non-BPS operators we need to diagonalize the $\mathfrak{so}(6)$ integrable spin chain Hamiltonian:

$$\mathcal{H}_{\mathfrak{so}(6)} = \sum_{l=1}^L \left(I_{l,l+1} - P_{l,l+1} - \frac{1}{2} K_{l,l+1} \right) \quad (\text{B.3})$$

where I, P and K are identity, permutation and trace operators respectively.

This spin chain Hamiltonian is proportional to the one loop dilatation operator in the $\mathfrak{so}(6)$ sector of $N = 4$ SYM. The basis of eigenstates of this Hamiltonian constitutes a basis for non-BPS operator of the one loop $\mathfrak{so}(6)$ sector, which (partially) lifts the original tree level degeneracy. The single trace operators of this sector are mapped to cyclic states of the spin chain as:

$$\text{Tr}(Z\bar{Z}XY\bar{X}) \longrightarrow |Z\bar{Z}XY\bar{X}\rangle + \text{cyclic permutations} \quad (\text{B.4})$$

where the elementary fields are given by the complex scalars fields:

$$Z \equiv \Phi_{12}, \quad X \equiv \Phi_{23}, \quad Y \equiv \Phi_{13}, \quad \bar{Y} \equiv \Phi_{42}, \quad \bar{X} \equiv \Phi_{14}, \quad \bar{Z} \equiv \Phi_{34}. \quad (\text{B.5})$$

These scalar fields form a multiplet of the antisymmetric $\mathbf{6}$ representation of $\mathfrak{su}(4)$, isomorphic to the vector representation of $\mathfrak{so}(6)$. This isomorphism is realized by the transformation.

$$\Phi_{ab} = \begin{pmatrix} 0 & \phi_1 + i\phi_4 & \phi_2 + i\phi_5 & \phi_3 - i\phi_6 \\ -\phi_1 - i\phi_4 & 0 & \phi_3 + i\phi_6 & -\phi_2 + i\phi_5 \\ -\phi_2 - i\phi_5 & -\phi_3 - i\phi_6 & 0 & \phi_1 - i\phi_4 \\ -\phi_3 + i\phi_6 & \phi_2 - i\phi_5 & -\phi_1 + i\phi_4 & 0 \end{pmatrix} \quad (\text{B.6})$$

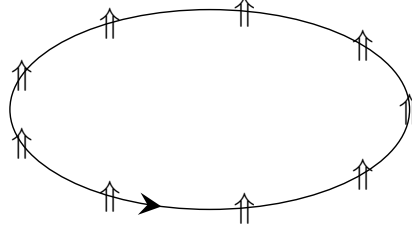
In this appendix we stick to the basis of complex scalars (B.5).

The ABA finds the spectrum of the $\mathfrak{so}(6)$ Hamiltonian by solving the eigenvalue problem of the transfer matrix, the trace of a monodromy operator. This operator is constructed by “scattering” a probe particle, in an auxiliary space $\mathbf{\Lambda}$ and spectral parameter (momentum) u , with all the spin chain sites. We can build various monodromies by choosing the auxiliary space to lie in any of the representations of the spin chain symmetry group:

$$T_{\Lambda}(u) = \text{---} \uparrow \uparrow \uparrow \uparrow \rightarrow \uparrow \uparrow \uparrow \uparrow \text{---}$$

(a) Monodromy matrix

$$\mathcal{T}(u) = \text{tr}_{\Lambda} T_{\Lambda}(u) =$$



(b) Transfer matrix

Figure B.2: $\mathfrak{so}(6)$ Monodromy and Transfer matrices with Λ auxiliary space. The spin chain sites represent any of the elementary fields $\uparrow \equiv \Phi_{ab}$ in (B.5)

From all these possibilities one is distinguished and corresponds to the choice of auxiliary space in the same representation as the spin chain sites. The trace of this special choice, the transfer matrix, is a generating function of a family of local conserved charges including the nearest-neighbour Hamiltonian of the spin chain. For our $\mathfrak{so}(6)$ spin chain the distinguished monodromy is T_6 , its trace generates local conserved charges such as the Hamiltonian (B.3). Other choices of auxiliary space do not generate the spin chain Hamiltonian, nevertheless their corresponding transfer matrices are in convolution with the distinguished one. This means that we can address the eigenvalue problem for the spin chain Hamiltonian and all the transfer matrices in convolution at once. So we can choose to solve the eigenvalue problem of the simplest transfer matrix. For our $\mathfrak{so}(6)$ spin chain the simplest choice corresponds to T_4 with auxiliary space in the $\mathbf{4}$ fundamental representation of $\mathfrak{su}(4)$ as:

$$(T_4(u))_{a; \Phi_{a_1 b_1} \dots \Phi_{a_L b_L}}^{b; \Phi_{c_1 d_1} \dots \Phi_{c_L d_L}} = \begin{array}{c} \Phi_{c_1 d_1} \quad \Phi_{c_2 d_2} \quad \Phi_{c_3 d_3} \quad \Phi_{c_4 d_4} \quad \dots \quad \Phi_{c_L d_L} \\ \uparrow \quad \uparrow \quad \uparrow \quad \uparrow \quad \quad \quad \uparrow \\ a \text{---} \rightarrow \bullet \rightarrow \bullet \rightarrow \bullet \rightarrow \bullet \rightarrow \dots \rightarrow \bullet \text{---} b \\ \uparrow \quad \uparrow \quad \uparrow \quad \uparrow \quad \quad \quad \uparrow \\ \Phi_{a_1 b_1} \quad \Phi_{a_2 b_2} \quad \Phi_{a_3 b_3} \quad \Phi_{a_4 b_4} \quad \dots \quad \Phi_{a_L b_L} \\ \theta_1 \quad \theta_2 \quad \theta_3 \quad \theta_4 \quad \quad \quad \end{array} \quad (B.7)$$

where $\Phi_{a_k b_k}$ and $\Phi_{c_k d_k}$ are the incoming and outgoing $\mathfrak{so}(6)$ flavours of the k^{th} spin chain site in the “scattering” with the auxiliary particle. The indexes a and b indicate the incoming and outgoing flavours in the auxiliary space, they take on values $\{1, 2, 3, 4\}$ of the $\mathbf{4}$ representation. The trace of this monodromy, the transfer matrix, is obtained by identifying the indexes a and b and summing over the four fundamental flavours. The set

of inhomogeneities $\{\theta_k\}$ must be taken to zero to describe the spin chain with Hamiltonian (B.3). However, we keep them finite as their presence do not affect our construction of the spectrum.

In section B.3 we build a Bethe basis that diagonalizes the transfer matrix of (B.7) and the Hamiltonian (B.3). This construction yields a wing-vertex model that renders a representation of the Bethe states as we present in the following section.

B.2 The $\mathfrak{so}(6)$ vertex model

In this section we introduce a vertex model obtained from the ABA in section B.3. The Bethe states can be obtained as partition functions of this vertex model when imposing appropriate boundary conditions.

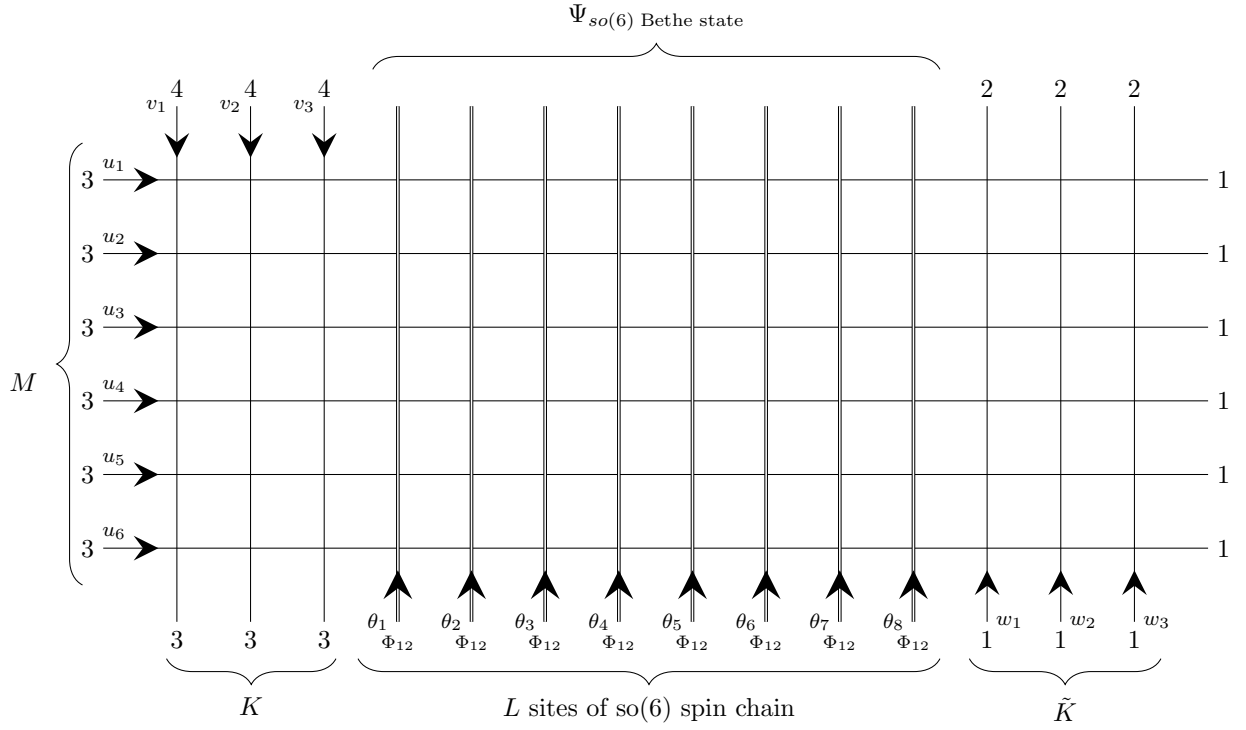


Figure B.3: $\mathfrak{so}(6)$ vertex model with $L = 8, K = 3, M = 6$ and $\tilde{K} = 3$. The arrows indicate the direction of flavour injection.

R -matrices in the lattice

The vertex model is given by the winged lattice in figure B.3. This lattice is composed by simple lines in the $\mathbf{4}$ fundamental representation spanned by flavours $\{1, 2, 3, 4\}$ and double

The boundary conditions and Bethe state

In order to obtain the $\mathfrak{so}(6)$ Bethe state from this vertex model we fix the boundaries of the wings as shown in figure B.3. With these restrictions the auxiliary spaces on the wings become effectively two-dimensional and the wing lattices render two 6-vertex models: $wing_{3,4}$ and $wing_{1,2}$, associated to $\mathfrak{su}(2)$ representations spanned by flavours $\{3, 4\}$ and $\{1, 2\}$ respectively.

To complete the boundary conditions we restrict the bottom of the double lines to have incoming flavour $Z \equiv \Phi_{12}$. This choice makes the vertex models $wing_{3,4}$ and $wing_{1,2}$ play the role of reservoirs. In this way the first wing injects $M - K$ units of flavour 3 and K units of flavour 4 to the double-lined lattice. The second wing absorbs $M - \tilde{K}$ units of flavour 1 and \tilde{K} of flavour 2.

Considering these boundary conditions we follow the flavour rules and Boltzmann weights in (B.10) and (B.11) to construct the $\mathfrak{so}(6)$ Bethe state, which can finally be read off from the top of the lattice in figure B.3. The Bethe state obtained from this vertex model has L sites and global charges:

$$\mathfrak{so}(6) \text{ charges : } [M - 2K, L + K - 2M + \tilde{K}, M - 2\tilde{K}] \quad (\text{B.12})$$

The Bethe state can be expressed as a linear combination of states in the $\mathfrak{so}(6)$ coordinate basis with charges (B.12) and length L . The states of this basis are composed of all allowed combinations of letters (B.5), considering their individual charges are:

$$Z : [0, 1, 0], X : [1, -1, 1], Y : [-1, 0, 1], \bar{Y} : [1, 0, -1], \bar{X} : [-1, 1, -1], \bar{Z} : [0, -1, 0]. \quad (\text{B.13})$$

As an example, for $L = 2$, $K = 1$, $M = 2$, $\tilde{K} = 1$ the total charge is $[0, 0, 0]$ and the corresponding coordinate basis is given by: $\{|Z\bar{Z}\rangle, |\bar{Z}Z\rangle, |X\bar{X}\rangle, |\bar{X}X\rangle, |Y\bar{Y}\rangle, |\bar{Y}Y\rangle\}$. The coefficient of one of these coordinate states, in the linear combination that renders the Bethe state, is determined by imposing the corresponding letters as boundary conditions at the top of the double lines of figure (B.3). Then we should consider all the possible paths the flavour can follow, consistent with the boundary conditions. Finally the coefficient is given by the sum of the Boltzmann weights associated to each possible path.

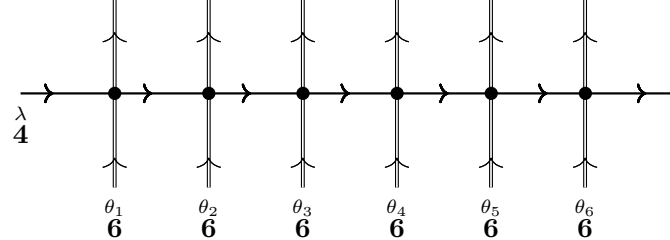
Following the rules of this vertex model it is possible to determine the general form of the Bethe state as a linear combination of the coordinate basis. We present this in section B.5 as a Coordinate Bethe Ansatz(CBA). In the following section we present the origin of this vertex model from the ABA.

B.3 The Algebraic Bethe Ansatz (ABA)

The monodromy T_4 and its elements

The “scattering” of a probe particle in the **4** representation with the spin chain sites in the **6** representation is given by a product of $R_{\mathbf{46}}$ matrices and renders the T_4 monodromy

matrix:

$$T_4(\lambda) = R_{46}(\lambda, \theta_L) \cdots R_{46}(\lambda, \theta_1) =$$

(B.14)

From the point of view of the auxiliary space the monodromy is a 4×4 matrix, whose elements are operators that act exclusively over the spin chain:

$$T_4(\lambda) = \begin{pmatrix} A_{11} & A_{12} & B_{13} & B_{14} \\ A_{21} & A_{22} & B_{23} & B_{24} \\ C_{31} & C_{32} & D_{33} & D_{34} \\ C_{41} & C_{42} & D_{43} & D_{44} \end{pmatrix} \quad (B.15)$$

In order to obtain the elements of this matrix in the graphical representation in (B.14), we simply fix the boundaries of the horizontal line to take specific flavour values $\{1, 2, 3, 4\}$. The corresponding transfer matrix, given by the trace of the monodromy (B.15), is:

$$\mathcal{T} = A_{11} + A_{22} + D_{33} + D_{44} \quad (B.16)$$

Now our aim is to construct the ABA to find the eigenvalues and eigenstates of this transfer matrix. For this we start by identifying one of its trivial eigenstates, the pseudo-vacuum:

$$|\Omega_L\rangle \equiv |Z^L\rangle \equiv |\Phi_{12}^L\rangle \quad (B.17)$$

We consider this pseudo-vacuum as a reference state to start the construction of the ABA. With this choice the action of the monodromy matrix organizes into 2×2 blocks. The pseudo-vacuum diagonalizes the A and D blocks:

$$\begin{aligned} \mathbb{A}(\lambda)|\Omega_L\rangle &= \begin{pmatrix} A_{11} & A_{12} \\ A_{21} & A_{22} \end{pmatrix} |\Omega_L\rangle = \begin{pmatrix} a(\lambda) & 0 \\ 0 & a(\lambda) \end{pmatrix} |\Omega_L\rangle \\ \mathbb{D}(\lambda)|\Omega_L\rangle &= \begin{pmatrix} D_{33} & D_{34} \\ D_{43} & D_{44} \end{pmatrix} |\Omega_L\rangle = \begin{pmatrix} d(\lambda) & 0 \\ 0 & d(\lambda) \end{pmatrix} |\Omega_L\rangle \end{aligned} \quad (B.18)$$

with (considering $\theta_k = 0$):

$$a(\lambda) = 1 \quad \text{and} \quad d(\lambda) = \left(\frac{\lambda + i/2}{\lambda - i/2} \right)^L \quad (B.19)$$

and it is annihilated by the \mathbb{C} -block elements:

$$\mathbb{C}(\lambda)|\Omega\rangle = \begin{pmatrix} C_{31} & C_{32} \\ C_{41} & C_{42} \end{pmatrix} |\Omega\rangle = 0 \quad (B.20)$$

The action of the B -operators over (B.17) is much less trivial. They create magnon-states or plane waves when acting over the pseudo-vacuum. The operator B_{jk} injects flavour $k \in \{3, 4\}$ and absorbs flavour $j \in \{1, 2\}$ from the state it acts over. When acting over the pseudovacuum (B.17) it creates a magnon of type Φ_{1k} when $j = 2$ or type Φ_{2k} when $j = 1$. For instance the operator B_{13} creates a $X \equiv \Phi_{23}$ magnon as:

$$|\Psi_X\rangle = \sum_{n=1}^L \psi_n(u) |Z \cdots \overset{n}{\downarrow} X \cdots Z\rangle = \sum_{n=1}^L \begin{array}{c} \text{Diagram} \end{array} \quad (\text{B.21})$$

The diagram shows a horizontal chain of six vertical lines, each labeled Φ_{12} at the bottom. A blue arrow labeled '3' enters from the left, and a red arrow labeled '1' exits to the right. At the fourth vertical line, a blue arrow labeled Φ_{23} points upwards, and a red arrow points downwards. The blue and red lines cross at this point.

with wave-function $\psi_n(u) = \left(\prod_{k=1}^{n-1} \frac{u - \theta_k + i/2}{u - \theta_k - i/2} \right) \left(\frac{-i}{u - \theta_n - i/2} \right)$ as can be read off from the lattice with Boltzmann weights (B.11).

Similarly we can create other magnon-states with different flavours or $\mathfrak{so}(6)$ charges by using operators B_{23} , B_{24} and B_{14} . The relationship between these creation operators and the $\mathfrak{so}(6)$ charges is summarized in the following figure:

$$\mathbb{B} = \begin{pmatrix} B_{13} & B_{14} \\ B_{23} & B_{24} \end{pmatrix}, \quad \begin{array}{ccccc} & & Y & & \\ & \xrightarrow{B_{23}} & & \xrightarrow{B_{14}} & \\ Z & \xrightarrow{B_{13}} & X & \xrightarrow{B_{13}} & \bar{X} \\ & \xrightarrow{B_{24}} & & \xrightarrow{B_{24}} & \\ & & \bar{Y} & & \bar{Z} \end{array} \quad (\text{B.22})$$

The diagram shows a directed graph with nodes Z, X, \bar{X}, \bar{Z} in a horizontal row and Y, \bar{Y} above and below X respectively. Curved arrows connect the nodes: $Z \rightarrow Y$ (labeled B_{23}), $Y \rightarrow \bar{Z}$ (labeled B_{14}), $Z \rightarrow X$ (labeled B_{13}), $X \rightarrow \bar{X}$ (labeled B_{13}), $X \rightarrow \bar{Y}$ (labeled B_{24}), $\bar{X} \rightarrow \bar{Z}$ (labeled B_{24}), $Z \rightarrow \bar{Y}$ (labeled B_{14}), and $\bar{Y} \rightarrow \bar{Z}$ (labeled B_{23}).

The Bethe Ansatz

The B creation operators play a key role in the construction of the spectrum of the transfer matrix. The states created by repeated action of B -operators over the reference state (B.17) serve as a basis to propose a general Ansatz for the eigenstates of the transfer matrix as:

$$|\Psi\rangle = \psi_{a_1 \dots a_M} \tilde{\psi}^{\tilde{a}_1 \dots \tilde{a}_M} B_{\tilde{a}_1 a_1}(u_1) \cdots B_{\tilde{a}_M a_M}(u_M) |\Omega_L\rangle \quad (\text{B.23})$$

where the indexes a_k and \tilde{a}_k take on flavour values $\{3, 4\}$ and $\{1, 2\}$ respectively, and the unconstrained tensors $\psi_{a_1 \dots a_M}$ and $\tilde{\psi}^{\tilde{a}_1 \dots \tilde{a}_M}$ weight the contributions of states constructed by different choices of $B_{\tilde{a}_m a_m}$ -operators.

We can rewrite the ansatz (B.23) by using 2×2 \mathbb{B} -blocks instead of individual $B_{\tilde{a}_k a_k}$ -operators. With this purpose we introduce the wing-auxiliary states $|\psi\rangle$ and $\langle\tilde{\psi}|$ as:

$$\psi_{a_1 a_2 \dots a_M} = \langle a_1 a_2 \cdots a_M | \psi \rangle \quad (\text{B.24})$$

$$\tilde{\psi}^{\tilde{a}_1 \tilde{a}_2 \cdots \tilde{a}_M} = \langle \tilde{\psi} | \tilde{a}_1 \tilde{a}_2 \cdots \tilde{a}_M \rangle \quad (\text{B.25})$$

with states $\langle a_1 a_2 \cdots a_M |$ and $|\tilde{a}_1 \tilde{a}_2 \cdots \tilde{a}_M \rangle$ forming coordinate basis in the tensor product of two-dimensional subspaces: $\mathbf{2}_1 \otimes \mathbf{2}_2 \cdots \otimes \mathbf{2}_M$ and $\tilde{\mathbf{2}}_1 \otimes \tilde{\mathbf{2}}_2 \cdots \otimes \tilde{\mathbf{2}}_M$ respectively. We define the \mathbb{B}_m -blocks as:

$$\mathbb{B}_m(u) = |\tilde{a}_m \rangle B_{\tilde{a}_m a_m}(u) \langle a_m | \quad (\text{B.26})$$

In this way the operator \mathbb{B}_m -block acts over the spin chain space and intertwines between the auxiliary spaces $\mathbf{2}$ (flavours $\{3, 4\}$) and $\tilde{\mathbf{2}}$ (flavours $\{1, 2\}$) as:

$$\mathbb{B}_m : \quad \mathbf{2}_m \otimes \mathbf{6}_1 \otimes \cdots \otimes \mathbf{6}_L \longrightarrow \tilde{\mathbf{2}}_m \otimes \mathbf{6}_1 \otimes \cdots \otimes \mathbf{6}_L \quad (\text{B.27})$$

while its action over other auxiliary spaces $\mathbf{2}_k$ and $\tilde{\mathbf{2}}_k$ is trivial for $k \neq m$.

Using \mathbb{B} -blocks and wing-auxiliary states we reformulate the Bethe Ansatz (B.23) as:

$$|\Psi\rangle = \langle \tilde{\psi} | \mathbb{B}_1(u_1) \cdots \mathbb{B}_M(u_M) |\psi\rangle \otimes |\Omega_L\rangle \quad (\text{B.28})$$

Using the Ansatz (B.28) we now need to solve the eigenvalue problem:

$$\mathcal{T}(\lambda)|\Psi\rangle = \Lambda(\lambda)|\Psi\rangle \quad (\text{B.29})$$

This means we need to find the restrictions over the auxiliary roots $\{u\}$ and the wings states such equation (B.29) holds. In what follows we sketch the steps to achieve this diagonalization. These will heavily rely on the Yang-Baxter algebra presented in section B.4.

We first reexpress the transfer matrix (B.16) by defining block operators \mathbb{A} and \mathbb{D} as:

$$\mathbb{A}_m(u) = |\tilde{a}_m \rangle A_{\tilde{a}_m \tilde{b}_m}(u) \langle \tilde{b}_m | \quad \text{and} \quad \mathbb{D}_m(u) = |a_m \rangle D_{a_m b_m}(u) \langle b_m | \quad (\text{B.30})$$

with non-trivial action over the spaces:

$$\mathbb{A}_a : \quad \tilde{\mathbf{2}}_a \otimes \mathbf{6}_1 \otimes \cdots \otimes \mathbf{6}_L \longrightarrow \tilde{\mathbf{2}}_a \otimes \mathbf{6}_1 \otimes \cdots \otimes \mathbf{6}_L \quad (\text{B.31})$$

$$\mathbb{D}_a : \quad \mathbf{2}_a \otimes \mathbf{6}_1 \otimes \cdots \otimes \mathbf{6}_L \longrightarrow \mathbf{2}_a \otimes \mathbf{6}_1 \otimes \cdots \otimes \mathbf{6}_L \quad (\text{B.32})$$

In this language the transfer matrix is now a sum of traces of \mathbb{A} and \mathbb{D} blocks and the eigenvalue problem has two pieces associated to these blocks:

$$\mathcal{T}(\lambda)|\Psi\rangle = \text{Tr}_a \mathbb{A}_a(\lambda)|\Psi\rangle + \text{Tr}_a \mathbb{D}_a(\lambda)|\Psi\rangle \quad (\text{B.33})$$

where “ a ” labels an auxiliary space $\tilde{\mathbf{2}}$ for the \mathbb{A} -block and $\mathbf{2}$ for the \mathbb{D} -block.

Now starting with equation (B.33) the strategy is to commute the \mathbb{A} and \mathbb{D} blocks through the product of \mathbb{B} -blocks until we reach the pseudo-vacuum that satisfies (B.18). This is possible using the commutation relations provided by the Yang-Baxter algebra (see section B.4). Once we follow this procedure the result has two type of terms: wanted and unwanted. From the wanted terms we can reproduce the eigenvalue equation (B.29) and read off the corresponding transfer matrix eigenvalue Λ . On the other hand the unwanted

terms spoil the eigenvalue equation and their vanishing is a necessary condition to satisfy (B.29). Here we only show the wanted terms:

$$\begin{aligned}
\mathcal{T}(\lambda)|\Psi\rangle = & \Phi_0(\lambda) \text{Tr}_a \langle \tilde{\psi} | T_a(u_1 \dots u_M | \lambda) \mathbb{B}_1(u_1) \cdots \mathbb{B}_M(u_M) \mathbb{A}_a(\lambda) |\psi\rangle \otimes |\Omega_L\rangle \\
& + \Theta_0(\lambda) \text{Tr}_a \langle \tilde{\psi} | \mathbb{B}_1(u_1) \cdots \mathbb{B}_M(u_M) \mathbb{D}_a(\lambda) T_a(\lambda | u_M \dots u_1) |\psi\rangle \otimes |\Omega_L\rangle \\
& + \text{unwanted terms from commuting } \mathbb{A} \text{ and } \mathbb{B}\text{-blocks} \\
& + \text{unwanted terms from commuting } \mathbb{D} \text{ and } \mathbb{B}\text{-blocks}
\end{aligned} \tag{B.34}$$

with:

$$\Phi_0(\lambda|\{u\}) = \prod_{j=1}^M \frac{\lambda - u_j + i}{\lambda - u_j} \quad \text{and} \quad \Theta_0(\lambda|\{u\}) = \prod_{j=1}^M \frac{\lambda - u_j - i}{\lambda - u_j} \tag{B.35}$$

As a by-product of the commutations of \mathbb{A} - \mathbb{B} and \mathbb{D} - \mathbb{B} blocks in (B.34) we obtain two auxiliary nested $\mathfrak{su}(2)$ monodromies⁵ acting in the spaces of $\langle \tilde{\psi} |$ and $|\psi\rangle$ respectively:

$$T_a(u_1 \dots u_M | \lambda) \equiv R_{1a}(u_1, \lambda) \cdots R_{Ma}(u_M, \lambda) \quad \text{with} \quad a \equiv \tilde{\mathbf{2}}_a \tag{B.36}$$

$$T_a(\lambda | u_M \dots u_1) \equiv R_{aM}(\lambda, u_M) \cdots R_{a1}(\lambda, u_1) \quad \text{with} \quad a \equiv \mathbf{2}_a \tag{B.37}$$

with R -matrices given by (B.9) but now restricted to act over $\mathfrak{su}(2)$ subspaces. Namely they read

$$R_{\mathbf{2}\mathbf{2}}(u, v) = \frac{u - v}{u - v - i} I_{\mathbf{2}\mathbf{2}} - \frac{i}{u - v - i} P_{\mathbf{2}\mathbf{2}}. \tag{B.38}$$

Furthermore we can directly act with \mathbb{A} over the pseudovacuum in the first line of (B.34), since it does not act non-trivially over the wing states. Similarly in the second line we can commute \mathbb{D}_a and the nested monodromy T_a in the presence of the trace and act over the pseudovacuum. Using the diagonalization properties (B.18) of pseudovacuum we can simplify (B.34) and obtain wing transfer matrices as traces of (B.36) and (B.37) :

$$\begin{aligned}
\mathcal{T}(\lambda)|\Psi\rangle = & \Phi_0(\lambda) a(\lambda) \boxed{\langle \tilde{\psi} | \text{Tr}_a T_a(u_1 \dots u_M | \lambda)} \mathbb{B}_1(u_1) \cdots \mathbb{B}_M(u_M) |\psi\rangle \otimes |\Omega_L\rangle + \cdots \\
& + \Theta_0(\lambda) d(\lambda) \langle \tilde{\psi} | \mathbb{B}_1(u_1) \cdots \mathbb{B}_M(u_M) \boxed{\text{Tr}_a T_a(\lambda | u_M \dots u_1) |\psi\rangle} \otimes |\Omega_L\rangle + \cdots
\end{aligned} \tag{B.39}$$

We now see that to reproduce the eigenvalue equation (B.29) from the “wanted” terms, the wing states must be eigenstates of the corresponding nested $\mathfrak{su}(2)$ transfer matrices of the monodromies (B.36) and (B.37). This auxiliary problem is simply solved by the standard $\mathfrak{su}(2)$ ABA [83]:

$$\langle \tilde{\psi} | = \langle \Omega_{\tilde{\mathbf{2}}} | \mathcal{C}(w_1) \cdots \mathcal{C}(w_{\tilde{K}}) \quad \text{and} \quad |\psi\rangle = \mathcal{B}(v_1) \cdots \mathcal{B}(v_K) |\Omega_{\mathbf{2}}\rangle \tag{B.40}$$

⁵This is analogous to the appearance of a nested $\mathfrak{su}(2)$ monodromy in the $\mathfrak{su}(3)$ Bethe Ansatz. But now we have two copies of nested monodromies, one for each wing $\langle \tilde{\psi} |$ and $|\psi\rangle$

where \mathcal{B} and \mathcal{C} are creation and annihilation operators extracted from the monodromies (B.37) and (B.36) respectively. They act over $\mathfrak{su}(2)$ vacuum states of the wings given by:

$$\langle \Omega_2 | \equiv \langle 1^M | \quad \text{and} \quad | \Omega_2 \rangle \equiv | 3^M \rangle \quad (\text{B.41})$$

In addition the sets of auxiliary roots $\{v\}$ and $\{w\}$ must be on-shell, that is they must fulfil $\mathfrak{su}(2)$ Bethe equations with the set $\{u\}$ as inhomogeneities. Assuming these conditions the $\mathfrak{su}(2)$ Bethe states (B.40) diagonalize the wing transfer matrices as:

$$\langle \tilde{\psi} | Tr_a T_a(u_{1\dots M} | \lambda) = \tilde{\Lambda}^{\mathfrak{su}(2)}(\lambda) \langle \tilde{\psi} | \quad \text{and} \quad Tr_a T_a(\lambda | u_{M\dots 1}) | \psi \rangle = \Lambda^{\mathfrak{su}(2)}(\lambda) | \psi \rangle \quad (\text{B.42})$$

With the wing-states on-shell, (B.39) becomes the eigenvalue equation (B.29) up to unwanted terms:

$$\mathcal{T}(\lambda) | \Psi \rangle = \left(\Phi_0 a \tilde{\Lambda}^{\mathfrak{su}(2)} + \Theta_0 d \Lambda^{\mathfrak{su}(2)} \right) | \Psi \rangle + \text{unwanted terms} \quad (\text{B.43})$$

More explicitly the transfer matrix eigenvalue is given in terms of the spectral parameter λ and the sets of auxiliary roots $\{u\}_M$, $\{v\}_K$ and $\{w\}_{\tilde{K}}$:

$$\begin{aligned} \Lambda(\lambda) = & \left(\prod_{j=1}^M \frac{\lambda - u_j + i}{\lambda - u_j} \right) \left(\prod_{k=1}^{\tilde{K}} \frac{\lambda - w_k - i}{\lambda - w_k} + \prod_{j=1}^M \frac{\lambda - u_j}{\lambda - u_j + i} \prod_{k=1}^{\tilde{K}} \frac{\lambda - w_k + i}{\lambda - w_k} \right) \\ & + \left(\frac{\lambda + i/2}{\lambda - i/2} \right)^L \left(\prod_{j=1}^M \frac{\lambda - u_j - i}{\lambda - u_j} \right) \left(\prod_{k=1}^K \frac{\lambda - v_k + i}{\lambda - v_k} + \prod_{j=1}^M \frac{\lambda - u_j}{\lambda - u_j - i} \prod_{k=1}^K \frac{\lambda - v_k - i}{\lambda - v_k} \right) \end{aligned} \quad (\text{B.44})$$

The vanishing of the unwanted terms puts constraints over the set of roots $\{u\}$. These constraints constitute the Bethe equations of the $\mathfrak{so}(6)$ middle node. Alternatively we can arrive to the same conditions by imposing the vanishing of the spurious poles at $\lambda = u_{1\dots M}$ of the transfer matrix eigenvalue (B.44). This latter method to obtain Bethe equations is the so called analytic Bethe Ansatz:

$$\text{Res}_{\lambda=u_m} \Lambda(\lambda) = 0 \quad \longrightarrow \quad \left(\frac{u_m + i/2}{u_m - i/2} \right)^L = \prod_{j \neq m}^M \frac{u_m - u_j + i}{u_m - u_j - i} \prod_{k=1}^{\tilde{K}} \frac{u_m - w_k - i}{u_m - w_k} \prod_{k=1}^K \frac{u_m - v_k}{u_m - v_k + i} \quad (\text{B.45})$$

To obtain the standard form of $\mathfrak{so}(6)$ Bethe equations we must perform the shifts⁶:

$$w \rightarrow w - i/2 \quad \text{and} \quad v \rightarrow v + i/2 \quad (\text{B.46})$$

In summary, the $\mathfrak{so}(6)$ Bethe state is given by the Ansatz in (B.28) with wing states given by the nested $\mathfrak{su}(2)$ Bethe states (B.40) and with the sets of auxiliary roots $\{u\}, \{v\}$ and

⁶ This is equivalent to define the $\mathfrak{su}(2)$ monodromies (B.36) and (B.37) with the Lax pair instead of the R -matrix. These two objects differ by a shift of $i/2$ in the spectral parameter

$\{w\}$ on-shell. The structure of the Bethe Ansatz presented in figure B.4 is equivalent to the vertex model in figure B.3.

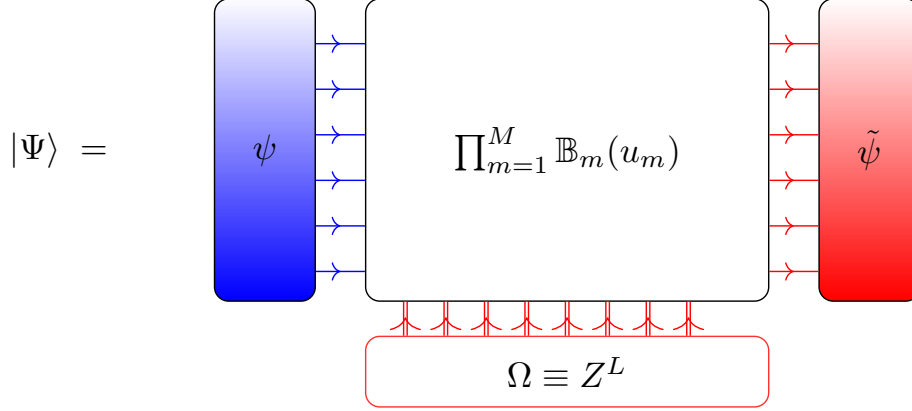


Figure B.4: The $\mathfrak{so}(6)$ Bethe state

B.4 The Yang-Baxter algebra

In this section we present the Yang-Baxter algebra of our $\mathfrak{so}(6)$ model. This algebra provides the technical steps to find the wanted and unwanted terms of the Bethe Ansatz in section B.3, as well as for our final result (B.83) for the scalar product (B.2).

The R matrices in (B.9) and (B.11) fulfil the Yang-Baxter equation:

$$R_{4_a 4_b}(u, v) R_{4_a 6}(u, \theta) R_{4_b 6}(v, \theta) = R_{4_b 6}(v, \theta) R_{4_a 6}(u, \theta) R_{4_a 4_b}(u, v) \quad (\text{B.47})$$

where a and b label two different spaces in the $\mathbf{4}$ fundamental representation.

This can be straightforwardly generalized to a Yang-Baxter relation for the monodromy in (B.14), the so called RTT relation⁷:

$$R_{ab}(u, v) T_a(u) T_b(v) = T_b(v) T_a(u) R_{ab}(u, v) \quad (\text{B.48})$$

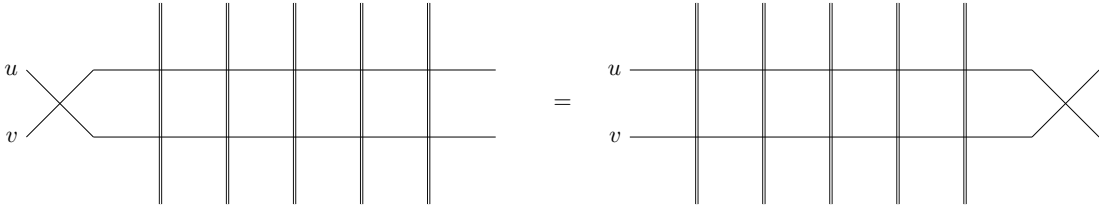


Figure B.5: $RTT = TTR$ relation

⁷ In our graphical representations the order of action of operators should be read from left to right. While in our equations we respect the usual order of operator action, that is operators on the right act first. In this way the left-hand side in figure B.5 represents the right-hand side on equation (B.48).

Furthermore, taking the trace over the 4-dimensional auxiliary spaces in (B.48) we obtain the commutation relation for the transfer matrices:

$$[\mathcal{T}(u), \mathcal{T}(v)] = 0 \quad \text{with} \quad \mathcal{T}(u) = \text{Tr}_a(T_a(u)) \quad (\text{B.49})$$

This latter relation gives a family of conserved local charges in convolution when expanding the transfer matrix around $u = -i/2$ (without inhomogeneities).

The RTT relation also provides the algebra of the monodromy elements in (B.15), known as the Yang-Baxter algebra. This is a set of commutation relations that can be obtained by specifying the boundary conditions in the four-dimensional auxiliary spaces: $a : (i) \rightarrow (k)$ and $b : (j) \rightarrow (l)$ as follows:

$$(R_{ab}(u, v))^{(k)(l)} (T_a(u))_{(i)} (T_b(v))_{(j)} = (T_b(v))^{(l)} (T_a(u))^{(k)} (R_{ab}(u, v))_{(i)(j)} \quad (\text{B.50})$$

where the lower indexes in parenthesis indicate the initial flavours and the upper indexes correspond to the final flavours. We leave implicit the intermediate flavours indexes over which we must sum over.

Expanding the R -matrices in (B.50) into identity and permutation as in (B.9) we obtain the following algebra of operators:

$$[T_{ki}(u), T_{lj}(v)] = \left(\frac{-i}{u-v} \right) (T_{li}(v) T_{kj}(u) - T_{li}(u) T_{kj}(v)) \quad (\text{B.51})$$

where $T_{13} \equiv B_{13}$ and likewise for other operators in (B.15).

The Yang-Baxter algebra (B.51) plays a key role in the construction of the ABA in section B.3 and also in the computation of the scalar product that gives the tree level structure constant in section B.6. In what follows we provide some of the details involved in these calculations.

The wanted and unwanted terms of the Bethe Ansatz

In the ABA construction we use the Yang-Baxter algebra organized into blocks. For this we restrict the four-dimensional auxiliary spaces in (B.48) to the subspaces $\mathbf{2}$ (flavours $\{3, 4\}$) or $\tilde{\mathbf{2}}$ (flavours $\{1, 2\}$), instead of strictly fixing the boundary conditions. For instance to derive the \mathbb{D} -block and \mathbb{B} -block commutation relation we restrict the auxiliary spaces as: $a : \mathbf{2}_{(3,4)} \rightarrow \mathbf{2}_{(3,4)}$ and $b : \mathbf{2}_{(3,4)} \rightarrow \tilde{\mathbf{2}}_{(1,2)}$:

$$(R_{ab}(u, v))^{(3,4)(1,2)} (T_a(u))_{(3,4)} (T_b(v))_{(3,4)} = (T_b(v))^{(1,2)} (T_a(u))^{(3,4)} (R_{ab}(u, v))_{(3,4)(3,4)} \quad (\text{B.52})$$

expanding the R -matrix of the left hand side we obtain:

$$\mathbb{D}_a(u) \mathbb{B}_b(v) = \left(\frac{u-v-i}{u-v} \right) \mathbb{B}_b(v) \mathbb{D}_a(u) R_{ab}(u, v) + \left(\frac{i}{u-v} \right) \mathbb{B}_b(u) \mathbb{D}_a(v) P_{ab} \quad (\text{B.53})$$

Under these restrictions now a and b label two-dimensional spaces.

Similarly, by making another appropriate choice of boundary conditions: $a : \tilde{\mathbf{2}}_{(1,2)} \rightarrow \tilde{\mathbf{2}}_{(1,2)}$ and $b : \mathbf{2}_{(3,4)} \rightarrow \tilde{\mathbf{2}}_{(1,2)}$, we obtain the \mathbb{A} - \mathbb{B} commutation relation:

$$\mathbb{A}_a(u)\mathbb{B}_b(v) = \left(\frac{u-v+i}{u-v}\right) R_{ba}(v,u) \mathbb{B}_b(v)\mathbb{A}_a(u) + \left(-\frac{i}{u-v}\right) P_{ab} \mathbb{B}_b(u)\mathbb{A}_a(v) \quad (\text{B.54})$$

Using these commutation relations, (B.53) and (B.54), we can compute the wanted and unwanted terms as a result of commuting \mathbb{A} and \mathbb{D} through the product of \mathbb{B} -blocks in the ansatz (B.28). These results are given by:

$$\begin{aligned} \mathbb{A}_a(\lambda) \mathbb{B}(u_{1\dots M}) &= \Phi_0(\lambda|\{u\}) \mathbb{T}_a(u_{1\dots M}|\lambda) \mathbb{B}(u_{1\dots M}) \mathbb{A}_a(\lambda) \\ &+ \sum_{k=1}^M \Phi_k(\lambda|\{u\}) \mathbb{T}_a(u_{1\dots M}|u_k) T_k(u_k|u_{k-1\dots 1}) \mathbb{B}(\lambda) \mathbb{B}(u_{1\dots \hat{k}\dots M}) T_k(u_{1\dots k-1}|u_k) \mathbb{A}_a(u_k) \end{aligned} \quad (\text{B.55})$$

where we use the short-hand notation:

$$\mathbb{B}(u_{1\dots M}) \equiv \prod_{m=1}^M \mathbb{B}_m(u_m) \quad \text{and} \quad \mathbb{B}(u_{1\dots \hat{k}\dots M}) \equiv \prod_{\substack{m=1 \\ m \neq k}}^M \mathbb{B}_m(u_m) \quad (\text{B.56})$$

as well as:

$$\begin{aligned} T_k(u_k|u_{k-1\dots 1}) &= R_{k\ k-1}(u_k, u_{k-1}) \cdots R_{k\ 2}(u_k, u_2) R_{k\ 1}(u_k, u_1) \\ T_k(u_{1\dots k-1}|u_k) &= R_{1\ k}(u_1, u_k) R_{k\ 1}(u_k, u_1) \cdots R_{k-1\ k}(u_{k-1}, u_k) \end{aligned} \quad (\text{B.57})$$

The Φ_k coefficients are:

$$\Phi_0(\lambda|\{u\}) = \prod_{j=1}^M \frac{u_j - \lambda - i}{u_j - \lambda} \quad \text{and} \quad \Phi_k(\lambda|\{u\}) = \frac{i}{u_k - \lambda} \prod_{\substack{j=1 \\ j \neq k}}^M \frac{u_j - u_k - i}{u_j - u_k} \quad (\text{B.58})$$

Similarly we commute a \mathbb{D} -block through a product of \mathbb{B} -blocks as:

$$\begin{aligned} \mathbb{D}_a(\lambda) \mathbb{B}(u_{1\dots M}) &= \Theta_0(\lambda|\{u\}) \mathbb{B}(u_{1\dots M}) \mathbb{D}_a(\lambda) T_a(\lambda|u_{M\dots 1}) \\ &+ \sum_{k=1}^M \Theta_k(\lambda|\{u\}) T_k(u_k|u_{k-1\dots 1}) \mathbb{B}(\lambda) \mathbb{B}(u_{1\dots \hat{k}\dots M}) T_k(u_{1\dots k-1}|u_k) \mathbb{D}_a(u_k) T_a(u_k|u_{M\dots 1}) \end{aligned} \quad (\text{B.59})$$

with coefficients:

$$\Theta_0(\lambda|\{u\}) = \prod_{j=1}^M \frac{\lambda - u_j - i}{\lambda - u_j} \quad \text{and} \quad \Theta_k(\lambda|\{u\}) = \frac{i}{\lambda - u_k} \prod_{\substack{j=1 \\ j \neq k}}^M \frac{u_k - u_j - i}{u_k - u_j} \quad (\text{B.60})$$

The C -commutation relations for the scalar product

When computing the scalar product (B.2), using the ABA, we will need of the commutation relations of the annihilation \mathbb{C} -block and the other elements of the monodromy. These can be obtained from the Yang-Baxter algebra (B.51) as:

$$[\mathbb{C}_a(u), \mathbb{B}_b(v)] = \left(\frac{-i}{u-v} \right) (\mathbb{A}_b(v) \mathbb{D}_a(u) P_{ab} - P_{ab} \mathbb{A}_a(u) \mathbb{D}_b(v)) \quad (\text{B.61})$$

$$[\mathbb{C}_a(u), \mathbb{A}_b(v)] = \left(\frac{-i}{u-v} \right) (\mathbb{A}_b(v) \mathbb{C}_a(u) P_{ab} - P_{ab} \mathbb{A}_a(u) \mathbb{C}_b(v)) \quad (\text{B.62})$$

$$[\mathbb{C}_a(u), \mathbb{D}_b(v)] = \left(\frac{-i}{v-u} \right) (P_{ab} \mathbb{D}_b(v) \mathbb{C}_a(u) - \mathbb{D}_a(u) \mathbb{C}_b(v) P_{ab}) \quad (\text{B.63})$$

B.5 The coordinate Bethe Ansatz (CBA)

As explained in section B.2 we can expand the Bethe states in terms of a coordinate basis as:

$$|\Psi_{\text{so}(6)}\rangle = \sum_{\text{coordinate basis}} \Psi_{ZX\ldots}(\{\textcolor{red}{v}\}, \{u\}, \{\textcolor{blue}{w}\}) |ZX\ldots\rangle \quad (\text{B.64})$$

where $|ZX\ldots\rangle$ stands for an element of the coordinate basis and the coefficient $\Psi_{ZX\ldots}$ is its corresponding wave-function. This wavefunction is obtained as a partition function in the lattice in figure B.3, with top boundary conditions imposed by the corresponding element of the coordinate basis.

The coordinate basis as strings of auxiliary roots

To introduce the wave-function of a given element in the coordinate basis we first define a one to one map between the elementary fields (B.5) and a set of rapidities:

$$Z \equiv \theta \quad X \equiv \overset{u}{\theta} \quad Y \equiv \overset{\overset{w}{u}}{\theta} \quad \bar{Y} \equiv \overset{\overset{\textcolor{red}{v}}{u}}{\theta} \quad \bar{X} \equiv \overset{\overset{\textcolor{red}{v}}{u}}{\overset{\textcolor{blue}{w}}{\theta}} \quad \bar{Z} \equiv \overset{\overset{\textcolor{red}{v}}{u_1} \textcolor{blue}{w}}{u_2} \theta, \quad (\text{B.65})$$

where θ 's are the inhomogeneities defined for each spin chain site. To make manifest the structure of the nested Bethe ansatz, here we represented the fields by stacking the roots: u is the root at the middle node whereas $\textcolor{blue}{w}$ and $\textcolor{red}{v}$ are the nested roots associated with the left and the right nodes respectively.

Using this representation, we can re-express the coordinate basis as a collection of (sets of) rapidities, for instance:

$$|Z_{(\theta_1)} X_{(\theta_2)} \bar{Z}_{(\theta_3)} \bar{Y}_{(\theta_4)}\rangle \equiv |\theta_1 \overset{u_1}{\theta_2} \overset{\overset{\textcolor{red}{v}_1}{u_2} \textcolor{blue}{w}_1}{u_3} \overset{\overset{\textcolor{red}{v}_2}{u_4}}{\theta_3} \theta_4\rangle \quad (\text{B.66})$$

Here we assigned a numeration to the auxiliary roots in the order of appearance⁸. In what follows, we call such a collection of rapidities a *string*. The full wave function (B.64) can then be written as

$$|\Psi_{\mathbf{s}0(6)}\rangle = \sum_{\mathbf{s} \in \text{all possible strings}} \Psi_{\mathbf{s}}(\{\mathbf{v}\}, \{u\}, \{\mathbf{w}\}) |\mathbf{s}\rangle \quad (\text{B.67})$$

The wave-function

The wavefunction $\Psi_{\mathbf{s}}$ for the string \mathbf{s} is given by a sum over weighted permutations over all the auxiliary roots:

$$\Psi_{\mathbf{s}} = \sum_{\pi \in \text{Per}(K_1)} S(\{\mathbf{v}\}_{\pi}) \sum_{\sigma \in \text{Per}(K_2)} S(\{u\}_{\sigma}) \sum_{\tilde{\pi} \in \text{Per}(K_3)} S(\{\mathbf{w}\}_{\tilde{\pi}}) \times \Psi_{\mathbf{s}}^{\text{bare}}(\{\mathbf{v}\}_{\pi}, \{u\}_{\sigma}, \{\mathbf{w}\}_{\tilde{\pi}}), \quad (\text{B.68})$$

where the notation $\{*\}_{\sigma}$ denotes that the set $*$ is permuted according to the permutation σ . The multiparticle S -matrix $S(\{u\}_{\sigma})$ brings the ordered momenta $\{u\}$ to the ordering $\{u\}_{\sigma}$ and is given by a factorized product of two-body S -matrices as in the examples:

$$\begin{aligned} S(\{u_3, u_2, u_1\}) &= S(u_1, u_2)S(u_1, u_3)S(u_2, u_3) \quad \text{with} \quad S(u_a, u_b) = \frac{u_a - u_b - i}{u_a - u_b + i} \\ S(\{u_3, u_1, u_2\}) &= S(u_1, u_3)S(u_2, u_3) \end{aligned} \quad (\text{B.69})$$

In a spin chain with L sites, the corresponding “bare” wavefunction $\Psi_{\mathbf{s}}^{\text{bare}}$ is given by

$$\Psi_{\mathbf{s}}^{\text{bare}}(\{\mathbf{v}\}, \{u\}, \{\mathbf{w}\}) = \prod_{n=1}^L \Phi(\mathbf{s}_n), \quad (\text{B.70})$$

where the individual wave function $\Phi(\mathbf{s}_n)$, defined for the n -th element of the string \mathbf{s} , is given by

$$\begin{aligned} \Phi(\theta) &= 1 \\ \Phi(\overset{u}{\theta}_n) &= \varphi_n(u|\{\theta\}) \\ \Phi(\overset{w}{\theta}_n) &= \varphi_n(u_m|\{\theta\}) \times \tilde{\varphi}_m(\mathbf{w}|\{u\}) \\ \Phi(\overset{v}{\theta}_n) &= \varphi_n(u_m|\{\theta\}) \times \tilde{\varphi}_m(\mathbf{v}|\{u\}) \\ \Phi(\overset{v \ w}{\theta}_n) &= (-1) \times \varphi_n(u_m|\{\theta\}) \times \tilde{\varphi}_m(\mathbf{v}|\{u\}) \times \tilde{\varphi}_m(\mathbf{w}|\{u\}) \\ \Phi(\overset{u_m \ v \ w}{\theta}_n) &= \frac{1}{2} \times \varphi_n(u_m|\{\theta\}) \times \varphi_n(u_{m+1}|\{\theta\}) \\ &\quad \times \left(\tilde{\varphi}_m(\mathbf{w}|\{u\}) - \tilde{\varphi}_{m+1}(\mathbf{w}|\{u\}) \right) \times \left(\tilde{\varphi}_m(\mathbf{v}|\{u\}) - \tilde{\varphi}_{m+1}(\mathbf{v}|\{u\}) \right) \end{aligned} \quad (\text{B.71})$$

⁸Since we later sum over all permutations of auxiliary roots this enumeration becomes irrelevant.

where we include the label of the rapidities (u_m) only when this is necessary to express the corresponding wavefunction. The factors φ and $\tilde{\varphi}$ are one-particle wave functions and are given by:

$$\begin{aligned}\varphi_n(u|\{\theta\}) &= \left(\prod_{l=1}^{n-1} \frac{u - \theta_l + i/2}{u - \theta_l - i/2} \right) \times \underbrace{\frac{1}{u - \theta_n - i/2}}_{\text{occupation factor}} \\ \tilde{\varphi}_m(w|\{u\}) &= \left(\prod_{l=1}^{m-1} \frac{w - u_l + i/2}{w - u_l - i/2} \right) \times \frac{1}{w - u_m - i/2}\end{aligned}\tag{B.72}$$

Needless to say, when the rapidities are permuted in (B.70), we should also permute the rapidities in the definitions of the wave functions, which are given by the right hand sides of (B.71), accordingly.

B.6 The scalar product: tree level structure constant

As we saw in the introduction of this Appendix, the tree level planar three-point function in figure B.1 is given by the scalar product between a rotated BMN vacuum and a Bethe state:

$$\begin{aligned}\mathcal{C}_{123} &= \langle \tilde{Z}^l | \Psi(\{v\}, \{u\}_M, \{w\}) \rangle_{l-Bethe} \\ &= \langle \tilde{Z}^l | \otimes \langle \tilde{\psi} | \mathbb{B}_1(u_1) \cdots \mathbb{B}_M(u_M) | \psi \rangle \otimes |\Omega_l\rangle\end{aligned}\tag{B.73}$$

where Bethe state is given by the Ansatz in figure B.4 but with the number of sites or elementary fields equal to the bridge “ l ”.

A global rotation

In order to compute the scalar product (B.73) using the machinery of the ABA, we first need to express the rotated vacuum in this language. This is achieved by means of a global rotation of the original vacuum:

$$|\tilde{Z}^L\rangle = e^{\mathbf{b}} |Z^L\rangle\tag{B.74}$$

The generator “ \mathbf{b} ” of this global rotation can be simply obtained from the B -block by taking the trace and sending to ∞ the spectral parameter “ u ”;

$$\lim_{u \rightarrow \infty} Tr \mathbb{B}(u) = \frac{i}{u} \mathbf{b}\tag{B.75}$$

this lowering generator is composed by the elements:

$$\mathbf{b} = \mathbf{b}_{13} + \mathbf{b}_{24}\tag{B.76}$$

When \mathbf{b}_{13} acts over the vacuum generates a X excitation, when \mathbf{b}_{24} acts generates $-\bar{X}$ and when both act over the same site a \bar{Z} excitation is generated. In this way we generate the rotated vacuum:

$$\tilde{Z} \equiv Z + \bar{Z} + X - \bar{X} \quad (\text{B.77})$$

In the scalar product (B.73) we must use instead the bra state for which we use the C -block as:

$$\langle \tilde{Z}^l | = \langle \Omega | e^{\mathbf{c}} \quad \text{with} \quad \lim_{u \rightarrow \infty} \text{Tr } \mathbb{C}(u) = \frac{i}{u} \mathbf{c} \quad (\text{B.78})$$

The scalar product

Now we outline the steps we take to compute the scalar product (B.73). The first step is to notice that the Bethe state has a defined $\mathfrak{so}(6)$ charge determined by the number of (finite) auxiliary roots $\{u\}_M, \{v\}$ and $\{w\}$. While in the expansion of global rotation $e^{\mathbf{c}} = 1 + \mathbf{c} + \dots$ only the term \mathbf{c}^M matches this $\mathfrak{so}(6)$ charge. So the scalar product (B.73) can be simplify to:

$$\mathcal{C}_{123} = \frac{1}{M!} \times \langle \Omega | \otimes \langle \tilde{\psi} | \mathbf{c}^M \mathbb{B}_1(u_1) \cdots \mathbb{B}_M(u_M) |\psi\rangle \otimes |\Omega\rangle \quad (\text{B.79})$$

The next step is to commute all the \mathbf{c} operators through the B -blocks, such as we can use their annihilation properties:

$$\mathbf{c} |\Omega\rangle = 0 \quad \text{and} \quad \langle \Omega | \mathbb{B}(u) = 0 \quad (\text{B.80})$$

The commutator of \mathbf{c} and B can be found from the Yang-Baxter algebra. Taking the limit (B.78) of (B.61) we obtain:

$$[\mathbf{c}, \mathbb{B}_a(u)] = \mathbb{D}_a(u) - \mathbb{A}_a(u) \quad (\text{B.81})$$

Since \mathbb{A} and \mathbb{D} blocks are generated we also need of their commutators with \mathbf{c} , which can be extracted in a similar way from (B.62) and (B.63) as:

$$[\mathbf{c}, \mathbb{D}_a(u)] = -\mathbb{C}_a(u), \quad [\mathbf{c}, \mathbb{A}_a(u)] = \mathbb{C}_a(u) \quad \text{and} \quad [\mathbf{c}, \mathbb{C}_a(u)] = 0 \quad (\text{B.82})$$

The final set of commutators we need are between \mathbb{C} and $\mathbb{A}, \mathbb{B}, \mathbb{D}$ blocks. These are given in section B.4.

All in all the result of commuting \mathbf{c}^M through a product of M B -block operators is given by a sum over bi-partitions:

$$\begin{aligned} \frac{1}{M!} \times \mathbf{c}^M \mathbb{B}_1(u_1) \cdots \mathbb{B}_M(u_M) = & \sum_{\alpha \cup \bar{\alpha} = \{u\}} (-1)^{|\alpha|} h_{\alpha, \bar{\alpha}} R_{\bar{\alpha}, \alpha} \mathbb{A}_{\alpha} \mathbb{D}_{\bar{\alpha}} R^{\alpha, \bar{\alpha}} \\ & + \mathbb{C}\text{-terms} + \mathbf{c}\text{-terms} \end{aligned} \quad (\text{B.83})$$

where we use the short-hand notation:

$$\mathbb{A}_\alpha = \prod_{u \in \alpha} \mathbb{A}(u), \quad \mathbb{D}_{\bar{\alpha}} = \prod_{u \in \bar{\alpha}} \mathbb{D}(u) \quad \text{and} \quad h_{\alpha, \bar{\alpha}} = \prod_{u \in \alpha, v \in \bar{\alpha}} \frac{u - v - i}{u - v} \quad (\text{B.84})$$

and the \mathbb{C} and \mathbf{c} -terms are products of operators that annihilate the $\mathfrak{so}(6)$ pseudo-vacuum.

The matrix operator $R^{\alpha, \bar{\alpha}}$ is a product of $\mathfrak{su}(2)$ R -matrices (B.38) that changes the order of the roots $\{u_1 \cdots u_M\}$ to the order $\{\alpha, \bar{\alpha}\}$, while the operator $R_{\bar{\alpha}, \alpha}$ takes the roots from the ordering $\{\bar{\alpha}, \alpha\}$ to the ordering $\{u_1 \cdots u_M\}$.

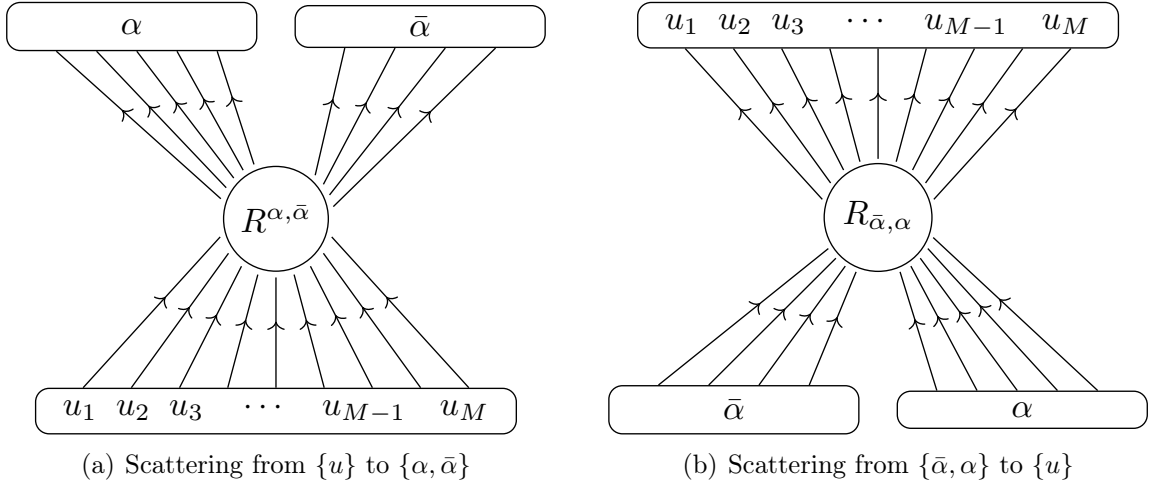


Figure B.6: multi-scattering R -matrices in (B.83) and (B.86)

For instance, when $\alpha = \{u_2, u_4\}$ and $\bar{\alpha} = \{u_1, u_3, u_5\}$, the multiparticle scattering operators are:

$$\begin{aligned} \{u_1, u_2, u_3, u_4, u_5\} &\xrightarrow{R^{\alpha, \bar{\alpha}}} \{\underbrace{u_2, u_4}_\alpha, \underbrace{u_1, u_3, u_5}_{\bar{\alpha}}\} : & R^{\alpha, \bar{\alpha}} &= R_{14} R_{12} R_{34} \\ \{\underbrace{u_1, u_3, u_5}_{\bar{\alpha}}, \underbrace{u_2, u_4}_\alpha\} &\xrightarrow{R_{\bar{\alpha}, \alpha}} \{u_1, u_2, u_3, u_4, u_5\} : & R_{\bar{\alpha}, \alpha} &= R_{32} R_{54} R_{52} \end{aligned} \quad (\text{B.85})$$

where we use the short-hand notation $R_{ab} = R_{ab}(u_a, u_b)$

Finally we can compute the scalar product (B.79) using (B.83) and the eigenstate relations of the pseudovacuum (B.18):

$$\mathcal{C}_{123} = \sum_{\alpha \cup \bar{\alpha} = \{u\}} (-1)^{|\alpha|} a_\alpha d_{\bar{\alpha}} h_{\alpha, \bar{\alpha}} \times \underbrace{\langle \tilde{\psi} | R_{\bar{\alpha}, \alpha} R^{\alpha, \bar{\alpha}} | \psi \rangle}_{\text{Matrix}_{\alpha, \bar{\alpha}}} \quad (\text{B.86})$$

with $a_\alpha = \prod_{u \in \alpha} a(u) = 1$ and $d_{\bar{\alpha}} = \prod_{u \in \bar{\alpha}} d(u) = \prod_{u \in \bar{\alpha}} \left(\frac{u+i/2}{u-i/2} \right)^L$. Needless to say, this expression is already strongly resembling the all loop expressions in the main text including the involved matrix part as proposed in [5].

Wings on-shell: simplifying the matrix part $\text{Matrix}_{\alpha, \bar{\alpha}}$

The matrix part can be further simplified considering that the wing-states are (on-shell) $\mathfrak{su}(2)$ Bethe states. In this case the action of the R -matrices has the simple effect of reshuffling the inhomogeneities $\{u\}$ of the wing-states so we obtain:

$$\langle \tilde{\psi} | R_{\bar{\alpha}, \alpha} = \langle \tilde{\psi}_{\bar{\alpha}, \alpha} | \quad \text{and} \quad R^{\alpha, \bar{\alpha}} |\psi\rangle = |\psi_{\alpha, \bar{\alpha}}\rangle \quad (\text{B.87})$$

where $|\psi_{\alpha, \bar{\alpha}}\rangle$ is the wing state $|\psi\rangle$ with the inhomogeneities order as in the top of figure B.6(a) and $\langle \tilde{\psi}_{\bar{\alpha}, \alpha} |$ is the wing $\langle \tilde{\psi} |$ with the ordering as in the bottom of figure B.6(b). In this way the matrix part is simply given by the scalar product of the states (B.87). To simplify this scalar product it is necessary to place the inhomogeneities of the two states in the same ordering. This can be achieved by using again the multi-scattering R matrix:

$$|\psi_{\alpha, \bar{\alpha}}\rangle = R_{\bar{\alpha}, \alpha}^{\alpha, \bar{\alpha}} |\psi_{\bar{\alpha}, \alpha}\rangle \quad (\text{B.88})$$

The special feature of this reordering scattering matrix is that it can be expressed as a product of nested $\mathfrak{su}(2)$ transfer matrices with spectral parameters $u \in \bar{\alpha}$ and inhomogeneities $\{u\}$:

$$R_{\bar{\alpha}, \alpha}^{\alpha, \bar{\alpha}} = \prod_{u \in \bar{\alpha}} \mathcal{T}^{su(2)}(u) \quad (\text{B.89})$$

Since our wing states are on-shell we can replace the transfer matrices by the corresponding eigenvalue and obtain the periodicity relation:

$$|\psi_{\alpha, \bar{\alpha}}\rangle = \left(\prod_{u \in \bar{\alpha}} \mathcal{T}^{su(2)}(u) \right) |\psi_{\bar{\alpha}, \alpha}\rangle = \left(\prod_{u \in \bar{\alpha}} \Lambda^{su(2)}(u) \right) |\psi_{\bar{\alpha}, \alpha}\rangle \quad (\text{B.90})$$

So for on-shell Bethe states the cost of reordering is just a phase. Then the matrix part is given by:

$$\text{Matrix}_{\alpha, \bar{\alpha}} = \left(\prod_{u \in \bar{\alpha}} \Lambda^{su(2)}(u) \right) \langle \tilde{\psi}_{\bar{\alpha}, \alpha} | \psi_{\bar{\alpha}, \alpha} \rangle \quad (\text{B.91})$$

We now have the scalar product of two on-shell Bethe states with inhomogeneities in the same ordering. Considering their orthogonality property we know this scalar product vanishes unless the set of wing roots are identical $\{v\} = \{w\}$ ⁹. Under this condition the scalar product is given by the Gaudin-determinant. This determinant is invariant under permutations of the inhomogeneities so it can be taken out of the sum over partitions. The final expression for the unnormalized tree level structure constant is:

$$\boxed{\mathcal{C}_{123}^{\text{so}(6)} = \text{Gaudin}_{\mathfrak{su}(2)\text{-wing}} \times \sum_{\alpha \cup \bar{\alpha} = \{u\}} (-1)^{|\alpha|} h_{\alpha, \bar{\alpha}} \times \prod_{u \in \bar{\alpha}} \left(\frac{u + i/2}{u - i/2} \right)^L \Lambda^{\mathfrak{su}(2)}(u)} \quad (\text{B.92})$$

where $\Lambda^{\mathfrak{su}(2)}(u) = \prod_{k=1}^K \frac{u - v_k + i/2}{u - v_k - i/2}$, after performing the shift (B.46).

⁹Here we refer to the shifted wing roots $v \rightarrow v + i/2$ and $w \rightarrow w - i/2$ which appear in the standard form of the $\mathfrak{so}(6)$ Bethe equations.

Appendix C

The $\mathfrak{su}(1, 1|2)$ spin chain

C.1 The coordinate Bethe Ansatz(CBA)

We construct the CBA for $\mathfrak{su}(1, 1|2)$ by considering a nesting of two $\mathfrak{su}(1|1)$ spin chains over a $\mathfrak{sl}(2)$ spin chain. For this purpose we identify the $\mathfrak{su}(1, 1|2)$ -excitations $\{D^n Z, D^n X, D^n \psi, D^n \tilde{\psi}\}$ with strings formed by a set $\{u\}$ of $\mathfrak{sl}(2)$ -roots and two copies $\{v\}$ and $\{w\}$ of auxiliary $\mathfrak{su}(1|1)$ roots:

$$\begin{aligned} D^n Z &\equiv \{\{\}, \{u_1, \dots, u_n\}, \{\}\} \\ D^n \psi &\equiv \{\{v\}, \{u_1, \dots, u_{n+1}\}, \{\}\} \\ D^n \tilde{\psi} &\equiv \{\{\}, \{u_1, \dots, u_{n+1}\}, \{w\}\} \\ D^n X &\equiv \{\{v\}, \{u_1, \dots, u_{n+1}\}, \{w\}\} \end{aligned} \tag{C.1}$$

Under this notation a state of L elementary fields is equivalent to a set of L strings of auxiliary roots. For example we identify a state of length 4 with 4 strings as follows:

$$\begin{aligned} |D^2 Z D X D^2 \psi \tilde{\psi}\rangle \longrightarrow \\ |\{\{\}, \{u_1, u_2\}, \{\}\}_1, \{\{\textcolor{red}{v}_1\}, \{u_3, u_4\}, \{\textcolor{blue}{w}_1\}\}_2, \{\{\textcolor{red}{v}_2\}, \{u_5, u_6, u_7\}, \{\}\}_3, \{\{\}, \{u_8\}, \{\textcolor{blue}{w}_2\}\}_4\rangle \end{aligned} \tag{C.2}$$

We assign indexes for the auxiliary roots in order of appearance. These indexes are important to describe the next step in our construction, however the final result for the wave-function does not depend on this labelling

To define the wave-function associated to an element of the coordinate basis, we first introduce the bare wave-function Ψ^{bare} . For a state $strings = |\mathfrak{S}_1, \dots, \mathfrak{S}_L\rangle$ with strings given by the sets of auxiliary roots: $\mathfrak{S}_j \equiv \{\mathbf{v}_j, \mathbf{u}_j, \mathbf{w}_j\}$ we define the bare wave-function as:

$$\Psi^{bare}(strings) = \prod_{j=1}^L \Psi^{bare}(\mathfrak{S}_j) \tag{C.3}$$

The bare wave-function of a single string is:

$$\Psi^{bare}(\mathfrak{S}_j) = \Psi^{\mathfrak{sl}(2)}(\mathbf{u}_j) \times \text{sign}_j \times \Psi^{\mathfrak{su}(1|1)}(\mathbf{v}_j|\mathbf{u}_j) \times \Psi^{\mathfrak{su}(1|1)}(\mathbf{w}_j|\mathbf{u}_j) \quad (\text{C.4})$$

where the free-particle wave-function $\Psi^{\mathfrak{sl}(2)}$ is given by:

$$\Psi^{\mathfrak{sl}(2)}(\mathbf{u}_j) = \prod_{u \in \mathbf{u}} \left(\frac{u + i/2}{u - i/2} \right)^j \quad (\text{C.5})$$

The sign factor is due to the fermionic nature of the nested auxiliary roots. We pick a minus sign each time a roots v passes a root w :

$$\text{sign}_j = \begin{cases} 1 & , \mathbf{v}_j = \{\} \\ (-1)^{\# \text{scatter}_{v,\mathbf{w}}} & , \mathbf{v}_j = \{v\} \end{cases} \quad \text{with} \quad \# \text{scatter}_{v,\mathbf{w}} = \sum_k^{j-1} |\mathbf{w}_k| \quad (\text{C.6})$$

The nested $\mathfrak{su}(1|1)$ wave-function is given by:

$$\Psi^{\mathfrak{su}(1|1)}(\mathbf{v}_j|\mathbf{u}_j) = \left(\prod_{u \in \bigcup_{k=1}^{j-1} \mathbf{u}_k} \frac{v - u - i/2}{v - u + i/2} \right) \times \sum_{k=1}^{|\mathbf{u}_j|} \left(\prod_m^{k-1} \frac{v - (\mathbf{u}_j)_m - i/2}{v - (\mathbf{u}_j)_m + i/2} \right) \frac{1}{v - (\mathbf{u}_j)_m + i/2} \quad (\text{C.7})$$

when $\mathbf{v}_j = \{v\}$ and it is simply 1 when $\mathbf{v}_j = \{\}$. The notation $(\mathbf{u}_j)_m$ refers to the m^{th} element on the list of roots \mathbf{u}_j .

With these definitions we can express the $\mathfrak{su}(1,1|2)$ wave-function of the state *strings* as sum over weighted permutations of the bare wave-function:

$$\Psi^{\mathfrak{su}(1,1|2)}(\text{strings}) = \sum_{\sigma \in \text{Per}(\mathbf{u})} \sum_{\pi \in \text{Per}(\mathbf{v})} \sum_{\tilde{\pi} \in \text{Per}(\mathbf{u})} \mathbb{S}^{\mathfrak{sl}(2)}(\sigma) \times \mathbb{S}^{\mathfrak{su}(1|1)}(\pi) \times \mathbb{S}^{\mathfrak{su}(1|1)}(\tilde{\pi}) \times \Psi^{bare}(\text{strings}) \quad (\text{C.8})$$

where $\mathbb{S}^{\mathfrak{sl}(2)}$ is the multi-particle $\mathfrak{sl}(2)$ S-matrix that we present for the following examples:

$$\begin{aligned} \mathbb{S}^{\mathfrak{sl}(2)}(\{u_1, u_2, u_3\}) &= 1 \\ \mathbb{S}^{\mathfrak{sl}(2)}(\{u_2, u_1, u_3\}) &= S(u_1, u_2) \\ \mathbb{S}^{\mathfrak{sl}(2)}(\{u_3, u_1, u_2\}) &= S(u_1, u_3)S(u_2, u_3) \quad \text{with} \quad S(u, v) = \frac{u - v + i}{u - v - i} \end{aligned} \quad (\text{C.9})$$

The multiparticle S-matrix of free fermions is simply:

$$\mathbb{S}^{\mathfrak{su}(1|1)}(\pi) = \text{Signature}(\pi) \quad (\text{C.10})$$

where **Signature** is a **Mathematica** function that provides the sign associated to a permutation of grassman variables.

Finally the Bethe states are constructed as liner combinations of coordinate states with wave-functions as in (C.8). Given the Bethe states are highest weights of the $\mathfrak{su}(1,1|2)$ and carry a definite charged, determined by the number of roots, we only need to consider

the coordinate states with the same charge. For example a Bethe state of length 2 can be expanded in the basis:

$$\text{coordinate basis} = \{|DZ X\rangle, |X DZ\rangle, |Z DX\rangle, |DX Z\rangle, |\psi \tilde{\psi}\rangle, |\tilde{\psi} \psi\rangle\} \quad (\text{C.11})$$

The Bethe state is given by:

$$|\Psi(\mathbf{v}, \mathbf{u}, \mathbf{w})\rangle = \sum_{\text{strings}}^{\text{coordinate basis}} \Psi^{\mathfrak{su}(1,1|2)}(\text{strings}) \times \text{Normalization}(\text{strings}) |\text{strings}\rangle \quad (\text{C.12})$$

where *strings* represent an element of the coordinates basis. A **Normalization** factor is introduced to have a normalized basis: $\langle \text{strings} | \text{strings} \rangle = 1$. For a state with length L : $\text{strings} = |\mathfrak{S}_1 \cdots \mathfrak{S}_L\rangle$ the corresponding normalization is:

$$\text{Normalization}(\text{strings}) = \prod_{j=1}^L = \text{Normalization}(\mathfrak{S}_j) \quad (\text{C.13})$$

where the normalization of a individual string $\mathfrak{S} = \{\mathbf{v}, \mathbf{u}, \mathbf{w}\}$ is:

$$\text{Normalization}(\mathfrak{S}) = \left(\frac{1}{\sqrt{|\mathbf{u}|}} \right)^{|\mathbf{v}|+|\mathbf{w}|} \quad (\text{C.14})$$

excluding the empty for which: $\text{Normalization}(\{\}) = 1$. More explicitly the normalization factors for all type of excitations are:

$$\begin{aligned} \text{Normalization}(D^{(n)}Z) &= 1, & \text{Normalization}(D^{(n)}X) &= \frac{1}{n+1} \\ \text{Normalization}(D^{(n)}\psi) &= \frac{1}{\sqrt{n+1}}, & \text{Normalization}(D^{(n)}\tilde{\psi}) &= \frac{1}{\sqrt{n+1}} \end{aligned} \quad (\text{C.15})$$

The representation (C.12) constitute an off-shell Bethe state, while the single trace operators are described by on-shell $\mathfrak{su}(1,1|2)$ cyclic states. For this the auxiliary roots $\{\mathbf{v}, \mathbf{u}, \mathbf{w}\}$ must satisfy the Bethe equations and zero momentum condition:

$$\begin{aligned} \text{left } \mathfrak{su}(1|1) \text{ wing, } v \in \mathbf{v}: & \quad 1 = \prod_{u \in \mathbf{u}} \frac{v - u + i/2}{v - u - i/2} \\ \text{middle } \mathfrak{sl}(2) \text{ node, } u \in \mathbf{u}: & \quad \left(\frac{u + i/2}{u - i/2} \right)^L = \prod_{\tilde{u} \in \mathbf{u}/\{u\}} \frac{u - \tilde{u} - i}{u - \tilde{u} + i} \prod_{v \in \mathbf{v}} \frac{u - v - i/2}{u - v + i/2} \prod_{w \in \mathbf{w}} \frac{u - w - i/2}{u - w + i/2} \\ \text{right } \mathfrak{su}(1|1) \text{ wing, } w \in \mathbf{w}: & \quad 1 = \prod_{u \in \mathbf{u}} \frac{w - u + i/2}{w - u - i/2} \\ \text{zero momentum:} & \quad 1 = \prod_{u \in \mathbf{u}} \frac{u + i/2}{u - i/2} \end{aligned} \quad (\text{C.16})$$

To obtain all the operators highest weights of the $\mathfrak{su}(1, 1|2)$ we need to find all solutions of these Bethe equations. This could be a hard task for high number of excitations. The Baxter equation or the **Fast analytic solver** based on the Q-system constitute better options to find the Bethe solutions. Using these methods we obtain Bethe solutions that we use for a explicit construction of the $\mathfrak{su}(1, 1|2)$ single trace operators using the CBA (C.12). We can further check the diagonalization of the $\mathfrak{su}(1, 1|2)$ Hamiltonian or one-loop dilation operator of the $\mathfrak{su}(1, 1|2)$ sector. When performing these checks we found some special cases corresponding to singular Bethe solutions. We devote the following section to this type of special operators.

C.2 Regularization of singular solutions in the $\mathfrak{su}(1, 1|2)$ sector at one loop level

When solving Bethe equations we encounter singular solutions. These contain a singular string formed by two middle node roots and one wing root from each wing :

$$\begin{aligned} \text{middle roots: } & \{u_{1,2} = \pm \frac{i}{2}, \underbrace{u_3, u_4, \dots}_{\text{regular roots}}\} \\ \text{wing roots: } & \{v = w = 0\} \end{aligned} \tag{C.17}$$

For these roots various factors become singular in the Bethe equations as well as in the CBA. Yet it is possible to use our CBA to obtain the singular operator provided we use a proper regularization of the singular string. For the singular solutions of type (C.17) we encounter the following regularization:

$$\begin{aligned} u_{1,2} &= \pm \frac{i}{2} + \epsilon + \lambda \epsilon^{L+1} \pm i \lambda \epsilon^{L+2} + \mathcal{O}(\epsilon^{L+3}) \\ v = w &= \epsilon + \mathcal{O}(\epsilon^{L+3}) \end{aligned} \tag{C.18}$$

where L is the length of the singular operator. The variable λ is determined by imposing that these regularized roots solve Bethe equations as we send the twist to zero: $\epsilon \rightarrow 0$. This allow us to find the λ as function of the regular roots: $\{u_3, u_4, \dots\}$:

$$\lambda = \prod_{u \in \{u_3, u_4, \dots\}} \frac{u + \frac{i}{2}}{u - \frac{3i}{2}} \tag{C.19}$$

The regularized roots (C.18) can be directly used over our CBA. The singular operator is obtained from the leading divergent power of the twist. In the following we show some explicit singular Bethe solutions, the corresponding regularization and the singular operators obtained from the CBA.

Finally we find a regularization of the singular string as:

$$\begin{aligned} u_{1,2} &\rightarrow \pm \frac{i}{2} + \epsilon + \kappa \epsilon^{L+1} \pm i^{L-1} \kappa \epsilon^{L+2} + \mathcal{O}(\epsilon^{L+3}) \\ v_1 = w_1 &\rightarrow \epsilon + \mathcal{O}(\epsilon^{L+3}) \end{aligned} \tag{C.20}$$

where the constant κ is determined from the regular roots as :

$$\kappa = \prod_{\substack{\text{\{regular middle roots\}} \\ u}} \frac{u + i/2}{u - 3i/2} \times \prod_{\substack{\text{\{regular wing roots\}} \\ v}} \frac{v - i}{v} \tag{C.21}$$

Appendix D

Superconformal Blocks

D.1 Cross ratios

Space-time cross ratios

We use the cross ratios:

$$u = \frac{x_{12}^2 x_{34}^2}{x_{13}^2 x_{24}^2} \quad \text{and} \quad v = \frac{x_{14}^2 x_{23}^2}{x_{13}^2 x_{24}^2} \quad (\text{D.1})$$

as well as the light-cone cross ratios:

$$z \bar{z} = u \quad \text{and} \quad (1 - z)(1 - \bar{z}) = v \quad (\text{D.2})$$

or in radial coordinates:

$$r^2 = u \quad \text{and} \quad e^{i\phi} = \sqrt{\frac{z}{\bar{z}}} \quad (\text{D.3})$$

R -charge cross ratios

Likewise for the R -space we use the cross ratios:

$$\sigma = \frac{(y_1 \cdot y_2)(y_3 \cdot y_4)}{(y_1 \cdot y_3)(y_2 \cdot y_4)} \quad \text{and} \quad \tau = \frac{(y_1 \cdot y_4)(y_2 \cdot y_3)}{(y_1 \cdot y_3)(y_2 \cdot y_4)} \quad (\text{D.4})$$

or

$$\alpha \bar{\alpha} = \sigma \quad \text{and} \quad (1 - \alpha)(1 - \bar{\alpha}) = \tau \quad (\text{D.5})$$

and radial coordinates:

$$\rho^2 = \sigma \quad \text{and} \quad e^{i\theta} = \sqrt{\frac{\alpha}{\bar{\alpha}}} \quad (\text{D.6})$$

D.2 The blocks

The super-OPE relies on the use of a superconformal block to resum the contributions of all the superconformal descendants of a given superconformal primary with weights Δ, s, m, n . In this appendix we record its expression when the superconformal primary that is flowing is either long or half-BPS and when the external operators are identical half-BPS superconformal primaries.

The non-BPS block presented in (D.7) can be read off from various references, e.g. [66, 67, 68, 69]. In contrast, less is written explicitly about the BPS block. Following [66, 67] it has become conventional to decompose the protected part of the four point function over an OPE-like basis of (single variable hypergeometric) functions [68, 66], which solve a SUSY version [69] of the Casimir eigenvalue equation [70]. These functions are however *not* identical to the BPS blocks we are after, as one can easily see by checking their content in usual conformal waves. We give in (D.11) the expression we have found for the BPS block by adding enough of the former functions together until we got the appropriate OPE content for an half-BPS multiplet.

Non-BPS blocks

These are given concisely by

$$\begin{aligned} \mathcal{F}_{\Delta,s,n,m}(z, \bar{z}, \alpha, \bar{\alpha}) &= (z - \alpha)(z - \bar{\alpha})(\bar{z} - \alpha)(\bar{z} - \bar{\alpha}) \times \\ &\times \left(F_{\Delta,s}(z, \bar{z}) = (-1)^s \frac{h_{\frac{\Delta+s}{2}}(z) h_{\frac{\Delta-s-2}{2}}(\bar{z}) - h_{\frac{\Delta-s-2}{2}}(z) h_{\frac{\Delta+s}{2}}(\bar{z})}{(z - \bar{z})/z\bar{z}} \right) \\ &\times \left(Y_{n,m}(\alpha, \bar{\alpha}) = \frac{(m!)^2((n+1)!)^2}{(2m)!(2n+2)!} \times \frac{P_m(\frac{2}{\alpha} - 1)P_{n+1}(\frac{2}{\bar{\alpha}} - 1) - P_{n+1}(\frac{2}{\alpha} - 1)P_m(\frac{2}{\bar{\alpha}} - 1)}{(\alpha - \bar{\alpha})\alpha\bar{\alpha}} \right), \end{aligned} \quad (\text{D.7})$$

where P_n are Legendre polynomials and where $h_\lambda(z) = z^\lambda {}_2F_1(\lambda+2, \lambda+2; 2\lambda+4; z)$, with the shifts in red being an $\mathcal{N} = 4$ SUSY shift. In AdS/CFT jargon, we can say that the first line is SUSY, the second is AdS and the third accounts for the sphere. The slightly unconventional normalization factor in the last line ensures that the R-charge blocks behave as $Y_{n,m}(\alpha, \bar{\alpha}) = 1 \times \alpha^{-n-2}\bar{\alpha}^{-m-2}(1 + \mathcal{O}(\alpha, \bar{\alpha}))$. The bosonic blocks are normalized so that $F_{\Delta,s}(z, \bar{z}) \simeq (\bar{z}z)^{\Delta/2}(-1)^s((\frac{z}{\bar{z}})^{\frac{s}{2}+\frac{1}{2}} - (\frac{\bar{z}}{z})^{\frac{s}{2}+\frac{1}{2}})/((\frac{z}{\bar{z}})^{1/2} - (\frac{\bar{z}}{z})^{1/2})$, in the OPE limit where $z, \bar{z} \rightarrow 0$ with z/\bar{z} fixed.

By sending $z, \bar{z} \rightarrow 0$, one reads out the $\mathfrak{su}(4)$ block of the superconformal primary, with Dynkin labels $[n - m, 2m, n - m]$,

$$Z_{n,m}(\alpha, \bar{\alpha}) = (\alpha\bar{\alpha})^2 Y_{n,m}(\alpha, \bar{\alpha}), \quad (\text{D.8})$$

while by sending $\alpha, \bar{\alpha} \rightarrow 0$ one recovers the conformal block of a SUSY descendent with

dimension $\Delta + 4$ and spin s ,¹

$$G_{\Delta+4,s}(z, \bar{z}) = (z\bar{z})^2 F_{\Delta,s}(z, \bar{z}). \quad (\text{D.9})$$

Equivalently, the $\mathfrak{so}(2, 4)$ block $G_{\Delta,s}$ for a conformal primary with dimension Δ and spin s is given [72] by $F_{\Delta,s}$ *without* the shifts in red in the arguments of the hypergeometric function h below (D.7).

BPS blocks

In order to find the $\frac{1}{2}$ -BPS block \mathcal{F}_Δ we can start with an Ansatz given by a linear combination of the solutions of the super-Casimir equation. Schematically this is

$$\mathcal{F}_\Delta = \mathcal{G}_\Delta^{\text{short}} + \sum_{k \in \text{zero modes}} c_{\Delta,k} \mathcal{F}_k^{\text{long}} \quad (\text{D.10})$$

which includes the short solution $\mathcal{G}_\Delta^{\text{short}}$ defined in [69]² and the long blocks of the form (D.7) with a vanishing super-conformal Casimir eigenvalue. This is such that \mathcal{F}_Δ satisfies the super-conformal Casimir equation with the same eigenvalue as $\mathcal{G}_\Delta^{\text{short}}$. We fix the coefficients $c_{\Delta,k}$ of the zero modes by demanding the correct OPE behaviour $\mathcal{F}_\Delta = (z\bar{z})^\Delta Z_{\Delta,\Delta}(\alpha, \bar{\alpha})(1 + (z, \bar{z}))$.

Our final result can be written as linear combinations of six bosonic blocks,

$$\begin{aligned} \mathcal{F}_\Delta = & G_{\Delta,0} Z_{\frac{\Delta}{2}, \frac{\Delta}{2}} + \frac{\Delta^2 G_{\Delta+1,1} Z_{\frac{\Delta}{2}, \frac{\Delta}{2}-1}}{2^4(\Delta-1)(\Delta+1)} + \frac{(\Delta+2)^2 \Delta^2 G_{\Delta+2,2} Z_{\frac{\Delta}{2}-1, \frac{\Delta}{2}-1}}{2^8(\Delta-1)(\Delta+1)^2(\Delta+3)} \\ & + \frac{(\Delta-2)^2 \Delta^2 G_{\Delta+2,0} Z_{\frac{\Delta}{2}, \frac{\Delta}{2}-2}}{2^8(\Delta-3)(\Delta-1)^2(\Delta+1)} + \frac{(\Delta-2)^2 (\Delta+2)^2 \Delta^2 G_{\Delta+3,1} Z_{\frac{\Delta}{2}-1, \frac{\Delta}{2}-2}}{2^{12}(\Delta-3)(\Delta-1)^2(\Delta+1)^2(\Delta+3)} \\ & + \frac{(\Delta-2)^2 (\Delta+2)^2 \Delta^4 G_{\Delta+4,0} Z_{\frac{\Delta}{2}-2, \frac{\Delta}{2}-2}}{2^{16}(\Delta-3)(\Delta-1)^3(\Delta+1)^3(\Delta+3)}. \end{aligned} \quad (\text{D.11})$$

The formula (D.11) agrees with those given in [71] for $\Delta = 2$ (irrep **20** = $[0, 2, 0]$) and $\Delta = 4$ (irrep **105** = $[0, 4, 0]$), see equations (8.17) and (8.24) in [71]. Each of the 6 conformal waves in (D.11) corresponds to one bosonic conformal primary, with zero hypercharge $Y = 0$ and in a left-right symmetric irrep of $\mathfrak{so}(3, 1)$ and $\mathfrak{su}(4)$, on the middle line of the half-BPS supermultiplet given in table (B.1) of [71]. For the stress tensor multiplet $\Delta = 2$, only the first three terms survive in (D.11), corresponding to the dimension 2 chiral primary, the dimension 3 R-symmetry current and the dimension 4 stress energy tensor, in agreement with the bosonic (hypercharge zero) components in the $\Delta = 2$ supermultiplet reviewed in table (2.15) of [71]. Notice that the dual and self-dual parts of the dilaton carry non zero hypercharges and thus decouple, in accord with the non-renormalization property of the BPS structure constant.

¹This descendent has shifted labels $n+2, m+2$ compared to those of the superconformal primary, see e.g. table (8.1) in [71].

²See section 6.2 therein.

D.3 The super-block of a long multiplet

The long multiplets appearing on the OPE decomposition of identical $\frac{1}{2}$ -BPS operators $\mathcal{O}_{[0,p,0]}$ have superprimaries with scaling dimension Δ , spin s and R -symmetry representations:

$$\mathcal{O}_{\Delta,s,[n-m,2m,n-m]} \quad \text{with} \quad 0 \leq m \leq n \leq p-2 \quad (\text{D.12})$$

The super-conformal block for these long representations is given by:

$$\mathcal{F}_{\Delta,s,n,m}(z, \bar{z}, \alpha, \bar{\alpha}) = \frac{(z - \alpha)(z - \bar{\alpha})(\bar{z} - \alpha)(\bar{z} - \bar{\alpha})}{(z\bar{z})^2} G_{\Delta+4,s}(z, \bar{z}) \times Y_{n,m}(\alpha, \bar{\alpha}) \quad (\text{D.13})$$

where $G_{\Delta,s}$ is the $\mathfrak{so}(4,2)$ scalar conformal block in (D.15) and the $\mathfrak{so}(6)$ harmonic function $Y_{n,m}$ is given in (D.19).

Similarly we can define $\mathcal{F}^{(d)}$ by replacing G by the derivative $G^{(d)}$ (see equation (D.17)):

$$\mathcal{F}_{\Delta,s,n,m}^{(d)}(z, \bar{z}, \alpha, \bar{\alpha}) = \frac{(z - \alpha)(z - \bar{\alpha})(\bar{z} - \alpha)(\bar{z} - \bar{\alpha})}{(z\bar{z})^2} \times G_{\Delta+4,s}^{(d)} \times Y_{n,m} \quad (\text{D.14})$$

These derivatives are useful to express the perturbative OPE expansion. When performing this expansion we are interested in the small cross-ratio series expansion of the conformal block. In what follows we provide such expansions in radial coordinates for both the $\mathfrak{so}(4,2)$ conformal block and the $\mathfrak{so}(6)$ R-symmetry block.

D.3.1 $\mathfrak{so}(4,2)$ conformal blocks

A 4D scalar conformal block for a exchanged primary of dimension Δ and spin s admits the radial expansion

$$G_{\Delta,s}(r, \phi) = r^\Delta \sum_{i=0}^{\infty} \sum_{j=0}^i A_{\Delta,s}^{(i,j)} r^i \frac{\sin((s+i-2j+1)\phi)}{\sin \phi} \quad (\text{D.15})$$

where each power of the radial cross ratio r corresponds to the scaling dimension of a descendant, see [100].

The coefficients A weighting each descendant contribution in (D.15) depend on the primary charges (Δ, s) and the level (i, j) (number of boxes $\square \equiv \mathcal{D}\bar{\mathcal{D}}$ and derivatives \mathcal{D}). An explicit expression for these coefficients is given in terms of Pochammers as:

$$A_{\Delta,s}^{(i,j)} = \frac{1}{j!(i-j)!} \frac{\left(\left(\frac{\Delta-s-2}{2}\right)_j\right)^2}{(\Delta-s-2)_j} \frac{\left(\left(\frac{\Delta+s}{2}\right)_{i-j}\right)^2}{(\Delta+s)_{i-j}} \quad (\text{D.16})$$

For the perturbative OPE expansion we define the following derivatives of the conformal blocks:

$$G_{\Delta_0,s}^{(d)}(r, \phi) = r^{\Delta_0} \sum_{i=0}^{\infty} \sum_{j=0}^i A_{\Delta_0,s}^{(d)(i,j)} r^i \frac{\sin((s+i-2j+1)\phi)}{\sin \phi} \quad (\text{D.17})$$

In this expansion the coefficients are given by derivatives of (D.16) with respect to the scaling dimension:

$$A_{\Delta,s}^{(n)(i,j)} = \frac{\partial^n}{\partial \Delta^n} A_{\Delta,s}^{(i,j)} \quad (\text{D.18})$$

D.3.2 $\mathfrak{so}(6)$ R-symmetry blocks

In radial coordinates (D.6) the R -symmetry blocks are given by the finite series:

$$Y_{n,m}(\rho, \theta) = \frac{m!^2 (n+1)!^2}{2m! (2n+2)!} \sum_{j=0}^{n+1} \sum_{k=0}^m B_{n,m}^{(j,k)} \rho^{-j-k-3} \frac{\sin((j-k)\theta)}{\sin \theta} \quad (\text{D.19})$$

This block corresponds to a $\mathfrak{so}(6)$ multiplet with highest weight $[n-m, 2m, n-m]$, with $n \geq m$. The coefficients B are:

$$B_{n,m}^{(j,k)} = M_{n+1,j} M_{m,k} \quad \text{with} \quad M_{m,k} = (-1)^{m-k} \frac{(m+k)!}{(k!)^2 (m-k)!} \quad (\text{D.20})$$

We find this expansion convenient when extracting OPE data from the supercorrelator. However when performing a R -charge projection on these blocks it is better to use the cross ratios $(\alpha, \bar{\alpha})$ or (σ, τ) .

D.4 Perturbative OPE expansion

A disadvantage of this weak coupling expansion is the huge degeneracy around the reference point $g = 0$. At this point we can only organize the degenerate primary operators into families that we name *Classes* distinguished by the global tree level quantum numbers $\{\Delta_0, s\}$. When turning on the coupling (weakly) this degeneracy is lifted and each primary operator can be identified by its corresponding (small) anomalous dimension $\delta\Delta = \Delta - \Delta_0$. Yet in the OPE, as shown in more detail in appendix D.4, the weak coupling expansion in powers of g^2 forces the OPE data to accumulate and appear only in sum rules $P_{\{\Delta_0, s\}}$ that mix loop corrections of structure constants and anomalous dimensions of primaries in the same *Class* $\{\Delta_0, s\}$.

The conformal block expansion of a four-point function depends on the OPE data: scaling dimension and structure constants of the intermediate operators. When working in a perturbative regime these dynamical data admits an expansion in the coupling g^2 as:

$$\begin{aligned} \Delta &= \Delta_0 + g^2 \gamma^{(1)} + g^4 \gamma^{(2)} + \dots \\ C_{pp\Delta} &= C^{(0)} + g^2 C^{(1)} + g^4 C^{(2)} + \dots \end{aligned} \quad (\text{D.21})$$

Similarly the reduced four-point function admits the coupling expansion:

$$\begin{aligned} \langle pppp \rangle &= \langle pppp \rangle^{(0)} + g^2 \langle pppp \rangle^{(1)} + g^4 \langle pppp \rangle^{(2)} + \dots \\ &= \sum_{a=0}^{\infty} (g^2)^a \langle pppp \rangle^{(a)} \end{aligned} \quad (\text{D.22})$$

We want to match this latter expansion against the conformal block decomposition:

$$\langle pppp \rangle = (\text{protected}) + \sum_{\{\Delta, l, n, m\}} C_{\Delta, l, n, m}^2 \mathcal{F}_{\Delta, l, n, m} \quad (\text{D.23})$$

where protected stands for short-multiplets which do not acquire anomalous dimensions. The sum is performed over all long multiplets with charges $\{\Delta, l, n, m\}$.

Since the scaling dimensions appear in the exponents of the radial cross ratio, in the limit $g^2 \rightarrow 0$, the correlator develops $\log(r)$ terms:

$$r^\Delta = r^{\Delta_0} + g^2 \gamma^{(1)} \log(r) r^{\Delta_0} + g^4 \left(\gamma^{(2)} \log(r) + \frac{1}{2} (\gamma^{(1)})^2 \log(r)^2 \right) r^{\Delta_0} + O(g^6) \quad (\text{D.24})$$

By plugging the expansions (D.21) into (D.23) we can find the loop corrections $\langle pppp \rangle^{(a)}$ in terms of the OPE data and the derivatives of the conformal blocks (D.14). The low loop corrections of the four-point function, organized according to their $\log(r)$ -singularities, are given by:

$$\begin{aligned} \langle pppp \rangle^{(0)} &= (\text{protected multiplets}) + \sum_{\{\Delta\}} (C^{(0)})^2 \mathcal{F}^{(0)} \\ \langle pppp \rangle^{(1)} &= \sum_{\{\Delta\}} \left(2 C^{(0)} C^{(1)} \mathcal{F}^{(0)} + \gamma^{(1)} (C^{(0)})^2 \mathcal{F}^{(1)} \right) + \left(\gamma^{(1)} (C^{(0)})^2 \mathcal{F}^{(1)} \right) \log(r) \\ \langle pppp \rangle^{(2)} &= \sum_{\{\Delta\}} \left((C^{(1)})^2 + 2 C^{(0)} C^{(2)} \right) \mathcal{F}^{(0)} + \left(2 C^{(0)} C^{(1)} \gamma^{(1)} + (C^{(0)})^2 \gamma^{(2)} \right) \mathcal{F}^{(1)} + \frac{1}{2} (C^{(0)} \gamma^{(1)})^2 \mathcal{F}^{(2)} \\ &\quad + \left((2 C^{(0)} C^{(1)} \gamma^{(1)} + (C^{(0)})^2 \gamma^{(2)}) \mathcal{F}^{(0)} + (C^{(0)} \gamma^{(1)})^2 \mathcal{F}^{(1)} \right) \log(r) \\ &\quad + \left(\frac{1}{2} (C^{(0)} \gamma^{(1)})^2 \mathcal{F}^{(0)} \right) \log(r)^2 \end{aligned} \quad (\text{D.25})$$

The sum on $\{\Delta\}$ (short for $\{\Delta, s, m, n\}$) runs over all long multiplets. The loop corrections $\gamma^{(a)}$ and $C^{(a)}$ should have labels (Δ) . While the blocks $\mathcal{F}^{(a)}$ depend only on the tree level ($g = 0$) charges (Δ_0) , fact that follows from (D.24).

We can then reorganize the sum over multiplets as follows:

$$\sum_{\{\Delta\}} \rightarrow \sum_{\{\Delta_0\}} \sum_{(\Delta) \in \text{Super-Class } \{\Delta_0\}} \quad (\text{D.26})$$

where a *Class* or *Super-Class* denotes a family of long multiplets that become degenerate with charges $\{\Delta_0\}$ when turning off the coupling $g = 0$. On the right hand side, the first sum runs over all admissible tree level charges $\{\Delta_0\}$ in the OPE. While the innermost sum runs over all multiplets (Δ) within a *Class* labeled by $\{\Delta_0\}$. In the OPE expansion we can

absorb this second sum within the definition of the sum rules:

$$\begin{aligned}
\mathcal{P}_{\{\Delta_0\}}^{(0,0)} &= \sum_{(\Delta) \in \text{Super-Class}\{\Delta_0\}} (C^{(0)})^2 \\
\mathcal{P}_{\{\Delta_0\}}^{(1,0)} &= \sum_{(\Delta)} 2 C^{(0)} C^{(1)}, \quad \mathcal{P}_{\{\Delta_0\}}^{(1,1)} = \sum_{(\Delta)} \gamma^{(1)} (C^{(0)})^2 \\
\mathcal{P}_{\{\Delta_0\}}^{(2,0)} &= \sum_{(\Delta)} (C^{(1)})^2 + 2 C^{(0)} C^{(2)}, \quad \mathcal{P}_{\{\Delta_0\}}^{(2,1)} = \sum_{(\Delta)} 2 C^{(0)} C^{(1)} \gamma^{(1)} + (C^{(0)})^2 \gamma^{(2)}, \\
\mathcal{P}_{\{\Delta_0\}}^{(2,2)} &= \sum_{(\Delta)} \frac{1}{2} (C^{(0)} \gamma^{(1)})^2
\end{aligned} \tag{D.27}$$

Using these sum rules we can rewrite (D.25) as:

$$\begin{aligned}
\langle pppp \rangle^{(0)} &= (\text{protected multiplets}) + \sum_{\{\Delta_o\}} \mathcal{P}^{(0,0)} \mathcal{F}^{(0)} \\
\langle pppp \rangle^{(1)} &= \sum_{\{\Delta_o\}} (\mathcal{P}^{(1,0)} \mathcal{F}^{(0)} + \mathcal{P}^{(1,1)} \mathcal{F}^{(1)}) + (\mathcal{P}^{(1,1)} \mathcal{F}^{(1)}) \log(r) \\
\langle pppp \rangle^{(2)} &= \sum_{\{\Delta_o\}} (\mathcal{P}^{(2,0)} \mathcal{F}^{(0)} + \mathcal{P}^{(2,1)} \mathcal{F}^{(1)} + \mathcal{P}^{(2,2)} \mathcal{F}^{(2)}) \\
&\quad + (\mathcal{P}^{(2,1)} \mathcal{F}^{(0)} + 2 \mathcal{P}^{(2,2)} \mathcal{F}^{(1)}) \log(r) \\
&\quad + (\mathcal{P}^{(2,2)} \mathcal{F}^{(0)}) \log(r)^2
\end{aligned} \tag{D.28}$$

The general definition of the sum rules in terms of the OPE data can be read off from the following generating function:

$$\sum_{(\Delta) \in \text{Super-Class}\{\Delta_0\}} C_{pp\Delta}^2 r^\Delta = r^{\Delta_0} \sum_{a=0}^{\infty} (g^2)^a \sum_{b=0}^a \log(r)^b \mathcal{P}_{\{\Delta_0\}}^{(a,b)} \tag{D.29}$$

with the OPE data C and Δ expanded as in (D.21).

With these definitions we can finally express the loop corrections $\langle pppp \rangle^{(a)}$ in terms of the OPE data and organized according to the log exponents as:

$$\langle pppp \rangle^{(a)} = \sum_{\{\Delta_0\}} \sum_{b=0}^a \log(r)^b \sum_{k=b}^a \binom{k}{b} \mathcal{P}_{\{\Delta_0\}}^{(a,k)} \mathcal{F}_{\{\Delta_0\}}^{(a-k)} \tag{D.30}$$

Appendix E

Comparison with Data : A Special Case

In this appendix we analyze in detail how to obtain the OPE data sum $\mathbb{P}_{\tau=6,s=0}^{n=0,m=0}$ in table 3.1 using the conjecture (2.56). Unlike the rest of the data that we have checked, this sum receives contributions from operators of different lengths. For these quantum numbers we have a total of 7 wing-symmetric Bethe solutions:

Lenght L	Field content at $\mathcal{O}(g^0)$	# Roots in $\mathfrak{sl}(2)$ -grading	# Wing-symmetric sols
4	$Tr(D\bar{D}Z\bar{Z}Z\bar{Z}) + \dots$	$\{1, 2, 3, 6, 3, 2, 1\}$	2
6	$Tr(Z\bar{Z}Z\bar{Z}Z\bar{Z}) + \dots$	$\{0, 2, 4, 6, 4, 2, 0\}$	5

(E.1)

The five solutions with $L = 6$ correspond to operators in the $so(6)$ sector at $\mathcal{O}(g^0)$. At loop level, their roots receive corrections in even powers of the coupling g and can be used straightforwardly in (2.56) to obtain the corresponding structure constants. These solutions behave in a standard way so we do not review them in this appendix.

The two solutions with $L = 4$ have roots in all the 7 nodes of the $\mathfrak{psu}(2, 2|4)$ Dynkin diagram. Hence it constitutes an interesting case that proves all the components of the conjecture (2.56). In the following we analyze in more detail these solutions.

At $g = 0$ these solutions contain two vanishing fermionic roots $v_1^{(3)} = v_1^{(1)} = 0$ (similary $w_1^{(3)} = w_1^{(1)} = 0$). These however are not associated to the action of supercharges. As we show in table E.1 these zeros receive corrections at loop order and are lifted to take opposite non-zero values. Their corrections start at $\mathcal{O}(g^1)$, unlike the rest of roots that start at $\mathcal{O}(g^2)$, and have an unusual expansion in odd powers¹ of g . In terms of the Zhukovski variables the relation between the fermionic roots translates into:

$$v_1^{(1)} = -v_1^{(3)} \rightarrow x(u_1^{(3)}) = -\frac{1}{x(u_1^{(1)})} \quad \text{with: } \frac{v}{g} = x(v) + \frac{1}{x(v)} \quad (\text{E.2})$$

¹The existence of these types of Bethe roots was first observed in [35], see section 5.2 therein.

At loop level we can perform a dynamical transformation of the fermionic roots, as explained in [35]. We can treat the roots of type (3) as of type (1), in both wings, by going through the cut ($x \rightarrow \frac{1}{x}$) and increasing the length of the operator. In this way, at loop order, the operator with length $L = 4$ and excitations $\{1, 2, 3, 6, 3, 2, 1\}$ has an alternative description with length $L = 6$ and excitations $\{0, 2, 4, 6, 4, 2, 0\}$. In this latter description the new fourth wing root $v_4^{(1)}$ of type (1) is simply identified with the root of type (3) in the former description and the corresponding Zhukovski variable changes as:

$$\begin{aligned}
\text{Zhukovsky:} \quad & x(v_1^{(3)}) \rightarrow x(v_4^{(1)}) = \frac{1}{x(v_1^{(3)})} \\
\text{Wing root:} \quad & v_1^{(3)} \rightarrow v_4^{(1)} = v_1^{(3)} \\
\text{Excitations:} \quad & \{1, 2, 3, 6, 3, 2, 1\} \rightarrow \{0, 2, 4, 6, 4, 2, 0\} \\
\text{Length:} \quad & L = 4 \rightarrow L = 6
\end{aligned} \tag{E.3}$$

	First solution up to $\mathcal{O}(g^4)$	Second solution up to $\mathcal{O}(g^4)$
$v_1^{(3)}$	$-2.1110824 g + 5.3821312 g^3 + \mathcal{O}(g)^4$	$-0.3000041 i g - 5.082979 i g^3$
$v_1^{(2)}$	$-0.37453099 - 3.8678404 g^2$	$-0.5540218 i - 1.802503 i g^2$
$v_2^{(2)}$	$+0.37453099 + 3.8678404 g^2$	$+0.5540218 i + 1.802503 i g^2$
$v_1^{(1)}$	$+2.1110824 g - 5.3821312 g^3$	$+0.3000041 i g + 5.082979 i g^3$
$v_2^{(1)}$	$-0.41330424 - 2.7636175 g^2$	$1.0820445 i + 1.8719637 i g^2$
$v_3^{(1)}$	$+0.41330424 + 2.7636175 g^2$	$-1.0820445 i - 1.8719637 i g^2$
u_1	$-0.074924705 g^2 - 0.43054180$	$-5.3834596 g^2 - 1.2029572$
u_2	$-0.4259447 - 0.5088469 i - (2.949711 + 0.111629 i) g^2$	$-3.9652234 g^2 - 0.53383287$
u_3	$-0.4259447 + 0.5088469 i - (2.949711 - 0.111629 i) g^2$	$-1.7006510 g^2 - 0.15250255$
u_4	$+0.4259447 - 0.5088469 i + (2.949711 - 0.111629 i) g^2$	$0.15250255 + 1.7006510 g^2$
u_5	$+0.4259447 + 0.5088469 i + (2.949711 + 0.111629 i) g^2$	$0.53383287 + 3.9652234 g^2$
u_6	$+0.43054180 + 0.074924705 g^2$	$1.2029572 + 5.3834596 g^2$

Table E.1: The two wing-symmetric Bethe solutions for $L = 4$, $\Delta_0 = 6$, $s = 0$, $n = 0$ and $m = 0$ in the $\mathfrak{sl}(2)$ -grading. The roots in red vanish at $\mathcal{O}(g^0)$ and have an unusual expansion in odd powers g , with $v_1^{(3)} = -v_1^{(1)}$. The next correction is of $\mathcal{O}(g^4)$ order for all the roots displayed.

When computing the corresponding normalized structure constants using the conjecture (2.56) we can use any of the two equivalent descriptions in (E.3). Using the roots in table E.1, the components of the conjecture behave as:

$$\mathcal{A}|_{L=4, \{1,2,3,6,3,2,1\}} = \mathcal{A}|_{L=6, \{0,2,4,6,4,2,0\}} \quad (\text{E.4})$$

and:

$$L \times \frac{\langle \mathbf{v} | \mathbf{v} \rangle^2}{\langle \mathbf{u} | \mathbf{u} \rangle} \Big|_{L=4, \{1,2,3,6,3,2,1\}} = L \times \frac{\langle \mathbf{v} | \mathbf{v} \rangle^2}{\langle \mathbf{u} | \mathbf{u} \rangle} \Big|_{L=6, \{0,2,4,6,4,2,0\}} \quad (\text{E.5})$$

Although a couple of fermionic roots in table E.1 have an expansion in odd powers of g , the resulting components (E.4) and (E.5) of the hexagon conjecture have the usual expansion in even powers of g . By a simple inspection of (2.53) we can check the Zhukovski variables in (E.2) fuse to give an expansion in even powers of g for the sum over partitions \mathcal{A} .

Finally to reproduce the corresponding OPE data in table 3.1 we plug the $\mathcal{O}(g^4)$ roots of the Bethe solutions (E.1) in formula (2.56) and sum over all 7 contributions obtaining:

$$\mathbb{P}_{\tau=6, s=0}^{n=0, m=0} \Big|_{y=0} = \sum_{\substack{2 \text{ solutions with} \\ L=4, \{1,2,3,6,3,2,1\}}} (C^{\circ\circ\bullet})^2 + \sum_{\substack{5 \text{ solutions with} \\ L=6, \{0,2,4,6,4,2,0\}}} (C^{\circ\circ\bullet})^2 = \frac{13}{210} - \frac{31}{63} g^2 + \mathcal{O}(g^4) .$$

Appendix F

Appendices for Octagon

F.1 More details on the octagon

In order to decode the sum in 4.5, in this appendix, we introduce the mirror states ψ and the hexagon form factors $\langle \mathcal{H} | \psi \rangle$ more explicitly.

F.1.1 The mirror states ψ

The spectrum on a mirror edge is given by the multi-particle states:

$$|\psi\rangle \equiv |u_1 \cdots u_n\rangle^{(A_1 \dot{A}_1) \cdots (A_n \dot{A}_n)} \quad (\text{F.1})$$

where each particle has a charged $(A \dot{A})$ under the residual symmetry of the BMN vacuum $\mathfrak{su}(2|2)_L \otimes \mathfrak{su}(2|2)_R$. The admissible representations of this group are label by the bound state number a . The elementary particle $a = 1$ lies in the bi-fundamental representation of $\mathfrak{su}(2|2)_L \otimes \mathfrak{su}(2|2)_R$, in this case A and \dot{A} can take four different flavors: two bosonic and two fermionic, making a total of 16 possible states. While the general a bound state particle lies in the a -th anti-symmetric representation of each $\mathfrak{su}(2|2)$ copy and can be obtained by fusion of a elementary particles.

The rapidity u is a continuous variable running from $-\infty$ to ∞ . In terms of this variable the measure μ_a , energy E_a and momentum p_a of the a -th bound state particle can be written as:

$$\begin{aligned} \mu_a(u) &= \frac{a}{g^2} \frac{(x^{[-a]} x^{[a]})^2}{(1 - (x^{[-a]})^2) (1 - x^{[-a]} x^{[a]})^2 (1 - (x^{[a]})^2)}, \\ e^{-E_a(u)} &= \frac{1}{x^{[-a]} x^{[a]}} \quad \text{and} \quad p_a(u) = u - g \left(\frac{1}{x^{[-a]}} + \frac{1}{x^{[a]}} \right) \end{aligned} \quad (\text{F.2})$$

where x is the Zhukovsky given in terms of the rapidity and the coupling as:

$$x^{[\pm a]}(u) = x(u \pm \frac{i a}{2}), \quad x(u) = \frac{u + \sqrt{u^2 - 4g^2}}{2g}, \quad \frac{u}{g} = x(u) + \frac{1}{x(u)} \quad (\text{F.3})$$

For our asymptotic multi-particle states (F.1) the total energy and momentum are computed by simply adding up the contributions of the composites, while the total measure is given by the simple product:

$$E_\psi = \sum_{j=1}^n E_{a_j}(u_j), \quad p_\psi = \sum_{j=1}^n p_{a_j}(u_j) \quad \text{and} \quad \mu_\psi = \prod_{j=1}^n \mu_{a_j}(u_j) \quad (\text{F.4})$$

This description of the mirror states allows us to make the sum in (4.5) more precise:

$$\sum_{\psi} \rightarrow \sum_{n=0}^{\infty} \frac{1}{n!} \sum_{a_1=1}^{\infty} \cdots \sum_{a_n=1}^{\infty} \int du_1 \cdots \int du_n \sum_{\substack{\text{internal flavour indexes} \\ \text{for each } a_k \text{ bound state}}} \quad (\text{F.5})$$

This sum includes: a sum over the number of particles $\sum_{n=0}^{\infty}$, where $n = 0$ corresponds to the mirror BMN vacuum and the factorial comes from Bose statistics. A sum over the bound state number $\sum_{a_i=1}^{\infty}$ and an integral $\int du_i$ for each particle. Finally a sum over all possible flavors ($A\dot{A}$) within each bound state representation.

F.1.2 The hexagon form factor $\langle \mathcal{H} | \psi \rangle$

The hexagon form factor for a multi-particle state is given by:

$$\langle \mathcal{H} | u_1 u_2 \cdots u_n \rangle^{(A_1 \dot{A}_1) \cdots (A_n \dot{A}_n)} = \prod_{i < j} h_{a_i a_j}(u, v) \times \mathcal{H}_{mat}^{(A_1 \dot{A}_1) \cdots (A_n \dot{A}_n)}(u_1, \cdots, u_n) \quad (\text{F.6})$$

where each A_j and \dot{A}_j group a a_j number of flavor indexes corresponding to a bound-state in a a_j -anti-symmetric representation of $\mathfrak{psu}(2|2)_L$ and $\mathfrak{psu}(2|2)_R$ respectively.

The first factor in (F.6) is given by a product of abelian two-particle hexagon form factors. For the elementary particles ($a = 1$), the two-particle form factor is:

$$h(u, v) = \frac{x^{[-]}(u) - x^{[-]}(v)}{x^{[-]}(u) - x^{[+]}(v)} \frac{1 - \frac{1}{x^{[-]}(u)x^{[+]}(v)}}{1 - \frac{1}{x^{[+]}(u)x^{[+]}(v)}} \frac{1}{\sigma(u, v)} \quad (\text{F.7})$$

where σ is the root-square of the BDS dressing phase.

By using fusion relations we can build the two-particle form factor for any bound state $h_{ab}(u, v)$, starting with a and b fundamental particles respectively. In our computation we do not need the explicit form of this function, but just the simpler symmetric product:

$$\begin{aligned} P_{ab}(u, v) &= h_{ab}(u, v) h_{ba}(v, u) \\ &= \mathcal{K}_{ab}^{++}(u, v) \mathcal{K}_{ab}^{+-}(u, v) \mathcal{K}_{ab}^{-+}(u, v) \mathcal{K}_{ab}^{--}(u, v) \end{aligned} \quad (\text{F.8})$$

with the \mathcal{K} function given in terms of Zchukovsky variables as:

$$\mathcal{K}_{ab}^{\pm\pm}(u, v) = \frac{x^{[\pm a]}(u) - x^{[\pm b]}(v)}{1 - x^{[\pm a]}(u) x^{[\pm b]}(v)} \quad (\text{F.9})$$

Fortunately in this symmetric product the dressing phase, with complicated analytic properties, drops out thanks to the relation $\sigma(u, v)\sigma(v, u) = 1$.

The matrix part \mathcal{H}_{mat} in (F.6) takes the incoming indexes in the $\mathfrak{psu}(2|2)_L$ and $\mathfrak{psu}(2|2)_R$ representation and combines them into a tensor invariant under a diagonal symmetry group $\mathfrak{psu}(2|2)_D$ (this is the residual symmetry preserved by the hexagon). To construct this tensor we use an arrangement of Beisert's $\mathfrak{su}(2|2)$ S-matrices realizing a scattering process with the $\mathfrak{psu}(2|2)_L$ particles as incoming and the $\mathfrak{psu}(2|2)_R$ as outgoing states. For a three-particle state this can be graphically depicted in figure F.1.

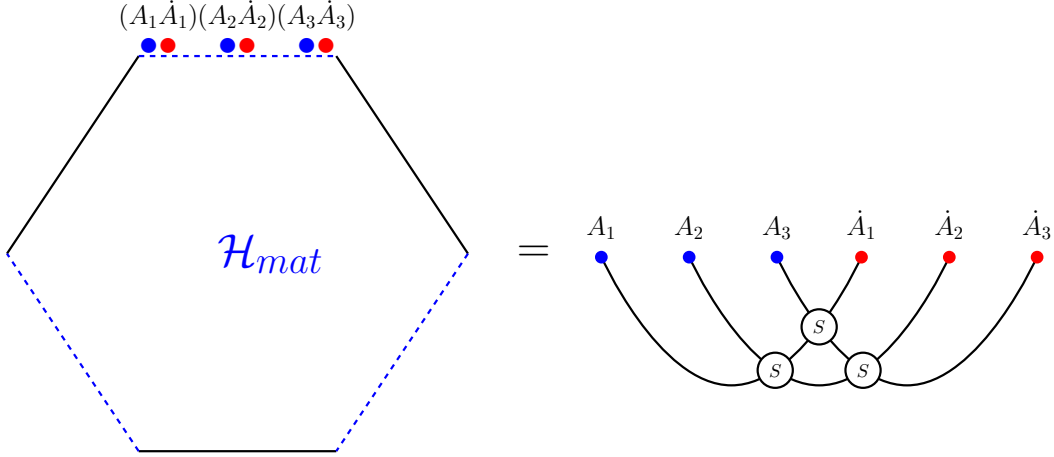


Figure F.1: The matrix part of the multi-particle hexagon form factor

The S-matrix for the fundamental representations can be found in [91], while the case of general mirror bound states has been worked out in [7] (see also [92]). In this paper we do not need the explicit form of the S-matrix but we just have to take into account the unitarity of the S-matrix $S_{ab}(u, v)S_{ba}(v, u) = 1$ which is graphically depicted as:

(F.10)

F.1.3 Summing over flavor indexes

We reorganize the summand by distinguishing between the elements that depend on the internal flavor and the ones which do not. We repackage this latter group into the weight $W^{(\text{flavour})}$ and rewrite the octagon as:

$$\begin{aligned} \mathbb{O}_l = \sum_{n=0}^{\infty} \frac{1}{n!} \sum_{a_1=1}^{\infty} \cdots \sum_{a_n=1}^{\infty} \int du_1 \cdots \int du_n \prod_{j=1}^n \mu_{a_j}(u_j) e^{-E_{a_j}(u_j)l} e^{ip_{a_j}(u_j) \log z \bar{z}} \prod_{i < j} P_{a_i a_j}(u_i, u_j) \\ \times W_{a_1 \cdots a_n}^{(\text{flavour})}(u_1, \cdots u_n) \end{aligned} \quad (\text{F.11})$$

The symmetric product $P_{ab}(u, v)$ in (F.8), appears from the product of the abelian part of hexagon form factor of ψ and its conjugate $\bar{\psi}$. The flavor weight $W^{(\text{flavour})}$ encodes the sum over internal flavor states for the subspace of n particles in representations $\{a_1 \cdots a_n\}$ and rapidities $\{u_1, \dots, u_n\}$ respectively, we label this subspace as $V_{a_1 \cdots a_n}$. The corresponding summand contains the matrix part of the hexagon form factors and the chemical potentials that depend on the angles θ, ϕ, φ :

$$W_{a_1 \cdots a_n}^{(\text{flavour})}(u_1, \dots, u_n) = \sum_{\psi \in V_{a_1 \cdots a_n}} \langle \mathcal{H}_{mat} | \psi \rangle e^{i L_\psi \phi} e^{i R_\psi \theta} e^{i J_\psi \varphi} \langle \psi | \mathcal{H}_{mat} \rangle \quad (\text{F.12})$$

In order to perform this sum we need to use the explicit $\mathfrak{su}(2|2)_L \otimes \mathfrak{su}(2|2)_R$ basis of the bound state representations. The cases $n = 1$ and $n = 2$ were worked out in great detail in [6] and [99]¹ respectively. In these references the choice of basis includes a prescription on how to include \mathcal{Z} markers. We are instructed to consider two ways of dressing the mirror basis with \mathcal{Z} -markers (two subspaces: $V_a = V_a^+ \oplus V_a^-$), perform the sum for each and then average over the two choices. Then the weight factor is composed as:

$$W_{a_1 \cdots a_n}^{(\text{flavor})} = \frac{W_{a_1 \cdots a_n}^{(\text{flavor})+} + W_{a_1 \cdots a_n}^{(\text{flavor})-}}{2} \quad (\text{F.13})$$

Both $W_{a_1 \cdots a_n}^{(\text{flavour})\pm}$ can be computed as shown in figure 4.4 for the case $n = 3$.

Thanks to the unitarity of the $\mathfrak{su}(2|2)$ S-matrix the flavour weight factorises into one-particle contributions which were computed in [6] and shown to be given by a $\mathfrak{su}(2|2)$ character:

$$W_{a_1 \cdots a_n}^{(\text{flavour})\pm} = \prod_{j=1}^n (\cos \phi - \cosh(\varphi \pm \theta)) \frac{\sin a_j \phi}{\sin \phi} \quad (\text{F.14})$$

notice the dependence on the rapidities totally drops.

Finally using (F.11), (F.13) and (F.14) we arrive to (5.2) in the main text.

F.2 An efficient way to evaluate the mirror integrals

In this appendix we show how to evaluate the integrals $\mathcal{I}_{n,l}$, see (F.17), at weak coupling. For this it is convenient to introduce the basis of integrals:

$$I_{m,n} = \sum_{a=1}^{\infty} \frac{\sin(a\phi)}{z - \bar{z}} a \int_{-\infty}^{\infty} du \frac{(z\bar{z})^{-iu}}{(u - \frac{i}{2}a)^m (u + \frac{i}{2}a)^n} \quad (\text{F.15})$$

For any non-negative m, n these integrals can be simply evaluated by taking the residue at the pole $u = \frac{i}{2}a$. Then performing the sum over the bound state number a we obtain the closed form expression:

$$I_{m,n} = (i)^{m+n} \sum_{k=0}^{m-1} (-1)^{n+k} \frac{\binom{m+n-k-2}{n-1}}{k!} \times \log(z\bar{z})^k \times \frac{\text{Li}_{m+n-k-2}(z) - \text{Li}_{m+n-k-2}(\bar{z})}{z - \bar{z}} \quad (\text{F.16})$$

¹see appendix D.2 therein.

We want to show that at any loop order the mirror integrals $\mathcal{I}_{n,l}$ can be expressed as a sum of products of the more elementary integrals in (F.16). To make this evident we explain the steps we follow to perform the loop expansion. We start by repeating some of the formulae of the main text to make this section self-contained.

The n -particle mirror integral $\mathcal{I}_{n,l}$ is given by:

$$\mathcal{I}_{n,l}(z, \bar{z}) = \frac{1}{n!} \sum_{a_1=1}^{\infty} \cdots \sum_{a_n=1}^{\infty} \int du_1 \cdots \int du_n \prod_{j=1}^n \bar{\mu}_{a_j}(u_j, l, z, \bar{z}) \times \prod_{j < k}^n P_{a_j a_k}(u_j, u_k) \quad (\text{F.17})$$

the effective measure packages the chemical potentials potentials:

$$\bar{\mu}_a(u, l, z, \bar{z}) = \frac{\sin(a\phi)}{z - \bar{z}} \times \mu_a(u) \times e^{-E_a(u)l} \times (z\bar{z})^{-ip_a(u)} \quad (\text{F.18})$$

and these are explicitly given in terms of the Zhukovskiy variable:

$$x^{[\pm a]}(u) = x(u \pm \frac{i a}{2}), \quad x(u) = \frac{u + \sqrt{u^2 - 4g^2}}{2g}, \quad \frac{u}{g} = x(u) + \frac{1}{x(u)} \quad (\text{F.19})$$

as:

$$\mu_a(u) = \frac{a}{g^2} \frac{(x^{[-a]} x^{[a]})^2}{(1 - (x^{[-a]})^2) (1 - x^{[-a]} x^{[a]})^2 (1 - (x^{[a]})^2)} \quad (\text{F.20})$$

$$e^{-E_a(u)l} = \left(\frac{1}{x^{[-a]} x^{[a]}} \right)^l \quad (\text{F.21})$$

$$(z\bar{z})^{-ip_a(u)} = (z\bar{z})^{-iu} (z\bar{z})^{ig \left(\frac{1}{x^{[-a]}} + \frac{1}{x^{[a]}} \right)} \quad (\text{F.22})$$

and the two-particle symmetric hexagon form factor is:

$$P_{ab}(u, v) = \mathcal{K}_{ab}^{++}(u, v) \mathcal{K}_{ab}^{+-}(u, v) \mathcal{K}_{ab}^{-+}(u, v) \mathcal{K}_{ab}^{--}(u, v) \quad (\text{F.23})$$

with:

$$\mathcal{K}_{ab}^{\pm\pm}(u, v) = \frac{x^{[\pm a]}(u) - x^{[\pm b]}(v)}{1 - x^{[\pm a]}(u) x^{[\pm b]}(v)} \quad (\text{F.24})$$

To perform the weak coupling expansion of the integrand we need the expansion of the Zhukovskiy variable:

$$x^{[\pm a]} = \frac{u \pm \frac{i}{2} a}{g} - \frac{g}{u \pm \frac{i}{2} a} - \frac{g^3}{(u \pm \frac{i}{2} a)^3} - \frac{2g^5}{(u \pm \frac{i}{2} a)^5} - \frac{5g^7}{(u \pm \frac{i}{2} a)^7} + \mathcal{O}(g)^9 \quad (\text{F.25})$$

This exhibits poles whose degree increases with each loop order. Likewise the integrand inherits these poles for each of the variables of integration. In particular we do not obtain

extra poles coupling two rapidities. Differences of rapidities coming from (F.23) only appear on the numerator so they can be easily expanded out to.

In order to make more explicit the pole structure of the integrand we propose the following change of variables:

$$\left(u - \frac{i}{2}a\right) \rightarrow \frac{1}{\mathcal{A}_-} \quad \text{and} \quad \left(u + \frac{i}{2}a\right) \rightarrow \frac{1}{\mathcal{A}_+} \quad (\text{F.26})$$

Similarly we use other letters for other pairs of rapidity-bound state number, for instance: \mathcal{B} for (v, b) , \mathcal{C} for (w, c) , etc.

Under this new notation the expansion in (4.14) looks like:

$$x^{[\pm a]}(u) = \frac{1}{g \mathcal{A}_\pm} - g \mathcal{A}_\pm - g^3 \mathcal{A}_\pm^3 - 2g^5 \mathcal{A}_\pm^5 - 5g^7 \mathcal{A}_\pm^7 + \mathcal{O}(g)^9 \quad (\text{F.27})$$

Plugging in this latter expansion for each rapidity in the components (F.20),(F.21),(F.22) and (F.23) we find the mirror integrand takes the schematic form:

$$\text{stripped integrand} = \sum_{m=0}^{\infty} (g^2)^m \sum_{k=0}^m \log(z\bar{z})^k \times \text{Polynomial}(\mathcal{A}, \mathcal{B}, \mathcal{C} \dots) \quad (\text{F.28})$$

where **stripped integrand** is the integrand after we have stripped out the **blue factors** in (F.18),(F.20),(F.21) for each rapidity. The expansion on $\log(z\bar{z})$ comes from the loop expansion of (F.22). The function **Polynomial** is a polynomial on the variables (F.26). Schematically for the $n = 3$ integrand it has the form:

$$\text{Polynomial}(\mathcal{A}, \mathcal{B}, \mathcal{C}) = \text{coef} \times \mathcal{A}_-^{m_1} \mathcal{A}_+^{n_1} \mathcal{B}_-^{m_2} \mathcal{B}_+^{n_2} \mathcal{C}_-^{m_3} \mathcal{C}_+^{n_3} + \dots \quad (\text{F.29})$$

where the dots represent analog terms with different coefficients and exponents (m_k, n_k) .

Now to go from the integrand (F.28) to the integral we just need to perform a replacement. Whenever we see a couple $\mathcal{A}_- \mathcal{A}_+$ in (F.29) we replace it by the basis in (F.16) as:

$$\begin{array}{ccc} \text{stripped integrand} & \Longrightarrow & \mathcal{I}_{n,l} \\ \mathcal{A}_-^{m_1} \mathcal{A}_+^{n_1} \mathcal{B}_-^{m_2} \mathcal{B}_+^{n_2} \mathcal{C}_-^{m_3} \mathcal{C}_+^{n_3} & \xrightarrow[\text{perform sums and integrals}]{\text{restore blue factors,}} & I_{m_1, n_1} I_{m_2, n_2} I_{m_3, n_3} \end{array} \quad (\text{F.30})$$

- **Maximal transcendentality:** using the explicit form of the basis (F.16) and collecting in logs we can make manifest the uniform and maximal transcendentality of the mirror integrals:

$$\mathcal{I}_{n,l} = \sum_{J=n(n+l)}^{\infty} (g^2)^J \sum_{k=0}^J \log(z\bar{z})^k \times \sum_{j_1+\dots+j_n=2J-k} \text{coe}_{j_1\dots j_n} \text{pl}_{j_1} \text{pl}_{j_2} \dots \text{pl}_{j_n} \quad (\text{F.31})$$

where all indexes j are positive and $\text{pl}_j \equiv \frac{\text{Li}_j(z) - \text{Li}_j(\bar{z})}{z - \bar{z}}$. Some of the coefficients $\text{coe}_{j_1, \dots, j_n}$ could be zero.

- **Single-valuedness:** The mirror integrals are single-value when z and \bar{z} are complex conjugates (euclidean regime).

Considering the integrand is invariant under the exchange $a \rightarrow -a$ we can argue that whenever we have the term with $\mathcal{A}_-^{m_1} \mathcal{A}_+^{n_1}$ we should also have a term with $\mathcal{A}_-^{n_1} \mathcal{A}_+^{m_1}$ and the same coefficients. Therefore there is a refinement of (F.30) which can allow us to express $\mathcal{I}_{n,l}$ into sums of products of the basis $I_{m,n} + I_{n,m}$. One can verified that this symmetric basis is single valued.

Taking into account this property we present our explicit results for some mirror integrals in terms of Ladder integrals. These belong to the family of single-valued polylogarithms.

- **Mathematica:** The loop expansion sketch in this appendix can be easily implemented in **Mathematica**. The key steps are the replacements (F.27) and (F.30). In our implementation of this algorithm we could obtain 17 loops in few minutes.

F.3 Mirror integrals up to nine loops

In this appendix we present some of the mirror integrals in a loop expansion.

The series expansion of the one-particle for any bridge parameter is given in terms of ladder integrals as:

$$\mathcal{I}_{n=1,l}(z, \bar{z}) = \sum_{k=l+1}^{\infty} (g^2)^k (-1)^{k-l-1} \binom{2k-2}{k-l-1} F_k(z, \bar{z}) \quad (\text{F.32})$$

For higher number of particles we were unable to find a closed form for the coefficients of the ladders. Here we only provide the expansion of the mirror integrals entering the nine loop *asymptotic* prediction in (4.54).

For $n = 2$ these include $l = 0, 1, 2$ (we leave z, \bar{z} dependence implicit):

$$\begin{aligned} \mathcal{I}_{n=2,l=0} = & g^8 \left(F_1 F_3 - \frac{1}{3} F_2^2 \right) + g^{10} (-6 F_1 F_4 + F_2 F_3) + g^{12} \left(28 F_1 F_5 + \frac{4}{5} F_2 F_4 - \frac{9}{5} F_3^2 \right) \\ & + g^{14} \left(-120 F_1 F_6 - 16 F_2 F_5 + \frac{36}{5} F_3 F_4 \right) \\ & + g^{16} \left(495 F_1 F_7 + \frac{690}{7} F_2 F_6 - \frac{9}{7} F_3 F_5 - \frac{486}{35} F_4^2 \right) \\ & + g^{18} \left(-2002 F_1 F_8 - \frac{979}{2} F_2 F_7 - \frac{1203}{14} F_3 F_6 + \frac{456}{7} F_4 F_5 \right) + \mathcal{O}(g^{20}) \end{aligned} \quad (\text{F.33})$$

$$\begin{aligned}
\mathcal{I}_{n=2,l=1} = & g^{12} \left(F_2 F_4 - \frac{1}{2} F_3^2 \right) + g^{14} \left(-8 F_2 F_5 + \frac{12}{5} F_3 F_4 \right) \\
& + g^{16} \left(45 F_2 F_6 + 2 F_3 F_5 - \frac{33}{5} F_4^2 \right) \\
& + g^{18} \left(-220 F_2 F_7 - \frac{380}{7} F_3 F_6 + \frac{240}{7} F_4 F_5 \right) + \mathcal{O}(g^{20})
\end{aligned} \tag{F.34}$$

$$\mathcal{I}_{n=2,l=2} = g^{16} \left(F_3 F_5 - \frac{3}{5} F_4^2 \right) + g^{18} (-10 F_3 F_6 + 4 F_4 F_5) + \mathcal{O}(g^{20}) \tag{F.35}$$

Finally the only $n = 3$ integral contributing at nine loops has $l = 0$:

$$\mathcal{I}_{n=3,l=0} = g^{18} \left(F_1 F_3 F_5 - \frac{3}{5} F_1 F_4^2 - \frac{1}{3} F_2^2 F_5 + \frac{1}{5} F_2 F_3 F_4 - \frac{1}{20} F_3^3 \right) + \mathcal{O}(g^{20}) \tag{F.36}$$

F.4 Prediction nine loop complete ope data of check

In this appendix we provide the primary and super-primary sum rules that could not fit in tables 4.5 and 4.2.

The missing primary sum rule in table 4.5 is given in terms of the following super-primary sum rules:

$$\begin{aligned}
\mathcal{P}_{\{26,2\}}^{(9,0)} = & \mathcal{P}_{\{22,2,9,9\}}^{(9,0)} + \mathcal{P}_{\{24,0,10,10\}}^{(9,0)} - \mathcal{P}_{\{24,0,11,9\}}^{(9,0)} - \frac{526199}{350175} \mathcal{P}_{\{24,0,11,11\}}^{(9,0)} + \mathcal{P}_{\{26,2,11,11\}}^{(9,0)} \\
& - \frac{27}{2102500} \mathcal{P}_{\{24,0,11,11\}}^{(9,1)} + \frac{2191}{1524312500} \mathcal{P}_{\{24,0,11,11\}}^{(9,2)} - \frac{59373}{276281640625} \mathcal{P}_{\{24,0,11,11\}}^{(9,3)} \\
& + \frac{8059143}{200304189453125} \mathcal{P}_{\{24,0,11,11\}}^{(9,4)} - \frac{263012022}{29044107470703125} \mathcal{P}_{\{24,0,11,11\}}^{(9,5)} \\
& + \frac{50158623078}{21056977916259765625} \mathcal{P}_{\{24,0,11,11\}}^{9,6} - \frac{10951243453584}{15266308989288330078125} \mathcal{P}_{\{24,0,11,11\}}^{(9,7)} \\
& + \frac{2694497074981488}{11068074017234039306640625} \mathcal{P}_{\{24,0,11,11\}}^{(9,8)} \\
& - \frac{737870670163918368}{8024353662494678497314453125} \mathcal{P}_{\{24,0,11,11\}}^{(9,9)}
\end{aligned} \tag{F.37}$$

These super sum rules on the right hand side can be computed by identifying the super-

multiplets (Bethe solutions) and using the BKV formula. These are our results:

$$\begin{aligned}
\mathcal{P}_{\{22,2,9,9\}}^{(9,0)} &= -\frac{3880272703256846017844314261170552101}{1008907523437500000000000000}, & \mathcal{P}_{\{24,0,11,11\}}^{(9,1)} &= 4175618304, \\
\mathcal{P}_{\{24,0,10,10\}}^{(9,0)} &= -\frac{1561516641881791110594032737679}{179687500000000000000}, & \mathcal{P}_{\{24,0,11,11\}}^{(9,2)} &= -3028140544, \\
\mathcal{P}_{\{24,0,11,9\}}^{(9,0)} &= -41148586528, & \mathcal{P}_{\{24,0,11,11\}}^{(9,3)} &= 1382002336, \\
\mathcal{P}_{\{24,0,11,11\}}^{(9,0)} &= -2755264512, & \mathcal{P}_{\{24,0,11,11\}}^{(9,4)} &= -438371648, \\
\mathcal{P}_{\{26,2,11,11\}}^{(9,0)} &= -\frac{24206493839806735477486708172518503089}{445073004000599941716074496}, & \mathcal{P}_{\{24,0,11,11\}}^{(9,5)} &= \frac{1506986624}{15}, \\
& & \mathcal{P}_{\{24,0,11,11\}}^{(9,6)} &= -\frac{250252288}{15}, \\
& & \mathcal{P}_{\{24,0,11,11\}}^{(9,7)} &= \frac{29139968}{15}, \\
& & \mathcal{P}_{\{24,0,11,11\}}^{(9,8)} &= -\frac{45540352}{315}, \\
& & \mathcal{P}_{\{24,0,11,11\}}^{(9,9)} &= \frac{4978688}{945}
\end{aligned} \tag{F.38}$$

Plugging these sum rules (F.38) into (F.37) we obtain the primary sum:

$$\mathcal{P}_{\{26,2\}}^{(9,0)} = -\frac{13565855042891885605834502859803364601}{1008907523437500000000000000} \tag{F.39}$$

which perfectly matches the sum rule listed in table 4.3 obtained from the nine-loop hexagonalization prediction of the *asymptotic* four point function.

Appendix G

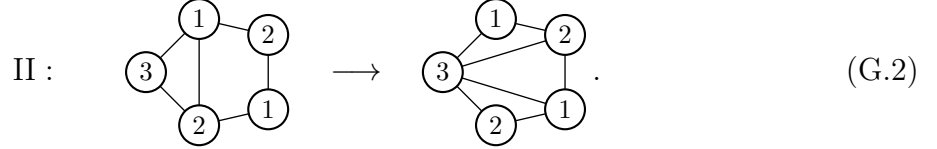
Non-planar appendices

G.1 Constructing Graphs Explicitly

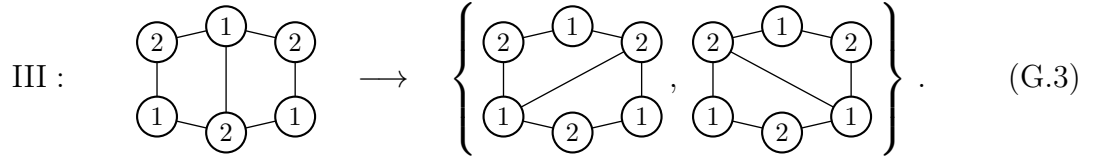
In the following, we want to explicitly construct all skeleton graphs up to a given genus. Listing the explicit graphs will allow us to compute the polynomials $P_{4g|g+1}(k_1, k_2, k_3, k_4)$ entering the correlator (7.14), and hence will provide an important cross-check of the results obtained with the help of matrix model techniques in Section 7.3 and Section 7.4. Moreover, constructing all contributing graphs explicitly is of more general interest: In the present paper, we consider the case where all bridges (propagator bundles) contain a large number of propagators, such that all faces are isolated from each other (the sum over mirror excitations / open string states reduces to the vacuum / ground state). Hence for the purpose of this paper, it is sufficient to know the *number of graphs* that can be formed from a given set of faces; how exactly these faces are arranged in each individual graph is irrelevant. However, the more general hexagonalization prescription [6, 7, 147, 148] for finite-charge operators requires to include non-trivial states that propagate between faces, hence one *does* have to know the local structure of each graph explicitly. Hence it is important to have techniques to construct the relevant graphs.

Mathematically, the graphs that we need to construct are *ribbon graphs* (also called fat graphs). In short, a ribbon graph is an ordinary graph equipped with a cyclic ordering of the edges incident to each vertex. More precisely, an ordinary graph consists of a set V of vertices, a set H of half-edges, a map $s : H \rightarrow V$ that maps each half-edge to the vertex that it is incident on, and a map $i : H \rightarrow H$ (involutive, without fixed points) that maps each half-edge to its other half. A ribbon graph is an ordinary graph (V, H, s, i) together with a bijection $\sigma : H \rightarrow H$ whose cycles correspond to the sets $s^{-1}(v)$ of half-edges incident on vertices $v \in V$. The ordering of each cycle prescribes the ordering of the incident half-edges at the vertex v . Topologically, each vertex of a ribbon graph can be thought of as a disk, and each edge as a narrow rectangle (or “ribbon”, hence the name “ribbon graph”) attached to two of the vertex disks. The boundaries of these ribbons together with segments of the vertex disks naturally form the *faces* of a ribbon graph (each face bounded by n ribbons is a cycle of $(i \circ \sigma)^n$). Inserting an open disk into each of these faces completes every ribbon

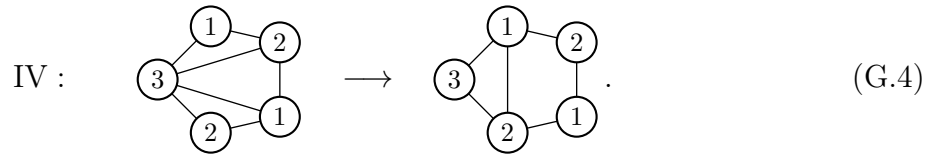
that, starting with *any single* triangulation, one can obtain *all* other triangulations by iteratively flipping edges. Since we can associate a triangulation to every maximal graph, we can also obtain all maximal graphs from a single maximal graph by flipping edges. This requires flipping real edges as well as fictitious edges that we added in order to split all squares into triangles. However, we can shortcut the introduction of fictitious edges by supplementing the flip operation (G.1) with further transformations that operate on squares. Namely, when an edge separates a triangle and a square, we have to consider the following transformation:



Here, the labels are again arbitrary, but their distribution is unique. An edge may also separate two squares. Such edges can be transformed in two inequivalent ways, and we have to include both of them:



The flip move (G.2) cannot be undone by iterations of move I without introducing self-contractions. In order to exhaust the space of maximal graphs, we thus also need to include the inverse of (G.2):



Again, the labels are arbitrary, but their distribution matters and is unique. Each of the transformations II–IV is the result of a sequence of simple flip moves (G.1) acting on real as well as fictitious bridges (that split the squares). By the above considerations, it is clear that the complete set of maximal graphs at a given genus can be obtained by starting with an arbitrary maximal graph and iterating the operations (G.1)–(G.4) in all possible ways.

The result of the above discussion is the following iterative algorithm that constructs all maximal graphs at a given genus:

1. Start with any maximal graph of the desired genus. This can for example be constructed by iteratively adding random edges to the empty graph until the target genus is reached, and then splitting all faces of the resulting graph with as many further edges as possible.

		genus				
		0	1	2	3	4
number of insertions	2 :	1	1	4	82	7325
	3 :	1	3	38	661	
	4 :	2	16	760	122307	
	5 :	4	132	18993		
	6 :	14	1571	487293		
	7 :	66	20465			
	8 :	409	278905			
	9 :	3078				
	10 :	26044				

Table G.1: Numbers of maximal graphs for various genera and numbers of insertions. Here, the vertices of the graphs are unlabeled, i. e. all vertices are treated as identical.

2. For each edge of each graph in the list constructed in the previous iteration step, generate a new graph by applying one of the transformations (G.1)–(G.3) to that edge (transformation III generates two new graphs). For each pair of adjacent edges with vertex structure as in (G.4), generate a new graph by applying transformation IV.
3. The list of graphs constructed in the previous step may contain graphs that are identical to graphs constructed in earlier iteration steps. It can also contain several copies of identical graphs. Drop all graphs that are identical to graphs already constructed earlier, and drop all duplicates. The resulting list contains the new graphs.
4. Iterate steps 2–3 until the list of new graphs is empty, i. e. until all edge transformations only generate copies of graphs already found earlier.

We can implement this algorithm on a computer, and construct the space of maximal graphs for various genera and numbers of insertions (vertices). In order to reduce overcounting, we treat all vertices as identical, i. e. we use unlabeled vertices.² The size of the space of graphs grows rapidly, see Table G.1. We note the following properties of maximal graphs of genus g with n vertices:

- The planar two-point graph has one edge.
- For $g = 0$ and $n \geq 3$, all maximal graphs consist of $2n - 4$ triangles and no squares, they have $3n - 6$ edges.
- For $g \geq 1$ and $n = 2$, all maximal graphs consist of $2g$ squares and no triangles, they have $4g$ edges.

²The algorithm works equally for labeled and unlabeled vertices.

- For $g \geq 1$ and $n \geq 3$, maximal graphs may consist of triangles and squares, their maximum edge number is $6g + 3n - 6$ (no squares, $2n + 4g - 4$ triangles), and their minimum edge number is $4g + 3n - 7$ ($2g + 1$ squares, $2n - 6$ triangles).

A note on the implementation: We found it convenient to represent ribbon graphs as lists of vertices, where each vertex is an ordered list of incident edges. For example, the graphs on the left in [Figure 7.9](#) can be represented in MATHEMATICA as

```
graph[v[1,2], v[1,3], v[2,4], v[3,4]]
graph[v[1,2,3], v[1,4,2,5,6], v[3,7,8], v[4,8,5,6,7]]
graph[v[1,2,3,4,5,6], v[1,7,8,3,9,10,5], v[2,4,11,6,12], v[7,11,8,9,12,10]]
```

Here, the edges have been given arbitrary integer labels. The bijection σ is explicit in this representation, whereas the incidence and half-edge identification maps s and i are implicit. Of course, graphs in this representation are separately invariant under (i) permuting the vertices $v[.]$ within $\text{graph}[.]$, (ii) rotating the edge labels within individual vertices $v[.]$, and (iii) relabeling the edges. When checking for equality of two graphs, these invariances have to be taken into account. A brute-force way of canonicalizing the representation is to tabulate over all permutations of the vertices $v[.]$ as well as over all possible rotations of the edge labels within each vertex, enumerating the edges in order of appearance in each of the resulting representations, and to select the lexicographically smallest representative of the set.

Now that we have obtained all maximal graphs at a given genus, it is easy to construct *all* graphs of that genus by iteratively removing bridges in all possible ways, taking care to drop duplicate graphs at each step. In particular, it is straightforward to obtain all graphs that contribute to the four-point correlator (7.14). Namely, the contributing graphs still have a maximal number of edges, but now under the constraint that \mathcal{O}_i only connects to $\mathcal{O}_{i\pm 1}$, but not to $\mathcal{O}_{i+2} \pmod{4}$. In other words, the four vertices of the graph have to split into two pairs, where the members of each pair are not connected by any edge. We call such graphs *maximal cyclic graphs*. To find them, we can take our list of maximal four-point graphs, group the four vertices into pairs in all (three) possible ways, and delete all edges connecting the members of each pair. Some of the resulting graphs will not be maximal,³ those have to be dropped (in practice, this can be done by keeping only graphs with $4g + 4$ edges). Following this procedure, we find 6, 215, and 26779 maximal cyclic graphs at genus 1, 2, and 3, respectively.

Armed with these lists of maximal cyclic graphs, we can now construct the polynomials $P_{4g|g+1}$. Since we have treated all vertices as identical (unlabeled) thus far, we first have to sum over all inequivalent vertex labelings for each unlabeled graph. In addition, each labeled graph comes with combinatorial factors from summing over all ways of distributing the propagators on all edges (bridges) of the graph. According to (7.6), summing over the distribution of k_i propagators on b_i bridges results in a factor $k_i^{b_i-1}/(b_i - 1)!$. Hence each

³For example, if one of the deleted edges was adjacent to a square, the resulting graph will have a non-minimal face and hence cannot be a maximal cyclic graph.

labeled graph comes with a combinatorial factor

$$\prod_{i=1}^4 \frac{k_i^{b_i-1}}{(b_i-1)!}, \quad (\text{G.5})$$

where b_i is the number of edges (bridges) connecting vertices (operators) \mathcal{O}_i and $\mathcal{O}_{i+1} \pmod{4}$ in the given graph.

There is one more point that we need to take into account: When we organize the sum over all Wick contractions into a sum over skeleton graphs and a sum over distributions of propagators on the edges of those skeleton graphs, it may happen that two or more seemingly *different* distributions of propagators on the same skeleton graph may actually represent *identical* Wick contractions. The reason for this is that we implicitly treat all edges as distinguishable (i.e. labeled) when we perform the sum over distributions of propagators. In particular, this assumption is implicit in the counting (7.6) leading to (G.5), therefore resulting in an overcounting that we have to compensate. At the level of skeleton graphs, this overcounting manifests itself in terms of non-trivial *ribbon graph automorphisms*. Such automorphisms are defined as follows: In a given ribbon graph (with unlabeled vertices and edges), temporarily pick unique labels for all vertices and edges, and mark a fixed point on the perimeter of each of the vertices, in between any two adjacent incident edges. There are many different possible positions for these marked points. A non-trivial automorphism is a combination of edge and vertex relabelings that transform the graph with any other choice of marked points to the same graph with the previously fixed chosen positions of marked points.⁴ The set of automorphisms for a given ribbon graph Γ form the automorphism group $\text{Aut } \Gamma$. This group does not depend on the initially chosen positions of marked points. In order to compensate the overcounting explained above, one has to divide the propagator-distribution factor (G.5) by the size $|\text{Aut } \Gamma|$ of the automorphism group.⁵ We find (1, 3, 24) graphs with $|\text{Aut } \Gamma| = 2$ at genus (1, 2, 3), two graphs with $|\text{Aut } \Gamma| = 3$ at genus two, and three graphs with $|\text{Aut } \Gamma| = 4$ at genus three. All other graphs up to genus three have trivial automorphism group.

Now all that remains is to count within each graph Γ the number $p(\Gamma)$ of faces that touch all four vertices. Each of these faces will be home to one octagon function \mathbb{O} , see (7.7). To construct the desired polynomials $P_{4g|g+1}$, we have to sum over the set $\mathbf{\Gamma}_g$ of all maximal cyclic ribbon graphs of genus g with four vertices, and, for each graph $\Gamma \in \mathbf{\Gamma}_g$, over all inequivalent ways ℓ of assigning the operators \mathcal{O}_i , $i = 1, \dots, 4$ to the four vertices. The

⁴In gauge-theory terms, automorphisms map different choices of “beginnings/end” of all operator traces to each other by relabeling the operators and edges. See the final part of Section 2.2 in [148] for a more detailed definition with examples.

⁵In order to find the automorphism group in practice for a graph graph [...] as represented above, we tabulate over all cyclic rotations of the edge labels within individual vertices v [...], and over all permutations of the vertices v [...] within graph [...]. For each element of the resulting list, we label the edges canonically (for example by enumeration in order of appearance). We then collect identical elements in the canonicalized list. The size of each group of identical elements (all groups have the same size) is the size $|\text{Aut } \Gamma|$ of the automorphism group.

polynomials then are⁶

$$P_{4g|g+1} = \sum_{\Gamma \in \Gamma_g} \frac{1}{|\text{Aut } \Gamma|} \sum_{\ell} \prod_{i=1}^4 \frac{k_i^{b_i(\Gamma_{\ell})-1}}{(b_i(\Gamma_{\ell}) - 1)!} \mathbb{O}^{p(\Gamma)}. \quad (\text{G.6})$$

Here, $b_i(\Gamma_{\ell})$ is the number of edges connecting vertices (operators) \mathcal{O}_i and \mathcal{O}_{i+1} in the labeled graph Γ_{ℓ} . This concludes the construction of the polynomials $P_{4g|g+1}$ from explicit graphs. We computed these polynomials up to $g = 3$ in this way, and found a perfect match with the polynomials computed with matrix-model techniques as explained in [Section 7.3](#) and [Section 7.4](#).

G.2 From Minimal to Maximal Graphs

In this appendix we present a complementary approach to that of [Appendix G.1](#) on the construction of skeleton graphs. We propose to start by finding the *minimal* graphs which are graphs with a single face or *minimum* number of edges for given fixed genus g and number of vertices n . Using these as a seed we can find all other graphs by adding new edges recursively such that we do not change the genus of the original graphs. This procedure stops when we saturate the graphs, such that any additional edge would change the genus. This final stage corresponds to the maximal graphs described in the previous appendix.

A graph with a fixed number of vertices n and genus g is minimal when it has a single face. From the Euler formula it follows that it also has the minimum number of edges

$$2 - 2g = (F_{\min} = 1) + (V = n) - E_{\min} \quad \rightarrow \quad E_{\min} = n + 2g - 1 \quad (\text{G.7})$$

An instance of a minimal graph with four punctures and genus one is presented in [Figure G.1](#). Another useful way of representing a minimal graph is given in [Figure G.2](#) (a), where we present the single face of the graph as a polygon whose sides represent the $2E_{\min}$ half-edges (these are of the form $1 \rightarrow 2$ and $2 \leftarrow 1$ which reconstruct an edge $1 \rightleftharpoons 2$ in the fat graph),⁷ and its vertices given by partitions of the original punctures of the graph. This latter representation allows us to recognize that a minimal graph can be found by starting with a $(2E_{\min})$ -gon and identifying its edges in a pairwise fashion such that we encapsulate n vertices or punctures. In more detail we follow these steps to construct the minimal graphs:

- We start with a polygon with $2E_{\min}$ sides and some orientation.
- We label the vertices with numbers from 1 to n in all possible ways, allowing for repetitions in order to cover all vertices, but we do not allow for neighboring vertices

⁶In addition to the number of faces \mathbb{O} , we can also count the numbers of all other types of vertices (7.7) and thus obtain a polynomial in all 9 types of faces. Doing so, we find a complete match with the result of [Section G.3.4](#), again up to genus three.

⁷Notice here we use a different notion of half-edge compared to [Appendix G.1](#)

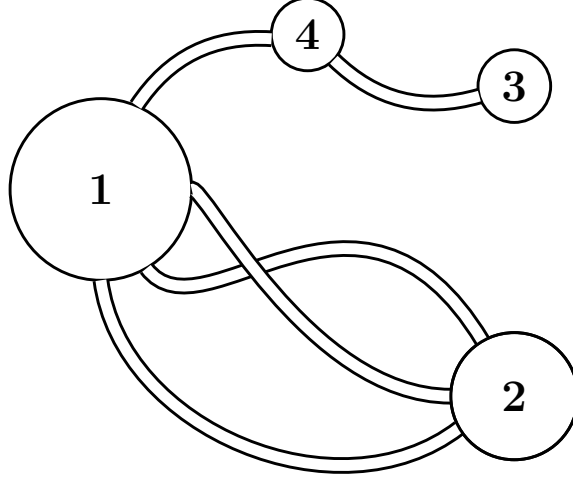


Figure G.1: Minimal graph example with $n = 4$ and $g = 1$.

with the same label as this would represent a self-contraction that we must dismiss. If we consider special polarizations as in the main text, then we should also dismiss the polygons with pairs of neighboring vertices labeled by operators that cannot connect.

- For each of the labeled polygons generated in the previous step, we identify pairs of sides (half-edges) of the form $1 \rightarrow 2$ and $1 \leftarrow 2$ to reconstruct the edges of the graph $1 \rightleftharpoons 2$. By doing so, all the vertices of the polygon with the same label also get together to reconstruct a puncture with that given label in the graph. We obtain a consistent graph when we get a total of n punctures with labels from 1 to n , with no repetition.

An alternative to this procedure can be found in the space of dual graphs, where we trade faces by vertices. The dual of a minimal graph has a single vertex, E_{\min} edges, and n faces. The advantage is that all these dual n -faced dual graphs can be found from Wick contractions in the Gaussian one-point function of a Hermitian matrix $\langle \text{tr}(\mathbb{M}^{2E_{\min}}) \rangle$. For instance see Figure G.2 (b), each Wick contraction there tells us how to identify the sides of the polygon in Figure G.2 (a). This dual point of view also facilitates the counting of the minimal graphs as nicely explained in [151] and derived in [178]. However the counting in those references has to be adapted to include labels in order to apply to the counting of our minimal graphs. We do not pursue this here, as our aim is only to provide a way to construct the minimal graphs.

Skeleton graphs with a higher number of edges can be simply constructed by adding edges to the minimal graphs. We would like to maintain the genus, so each additional edge must increase the number of faces by one to satisfy the Euler formula

$$2 - 2g = (1 + F_{\text{add}}) - n + (E_{\min} + E_{\text{add}}) \quad \Rightarrow \quad F_{\text{add}} = E_{\text{add}}. \quad (\text{G.8})$$

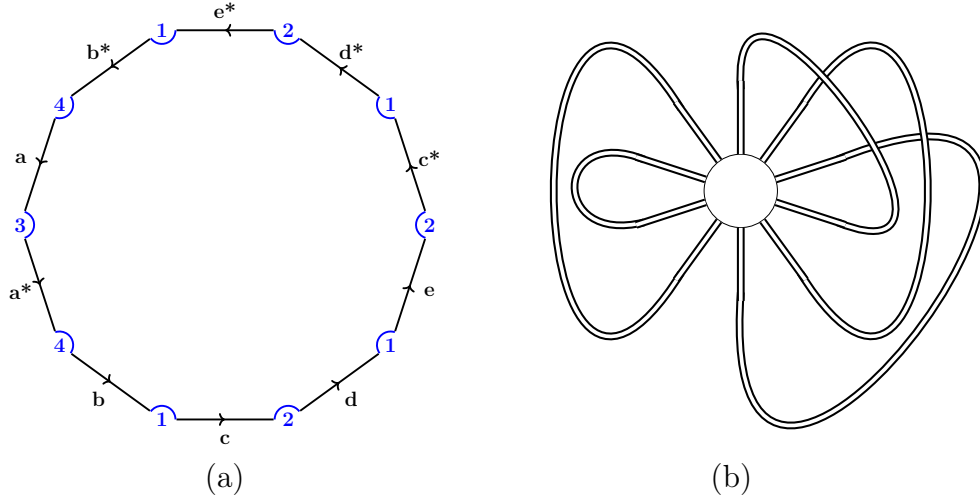


Figure G.2: The genus-one minimal graph of [Figure G.1](#) represented as the polygon of its single face (a), and its dual represented by Wick contractions in a one-point matrix correlator (b).

To achieve this we simply start with the polygon representing a minimal graph, and consider the additional edges as non-intersecting diagonals of the polygon. These divide the polygon into sub-polygons which represent the faces of the new non-minimal graphs.

Furthermore, we should only allow for diagonals that connect vertices of the polygon with different labels, otherwise we would be including self-connections. In the case of special polarizations, as considered in the main body of this paper, we should also disallow diagonals representing prohibited connections.

Adding non-intersecting diagonals one by one to each polygon of a minimal graph, we generate all skeleton graphs. In general the saturation of the number of edges happens when we turn on all possible non-intersecting diagonals forming a triangulation of the polygon of a minimal graph, see [Figure G.3](#) (a). From this consideration it follows that the maximum number of edges and faces a maximal graph can have are

$$\begin{aligned} E_{\max} &= (E_{\min} = n + 2g - 1) + (E_{\text{add}} = 2E_{\min} - 3) = 3(E_{\min} - 1) \\ &= 3(n + 2g - 2), \end{aligned} \tag{G.9}$$

$$F_{\max} = 2E_{\min} - 2 = 2(n + 2g - 2), \tag{G.10}$$

where the additional number of edges E_{add} simply corresponds to the maximal number of non-intersecting diagonals in the $(2E_{\min})$ -gon and the maximum number of faces F_{\max} is the number of triangles.

Due to the restriction of no self-connections, the saturation of edges can also happen before we reach the maximum value of edges ([G.9](#)). This is the case for the maximal graph in [Figure G.3](#) (b) represented by a tessellation containing both triangular and square faces.

In order to find all maximal graphs, we need to find all ways of triangulating the polygons of the minimal graphs. This can be achieved by following a recursive procedure

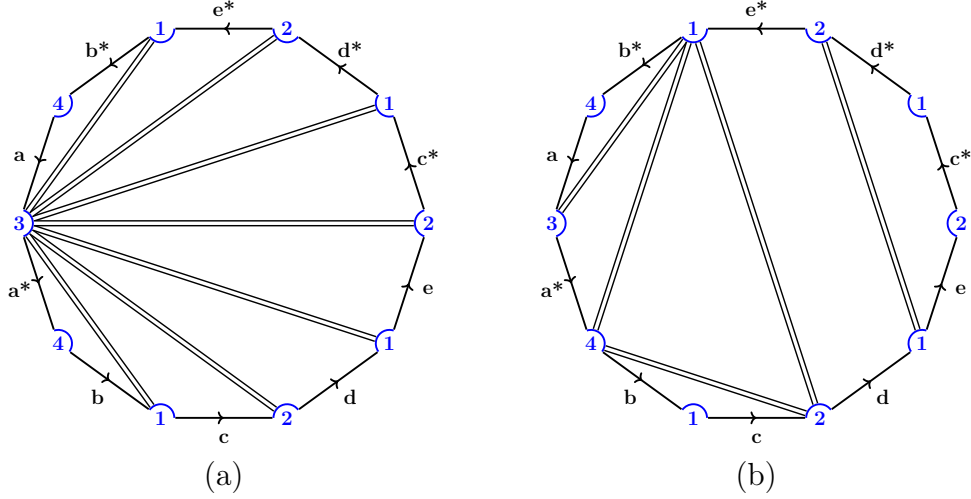


Figure G.3: Genus One: A maximal skeleton graph with only triangular faces (a), and an edge-saturated skeleton graph with triangular and square faces (b).

of bifurcation of polygons. Performing this procedure, we generate the list of all maximal graphs starting with the minimal graphs as a seed. We obtained results up to genus 3 which confirm the maximal graph generating algorithm of [Appendix G.1](#). The disadvantage is that the final list of graphs is redundant, since some originally different minimal graphs get identified after adding new edges. In practice we noticed that we only need to consider triangulations of relatively few minimal graphs to obtain the full list of maximal graphs. It would be nice to better understand how to single out a minimal subset of all minimal graphs that generates all maximal graphs.

G.3 Counting Quadrangulations Including Couplings

G.3.1 Introduction

For the correlator studied in this paper we have specific polarizations that restrict the connections to be only between neighbors $1 - 2 - 3 - 4 - 1$. This condition dismisses triangles, so we only need to consider squares to find the corresponding maximal graphs that dominate in the double scaling limit (DSL) considered in the main text.

In [Figure G.4 \(a\)](#) we present a genus-one quadrangulation obtained from the minimal graph of [Figure G.2 \(a\)](#) by adding non-intersecting charged-allowed diagonals only, or from the (truly) maximal graph in [Figure G.3 \(a\)](#) by erasing the charge-disallowed connections $1 - 3$ and $2 - 4$.

The squares entering a quadrangulation of our correlator can be classified according to the labels (operators 1,2,3 or 4) at its vertices. We have three types of squares as presented in [\(7.7\)](#) and in [Figure G.5](#). The first type includes the non-BPS squares $[1234]$ and $[4321]$ that evaluate to 1 in the free theory, and to the octagon function \mathbb{O} when the coupling is

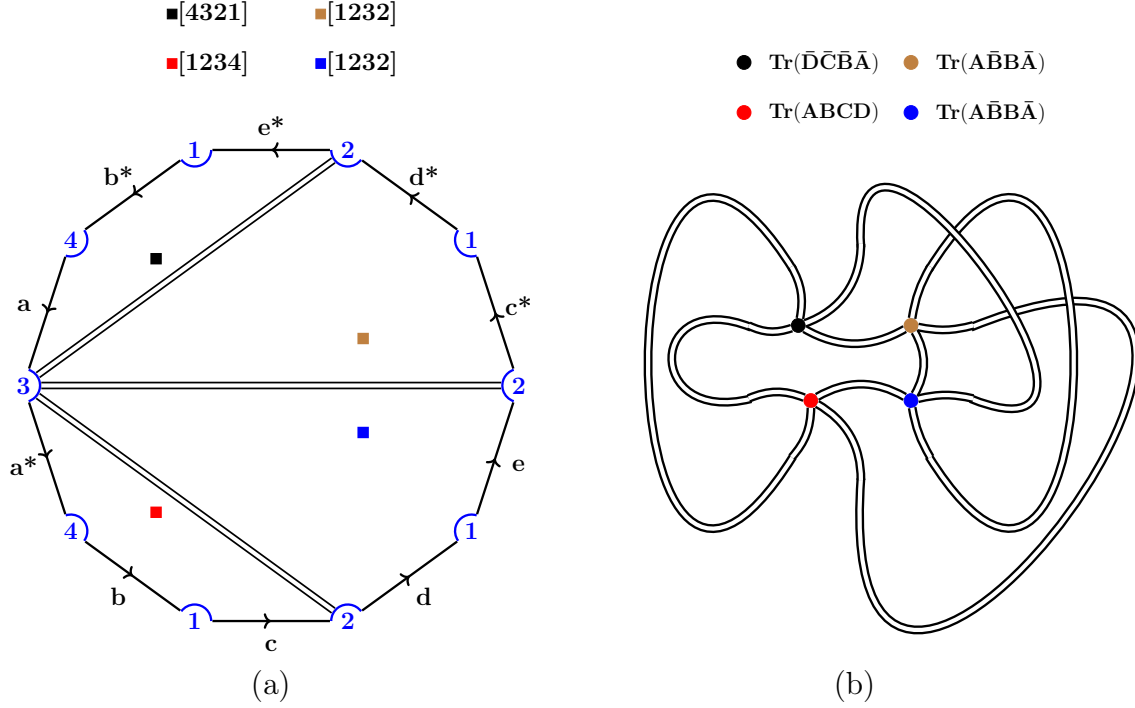


Figure G.4: A genus-one quadrangulation and its graph dual as Wick contractions of four-valent vertices.

turned on. The other two types are BPS squares of them form $[abcb]$ and the other four of form $[abab]$. These latter squares still evaluate to 1 when turning on the coupling.

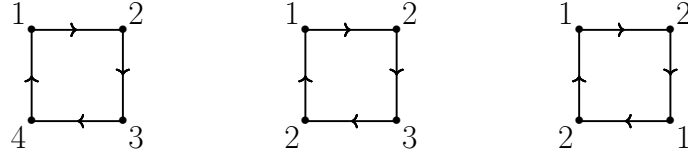


Figure G.5: The three types of squares that enter a quadrangulation. The vertices denote the punctures.

In order to find the graph's form by gluing these squares, we prefer to work in the dual space, where these faces are traded by four-valent vertices, see [Figure G.6](#). In this dual space, we have a total of 10 vertices, which define a matrix model with action

$$\begin{aligned}
S = & -\text{tr } A\bar{A} - \text{tr } B\bar{B} - \text{tr } C\bar{C} - \text{tr } D\bar{D} + \mathbb{O} \left(\text{tr } (ABCD) + \text{tr } (\bar{D}\bar{C}\bar{B}\bar{A}) \right) \\
& + \frac{\alpha_1}{2} \text{tr } (A\bar{A}A\bar{A}) + \frac{\alpha_2}{2} \text{tr } (B\bar{B}B\bar{B}) + \frac{\alpha_3}{2} \text{tr } (C\bar{C}C\bar{C}) + \frac{\alpha_4}{2} \text{tr } (D\bar{D}D\bar{D}) \\
& + \beta_1 \text{tr } (DA\bar{A}\bar{D}) + \beta_2 \text{tr } (AB\bar{B}\bar{A}) + \beta_3 \text{tr } (BC\bar{C}\bar{B}) + \beta_4 \text{tr } (CD\bar{D}\bar{C}) \quad (\text{G.11})
\end{aligned}$$

Unlike the action in (7.11), which only includes the coupling \mathbb{O} for non-BPS squares, here we include couplings associated to each four-valent vertex to distinguish each type

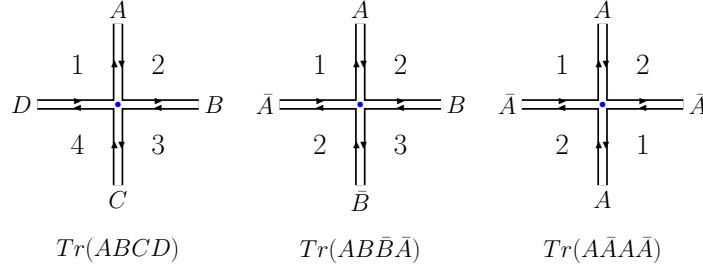


Figure G.6: The three types of squares that enter a quadrangulation. The original vertices 1, 2, 3, 4 are now faces that lie between the new edges.

of square. This gives the advantage of keeping track of the specific squares that form a quadrangulation, which can help recognizing symmetries or patterns essential for a genus resummation.

In this dual space, a quadrangulation is given by Wick contractions in a Gaussian correlator as represented in Figure G.4 (b). The correlator of this particular set of (dual) vertices can be explicitly computed as:

$$\frac{1}{2!} \langle \text{tr}(ABCD) \text{tr}(\bar{D}\bar{C}\bar{B}\bar{A}) \text{tr}(AB\bar{B}\bar{A})^2 \rangle = N^4 + 12N^6 + \frac{9}{2}N^8 + \frac{1}{2}N^{10} \quad (\text{G.12})$$

On the left hand side we add a symmetry factor due to the two identical vertices in the correlator. The result on the right hand side is given as a polynomial in N , the rank of the complex matrices, and from the exponents we can read off the number of faces of the graphs constructed by Wick contractions. We are only interested in the four-faced graphs, as they give the original four operators when dualized back. Furthermore in order to guarantee the dualized four faces give four different operators, we must have all A, B, C, D matrices present in our correlators of four-valent vertices.

The relevant 4-faced partition function, extracted from the matrix model with action (G.11), is explicitly given by

$$\mathbf{Z}(\mathbb{O}, \alpha_i, \beta_i) = \sum_{g=0}^{\infty} \sum_{T_g = \{t_1, \dots, t_{2g+2}\} \in V_4} \frac{1}{\text{sym}(T_g)} \left\langle \prod_{m=1}^{2g+2} t_m \right\rangle_{4 \text{ faces}} \quad (\text{G.13})$$

where we use the notation $\langle \dots \rangle_{4 \text{ faces}}$ to indicate we extract the coefficient of N^4 only. The subset $T_g = \{t_1, \dots, t_{2g+2}\}$ is a list of $2g + 2$ vertices, which are picked from the list of ten four-valent vertices with couplings $V_4 = \{\mathbb{O} \text{tr}(ABCD), \dots, \beta_4 \text{tr}(CD\bar{D}\bar{C})\}$ announced in (G.11), with the extra condition of containing all matrices A, B, C, D . The symmetry factor $\text{sym}(T_g)$ contains a factor of 2 for each vertex of the form $\text{tr}(X\bar{X}X\bar{X})$ and a factor $n!$ when we have n identical vertices t_m .

The partition functions \mathbf{Z} of (G.13) and \mathcal{Z} of (7.16) or (7.20) are identical up to a simple replacement of couplings:

$$k_1 k_2 k_3 k_4 \mathcal{Z}(\mathbb{O}, k_i) = \mathbf{Z}(\mathbb{O}, \alpha_i, \beta_i) \Big|_{\alpha_i \rightarrow k_i^2, \beta_i \rightarrow k_{i-1} k_i, \mathbb{O}^2 \rightarrow \mathbb{O}^2 k_1 k_2 k_3 k_4} \quad (\text{G.14})$$

As explained in [Section 7.3](#), the partition function \mathcal{Z} requires a Borel-type transformation to give the cyclic correlator \mathcal{A} , see (7.18). The analog transformation for \mathbf{Z} defines the partition function

$$\mathbf{A} = \sum_{g=0}^{\infty} \sum_{T_g=\{t_1, \dots, t_{2g+2}\} \in V_4} \frac{1}{\text{sym}(T_g)} \frac{1}{\text{weight}(T_g)} \left\langle \prod_{i=1}^{2g+2} t_i \right\rangle_{4 \text{ faces}} \quad (\text{G.15})$$

where the sole difference with (G.13) is the inclusion of the factorials:

$$\text{weight}(T_g) = (n_A - 1)!(n_B - 1)!(n_C - 1)!(n_D - 1)! \quad (\text{G.16})$$

with n_X counting the number of appereances of X in the subset T_g of $2g + 2$ vertices. Notice by construction we always demand $n_X \geq 1$.

The partition function \mathbf{A} of (G.15) is identified with the cyclic correlator \mathcal{A} under the replacement

$$\zeta_1 \zeta_2 \zeta_3 \zeta_4 \mathcal{A}(\mathbb{O}, \zeta_i) = \mathbf{A}(\mathbb{O}, \alpha_i, \beta_i) \Big|_{\alpha_i \rightarrow \zeta_i^2, \beta_i \rightarrow \zeta_{i-1} \zeta_i, \mathbb{O}^2 \rightarrow \mathbb{O}^2 \zeta_1 \zeta_2 \zeta_3 \zeta_4} \quad (\text{G.17})$$

with $\zeta_i = k_i / \sqrt{N_c}$.

By a direct computation of the correlators $\langle \dots \rangle_{4 \text{ faces}}$ in (G.15) we obtain, up to genus one:

$$\begin{aligned} \mathbf{A}(\mathbb{O}, \alpha_i, \beta_i) &= \mathbb{O}^2 + \frac{1}{2} \mathbb{O}^4 \\ &+ \mathbb{O}^2 \left(\sum_{i=1}^4 \left(\frac{1}{24} \alpha_i^2 + \frac{1}{6} \alpha_i (\beta_i + \beta_{i+1}) + \frac{1}{4} \beta_i^2 \right) + \frac{1}{2} (\beta_1 + \beta_3)(\beta_2 + \beta_4) \right) + \beta_1 \beta_2 \beta_3 \beta_4 + \dots \end{aligned} \quad (\text{G.18})$$

where the dots indicate contributions from genus two and higher. This latter expression can be compared with (8.4) under the replacement (G.17) and after setting $\zeta_i = \zeta$.

At higher genus, the correlators $\langle \dots \rangle_{4 \text{ faces}}$ become computationally more demanding, so in order to simplify them we use integrating-in and -out operations that we describe in the following section.

G.3.2 Graph Operations

In order to simplify the correlators $\langle \dots \rangle_{4 \text{ faces}}$ of four-valent vertices, we now introduce operations that reduce them to correlators with less number of faces. We will present these operations at the level of graphs, nevertheless they have an obvious translation into matrix theory language as integrating-in and -out matrix fields.

Integrating-In: Adding Edges

We use this operation to split a four-valent vertex into two three-valent vertices. This can be useful to restructure a graph and set it up for the application of other simplifying operations.

This operation is performed in two steps as shown in Figure G.7. In the first step we introduce a new edge and increase the number of vertices by one, such that the genus of the graph is maintained. As shown in the middle column of Figure G.7, there are two possibilities to add this intermediate edge. In this specific example the two different options require two different types of edges. The top type needs an edge with different faces on its sides and can be represented by a complex matrix in the matrix language. The bottom type needs an edge with the same face on its sides and can be represented by a Hermitian matrix. Finally in the second step we split this new edge resulting in two new three-valent vertices.

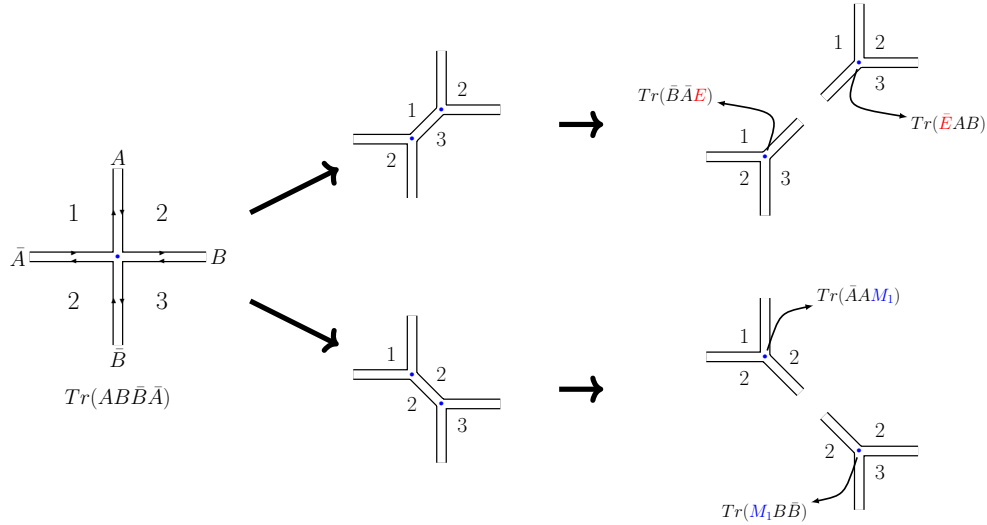


Figure G.7: Adding an extra intermediate edge

Ultimately, we want to connect back the intermediate edge to reconstruct the graph. But typically, we will first perform other simplifications, such as integrating-out, before restoring the intermediate edge, such that the final result will be simpler than the original graph.

Integrating-Out: Removing A Face

We use this operation to decrease the number of faces, vertices and edges all at the same time, such that the genus of the graph does not change. In the matrix language, this corresponds to integrating out one or more matrix fields.

To perform this operation, we first choose a reference face, labeled by 1 for instance. Then we organize all vertices that have a 1 appearing between their edges around the reference face as shown on the left panel of Figure G.8. The next step is to remove the reference face, such that all vertices on its perimeter get contracted to a single effective vertex that inherits all the outer edges, as shown on the right panel of Figure G.8.

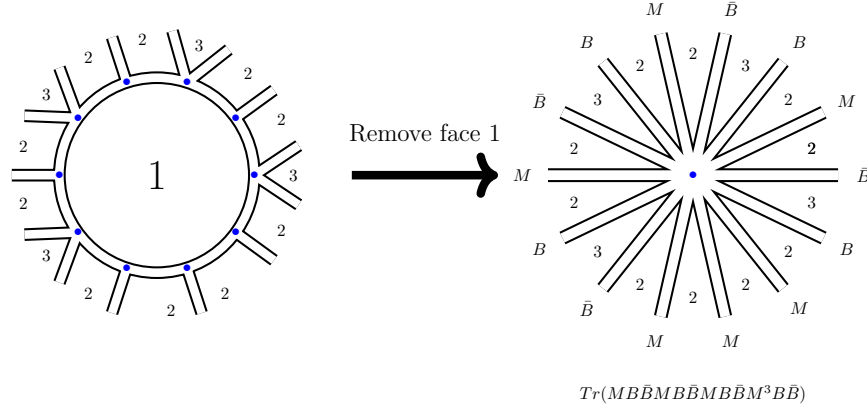


Figure G.8: Vertices organize around a reference face

In some cases it is possible to choose more than one reference face, such that all vertices participate in an integrating-out operation. On the other hand, in some cases it is not possible to pick a reference face at first, for instance we can not place four-valent vertices with faces between edges $[1212]$ around a reference face 1 or 2. In these cases, making an integrating-in operation first can allow to organize the resulting vertices of lower valence around a reference face. In the following sections, we will perform combinations of these graph operations to simplify the counting of quadrangulations.

G.3.3 Non-BPS Quadrangulations

As a warm-up, we consider quadrangulations formed by squares $[1234]$ and $[4321]$ only. As described in the main text, this addresses the limit of large coupling \mathbb{O} . In the dual space, the relevant matrix model has action

$$S_{\text{large } \mathbb{O}} = -\text{tr } A\bar{A} - \text{tr } B\bar{B} - \text{tr } C\bar{C} - \text{tr } D\bar{D} + \mathbb{O} \left(\text{tr } (ABCD) + \text{tr } (\bar{D}\bar{C}\bar{B}\bar{A}) \right). \quad (\text{G.19})$$

The simplicity of this problem allows for the application of different graph operations, which lead to different simplified outcomes. In what follows, we list some of these results, summarized in Section G.3.3.

As a 1-vertex and 3-faces problem

Having only vertices $\text{tr } (ABCD)$ and $\text{tr } (\bar{D}\bar{C}\bar{B}\bar{A})$, we can easily apply the integrating-out technique by picking as reference the face 1 (or any of the other three). Then, as shown

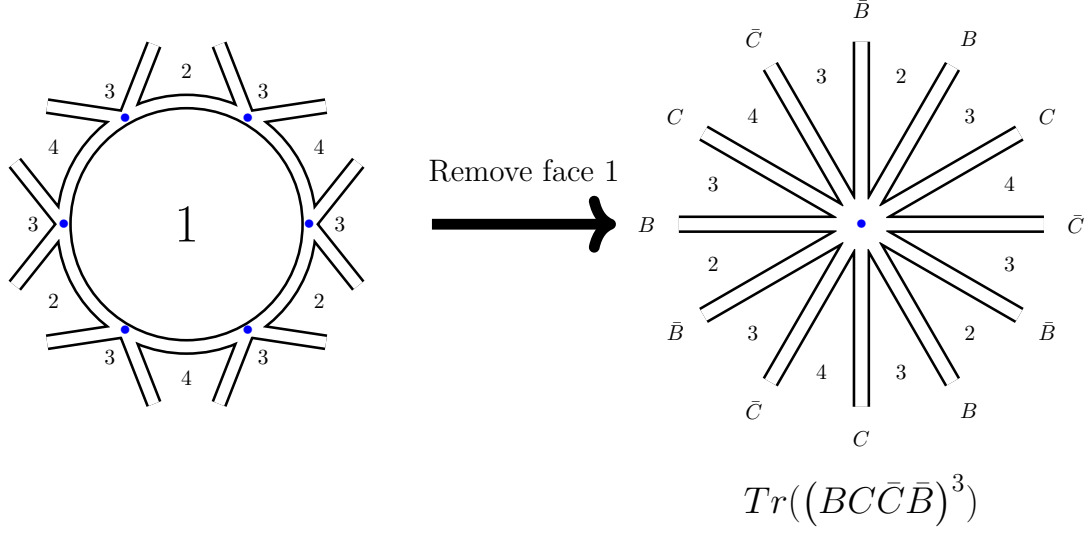


Figure G.9: Genus-two example: The unique way of organizing the four-valent vertices around a reference face 1, which leads to a single effective vertex, once we remove the reference face.

in Figure G.9, there is a unique way of organizing the vertices on the perimeter of this reference face, that is alternating the two types of vertices. After removing the reference face 1, the result is an effective vertex with fields B and C (and conjugates) only, the fields A and D are integrated out.

The non-BPS quadrangulations counted by the correlator of four-valent vertices $\langle \cdots \rangle_{4 \text{ faces}}$ can now be counted by a one-point correlator $\langle \text{tr}(\cdots) \rangle_{3 \text{ faces}}$, see equation (G.23).

As a 2-vertices and 2-faces problem

Another simplification of the non-BPS counting can be achieved by first integrating-in complex fields in the non-BPS vertices as shown in figure Figure G.10. After splitting the

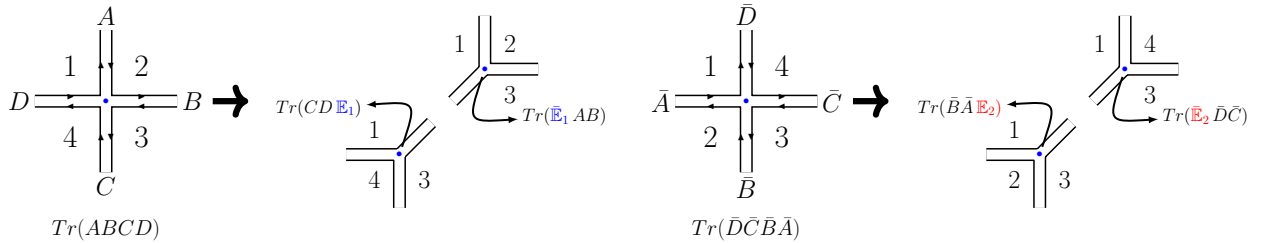


Figure G.10: Splitting non-BPS vertices.

four-valent vertices, we can arrange all three-valent vertices around two reference faces (2 and 4) as shown in Figure G.11.

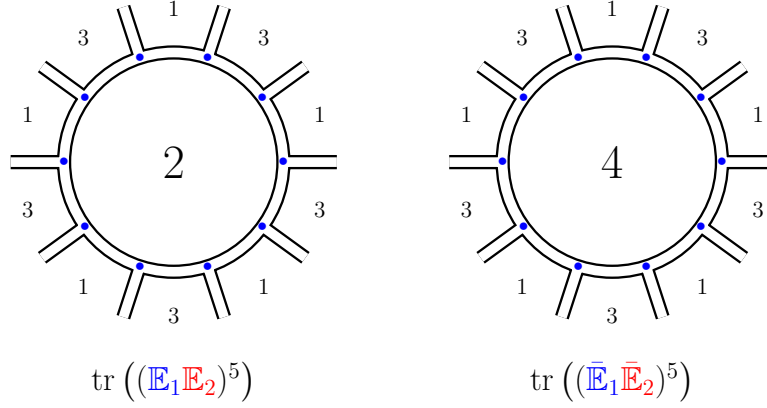


Figure G.11: Genus four non-BPS example: Integrating out faces 2 and 4 gives a single two-point function of traces with two complex matrices.

Then we remove these faces 2 and 4, which effectively integrates out all A, B, C, D , and obtain two effective vertices that contain only the fields \mathbb{E}_1 and \mathbb{E}_2 (and conjugates). Now the quadrangulation counting can be found by computing a two-point function $\langle \text{tr}(\cdots) \text{tr}(\cdots) \rangle_{2 \text{ faces}}$, see equation (G.24).

As a 3-vertices and 1-face problem

Naturally, dualizing the 1-vertex and 3-face problem, we obtain a 3-vertices and 1-face problem. We have not worked out in detail the necessary graph operations to get this latter outcome starting with the four-valent vertices. Nevertheless, by working out a few examples, we figured out what the correlator is, and present it in equation (G.25)

Summary for Non-BPS squares

We use \mathcal{N}_g to denote the number of non-BPS quadrangulations weighted by their corresponding symmetry factors (automorphisms). From genus $g = 0$ to $g = 5$ these numbers, not necessarily integers, are:

$$\{\mathcal{N}_g\} = \left\{1, \frac{1}{2}, 1, 5, \frac{248}{5}, 840, \dots\right\} \quad (\text{G.20})$$

they appear in the large \mathbb{O} limit of \mathcal{A} , see (7.32), as:

$$\mathcal{A} = \frac{1}{\zeta_1 \zeta_2 \zeta_3 \zeta_4} \sum_{g=0}^{\infty} \frac{(\zeta_1 \zeta_2 \zeta_3 \zeta_4 \mathbb{O}^2)^{g+1}}{g!^4} \mathcal{N}_g \quad (\text{G.21})$$

and can be computed in four different and equivalent ways

$$\mathcal{N}_g = \frac{\langle (\text{tr } (ABCD) \text{tr } (\bar{D}\bar{C}\bar{B}\bar{A}))^n \rangle_{4 \text{ faces}}}{n!^2} \quad (\text{G.22})$$

$$= \frac{\langle \text{tr } ((BC\bar{C}\bar{B})^n) \rangle_{3 \text{ faces}}}{n} \quad (\text{G.23})$$

$$= \frac{\langle \text{tr } ((BC)^n) \text{tr } ((\bar{B}\bar{C})^n) \rangle_{2 \text{ faces}}}{n^2} \quad (\text{G.24})$$

$$= \frac{\langle \text{tr } (B^n) \text{tr } (C^n) \text{tr } ((\bar{B}\bar{C})^n) \rangle_{1 \text{ face}}}{n^3}, \quad (\text{G.25})$$

where $n = g + 1$.

Notice that the weights in our correlators, denominators in (G.22) until (G.25), correspond to symmetry factors. We have the factor $n!$ for n identical vertices, and the factor n for traces of the form $\text{tr } (X^n)$.

G.3.4 All quadrangulations

We now address the full problem of counting quadrangulations including all ten vertices. Out of the three possibilities we presented for the non-BPS squares ([1234] and [4321]) sector in Section G.3.3, we found only the two-face simplification can be deformed to include the BPS squares ($[abcb]$ and $[abab]$) and count all quadrangulations.

To get to this two-face simplification, we first integrate-in auxiliary Hermitian matrices $\mathbb{M}_1, \mathbb{M}_2, \tilde{\mathbb{M}}_1, \tilde{\mathbb{M}}_2$ and complex matrices \mathbb{X}, \mathbb{Y} to split the BPS vertices as shown in Figure G.12 and Figure G.13. In addition to that, to be consistent with this new auxiliary matrices, we relabel the complex matrices in the splitting of the non-BPS vertices as shown in Figure G.14.

In order to reconstruct the couplings α_i, β_i we impose the auxiliary matrices satisfy:

$$\begin{aligned} \langle \mathbb{M}_1 \mathbb{M}_1 \rangle &= \alpha_1 & \langle \mathbb{X} \bar{\mathbb{X}} \rangle &= \beta_2 \\ \langle \mathbb{M}_2 \mathbb{M}_2 \rangle &= \alpha_2 & \langle \mathbb{Y} \bar{\mathbb{Y}} \rangle &= \beta_4 \\ \langle \tilde{\mathbb{M}}_2 \tilde{\mathbb{M}}_2 \rangle &= \alpha_3 & \langle \mathbb{M}_2 \tilde{\mathbb{M}}_2 \rangle &= \beta_3 \\ \langle \tilde{\mathbb{M}}_1 \tilde{\mathbb{M}}_1 \rangle &= \alpha_4 & \langle \mathbb{M}_1 \tilde{\mathbb{M}}_1 \rangle &= \beta_1 \end{aligned} \quad (\text{G.26})$$

and similiary for the non-BPS coupling:

$$\langle \mathbb{X} \bar{\mathbb{Y}} \rangle = \langle \bar{\mathbb{X}} \mathbb{Y} \rangle = \mathbb{O} \quad (\text{G.27})$$

We can now arrange the three-valent vertices around reference faces 2 and 4 as shown in Figure G.15. After removing these faces we obtain effective vertices of the form:

$$T_{\{L, \{m_i\}, \{n_i\}\}} = \text{tr} \left(\prod_{i=1}^L (\mathbb{M}_1^{m_i} \mathbb{X} \mathbb{M}_2^{n_i} \bar{\mathbb{X}}) \right) \quad \text{and} \quad \tilde{T}_{\{\tilde{L}, \{\tilde{m}_i\}, \{\tilde{n}_i\}\}} = \text{tr} \left(\prod_{i=1}^{\tilde{L}} (\tilde{\mathbb{M}}_1^{\tilde{m}_i} \mathbb{Y} \tilde{\mathbb{M}}_2^{\tilde{n}_i} \bar{\mathbb{Y}}) \right) \quad (\text{G.28})$$

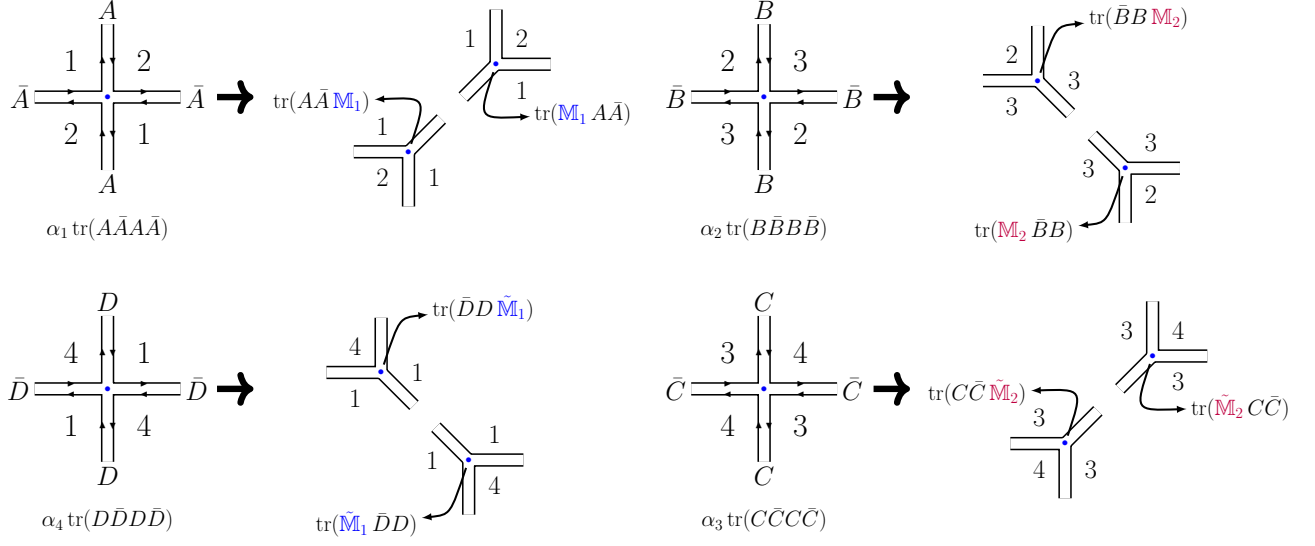


Figure G.12: Splitting vertices with couplings α_i

The counting of quadrangulations now follows from computing the two-point functions of these effective vertices with Wick contractions dictated by (G.26) and (G.27) and extracting the two-face coefficient $\langle T \tilde{T} \rangle_{2 \text{ faces}}$. For instance, at genus two we have a contribution from:

$$\begin{aligned}
 \langle \text{tr} (\mathbb{M}_1^2 \mathbb{X} \mathbb{M}_2 \bar{\mathbb{X}} \mathbb{M}_1 \mathbb{X} \bar{\mathbb{X}}) \text{tr} (\tilde{\mathbb{M}}_1 \mathbb{Y} \tilde{\mathbb{M}}_2^2 \bar{\mathbb{Y}} \mathbb{Y} \tilde{\mathbb{M}}_2 \bar{\mathbb{Y}}) \rangle_{2 \text{ faces}} = \\
 4 \mathbb{O}^4 \alpha_1 \alpha_2 \alpha_3 \beta_1 + 16 \mathbb{O}^4 \alpha_1 \beta_1 \beta_3^2 + 16 \mathbb{O}^2 \alpha_1 \alpha_2 \alpha_3 \beta_1 \beta_2 \beta_4 \\
 + 55 \mathbb{O}^2 \alpha_1 \beta_1 \beta_2 \beta_3^2 \beta_4 + 4 \alpha_1 \alpha_2 \alpha_3 \beta_1 \beta_2^2 \beta_4^2 + 12 \alpha_1 \beta_1 \beta_2^2 \beta_3^2 \beta_4^2. \quad (\text{G.29})
 \end{aligned}$$

In order to compute the two-face partition function, we must consider all possible effective vertices and their corresponding symmetry factors:

$$\mathbf{Z}(\mathbb{O}, \alpha_i, \beta_i) = \sum_{g=0}^{\infty} \sum_{\{\mathcal{N}, \tilde{\mathcal{N}}\} \in \mathcal{M}_g} \frac{1}{s_{\mathcal{N}} s_{\tilde{\mathcal{N}}}} \langle T_{\mathcal{N}} \tilde{T}_{\tilde{\mathcal{N}}} \rangle_{2\text{-faces}}, \quad (\text{G.30})$$

where we group the collections of indices as

$$\mathcal{N} \equiv \{L, \{m_i\}, \{n_i\}\} \quad \tilde{\mathcal{N}} \equiv \{\tilde{L}, \{\tilde{m}_i\}, \{\tilde{n}_i\}\}. \quad (\text{G.31})$$

Allowing for different orderings of $\{m_i\}$ and $\{n_i\}$ ($\{1, 2\} \neq \{2, 1\}$) in the inner sum of (G.30),⁸ then the symmetry factors are simply giving by:

$$s_{\mathcal{N}} = L \quad \text{and} \quad s_{\tilde{\mathcal{N}}} = \tilde{L}. \quad (\text{G.32})$$

⁸We could alternatively mod out orderings $\mathcal{N} \equiv \{L, \{m_i\}, \{n_i\}\}$ that are cyclically equivalent within the trace. In that case we would have to modify the symmetry factor $s_{\mathcal{N}} = \frac{L}{\# \text{ equivalent orderings}}$

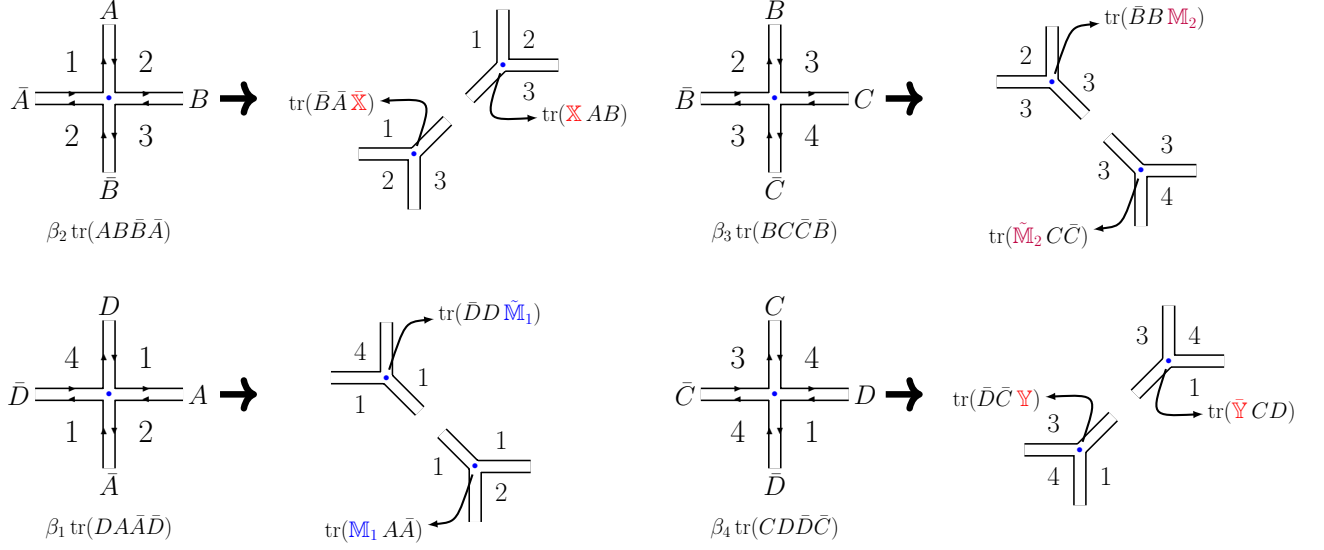


Figure G.13: Splitting vertices with couplings β_i

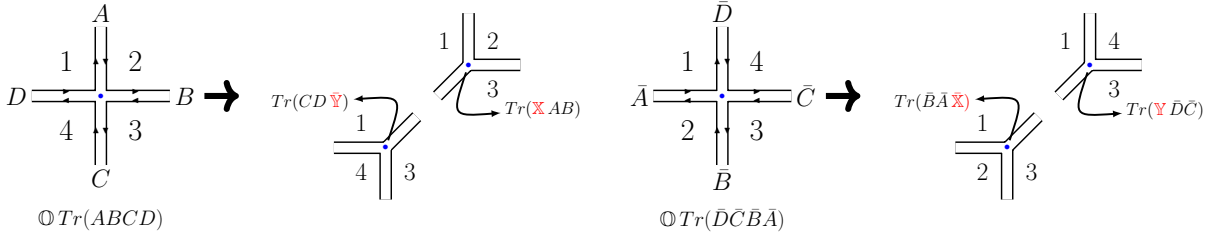


Figure G.14: Splitting vertices with coupling \mathbb{O} using complex matrices.

Furthermore the inner sum is restricted to run over the group \mathcal{M}_g , whose elements are all $\{\mathcal{N}, \tilde{\mathcal{N}}\}$ that satisfy:

$$2(L + \tilde{L}) + \sum_{i=1}^L (n_i + m_i + \tilde{n}_i + \tilde{m}_i) = 4g + 4, \quad (\text{G.33})$$

such that for each genus g the number of fields is $4g + 4$, leading two $2g + 2$ squares after Wick contractions. Furthermore, from (G.26) it follows that only when $\sum_i m_i + \tilde{m}_i$ and $\sum_i n_i + \tilde{n}_i$ are even numbers are the two-point correlators non-vanishing.

The expression (G.30) admits a resummation that leads to the compact formula:

$$\mathbf{Z}(\mathbb{O}, \alpha_i, \beta_i) = \left\langle \text{tr} \log \left(\mathbb{I} - \frac{1}{\mathbb{I} - \mathbb{M}_2} \bar{\mathbb{X}} \frac{1}{\mathbb{I} - \mathbb{M}_1} \mathbb{X} \right) \text{tr} \log \left(\mathbb{I} - \frac{1}{\mathbb{I} - \tilde{\mathbb{M}}_2} \bar{\mathbb{Y}} \frac{1}{\mathbb{I} - \tilde{\mathbb{M}}_1} \mathbb{Y} \right) \right\rangle_{2 \text{ faces}} \quad (\text{G.34})$$

This is the analog of (7.22), but now with couplings α_i and β_i for the BPS squares. Notice that the expansion of the logs in (G.34) leads to terms which do not satisfy the restriction (G.33). However, these unwanted terms do not have a two-face contribution,

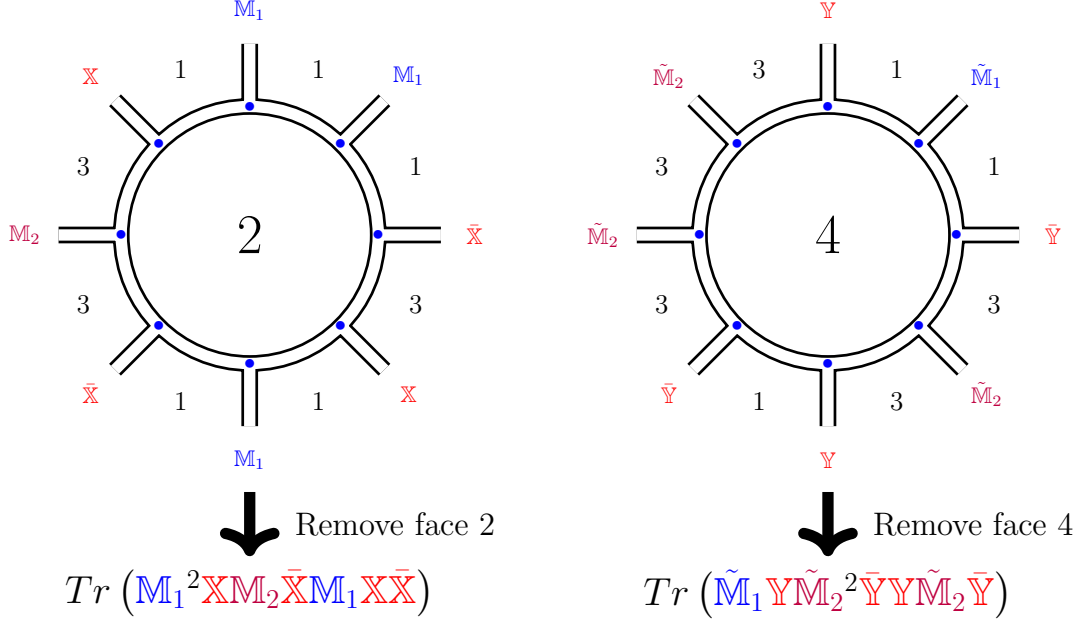


Figure G.15: Integrating-out faces 2 and 4 gives two effective vertices, which under Wick contractions should encapsulate two faces: 1 and 3.

$\langle \text{unwanted} \rangle_{2 \text{ faces}} = 0$.⁹ So effectively, (G.30) and (G.34) are identical.

The partition function \mathbf{A} that makes direct contact with the cyclic correlator studied in this paper is now given by:

$$\mathbf{A}(\mathbb{O}, \alpha_i, \beta_i) = \sum_{g=0}^{\infty} \sum_{\{\mathcal{N}, \tilde{\mathcal{N}}\} \in \mathcal{M}_g} \frac{1}{s_{\mathcal{N}} s_{\tilde{\mathcal{N}}}} \frac{1}{w_{\mathcal{N}} w_{\tilde{\mathcal{N}}}} \langle T_{\mathcal{N}} \tilde{T}_{\tilde{\mathcal{N}}} \rangle_{2\text{-faces}} \quad (\text{G.36})$$

with weights:

$$w_{\mathcal{N}} \equiv w_{\{L, \{m_i\}, \{n_i\}\}} = \left(-1 + \sum_{i=1}^L (m_i + 1) \right)! \left(-1 + \sum_{i=1}^L (n_i + 1) \right)!, \quad (\text{G.37})$$

for which we have not found a compact re-summed formula as (G.34).

Perturbative genus computation

The two-face formulations (G.30) and (G.36) allows us to efficiently compute the partitions \mathbf{Z} or \mathbf{A} up to genus 4. Then under the replacement (G.17) we obtain the perturbative result in (8.4).

⁹This follows from the Euler formula. We have two vertices and demand two faces, so the number of edges must be:

$$2 - 2g = (F = 2) + (V = 2) - E \quad \Rightarrow \quad E = 2g + 2, \quad (\text{G.35})$$

which means that only two-point correlators with a total number of composite matrices given by a multiple of four, condition (G.33), contribute to $\langle \cdots \rangle_{2 \text{ faces}}$.

In the BPS limit $\mathbb{O} \rightarrow 0$, we carry on up to genus 6 by integrating out the complex matrices, and then evaluating one-face correlators of Hermitian matrices as explained in [Section 7.4](#). This larger amount of data, and the inspiration we get from the extremal correlator in [Appendix G.4.1](#) allows us to guess the re-summed series as:

$$\mathbf{A}(\mathbb{O} = 0, \alpha_i, \beta_i) = \prod_{i=1}^4 \beta_i \frac{\sinh \frac{1}{2} (\beta_i + \alpha_i + \beta_{i+1})}{\frac{1}{2} (\beta_i + \alpha_i + \beta_{i+1})}. \quad (\text{G.38})$$

Under the replacement [\(G.17\)](#), we obtain the result in [\(7.30\)](#).

In fact we further found that formula [\(G.38\)](#) can be extended to find the BPS part of a larger class of cyclic correlators, as we present in [Appendix G.4.2](#).

G.4 Other Results On Quadrangulations

G.4.1 $(n + 1)$ -Point Extremal Correlators in DSL

In this appendix, we review the computation of protected extremal correlators of the form^{[10](#)}

$$E_n = \langle \text{tr} (Z^{J_1}) \text{tr} (Z^{J_2}) \cdots \text{tr} (Z^{J_n}) \text{tr} (\bar{Z}^{J_R}) \rangle \quad (\text{G.39})$$

with $J_R = J_1 + \cdots + J_n$, in the double scaling limit $J_i \rightarrow \infty$, $N_c \rightarrow \infty$ and $J_i/\sqrt{N_c}$ fixed. In fact the result is known at finite N_c and J_i from [\[141, 143\]](#). In the DSL it is given by:

$$E_n(J_i, N_c) \stackrel{\text{DSL}}{=} J_R^{-2} (2N_c)^n \prod_{i=1}^n \sinh \left(\frac{J_i J_R}{2N_c} \right). \quad (\text{G.40})$$

Here, we would like to present how to reproduce this result by counting quadrangulations and using integrating-in and -out graph operations.

In the DSL, the correlator E_n can be reconstructed in a similar fashion as the cyclic correlator of this article. The skeleton graphs that dominate are also given by quadrangulations, and to obtain E_n we must count them and dress them with the lengths J_i by performing a Borel-type transformation.

All squares involved include the reservoir R twice, and the corresponding dual four-valent vertices are given in the matrix action:

$$S_n^{(\text{E})} = - \sum_{a=1}^n \text{tr} (A_a \bar{A}_a) + \frac{1}{2} \sum_{a=1}^n \sum_{b=1}^n \alpha_{a,b} \text{tr} (A_a A_b \bar{A}_b \bar{A}_a) \quad (\text{G.41})$$

with couplings $\alpha_{a,b} = \alpha_{b,a}$ associated to squares of the form $[\text{RaRb}]$.

¹⁰Here, the normalization is such that the genus expansion goes as $N_c^0(\cdots) + N_c^{-2}(\cdots) + \cdots$

The relevant Borel-transformed partition function (the analog of (G.15)) coming from the matrix model (G.41) is

$$\mathbf{A}_n^{(E)}(\alpha_{a,b}) = \sum_{g=0}^{\infty} \sum_{T_g = \{t_1, \dots, t_{n+2g-1}\} \in V_4^{(E)}} \frac{1}{\text{sym}(T_g)} \frac{1}{\text{weight}(T_g)} \left\langle \prod_{m=1}^{n+2g-1} t_m \right\rangle_{(n+1) \text{ faces}}, \quad (\text{G.42})$$

where now T_g is a subset of $(n + 2g - 1)$ four-valence vertices with couplings chosen from $V_4^{(E)} = \{\alpha_{a,b} \text{tr}(A_a A_b \bar{A}_b \bar{A}_a)\}_{a,b=1, \dots, n}$ with at least one occurrence of A_a for $a = 1, \dots, n$.

The symmetry factor $\text{sym}(T_g)$ has a factor of 2 for each vertex of the form $\text{tr}(A_a A_a \bar{A}_a \bar{A}_a)$, and a $k!$ when T_g contains a vertex repeated k times. The weight factor is given by:

$$\text{weight}(T_g) = \prod_{i=1}^n (m_{A_i} - 1)! \quad (\text{G.43})$$

where m_{A_i} counts the number of occurrences of A_i in the subset T_g .

This partition function \mathbf{A} can be identified with the DSL of the extremal correlator under the replacement:

$$E_n(J_i, N_c) \stackrel{\text{DSL}}{=} N_c^{n-1} \mathbf{A}_n^{(E)}(\alpha_{a,b}) \big|_{\alpha_{a,b} \rightarrow J_a J_b / N_c} \quad (\text{G.44})$$

We can simplify the correlators $\langle \dots \rangle_{(n+1) \text{ faces}}$ in (G.42) by performing integrating-in and -out operations. First, we integrate-in to obtain three-valent vertices where the faces lying between their edges are $(R R a)$ as shown in figure Figure G.16. Then, we can arrange all

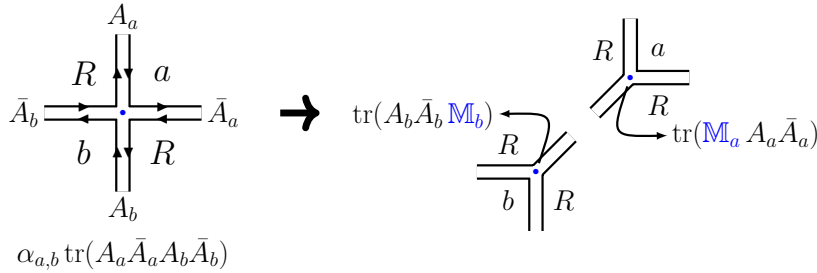


Figure G.16: Splitting a BPS vertex by introducing hermitian matrices \mathbb{M}_a and \mathbb{M}_b , which satisfy $\langle \mathbb{M}_a \mathbb{M}_b \rangle = \alpha_{a,b}$.

vertices of the form $(R R a)$ around the face a , for all $a = 1, \dots, n$, as shown in Figure G.17.

Finally, by removing these n reference faces, we obtain n effective vertices, with the only remaining face being the reservoir R . So the partition $\mathbf{A}_n^{(E)}$ is now effectively computed by a sum of one-face correlators:

$$\mathbf{A}_n^{(E)}(\alpha_{a,b}) = \sum_{g=0}^{\infty} \sum_{i_1 + \dots + i_n = 2(n+2g-1)} \frac{\langle \text{tr}(\mathbb{M}_1^{i_1}) \dots \text{tr}(\mathbb{M}_n^{i_n}) \rangle_{1 \text{ face}}}{i_1! \dots i_n!} = \left\langle \prod_{a=1}^n \text{tr}(e^{\mathbb{M}_a} - \mathbb{I}) \right\rangle_{1 \text{ face}} \quad (\text{G.45})$$

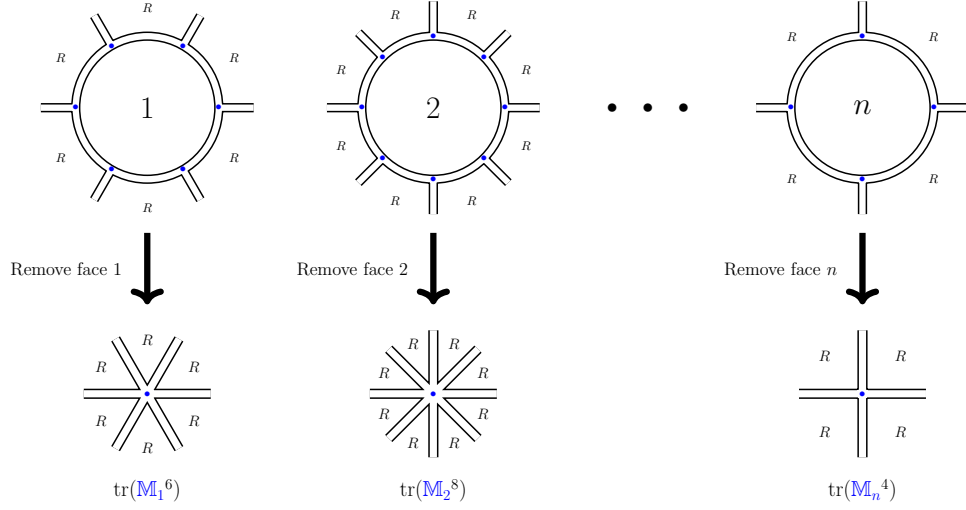


Figure G.17: Integrating-out all faces except the reservoir R .

where all indices $i_m > 0$, and the couplings appear in the Wick contractions as:

$$\langle \mathbb{M}_a \mathbb{M}_b \rangle = \alpha_{a,b}. \quad (\text{G.46})$$

We have computed this partition function (G.45) for the first few genera, and found a match against (G.40) under the replacement (G.44). We have further recognized that in terms of couplings $\alpha_{a,b}$, the partition function evaluates to:

$$\mathbf{A}_n^{(\text{E})}(\alpha_{a,b}) = \left\langle \prod_{a=1}^n \text{tr} \left(e^{\mathbb{M}_a} - \mathbb{I} \right) \right\rangle_{1 \text{ face}} = P_n(\alpha_{a,b}) \prod_{a=1}^n \frac{\sinh \left(\frac{1}{2} \sum_{b=1}^n \alpha_{a,b} \right)}{\frac{1}{2} \sum_{b=1}^n \alpha_{a,b}}. \quad (\text{G.47})$$

The prefactor P_n is a non-factorizable homogeneous polynomial of degree $n - 1$ in the couplings $\alpha_{a,b}$, with $a \neq b$, and is independent of the genus. For $n = 3$ and $n = 4$, it is simply given by:

$$P_{n=3} = \alpha_{1,2} \alpha_{1,3} + \alpha_{1,2} \alpha_{2,3} + \alpha_{1,3} \alpha_{2,3}, \quad (\text{G.48})$$

$$\begin{aligned} P_{n=4} = & \alpha_{1,2} \alpha_{3,4} (\alpha_{1,3} + \alpha_{1,4} + \alpha_{2,3} + \alpha_{2,4}) + \alpha_{1,3} \alpha_{2,4} (\alpha_{1,2} + \alpha_{1,4} + \alpha_{2,3} + \alpha_{3,4}) \\ & + \alpha_{1,4} \alpha_{2,3} (\alpha_{1,2} + \alpha_{1,3} + \alpha_{2,3} + \alpha_{2,4}) + \alpha_{1,2} \alpha_{1,3} \alpha_{1,4} + \alpha_{1,2} \alpha_{2,3} \alpha_{2,4} \\ & + \alpha_{1,3} \alpha_{2,3} \alpha_{3,4} + \alpha_{1,4} \alpha_{2,4} \alpha_{3,4}. \end{aligned} \quad (\text{G.49})$$

We have not found its closed form for generic n , although we know it explicitly up to $n = 6$. It is related to the planar contribution of the DSL of the extremal correlator:

$$\lim_{N_c \rightarrow \infty} E_n^{\text{DSL}} P_n(\alpha_{a,b}) \big|_{\alpha_{a,b} \rightarrow J_a J_b} = (J_1 + \dots + J_n)^{n-2} \prod_{i=1}^n J_i = J_R^{n-2} \prod_{i=1}^n J_i. \quad (\text{G.50})$$

G.4.2 n -Point Cyclic Correlators In DSL

Finally, we consider the n -point cyclic correlator shown in Figure G.18. For $\mathcal{N} = 4$ SYM, only the correlators with $n \leq 6$ are realizable, while for higher n the theory does not admit

enough R-charge polarizations to prevent other connections that break the cyclic pattern. Furthermore for $n > 4$ only BPS quadrangulations dominate.

The relevant matrix model to count these quadrangulations has the action

$$S_n^{(C)} = - \sum_{i=1}^n \text{tr} (A_i \bar{A}_i) + \sum_{i=1}^n \frac{\alpha_i}{2} \text{tr} (A_i \bar{A}_i A_i \bar{A}_i) + \beta_i \text{tr} (A_i \bar{A}_i \bar{A}_{i-1} A_{i-1}) \quad (\text{G.51})$$

Based on direct computations of the relevant correlators of four-valent vertices up to genus two, we predict the generalization of (G.38) is:

$$\mathbf{A}_n^{(C)}(\alpha_i, \beta_i) = \prod_{a=1}^n \beta_i \frac{\sinh\left(\frac{1}{2}(\beta_i + \alpha_i + \beta_{i+1})\right)}{\frac{1}{2}(\beta_i + \alpha_i + \beta_{i+1})}, \quad (\text{G.52})$$

where $\mathbf{A}_n^{(C)}$ is defined analogously to (G.15), with the four-valent vertices in (G.51), and demanding now n faces ($\langle \cdots \rangle_{n \text{ faces}}$). The corresponding cyclic correlator in the DSL is obtained by introducing the bridge lengths k_i with the replacement $\alpha_i \rightarrow k_i^2/N_c^2$ and $\beta_i \rightarrow k_{i-1}k_i/N_c$ with $k_0 \equiv k_n$.

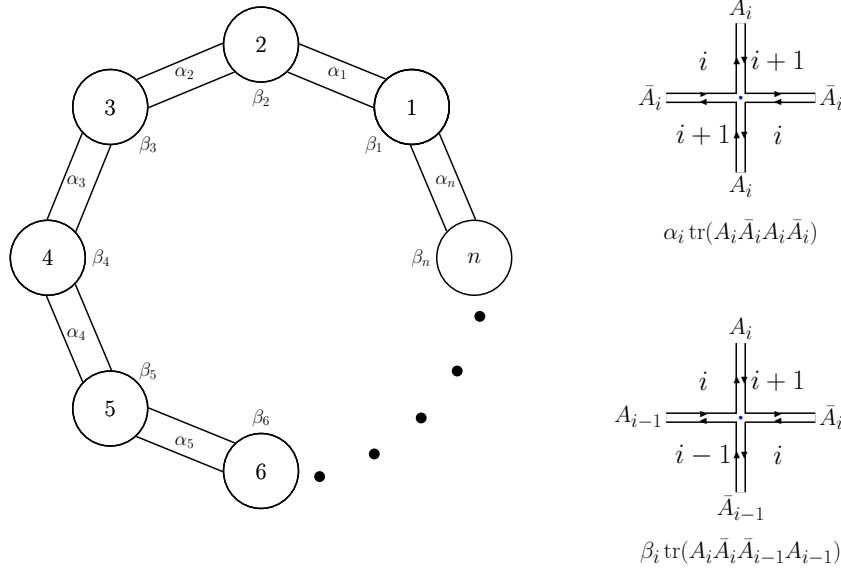


Figure G.18: Cyclic correlator and four-valent vertices dual to the BPS squares $[i(i+1)i(i+1)]$ and $[i(i+1)i(i-1)]$.